Competitive Traits of El Tor *V. cholerae*

By

Benjamin Kostiuk

A thesis submitted in partial fulfillment of the requirements for the degree of

Doctor of Philosophy
in
Bacteriology

Department of Medical Microbiology and Immunology
University of Alberta

Abstract

Vibrio cholerae is a diverse bacterial species that causes a wide range of disease, ranging from the diarrheal disease cholera by toxigenic strains to mild gastroenteritis caused by non-toxigenic strains. Toxigenic strains are able to cause more severe disease due to the secretion of cholera toxin. During its lifecycle, *V. cholerae* inhabits chitinous surfaces and the human host. This diversity within the species and environmental conditions results in opportunities for competition among *V. cholerae* strains and with other microorganisms.

V. cholerae uses the type VI secretion system (T6SS) to mediate competition with other bacteria and eukaryotes. The T6SS is a molecular syringe-like apparatus that contracts in the host bacterium, sending a spike decorated with effector proteins into neighbouring bacterial or eukaryotic cells. Effector translocation is lethal unless the target cell produces cognate immunity proteins specific to the incoming effectors. Despite the T6SS being ubiquitous amongst all sequenced *V. cholerae* strains, different strains encode different effectors and immunity genes. Therefore, each strain carries three effector genes but also three immunity genes to neutralize these effectors. This phenomenon allows competition not just with other species of bacteria, but also between *V. cholerae* strains. If bacteria encode the same effectors, they are able to coexist, while encoding different effectors causes competition. The T6SS effectors appear to be horizontally shared based on strong bioinformatics evidence and early experimental data.

All sequenced toxigenic strains encode the same three effectors – termed the AAA module set. Initial experiments have demonstrated that toxigenic strains are all able to coexist while being able to outcompete non-toxigenic strains in a T6SS dependent manner. My Ph.D. work focused on better understanding aspects of the T6SS that are unique to toxigenic strains. Specifically, my thesis characterizes unique aspects of the toxigenic T6SS, including the acquisition of the AAA effector modules, the evolution of the T6SS over time, host regulation of the system, and both the advantages of the system of intra- and interspecies competition.

First, I tested a potential mechanism by which T6SS effectors can be exchanged and the consequences of effector exchange. Briefly, using next generation sequencing, I found that T6SS effectors modules can be exchanged with no change to the structural genes. Additionally, that pressure to exchange T6SS genes also results in the exchange of genes elsewhere on the chromosome. Lastly, through competition assays I studied the consequences of acquiring the AAA module set, and the ability to outcompete non-AAA strains as well as coexist with other toxigenic strains.

Second, I looked at the differences between modern toxigenic strains belonging to the 7th cholera pandemic, and ancient toxigenic strains belonging to the 2nd and 6th pandemics. By mutating modern *V. cholerae* strains to resemble the classical strains from the 2nd and 6th pandemic, my data suggest that while the ancient toxigenic strains encode the genes for the T6SS and the AAA module set, mutations were accumulated making the system inactive. In general these findings suggest that the T6SS has changed from being inactive to active throughout pandemics.

Third, I investigated host regulation of the T6SS. While most non-toxigenic strains have constitutively active T6SSs, toxigenic strains tightly regulate the T6SS. I found that mucin, the proteinaceous component of mucus, is able to active the T6SS. I also found that bile salts are able to modulate the magnitude of that activity. Activating the T6SS in the host is advantageous as it allows *V. cholerae* to participate in intraspecies competition and exclude nontoxigenic strains during infection.

Lastly, in partnership with David Fast (from Dr. Foley's laboratory) within our department, I was able to investigate the role of the T6SS in interspecies competition within the *Drosophila melanogaster* model of infection. We found that a T6SS-positive toxigenic strain was more pathogenic in this model, as determined by increased diarrheal symptoms and survivability. The increased virulence was dependent on both the presence of the T6SS and a T6SS prey, *Acetobacter pasteurianus.* Furthermore, this interaction between the T6SS and *A. pasteruianus* also evoked the host immune system. Altogether this suggests that the T6SS of *V. cholerae,* the host immune system and *A. pasteurianus* all interact to contribute to host death.

My thesis demonstrates that acquiring the AAA compatibility group in an inducible 7th pandemic *V. cholerae* strain results in superior competition both within and outside the *V. cholerae* species in a host environment.

Acknowledgements:

First and foremost I would like to thank Dr. Stefan Pukatzki for accepting me as a summer student in 2012 and again as a graduate student in 2013. It has been an extremely fun and rewarding 6 years, and I feel I have grown as both a scientist and a person working in your lab. I appreciate your attitude towards science, and have enjoyed all of our conversations about science and life. I appreciate all the opportunities you gave me, to be a TA, to travel to international conferences, and to co-author several papers. Finally, I am thankful for how well we were able to maintain our relationship, both personally and scientifically, after you moved to Colorado. I wish you and your new lab nothing but success.

Change is never easy, but I thank Dr. Maya Shmulevitz, for making my transition into a new laboratory both smooth and fun. I appreciate how much you cared for me and my project and really took the time to learn all you could about *V. cholerae*. I thank you for always having an open door to talk about science as well as my future. I know it took a lot of effort, but from my perspective it was absolutely worth it.

All of the chapters of my thesis would not be possible without the entire lab, both past and present. I thank Teresa Brooks for being my first mentor in the lab, I learned a lot from you. I thank Dr. Daniel Unterweger, and Dr. Verena Bachmann for starting projects with me when I was new in the lab. I thank Sarah Kane for all your guidance when I was a new graduate student. I would also Laura Satizibal-Diaz for all our helpful discussions and your scientific expertise as well as Ashley Wagner for all the animal experiments than you have completed. Lastly, I would like to thank Frank Santoriello for help with bioinformatics, I am glad I got a chance to collaborate and meet you.

To my adopted lab, thank you Dr. Heather Eaton, Dr. Adil Mohammed, Fran Cristi Munoz, Wan Kong Yip for accepted me so quickly and embracing the *Vibrio* half of the lab.

To all my collaborators outside the lab. Thank you. Thank you David Fast for being a part of such a fun project and allowing me to learn more about the fly. Thank you Dr. Edan Foley for supporting this partnership and always being around for exciting scientific discussion. I hope your T6SS project continues to flourish. Dr. Stephen Ogg, thank you for all your scientific advice and microscopy guidance. Dr. Daniele Provenzano, thank you for your helpful scientific discussions over the years. I also want to thank Dr. Yildiz Fitnat and your entire lab, especially Avatar Joshi, for hosting me at UCSC and for the opportunity to write a review together.

I would like to thank Dr. Tracy Raivio and Dr. Troy Baldwin for being an excellent examining committee and disproving the myth that committee meetings are something to be feared. I would like to thank Dr. Eytan Wine and Dr. Jim Bina for serving as externals for my exam.

Thank you to my funding sources: NSERC, CHIR and the University of Alberta.

Additionally, I would like to thank the entire MMI department, especially our fantastic student group. We are really one of a kind, and I know it will continue to grow.

Finally, I would like to thank my friends both in the department and outside of it. It has been a long journey and it has always been made easier by you all. Thank you to my family: mum, dad, Alex, Nick and Sylwia. I love you all.

I am excited for what comes next!

Table of Contents

List of Tables and Figures

Chapter 1

Chapter 2

Chapter 3

Chapter 4

Chapter 5

Chapter 6

Chapter 7

Chapter 1: Introduction

1-1.1 *Vibrio cholerae* in the environment.

Vibrio cholerae is a pathogen, however, it spends the majority of its life cycle in brackish water and coastal environments (Nelson et al., 2009). In order to thrive in this environment, *V. cholerae* must survive fluctuating temperature, nutrient scarcity and predation from phage and amoeba (Conner et al., 2016). In this section I will describe the life cycle of *V. cholerae,* and how it deals with these challenges. Finally, I will discuss how diversity serves as a strength for *V. cholerae* as a species.

1-1.2 Life cycle of *V. cholerae*

Vibrio cholerae is a Gram-negative bacterium belonging to the phylum Proteobacteria and the family of *Vibrionaceae*. *V. cholerae* is a curved rod with a polar flagellum for motility (Utada et al., 2014). *V. cholerae* is ubiquitous in the world and has been isolated on 6 continents – all but Antarctica – likely because the bacterium is sensitive to low temperatures (Ali et al., 2012; Boucher et al., 2015; Das et al., 2016; Dutta et al., 2013a; Kirchberger et al., 2016).

In the environment, *V. cholerae* inhabits estuarine and coastal waters, and can be found as free-living bacteria, in a viable but non-culturable state (VBNC), or associated as a biofilm to a number of abiotic or biotic surfaces (Conner et al., 2016). For example, *V. cholerae* can be found on algae, copepods, shellfish, as well as vertebrates such as fish and birds. Additionally *V. cholerae* can be found on chitinous debris (Almagro-Moreno and Taylor, 2013).

Nutrients are scarce in the environment, and *V. cholerae* uses a variety of nutrients to satisfy its prototrophic lifestyle (Conner et al., 2016). *V. cholerae* has the ability to recycle *N*-acetylglucosamine – a carbon chain sequestered as an insoluble polymer in chitin (Huq et al., 1983; Meibom et al., 2004; Nalin et al., 1979). This provides not only an ample source of nitrogen and carbon for the bacteria, but also signals to *V. cholerae* as a site of chemotaxis and biofilm formation (Haugo and Watnick, 2002; Meibom et al., 2004). This composition of chitin skews *V. cholerae* colonization to invertebrates, where chitin makes up their shell. Using its polar flagellum, *V. cholerae* swims towards the chitin, makes contact using the mannose-sensitive hemagglutinin type IV pilus (MSHA) pilus and the chitin-binding protein GbpA (Chiavelli et al., 2001; Kirn et al., 2005; Meibom et al., 2004).

This attachment serves as the first step for biofilm formation (Haugo and Watnick, 2002). Additionally, chitin is catabolized by chitinases (Nalin et al., 1979). Chitin also upregulates the uptake of DNA for purposes of nutrients or genetic information in order to diversify, and the type six secretion system (T6SS) to engage in competition (Veening and Blokesch, 2017). Altogether, intimate contact with chitin allows *V. cholerae* to gain nutrients, acquire new traits, become more competitive and increase transmission.

Attachment to chitinous creatures also provides many other advantages to *V. cholerae.* When attached to chitin, *V. cholerae* has been shown to have an increased resistance to changes in pH and salinity when compared to growth in a free living state (Huq et al., 1984). Interestingly, there are structural similarities between chitin and mucin – specifically the *N*-acetylglucosamine of chitin is also a major sugar glycosylated onto the protein backbone of mucin – the major component of mucus (Chourashi et al., 2016a; Shi et al., 2004). Therefore, another consequence of *V. cholerae* promoting a lifestyle to thrive on chitin is that *V. cholerae* has potentially also evolved to thrive in the host. For example, the same sensor protein that recognizes chitin, ChiS, also recognizes mucin and is important for virulence (Chourashi et al., 2016a). *V. cholerae* lacking ChiS is attenuated in the host (Chourashi et al., 2016a). Another example is the chitin-binding protein, GbpA (Bhowmick et al., 2008; Chiavelli et al., 2001). This protein is used by *V. cholerae* as the first step in biofilm formation when binding both chitin and mucin (Bhowmick et al., 2008). This is an exciting observation that blurs the line for what constitutes a virulence factor.

Along with the advantages of living on chitin come disadvantages as many competitors either graze off the high density of *V. cholerae* or compete for space. The major competitors for *V. cholerae* are bacteriophage, protozoa and other bacteria (Almagro-Moreno and Taylor, 2013; Conner et al., 2016).

Vibriophage are a class of bacteriophage that are specific to *V. cholerae.* Amongst the 200 bacteriophage types that infect *V. cholerae* is the lysogenic CTXΦ that encodes and disseminates cholera toxin (Nelson et al., 2009; Waldor and Mekalanos, 1996). The phage is specific to the LPS O antigen encoded by *V. cholerae* (Nelson et al., 2009). Vibriophage often have a narrow host range and are lytic (Nelson et al., 2009). In the environment, vibriophage titres display a delayed positive correlation with the number of cases of cholera in the region (Faruque et al., 2005). This indicates that as *V. cholerae*

increases in the environment, the numbers of vibriophage subsequently increase causing a decrease in *V. cholerae* levels (Faruque et al., 2005). This relationship is cyclical in nature. This observation suggests that vibriophage controls *V. cholerae* levels, and might be a plausible way for human intervention to control pandemic transmissions, or as a therapeutic (Nelson et al., 2009).

Protozoa, specifically phagocytic amoeba, have been shown to thrive on *V. cholerae* and both the amoeba and *V. cholerae* have evolved mechanisms to deal with one another (Pukatzki et al., 2006a; Valeru et al., 2012; Van der Henst et al., 2016; Zheng et al., 2011). In addition to preying on one another, *V. cholerae* uses some amoeba as a replicative niche, helping in their dissemination and increasing their titres (Van der Henst et al., 2016). This relationship presents yet another example of overlap in bacterial proteins that help for survival in the environment and in the human host. HapA is a secreted protease that is a virulence factor in the infant mouse model of *V. cholerae* as well as a protease important for intracellular survival in amoeba (Silva et al., 2003; Van der Henst et al., 2016). The T6SS is a known virulence factor in several host organisms, but is also a mechanism to prevent grazing by *Dictyostelium discoideum* (Fu et al., 2018; Pukatzki et al., 2006a; Zhao et al., 2018; Zheng et al., 2011). One hypothesis for this, is that amoeba share many characteristics with phagocytic immune cells such as macrophages. However, there is little evidence that macrophages are involved in a *V. cholerae* infection.

Finally, other bacteria also compete with *V. cholerae. Long et al.* investigated the ability of a group of 66 marine bacteria – representing three phylogenetic classes – to inhibit the growth of *V. cholerae* (Long et al., 2005). A mixture of these 66 marine bacteria was spotted on *V. cholerae* impregnated into soft agar, and inhibition was seen in 7 different *V. cholerae* strains. This competition was also demonstrated in a colonization assay of glass beads (Long et al., 2005). *V. cholerae* has ways to fight back, including the T6SS. In addition, as *V. cholerae* is an extremely diverse species, competition also exists between *V. cholerae* strains (Unterweger et al., 2012).

1-1.3 Diversity of *V. cholerae*

V. cholerae is a species with over 200 serogroups (Harris et al., 2012). This serological diversity is matched with phylogenetic diversity (Choi et al., 2016; Chun et al.,

2009; Kirchberger et al., 2016). These strains are diverse with respect to their environment lifestyle, phage resistance as well as virulence potential. Part of this diversity stems from the fact that *V. cholerae* is present in many different areas in the world, from Mexico, the United States, Haiti, Nepal, India, China, Southern Africa and beyond (Ali et al., 2012). Genomic diversity of *V. cholerae* has been associated with many phenotypic differences.

One example of how the diversity of *V. cholerae* causes phenotypic differences is in OmpU (Karunasagar et al., 2003). OmpU is a porin protein that is important for resistance to bile. *ompU* is non-uniformly distributed across *V. cholerae* and therefore resistance to bile is also more prominent in clinical versus environmental strains (Karunasagar et al., 2003). Another source of diversity relates to the propensity to form biofilms. The diversity for this comes within *hapR* (Hammer and Bassler, 2003; Matz et al., 2005). HapR is a regulator of quorum sensing – the ability for bacteria to sense their cell density (Hammer and Bassler, 2003). Frameshift mutations in *hapR* are common amongst toxigenic and non-toxigenic *V. cholerae* strains (Hammer and Bassler, 2003). A functional HapR gives *V. cholerae* an advantage when biofilm associated. A frameshift in *hapR* has a great disadvantage in these cases, however, they have a survival advantage when being grown planktonically (Hammer and Bassler, 2003). This shows how genomic diversity can drive *V. cholerae* towards a specific lifestyle. Finally, as discussed earlier, the diversity in phage matches the diversity in *V. cholerae* (Nelson et al., 2009). As phages are serogroup specific, *V. cholerae* diversity and relative levels are at the behest of the phage population in the environment. To overcome phage predation, *V. cholerae* can undergo serogroup conversion (Blokesch and Schoolnik, 2007). An example of this is the acquisition of the O139 gene cluster by strains previously O1 (Blokesch and Schoolnik, 2007). In this example, the new *V. cholerae* O139 – harbouring the pathogenic O1 traits – was able to increase prevalence by escaping killing from vibriophage specific to the O1 serogroup (Blokesch and Schoolnik, 2007). This example is intriguing because it suggests there is a mechanism in place to facilitate gene transfer between the diverse *V. cholerae* strains.

It has been proposed that chitin-induced natural transformation is a plausible mechanism by which diversification of *V. cholerae* could have occurred (Blokesch and Schoolnik, 2007). Three signals are necessary for this process to occur. First, chitin must

be degraded into the chitin di-hexamers (N-Acetyl Chitohexaose) (Matthey and Blokesch, 2016). This cleaved chitin is recognized by the response regulator ChiS, which through the post-transcriptional regulation by the sRNA TfoR increased translation of *TfoX* mRNA (Matthey and Blokesch, 2016). TfoX is a regulator for many genes involved in the apparatus of physically acquiring the DNA (Matthey and Blokesch, 2016). The second signal is increased cAMP levels inside the cell. This indicates that chitin, or at least non-glucose carbon sources must be the only sources of carbon available to *V. cholerae* (Matthey and Blokesch, 2016). This could indicate that the nutritional value of DNA might also be important in this process as cAMP is associated with a low nutritional state (Kariisa et al., 2015). The third pathway is quorum sensing. A functional LuxO and HapR are required for natural transformation. At high cell densities LuxO's repression of HapR is relieved. HapR not only downregulates the DNAse *dns* but also increases regulation of *comEA* a component of the DNA acquiring machinery (Matthey and Blokesch, 2016).

The first step in the acquisition of foreign DNA is the creation of the pilin (Seitz et al., 2014). PilA is the major pilin, and is processed by the peptidase PilD (Seitz et al., 2014). The pilin is assembled in an ATP-dependent manner, by PilB. When PilA makes contact with double stranded DNA, the ATPase PilT causes the retraction of the pilus, bringing the DNA in through the PilQ channel. In the periplasm, the DNA is bound by the ssDNA binding protein ComEA (Seitz et al., 2014). ssDNA is necessary to move through the channel, ComEC, in the inner membrane. The DNA is now in the cytoplasm and is recruited by recombination machinery to integrate into the genome (Meibom et al., 2005).

The ability to acquire and integrate foreign DNA into the genome allows for the diversification of *V. cholerae* (Kirchberger et al., 2016). This is likely responsible for serogroup conversion (Blokesch and Schoolnik, 2007). Lastly, horizontal gene transfer, including natural competence, has been implicated in crafting the current pandemic strain through DNA acquired in the natural environment (Chun et al., 2009).

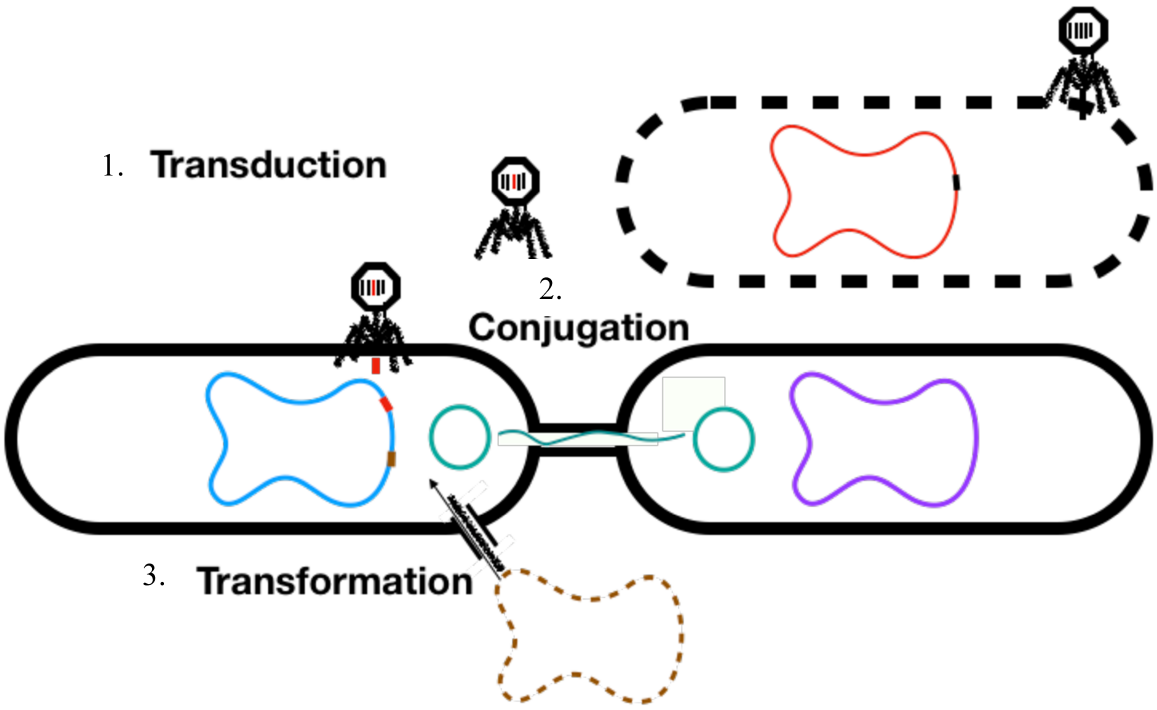

Figure 1-1 **Mechanisms of Horizontal Gene Transfer.** Gram-negative bacteria, including *Vibrio cholerae,* have three main mechanisms to acquire new genes: transduction, conjugation and transformation. Transduction involves the mispacking of viral genomes during the lytic phage to include parts of the bacterial genome. When the phage exits the bacterium, it infects neighboring bacteria, introducing into it not only phage DNA but bacterial DNA. This can recombine into the bacterial DNA through homologous recombination. Conjugation has a similar mechanism of action, except that instead of a phage it is a mobile plasmid. Conjugative plasmids encode genes for a pilus to form between two bacteria in contact. This pilus facilitates the transfer of the plasmid to the neighboring cell. Similarity to transduction, host DNA can be transferred during the transfer of plasmid DNA. Lastly, transformation occurs when the bacteria scavenges for bacteria in the environment. The bacteria can use this DNA as a source of nutrients, or as a source of DNA for recombination.

1-2 Mechanisms of horizontal gene transfer and recombination

Transformation via natural competence is not the only mechanism for horizontal gene transfer. In this chapter, I will discuss conjugation and transduction, as well as barriers to horizontal gene transfer and advantages to horizontal gene transfer. The three mechanisms of horizontal gene transfer are summarized in Figure 1 (above).

1-2.1 Conjugation

Conjugation is a mechanism for bacteria to transfer DNA from one to another using a class of the type IV secretion system (T4SS) (Ilangovan et al., 2015). The T4SS can be used for secreting proteins or toxins, but in some bacteria it is modified to be involved in obtaining DNA via transformation, or by conjugation (Llosa et al., 2002). In the case of conjugation, the T4SS can be divided into three functional components; a translocation channel, a T4SS ATPase, and the pilus component (Ilangovan et al., 2015). The translocation channel spans the inner and outer membrane from the cytoplasm through the periplasm and into the extracellular space. The pili, which is secreted out of the translocation channel, is brought back in after contact is made with the recipient cell. The ATPase components are responsible for assembling and disassembling the pilin. In the case of conjugation, bacteria-bacteria contact is necessary (Thomas and Nielsen, 2005). The first step is the synthesis of the pilus. The pilus of the donor cell then binds the membrane of the recipient cell and retracts, causing a membrane fusion event (Ilangovan et al., 2015). When the membranes fuse, a relaxasome transferasome complex unwinds plasmid DNA and delivers it single stranded into the neighbouring cell (Ilangovan et al., 2015). The evolution of conjugation is likely a mechanism for parasitic DNA to survive and spread (Thomas and Nielsen, 2005). However, during this process, host genes, hypothesized by accident, are able to pass through the transferasome complex and spread along with the plasmid DNA (de la Cruz and Davies, 2000).

1-2.2 Transduction

Transduction is a mechanism of lateral gene transfer that uses a bacteriophage as the DNA carrier (Thomas and Nielsen, 2005). Transduction is the most common mechanism of horizontal gene transfer between bacteria (Redfield, 2001). Specialized transduction is caused when bacteriophage enter its lytic phage. Errors in DNA packaging within the donor bacteria can cause host genes to be incorporated into the bacteriophage head (Redfield, 2001). When the phage enters a nearby recipient bacteria and enters a lysogenic phase, the donor genes are also incorporated into the recipient bacteria along with the phage DNA. After the DNA is integrated, it becomes vertically transmitted

(Waldor and Mekalanos, 1996). Transduction is an important concept for lateral gene transfer in *V. cholerae.* The important *Vibrio* pathogenicity island (VPI) is encoded on the cholera-toxin phage (CTXΦ) (Karaolis et al., 1999; Waldor and Mekalanos, 1996). This allows these virulence factors to be spread amongst strains. Interestingly, CTXΦ is excised during infection (Waldor and Mekalanos, 1996). The relationship between *V. cholerae* and vibriophage run deeper, as another filamentous bacteriophage, VPIΦ, encodes the other major virulence factor, TcpA, which acts as both the receptor for CTXΦ, a colonization factor, and the coat protein for VPIΦ (Karaolis et al., 1999). However, it is unknown whether or not the TCP island is in fact carried on a phage or is horizontally transferred by another mechanism (Faruque et al., 2003a).

1-2.3 Consequences of horizontal gene transfer

In addition to the spread of cholera toxin, horizontal gene transfer is an extremely important mechanism of bacterial diversification (de la Cruz and Davies, 2000; Thomas and Nielsen, 2005). One of the most abundant class of genes spread by horizontal gene transfer is antibiotic resistance (Kitaoka et al., 2011a; Salyers et al., 2004; Úbeda et al., 2005). One of the biggest reservoirs for antibiotic resistance genes is in the human intestine (Salyers et al., 2004). This is because the human intestine is full of a wide variety of bacteria that has both a stable resistant population, but is also an environment where other bacteria are constantly passing through (Salyers et al., 2004). These bacteria can be other commensals, pathogens, or belong to neither group. Several studies have demonstrated the spread of antibiotic resistance between commensals in Enterococci, Lactococcus, Bacteroides (Salyers et al., 2004). This spread is not only observed within species or family – but has also been shown between Gram-positive and Gram-negative bacteria (Salyers et al., 2004).

However, like all changes to the genome of a bacterium, the majority are deleterious while few offer an advantage. The same is true for horizontal gene transfer (Baltrus, 2013). Horizontally transferred genes can be recombined out of frame, make incomplete gene products or simply confer no advantage (Baltrus, 2013). Therefore, especially in a static environment, it has been mathematically shown that there might be no benefit at all to

horizontal gene transfer and that it actually negatively effects the fitness of a population (Baltrus, 2013).

This hypothesis suggests that bacteria must have a way to regulate horizontal gene transfer, either upregulating it during dynamic environmental changes or preventing it in static environments. Further evidence that suggests horizontal gene transfer is depressed as there does not appear to be any homogenized genetic bacteria, or a compromised phylogenetic tree (Thomas and Nielsen, 2005). This indicates that horizontal gene transfer events are still the exception to the rule.

1-2.4 Mechanisms to enhance or decrease horizontal gene transfer

As horizontal gene transfer can be positive or negative, bacteria have developed the means to fine tune the frequency. It has been hypothesized that under times of bacterial stress, there is a larger advantage to horizontal gene transfer than during static times. In *V. cholerae* the integrating conjugative element, SXT, can be spread between other *V. cholerae* as well as other bacterial species (Beaber et al., 2004). The SXT element contains genes to resist antibiotics and heavy metal resistance (Beaber et al., 2004). The transcriptional regulator, SetR, represses the activators of SXT transfer during times without stress. However, this repression is relieved during the so called "SOS response" (Beaber et al., 2004). The SOS response is in response to DNA damage, and amongst many other phenotypes causes an increase in conjugation. Interestingly, antibiotic exposure has been shown to induce the SOS response (Beaber et al., 2004). Therefore, exposure to antibiotics causes the spread of antibiotic resistance genes. A similar phenomenon has been identified in *Staphylococci* (Úbeda et al., 2005). Finally, gut inflammation has been shown to increase the frequency of horizontal gene transfer between pathogenic *Salmonella* enterica and commensal *E. coli* (Stecher et al., 2012). This could turn commensal bacteria into pathogens, or at the very least increases the reservoir of pathogenic genes in the host microbiome (Stecher et al., 2012).

There are also mechanisms in place to reduce horizontal gene transfer. One mechanism is through the CRISPR/Cas system (Marraffini and Sontheimer, 2008). CRISPR is a system that has been associated with resistance towards bacteriophage. The system works by producing short lengths of mRNA (20-50 nucleotides) (Thurtle-Schmidt

and Lo, 2018). If these are complimentary to foreign DNA, the DNA is degraded. This system has been shown to reduce transduction by degrading the foreign DNA (Thomas and Nielsen, 2005). However, this might not be the function of the system, as phage resistance is not necessarily synonymous with horizontal gene transfer resistance (Thomas and Nielsen, 2005). However, *Staphyloccous epidermidis* has been shown to have CRISPR spacers that are specific to the nickase gene present in all *Staphyloccoal* conjugative plasmids (Marraffini and Sontheimer, 2008). This feature blocks conjugation and transformation. Another way to reduce DNA transfer is simply by degrading incoming DNA. Bacterial DNA is methylated in specific patterns on cytosine and guanine. As bacteriophage DNA is not methylated in this manner, restriction enzymes specific to unmethylated DNA are used by bacteria to degrade phage DNA (Labrie et al., 2010). A final example of resistance to horizontal gene transfer is the type six secretion system of *Pseudomonas aeruginosa* (Ho et al., 2013). This system responds to T4SS-mediated conjugation by attacking, and killing the donor bacterial cell (Ho et al., 2013).

Altogether, bacteria have developed many mechanisms to facilitate horizontal gene transfer, such as natural transformation and conjugation, and are subjected to other mechanisms by external forces such as bacteriophage. While great benefits can arise through horizontal gene transfer, such as phage resistance, acquisition of virulence factors or antibiotic resistance cassettes, there are also disadvantages that can reduce bacterial fitness. Because of the potential advantages and cost of horizontal gene transfer bacteria have developed mechanisms to either encourage or discourage the process. *V. cholerae*'s large genetic diversity between strains results in opportunities to share genetic traits with similar strains. This sharing of genetic material can result in *V. cholerae* becoming more pathogenic and causing the disease cholera.

1-3 The disease cholera

Cholera is often incorrectly described as an ancient disease. Although evidence of outbreaks have stretched back thousands of years and seven distinct pandemics have been recorded in human history, the disease persists today (Harris et al., 2012). Characterized by diarrhea, dehydration and death, cholera patients can lose up to 20L of diarrhea a day (Harris et al., 2012). In this section, the disease, epidemiology and major virulence factors

of the disease will be discussed. The major events in *V. cholerae* history and the pandemics are visually represented as a timeline in Figure 2.

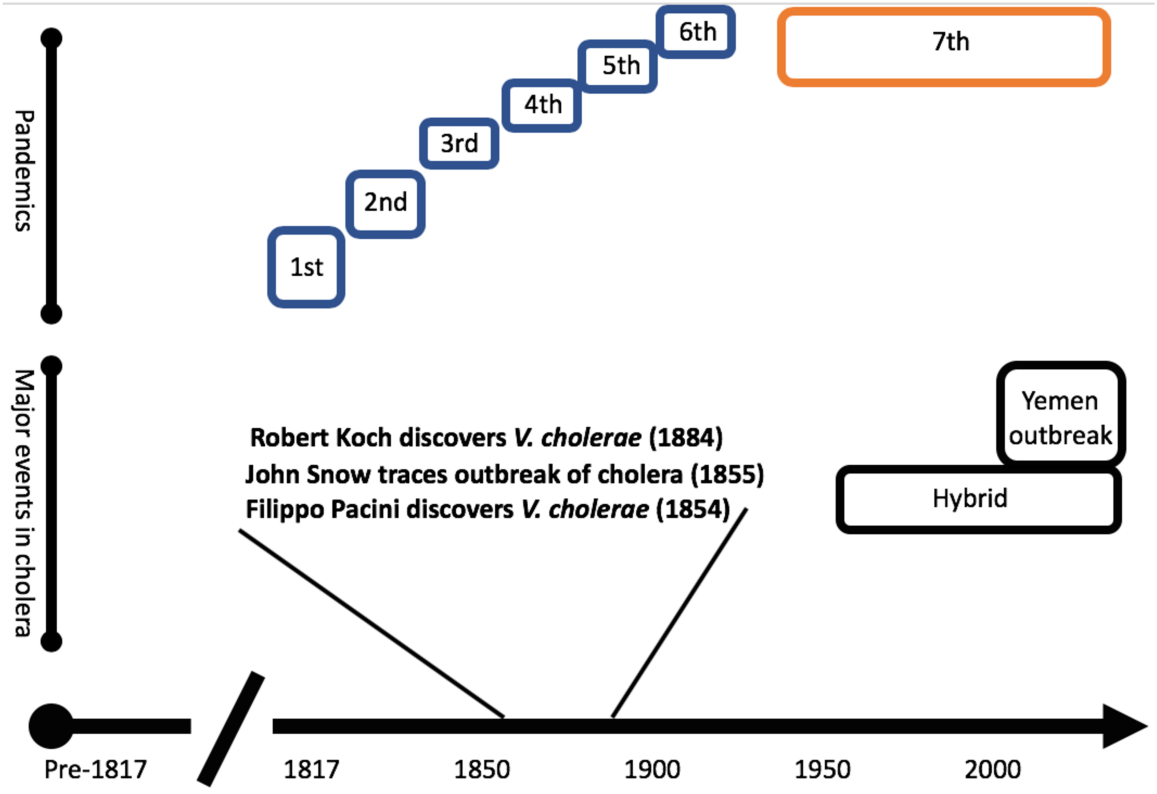

Figure 1-2. **History of cholera.** This timeline includes major cholera events from the first pandemic in 1817 to the ongoing outbreak in Yemen. For the 7 pandemics, they are coloured coded by which strain dominated the pandemic. In blue are the pandemics caused by classical strains and in orange the pandemic caused by El Tor *V. cholerae.*

1-3.1 History of cholera

The connection between *V. cholerae* and the disease cholera have been associated since the mid 19th century when *V. cholerae* was concurrently implicated as the cause of cholera by the Italian anatomist Filippo Pacini and German physician Robert Koch in 1854 and 1884, respectively (Koch, 1884; Pacini, 1854). However the disease cholera had plagued humanity for much longer than that. 7 cholera pandemics have been recorded in human history (Barua, 1992). The first pandemic began in Bengal and India in the early 19th century and spread throughout Asia. The second pandemic extended this disease to Europe and Africa, with some reports of the disease extending to North America. It was not until the 3rd pandemic, that *something* was implicated as the cause. During this pandemic the English physician John Snow developed basic epidemiology to identify the source of the cholera outbreak as a contaminated well in Soho, London (Snow, 1857). It was hypothesized that dirty water was responsible for this disease (Snow, 1857). This observation allowed public health measures to greatly reduce the burden of disease (Barua, 1992). The fourth cholera pandemic once again began in Bengal, before travelling during the Muslim pilgrimage to Mecca (Barua, 1992). From there it moved north before affecting those fighting in the Austro-Prussian War. This feature of cholera repeats throughout history. This disease is most likely to affect people in war-torn or disaster-struck areas due to compromised water purification systems, poor sewage treatment and at high population densities. Finally, in the fifth cholera pandemic, Robert Koch developed the germ theory of disease to isolate the cause of cholera to be *V. cholerae* (Koch, 1884). The sixth cholera pandemic had major casualties in the Philippines and the Ottoman empire (today's Turkey) (Barua, 1992). This is the first pandemic for which there are significant strains repositories. These strains, termed classical O1 *V. cholerae* are hypothesized to have caused the preceding five pandemics (Barua, 1992). The 7th pandemic is ongoing and the classical strains have been replaced by a new class of strains, termed El Tor strains. This pandemic started in the Philipeans, and spread throughout India, North Africa and the South Pacific. Although not specifically apart of the pandemic, these El Tor strains continue to cause outbreaks worldwide (Barua, 1992). Most recently, El Tor strains are responsible for the ongoing 2016 outbreak in Yemen (Camacho et al., 2018). There are over one million suspected cases of cholera in this outbreak, which has been attributed to the lack of clean water during a civil war (Camacho et al., 2018).

1-3.2 Epidemiology of cholera

There are an estimated 3 million cases of cholera, and 100,000 deaths worldwide, although these numbers are low estimates as the disease is vastly underreported (Lancet, 2017). Cholera is a global disease, but tends to primarily affect areas with inadequate access to clean water. This is often due to limited resources, war or natural disaster. Currently, cholera is endemic in around 50 countries – mostly in Africa and Asia (Mintz, 2018). In addition to endemic cholera, there are also epidemics (Mintz, 2018).

Cholera endemics follow a seasonal distribution, striking before and after the rainy season (Faruque et al., 2005). Before the rainy season, the hot weather evaporates water and keeps the river levels low. This increases the salinity and chlorophyll levels in the water which supports the growth of copepods which carry *V. cholerae* (Faruque et al., 2005). After the rainy season, there is flooding which helps spread contaminated water. Therefore, based on weather patterns, endemic cholera can be predicted with accuracy (Nishiura et al., 2018). Epidemic cholera is more difficult to predict. Epidemics are often associated when *V. cholerae* is introduced into an area where the immunologically naive population lack a clean water supply (Nishiura et al., 2018). Such was the case when United Nations stabilization forces introduced *V. cholerae* to Haiti after an earthquake (Ali et al., 2011).

Those infected with *V. cholerae* exhibit a wide variety of symptoms. This ranges from asymptomatic to severe disease and death. The ratio of asymptomatic to severe disease has increased from the sixth pandemic to the seventh pandemic (Khan and Shahidullah, 1980). After ingestion of *V. cholerae,* there is an incubation period between several hours and 5 days, with a mean time of 2 days (Azman et al., 2013). After this period, mild to severe diarrhea occurs – while mild cases cannot be distinguished from other food or water born gastrointestinal distress – severe cases run a distinct course (Azman et al., 2013). In these cases, cholera can result in up to 1 liter per hour of purged diarrhea, starting with bile and fecal content before becoming a profuse “rice-water” stool with water, salts, bacteria and mucous (Alexakis, 2017). This diarrhea results in severe dehydration and electrolyte loss causing hypovolemia – a reduction in blood volume as well as hypokalemia and hypoglycemia (Sharifi-Mood and Metanat, 2014). This can result in renal or heart

failure. *V. cholerae* is a self-limiting disease and therefore treatment with water and electrolytes, mortality can reduce from 50 – 70% to 0.5% (Sharifi-Mood and Metanat, 2014). The diversity of response to a *V. cholerae* infection is a mixture of immune status, age, treatment options and the virulence factors encoded by the *V. cholerae* strain (Sharifi-Mood and Metanat, 2014).

1-3.3 Cholera across the pandemics

Out of the over 200 serogroups of *V. cholerae*, only one, O1 *V. cholerae,* has been implicated in cholera pandemics (Barua, 1992). A subgroup of O1 strains, named classical *V. cholerae,* is hypothesized to be responsible for the first six pandemics – with strains available from the second and sixth pandemics both supporting the hypothesis (Barua, 1992). The seventh pandemic represented a departure from the classical strains and the emergence of El Tor *V. cholerae* (Barua, 1992).

To differentiate between the two biotypes, many assays can be performed. El Tor strains have the ability to agglutinate red blood cells, produce acetoin and resist polymyxin B (Beyhan et al., 2006; Jonson et al., 1990). Since deep sequencing of bacterial strains became more frequent, phylogenetic analysis easily distinguishes strains on a genetic level (Beyhan et al., 2006). Another important difference between classical and El Tor *V. cholerae* is the sequence of the cholera toxin gene, *ctxB* (Murley et al., 2000). The classical and El Tor variants of the CtxB protein differ by two amino acids (Murley et al., 2000). Interestingly, recent El Tor strains – termed El Tor hybrids –encode the classical allele of *ctxB* (Das et al., 2016). This observation implies that the sequence difference has phenotypic or pathogenic consequences. In addition to differences in the sequence of cholera toxin, the regulatory network surrounding the production of cholera toxin, and the amount of cholera toxin produced also differs. Differences in the promoter of *tcpPH* result in significantly reduced cholera toxin production by the regulator AphB in El Tor strains (Kovacikova and Skorupski, 2000; Murley et al., 2000). On the genetic level, amongst virulence factors, the biggest difference between El Tor and classical *V. cholerae* strains is within *tcpA* where over 20% of the gene is different between the two groups of strains (Heidelberg et al., 2000; Shaw and Taylor, 1990). In addition between these differences, El Tor *V. cholerae* strains also encode a number of auxiliary toxins, such as MATRX and

HA toxins, that are not encoded by classical *V.* cholerae (Heidelberg et al., 2000; Olivier et al., 2007).

It is poorly understood which, if any, of these genotypic and phenotypic differences results in pathogenicity differences between these two sets of strains, however clinical studies indicate different pathologies (Bart et al., 1970; Barua, 1992; Khan and Shahidullah, 1980; Narkevich et al., 1993; Niyogi, 1979; Oseasohn et al., 1966; Sack et al., 2003). El Tor infections exhibit many characteristics that suggest lower pathogenicity than classical *V. cholerae.* One indicator is the ratio of total infections to the number of infections that require hospitalization. In some studies hospitalization rates for El Tor carriers are as low as 6%, whereas lower estimates for classical infections are 25% (Khan and Shahidullah, 1980). Another indication of differences in pathogenesis is that El Tor strains have much greater rates of being asymptomatic then classical strains (Bart et al., 1970; Sack et al., 2003). Despite these indicators, El Tor infection results in over a 23% longer excretion time (Niyogi, 1979; Oseasohn et al., 1966). These statistics indicate a paradigm change between a violent and brief disease to a more mild and prolonged disease course.

Non-pandemic *V. cholerae* still retain the ability to cause disease, although this is often indistinguishable from gastroenteritis (Anderson et al., 2004). These differences are likely associated with the virulence factors produced by *V. cholerae.*

1-3.4 Virulence factors of *V. cholerae*

There are many proteins produced by *V. cholerae* that have been shown to have negative effects on host health while promoting the transmission and bacterial load of the pathogen. It is using these metrics that I am defining a virulence factor. I will start with briefly introducing the ToxR regulon – the master regulator of *V. cholerae* virulence. The quintessential *V. cholerae* virulence factors are cholera toxin (CT) and the toxin-coregulated pilus (TCP) (Holmgren, 1981; Krebs and Taylor, 2011). However, *V. cholerae* also uses the type 3 and 6 secretion systems as well as biofilm formation (Figure 4).

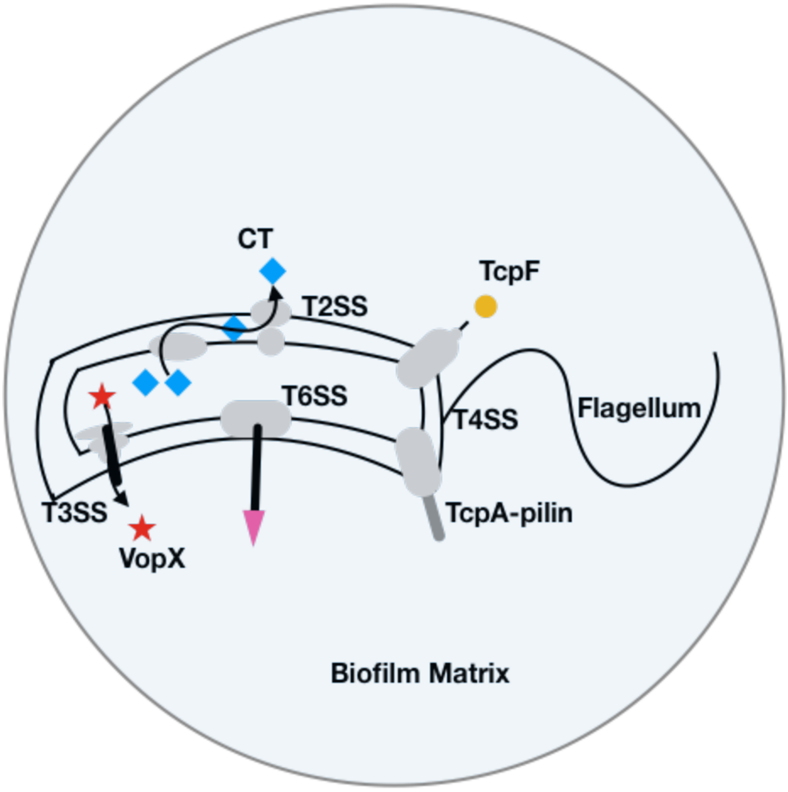

Figure 1-3. **Virulence factors of *V. cholerae.*** This figure shows the major virulence factors of *V. cholerae.* The T2SS secretes CT (blue square). The T3SS secretes many proteins that target eukaryotic cells including the apoptotic VopX (red circle). The T6SS injects a molecular spear decorated with toxins (pink triangle). Also included are TCP (dark grey), the flagellum (black) and a biofilm matrix (light blue).

The ToxR regulon is a regulatory cascade, started by the interaction of ToxR with ToxS and TcpPH, that results in the downstream coordination of several factors involved in virulence (Childers and Klose, 2007). There are two main arms of the ToxR regulon, those that work through ToxT and those that do not. ToxR responds to environmental stimuli including acidity and bile (Merrell et al., 2001; Provenzano and Klose, 2000). ToxR positively regulates the outer membrane proteins *ompU,* which is a porin that aids in the diffusion of bile out of *V. cholerae* (Provenzano and Klose, 2000).ToxR also negatively regulates *ompT*, resulting in only one of the two porins being made. ToxR directly increases transcription of *leuO,* which also contributes to bile resistance independent of OmpU and RND efflux pumps (Ante et al., 2015). In addition to bile salts, LeuO also contributes to resistance to cationic antimicrobial peptides (Bina et al., 2016). Lastly, LeuO

works to downregulate virulence factor production, providing negative feedback to the ToxR regulon (Bina et al., 2013). Through ToxT, *V. cholerae* regulates many virulence factors including TCP and CT which will be discussed below (Childers and Klose, 2007).

TCP serves three functions in the pathogenesis of *Vibrio cholerae.* The first is the secretion of TcpF. While the function of TcpF is unknown, it is critical for the colonization of the infant mouse model of cholera (Kirn et al., 2003). Unlike most other pili, TCP does not serve to adhere with the host intestine (Childers and Klose, 2007; Tamamoto et al., 1998). In contrast to making interactions with the host intestine, TCP also makes interactions with other *V. cholerae* (Jude and Taylor, 2011*)*. This causes the formation of microcolonies, where bacterial density is higher than without a TCP mediated interaction. Microcolonies are an essential component of a *V. cholerae* infection (Silva and Benitez, 2016). Microcolonies are shown to be important in infection for unknown reasons, but *in-vitro* evidence demonstrates that microcolonies resist bile to a higher degree than planktonic bacteria (Silva and Benitez, 2016). The third function of TCP is to bind and internalize the cholera toxin phage (Waldor and Mekalanos, 1996). This property allows the incorporation of a transposon containing multiple virulence factors into the genome of *V. cholerae,* increasing its pathogenicity (Waldor and Mekalanos, 1996). In pandemic *V. cholerae* deletion of the major pilin, *tcpA*, results in loss of colonization ability in the infant mouse and the infant rabbit (Ritchie et al., 2010). Additionally, in human volunteers, a *tcpA* mutant is unable to be detected in the stool (Herrington et al., 1988).

When integrated into the genome of *V. cholerae,* cholera toxin is responsible for severe diarrhea (Holmgren, 1981; Levine et al., 1988; Ritchie et al., 2010) . Cholera toxin is an AB_5 toxin secreted by the type two secretion system (Holmgren, 1981). An AB_5 toxin is a protein complex with 1 active subunit (A) and 5 binding subunits (B) that facilitate the A subunit to get to the desired target (Holmgren, 1981). Transcription of cholera toxin is promoted by ToxT, after ToxR responds to cues in the host intestine, such as intestinal bile. Once secreted into the extracellular space, the B-subunits binds GM_1 gangliosides that coat the intestinal epithelial cells. Next, the toxin is internalized via endocytosis and is transported to the endoplasmic reticulum (ER). In the ER, the foreign protein triggers the misfolded protein response, and as a result the B subunits are cleaved from the A subunit (Holmgren, 1981). After cleavage, the A-subunit is refolded and released back in the

cytosol. There, CtxA works as an ADP-ribosyltransferase preventing adenylate cyclase from recycling, and keeping it in its active confirmation (Holmgren, 1981). This constitutively active adenylate cyclase increases cAMP in the cell thereby activating Protein Kinase A (PKA) (Holmgren, 1981). PKA phosphorylates the cystic fibrosis transmembrane conductance regulation which increases the secretion of chloride and sodium ions into the intestinal lumen (Holmgren, 1981). This causes water to leave the host into the intestine through osmosis. This results in the watery diarrhea that is characteristic of cholera (Levine et al., 1988). When *V. cholerae* lacking the ability to secrete cholera toxin in inoculated into the infant mouse, there is an approximately 100-fold decrease in colonization compared to wild-type *V. cholerae* (Marsh and Taylor, 1998). Additionally, to measure the importance of cholera toxin as a driver of disease, the lethal dose required to kill 50% of the mice was measured (Marsh and Taylor, 1998). For wild-type *V. cholerae* this is 10^6 bacteria after a 48 hours infection, however, for *V. cholerae* unable to secrete cholera toxin, this dose goes up to 10^8 (Marsh and Taylor, 1998). Because of the importance of cholera toxin, it has been thoroughly studied, and even studies in human volunteers have been conducted. When 10^6 *V. cholerae* were ingested by human volunteers, 92% of the participants experienced diarrhea with the average participant expelling 4.2L over 15.2 stools over a period of 24 hours (Levine et al., 1988). At the same dose, *V. cholerae* without cholera toxin only caused diarrhea in 1/4 of the participants with 9-fold less volume of diarrhea. Even at an inoculum over 1000-fold higher, the levels of diarrhea do not approach that of wild-type *V. cholerae* (Levine et al., 1988). This implicates cholera toxin as the premier virulence factor for pandemic *V. cholerae.* However, both in the infant mouse and in the human, *V. cholerae* is still virulent and still colonizes without cholera toxin (Levine et al., 1988; Marsh and Taylor, 1998). This suggests that other virulence factors are encoded which contribute to disease.

Cholera-toxin negative *V. cholerae* still cause disease, as there are many of non-pandemic strains that do not encode cholera toxin and still cause gastroenteritis (Anderson et al., 2004; Dutta et al., 2013a; Morris, 1990). For example, the *V. cholerae* strain AM19226 lacks both cholera toxin and TCP. While the exact mechanism is unclear, AM19226 is unique amongst *V. cholerae* strains as it encodes a T3SS which is indispensable for colonization in the infant mouse model of infection (Chaand et al., 2015).

Other auxiliary virulence factors are encoded by El Tor *V. cholerae* but not classical *V. cholerae* strains. It has been hypothesized that these virulence factors may account for the longer excretion time of El Tor infections or simply make up for the decrease in cholera toxin expression (Olivier et al., 2007; 1992). These virulence factors are a multifunctional auto processing RTX (MARTX) toxin, a zinc metalloprotease hemagglutinin (HA) and a pore-forming hemolysin (Benitez and Silva, 2016; Cordero et al., 2007; Vaitkevicius et al., 2006). The MARTX toxin has actin cross-linking activity and inhibits Rho – a protein critical for eukaryotic transcription (Cordero et al., 2007). The HA toxin degrades the protein occluding in tight junctions within the intestine (Benitez and Silva, 2016). The hemolysin has both hemolytic and cytolytic activity (Vaitkevicius et al., 2006). The infant mouse model has proven ineffectual to study these proteins, potentially because the effects of cholera toxin overshadows their effect or because the infant mouse model can only be used to study acute infections and these proteins might have activity later in infection (Fullner, 2003). In line with this hypothesis, in the adult mouse these three auxiliary toxins extend the infection of El Tor *V.* cholerae (Olivier et al., 2007). Finally, the type-six secretion system of *V. cholerae* has been shown to increase colonization through competition with commensal bacteria in the infant mouse (Zhao et al., 2018).

The last set of virulence factors are ones that reduce the infectious dose of *V. cholerae* yet are not prescribed a specific pathogenic effect. In the environment, *V. cholerae* colonizing chitin and copepods are often biofilm associated (Almagro-Moreno and Taylor, 2013; Silva and Benitez, 2016). Biofilm associated *V. cholerae* have a reduced infectious dose, this is hypothesized to be due to their increased acid tolerance (Silva and Benitez, 2016). Other virulence factors that reduce the infectious dose of *V. cholerae* are type IV pili, including the predominantly environmental mannose-sensitive hemagglutinin (MshA) pili and PilA (Almagro-Moreno and Taylor, 2013). The more pili that *V. cholerae* encodes the better chance it has to attach to the host surface and make microcolonies (Alam et al., 2005). This mechanism of lowering the infectious dose in this case appears to be important for human-to-human transmission. Upon leaving the host, *V. cholerae* has these factors upregulated, putting *V. cholerae* in a hyperinfectious state to infect the next host (Alam et al., 2005).

As *V. cholerae* has a plethora of virulence factors, finding appropriate animal models to study these virulence factors is difficult as no model is perfect at recapitulating the human host. To deal with this, researchers have developed many model to study *V. cholerae* infection.

1-4 Animal models of cholera

There is no animal model for cholera appropriate to deal with all the strains and virulence factors. This extreme diversity makes studying *V. cholerae* difficult. However, many animal models have been developed. This allows many interesting observations to be made. For example, common themes that persist across the models can begin to be thought of as truths of the pathogen. Alternatively, if an observation is made only in one model, that can help isolate a specific host pathway. In this section, I will introduce the two most prominent models for infection, the infant mice and rabbits. Next, more modern models such as the adult mouse, the zebra fish model and the fruit fly model will be discussed. For each model, I will briefly outline the infection protocol, what this model has taught the field, and major disadvantages.

1-4.1 The infant mouse model

The earliest model to study *V. cholerae* infection is the suckling mouse, or infant mouse model of infection (Herrington et al., 1988; Matson, 2018). In this model the infection route is oral gavage. The standard dose for this is 10^5 – 10^6 CFUs, however, inoculum levels up to 10^9 have been reported and well tolerated in mice between 3-5 days old (Ma and Mekalanos, 2010a; Matson, 2018). The infant mouse model has been used to identify the majority of important virulence factors. Early experiments demonstrated the importance of the LPS O-antigen (Chiang and Mekalanos, 1998). Additionally, this work demonstrated the importance of many metabolic proteins *in-vivo,* including iron scavenging molecules and genes involved in motility (Chiang and Mekalanos, 1998). Additionally, the toxin hemagglutinin was shown to be important. These genes were discovered to be important by unbiased methods, such as transposon mutagenesis to look for genes critical for infection or reporter constructs to demonstrate *in-vivo* expression

(Camilli and Mekalanos, 1995; Chiang and Mekalanos, 1998). Studying of *V. cholerae in-vivo* has resulted in the development of these tools that have been used for other bacteria.

One of the most important discoveries about *V. cholerae* from the infant mouse is the importance of TCP (Taylor et al., 1987). Such studies are performed by coinfecting the mouse with two strains, one, a wild-type *V. cholerae* strain with *lacZ* (or *phoA*) genetically removed, and the other with *tcpA* genetically removed. *lacZ* is a gene which encodes a protein that metabolizes galactose (Matson, 2018). When WT *V. cholerae* is grown on X-gal media, *V. cholerae* colonies grow blue, however, a *lacZ*$^-$ strain grows white. This allows the differentiation between two isogenic strains *in-vivo* (Matson, 2018). In these experiments, a *tcpA* mutant is unable to colonize when introduced in combination with wild type *V. cholerae.* This observation was confirmed in human volunteers (Herrington et al., 1988). This confirmation of the infant mouse model solidified it as the best model to study a *V. cholerae* infection. In addition to TCP, its major regulator ToxR was also shown to be essential for colonization in the infant mouse and in humans (Herrington et al., 1988). This confirmation gives validity to other findings. More recently, the infant mouse has been used to show the importance of the type six secretion system *in-vivo* (Zhao et al., 2018). Additionally, this model has been used to show that *V. cholerae* leaving the human host is hyper infectious compared to *V. cholerae* in the environment (Alam et al., 2005).

The major disadvantages of this model are that the infant mouse is immature in many ways. First, the infant mouse intestines lack bile (Russell et al., 2013a). The adaptive immune system is underdeveloped as is the intestine, while the innate immune response is intact (Richardson, 1994). The intestine potentially has an underdeveloped microbiome (Tanaka and Nakayama, 2017). This makes studies involving competition with the microbiome difficult. Additionally, the infection cannot be made long term, as mice become naturally immune to *V. cholerae* when they are 5 days old (Matson, 2018). This limits studies of the infant mouse to 16-24 hours. Another limitation of *V. cholerae* infected infant mice is that they do not develop symptoms, most importantly, they do not develop the hallmark diarrhea associated with cholera (Klose, 2000).

1-4.2 The infant rabbit model

Infant rabbits are not reliably infected with *V. cholerae* (Ritchie et al., 2010). There is huge variability on which animals gets colonized and which do not (Ritchie et al., 2010). It was shown that inoculating the small intestine directly overcame this variability (Dutta and Habbu, 1955). Therefore, researchers hypothesized that the stomach acid was responsible for the variability in a *V. cholerae* infection (Ritchie et al., 2010). This lead Ritchie *et al*. to develop a model of infection with pre-treatment with cimetidine (Ritchie et al., 2010). Cimetidine is a histamine H_2 receptor antagonist, that inhibits stomach acid production. This drug causes a 3-log increase in the pH of the stomach, which allows orogastric inoculation of 10^9 *V. cholerae* to cause reliable disease in the infant rabbits (Ritchie et al., 2010). This resulted in severe diarrhea, a 10% loss in body weight, and a colon distended and full of liquid (Ritchie et al., 2010). Additionally, *V. cholerae* colonizes the intestine at high numbers. This models the disease cholera much stronger than in the infant mouse (Ritchie et al., 2010). Additionally, *V. cholerae* virulence factors play a role in infection. Cholera toxin plays a role in host inflammation but not in the numbers of *V. cholerae* (Ritchie et al., 2010). This allows modeling of the disease symptoms by cholera toxin, but not the amplification of *V. cholerae* which was seen in human volunteers (Herrington et al., 1988; Ritchie et al., 2010). A *tcpA* mutant was both deficient in colonization and disease symptoms (Ritchie et al., 2010). Therefore, this suggests cholera toxin action is downstream of TCP's action.

As the infant rabbit responds to cholera toxin by inflammation and fluid in the cecum, this cecum can be analyzed to look at the host response to *V. cholerae* and what molecules *V. cholerae* encounters (Ritchie et al., 2010). In contrast to an uninflamed mouse gut, *V. cholerae* encounters long chained fatty acids, sulfate containing compounds, and heme (Mandlik et al., 2011). The presence of heme in the small intestine of rabbits but not infant mice during infection is interesting, and might indicate that *V. cholerae's* permeabilization of the small intestine might result in the usually scarce iron to be introduced at higher levels (Mandlik et al., 2011).

The infant rabbit model of *V. cholerae* infection models the disease very well, but does not mimic the replicative burst that *V. cholerae* gets through the action of cholera toxin. Furthermore, similarly to the infant mouse model, there is not an option to study the long term dynamics of infection or interaction with the microbiome.

1-4.3 The adult mouse model

The adult mouse was initially dismissed as a viable model to study *V. cholerae* as *V. cholerae* appeared unable to colonize the intestine (Knop and Rowley, 1975). In 2000, Ryan *et al*. showed that *V. cholerae* could colonize a germ-free mouse, implicating the microbiome as a mechanism to resist *V. cholerae* in an adult mouse (Ryan et al., 2000a). These data were matched by adult mice treated with the antibiotic streptomycin, presumably to remove the commensal bacteria (Merrell and Camilli, 1999). This allows *V. cholerae* infection to be monitored over several days (Merrell and Camilli, 1999).

While cholera toxin and TCP are dispensable in this model, the adult mouse allows the study of auxiliary virulence factors that appear to have no effect in the infant models (Olivier et al., 2007). Additionally, as the adult mouse has a fully matured immune system, the involvement of immune cells can be studied (Queen and Satchell, 2012). Lastly, the adult mouse intestine has bile (Li-Hawkins et al., 2000).

In the adult mouse, many virulence factors have been shown to be important for prolonged colonization, including the three auxiliary toxins only found in El Tor *V. cholerae* and not within classical *V. cholerae* strains (Olivier et al., 2007). These toxins are the multifunctional auto processing RTX (MARTX) toxin, a zinc metalloprotease hemagglutinin (HA) and a pore-forming hemolysin toxin (Olivier et al., 2007). The mechanism behind how these toxins impact colonization appears to be through their ability to kill neutrophils (Queen and Satchell, 2012). Another toxin with a described mechanism that is important in the adult mouse is the zinc-transporter (Sheng et al., 2015). To study this transporter, Sheng *et al.* adapted the adult mouse model. After reducing the microbiome with streptomycin, the researchers inoculated the mouse with *V. cholerae* and stopped the antibiotic treatment, allowing the microbiome to return (Sheng et al., 2015). The researchers then measured the time it took for the returning microbiome to clear the infection (Sheng et al., 2015). Their rationale was that the longer *V. cholerae* remained in the gut, the better it was able to outcompete the commensal bacteria. In this case, *V. cholerae* is hypothesized to utilize its zinc uptake systems to steal the scarce nutrient from the returning commensals and contribute to a longer disease (Sheng et al., 2015).

With a competent immune system, this model has allowed the study of the immune response to *V. cholerae.* In one such study, the authors looked at the ability of neutrophils to contain *V. cholerae* during early stages of infection (Queen and Satchell, 2012). It was shown that neutrophils were indispensable for reducing systemic inflammation and reducing extra-intestinal infections (Queen and Satchell, 2012).

While a powerful model, without causing disease symptoms or needing traditional virulence factors that are shown to be important in the human it is far from a perfect model. Additionally, while microbiome studies can be performed, the manipulations of the microbiome needed does not allow bacterial competition to be studied in a natural setting.

1-4.4 The zebra fish model

The zebrafish model is a nonmammalian model for many bacterial infections (Sullivan and Kim, 2008). For *V. cholerae* it is scarcely used, but has lots of advantages over traditional animal models (Runft et al., 2014). For one, zebrafish is a natural reservoir of *V. cholerae,* so *V. cholerae* infects zebrafish naturally without any need for pre-treatment with drugs (Runft et al., 2014). Zebrafish also models the symptoms of cholera which can be measured by the optical density of the fish tank. The water in the fish tank gets murky due to the presence of mucous from the diarrhea (Runft et al., 2014).

The zebrafish appears to be a great model to study the differences between classical and El Tor strains. These studies showed that El Tor strains colonize better and colonize longer and that this advantage is due to the auxiliary toxins (Runft et al., 2014). This is very similar to the work completed in the adult mice. Another study using the zebrafish demonstrated the ability of the *V. cholerae* type six secretion system to clear commensals from the gut. The mechanism behind this appears to be the anti-eukaryotic rather than the anti-bacterial activities of this secretion system. The anti-eukaryotic effect of the T6SS causes contraction of the intestine and expulsion of the commensal bacteria (Logan et al., 2018).

Similar to the adult mouse model, this model does not allow the study of *V. cholerae*'s primary virulence factor TCP or cholera toxin as their regulator ToxT is dispensable for both colonization and diarrhea (Olivier et al., 2007; Runft et al., 2014).

Also, as the host symbionts are cleared by an immune response to the pathogen, it is difficult to study bacterial-bacterial competition (Logan et al., 2018).

1-4.5 The fruit fly model

Another non-mammalian model of cholera is *Drosophila melanogaster* (Blow et al., 2005). The fruit fly is used frequently as a model for intestinal infections do the similarity of the fly midgut to the human small intestine (Dionne and Schneider, 2008). Although it lacks an adaptive immune system, there is an innate immune system that has analogous systems to the mammal (Lemaitre and Miguel-Aliaga, 2013).

For the cholera model this works by feeding a *V. cholerae* culture to the fly continuously during infection (Blow et al., 2005). The flies eat the culture and die of the infection without the need for pharmacological manipulation. Cholera toxin appears to be a virulence factor in the fruit fly, but is not responsible for all of the virulence (Blow et al., 2005). Other virulence factors that appear to be important include the ability to form biofilms, along with the ability to participate in quorum sensing (Kamareddine et al., 2018; Purdy and Watnick, 2011). The main virulence factor was proposed to be the consumption of acetate by *V. cholerae* which disrupts host metabolic signaling (Hang et al., 2014).

Like mammals, *D. melanogaster* responds to intestinal pathogens by increasing proliferation in the intestine to shed intestinal cells and with it the bacteria (Lemaitre and Miguel-Aliaga, 2013). This proliferative response however is not seen with *V. cholerae* implying there is a means to actively supress stem cell division (Berkey et al., 2009). This is an observation that has not been investigated in higher order animals.

The fruit fly model is however, underutilized, and so many aspects of cholera have been unexplored. One disadvantage of this system is a technical aspect. The infection must be ongoing for *V. cholerae* to be able to kill the host, this suggests that *V. cholerae* colonization does not persist and that aspects of colonization might not be able to be studied in this model (Blow et al., 2005). In my thesis, we utilized this model to look at the activity of the T6SS in infection.

1-5 The Type Six Secretion System

The type six secretion system (T6SS) is a molecular syringe used by over a quarter of Gram-negative bacteria to deliver protein effector molecules into neighbouring Gram-negative bacteria or eukaryotic cells (Boyer et al., 2009). The outcome of this secretion is extremely diverse but often results in cell death for the prey cell. In this section, I will introduce and describe the T6SS in broad terms, focusing on aspects of the system that are well conserved across proteobacteria. In particular, I will examine the structure and mechanics of the system, the diversity of the effectors secreted, and end with examples of how the system is used in pathogenesis. As the next section will focus exclusively on *V. cholerae*, this section will primarily look at other bacteria.

1-5.1 Structure assembly and delivery of the T6SS

The T6SS is a multicomponent toxin-delivery apparatus that has structural and functional homology to the T4 bacteriophage tail spike and tube (Leiman et al., 2009). Imaging studies suggest that translocation of T6SS effector proteins occurs through a contraction event that propels a membrane-puncturing complex into neighboring cells (Basler and Mekalanos, 2012). Assembly of the T6SS begins with the assembly of the membrane complex, followed by recruitment of baseplate proteins that anchor the outer sheath and the inner tube to the lipid membranes of the bacteria (Brunet et al., 2015). The membrane complex is comprised of the three proteins TssJLM, which span the inner membrane and provide structural support to the system (Brunet et al., 2015). The cytoplasmic proteins that form the baseplate complex, TssEFGK and VgrG1-3, are then recruited to the membrane complex and are anchored to the inner membrane (Brunet et al., 2015; Zoued et al., 2013). These baseplate subunits are required for proper formation of the tail complex, which is assembled onto the VgrG1-3 trimer that forms the tip of the T6SS apparatus (Brunet et al., 2015). Though not shown to be essential components of the baseplate, proteins containing repeating proline-alanine-alanine-arginine (PAAR) motifs cap the VgrG1-3 trimer and act to sharpen the T6SS spike complex (Shneider et al., 2013). The tail complex is composed of an inner tube formed by hemolysin coregulated protein (Hcp) hexamers encased within an outer VipA/VipB tube complex (Brunet et al., 2015; Shneider et al., 2013; Zoued et al., 2013). The outer and inner tubes polymerize into the

cytosolic space over the course of approximately 30 seconds and can remain fully extended for several minutes until a signal triggers rapid contraction of the outer sheath (~5 ms) and translocation of the inner tube into the extracellular space (Basler and Mekalanos, 2012; Basler et al., 2012). The signals and mechanisms that govern contraction are beginning to be uncovered. The current model suggests that the VipA/B sheath continues to grow until it makes contact with the inner membrane at the other end of the cell (Vettiger et al., 2017a). At this point, a conformational change is made that involves the N-terminal linker for VipA that causes destabilization of an interaction within VipA which keeps the T6SS in the extended conformation (Vettiger et al., 2017a). After contraction and secretion occur, the ClpV ATPase is recruited to disassemble and recycle the VipA/VipB tube components (Vettiger et al., 2017a). Analysis performed in a variety of species suggests that effectors can associate with Hcp, PAAR motif proteins, and VgrG (Shneider et al., 2013). To date, all characterized *V. cholerae* T6SS effectors are either loaded onto the VgrG tip or are part of the tip proteins themselves (Unterweger et al., 2017). 'Cargo effectors' are loaded directly onto the tip of the T6SS (Unterweger et al., 2015). Cargo effector loading is facilitated by chimeric adaptor proteins that bind both the effector and the VgrG protein yet are not themselves secreted. Finally, the so-called PAAR-motif proteins, which assemble into a cone-like structure at the tip of the T6SS and form a sharp point that facilitates membrane puncture, have also been shown to harbor C- or N-terminal effector domains or to bind and load additional effectors (Shneider et al., 2013).

1-5.2 Diversity of T6SS effectors

The assembly, contraction and mechanisms of secretion are all very highly conserved amongst bacterial strains, however, the effectors themselves vary greatly not only on the sequence level but their function. The four major classifications appear to be effectors that kill bacteria, effectors that kill eukaryotic cells, effectors that modulate eukaryotic cells and effectors that are involved in self/non-self-recognition to modulate group behaviors (Pukatzki et al., 2007; Saak and Gibbs, 2016; Unterweger et al., 2014a). Antibacterial effectors are a major class of T6SS effectors. These effectors tend to act on conserved features of bacteria exclusively associated with virulence against Gram-negative bacteria. For example, the T6SS of *Pseudomonas aeruginosa* secretes multiple lipases that

are specific for the inner membrane (Russell et al., 2013a). In *Acinetobacter baumannii*, an effector also targets the periplasm and degrades the peptidoglycan (Weber et al., 2015). However, not all antibacterial effectors target the periplasm. In *Agrobacterium tumefaciens,* the T6SS gene clusters encode a protein that degrades DNA (Ma et al., 2014). This indicates that potentially the system could be used to target Gram-positive bacteria as there are effectors that can hypothetically target them. It has, however, been speculated that a thick peptidoglycan layer might help protect from T6SS (MacIntyre et al., 2010). This was recently corroborated by a report that demonstrates the T6SS can be defended against by a capsule (Toska et al., 2018).

Antibacterial effectors that target conserved cellular components necessitate the need for immunity proteins (Dong et al., 2013; Miyata et al., 2013). These proteins are necessary to avoid toxicity from sister cells. All examples of these proteins work by directly binding and sequestering the effectors (Benz and Meinhart, 2014; Brooks et al., 2013; Dong et al., 2013).

Other T6SS are toxic towards eukaryotic cells. These effectors have been shown to be important against a variety of eukaryotic cells including fungi, amoeba, host epithelial cells and immune cells (Jiang et al., 2016; Ray et al., 2017; Russell et al., 2013a; Suarez et al., 2010; Trunk et al., 2018). In *Aeromonas hydrophila,,*an effector covalently linked to the VgrG protein exhibits ADP ribosyltransferase activity which activates caspase 9 in HeLa cells resulting in apoptosis (Suarez et al., 2010). *Serratia marcescens* use their T6SS effector to target the fungus, *Candida saccharomyces* (Trunk et al., 2018). The effector, Tfe1 disrupts amino acid metabolism resulting in cell death through autophagy (Trunk et al., 2018). Other anti-eukaryotic effectors include the same toxins that target the inner membranes of bacterial cells (Russell et al., 2013a). Such effectors target both the inner membrane of bacteria and lipids within eukaryotic cells. These effectors have been called cross-kingdom effectors (Russell et al., 2013a).

Another class of bacterial effector is used for self-recognition without toxicity. The swarming bacteria *Proteus mirabilis* uses a T6SS as a means to recognize similar strains (Saak and Gibbs, 2016). When the effector and immunity proteins bind, the protein complex acts as a signal to initiate swarming (Saak and Gibbs, 2016). This functions to restrict a beneficial cooperative behavior to kin bacteria (Saak and Gibbs, 2016).

Lastly, bacteria use their T6SS to modulate eukaryotic cell behavior. The two main changes the bacteria look to make are to increase endocytosis or to decrease immune activity. VgrG2b, a *P. aeruginosa* effector, helps aid in endocytosis of *P. aeruginosa* into non-phagocytic cells by binding γ-tubulin (Sana et al., 2016a). Similarly, VgrG5 from the intracellular bacteria *Burkholderia pseudomallei* helps fuse eukaryotic cells together so that the bacteria can be easily trafficked between the two eukaryotic cells (Schwarz et al., 2014). The fish pathogen *Edwardsiella tarda* encodes an effector, EvpP, which prevents the oligomerization of ASC – an important host protein necessary for inflammasome production (Chen et al., 2017; Wang et al., 2009). Inflammasome production results in pyroptosis and cell death, and in turn the death of the intracellular pathogen (Chen et al., 2017).

Whether manipulating the immune system or killing other bacteria, the T6SS can likely play a role in infection for pathogenic bacteria. In the next sub-section I will introduce the variety of ways in which the T6SS can be used for pathogenesis.

1-5.3 The involvement of the T6SS in pathogenesis

While many pathogenic roles for the T6SS have been hypothesized based on the biological activity of the effector proteins, there have also been well documented roles of the T6SS being important for *in-vivo* virulence. This section will again look at anti-bacterial killing, anti-eukaryotic killing as well as the manipulation of the host immune system.

Antibacterial T6SS activity has been implicated in increased virulence in a niche replacement model, i.e. the antibacterial activity kills the commensal bacteria living on or in the host and allows the pathogenic bacteria to take their spot. *Salmonella* Typhimurium uses its T6SS *in-vivo* to kill the commensal *Klebsiella oxytoca* (Sana et al., 2016b). This allows *S.* Typhimurium to colonize the adult mouse model more effectively, specifically by increasing the duration of colonization. Another example is the plant pathogen *Agrobacterium tumefaciens,* its T6SS is used to kill T6SS-negative *A.tumefaciens in-planta* to increase colonization (Ma et al., 2014).

Anti-eukaryotic activity comes in many different ways. For example, *Campylobacter jejuni* uses its T6SS to adhere to epithelial cells, and is unable to colonize

the mouse without its activity (Lertpiriyapong et al., 2012). It is likely that the T6SS of *C. jejuni* also is involved in internalization of the bacteria into non-phagocytic cells allowing an intracellular infection (Lertpiriyapong et al., 2012). Some T6SS activity is used to supress the immune system. Once phagocytized by a macrophage, enterohemorrhagic *Escherichia coli* uses its T6SS to prevent the antibacterial activity of reactive oxygen species by secreting a catalase, KatN (Wan et al., 2017). This allows EHEC to increase its ability to kill the mouse model of infection (Wan et al., 2017). A final example is the respiratory pathogen *Bordetella bronchiseptica*, which uses the T6SS in the mouse lung to reduce cytokine production (Bendor et al., 2015) . This in turn reduces mucus clearance in the lung, allowing the bacteria to persist longer and cause a much more severe disease (Bendor et al., 2015).

Altogether, the T6SS has a conserved structure and mechanism, yet is able to secrete a diverse array of effectors that contribute to bacterial competition, competition with eukaryotic cells and pathogenesis within the host. In the next section I will discuss specifically how these general themes relate to *V. cholerae*.

1-6 *Vibrio cholerae's* Type VI Secretion System

The T6SS was first discovered in *V. cholerae* and it has remained one of the best characterized amongst other bacteria. One reason it is readily studied is that *V. cholerae* only encodes one T6SS, and there are strains that have a constitutively active T6SS. In this section I will examine several studied aspects of the *V. cholerae* T6SS. Starting with the T6SS on a genetic level, both what is conserved amongst strains and where diversity exists. Next, I will discuss how this diversity contributes to competition between *V. cholerae* isolates – specifically those from the pandemics and the environmental strains. Then I will describe the regulatory networks that govern T6SS activity, specifically focusing on the host derived components which will lead to an examination of how the T6SS contributes to virulence. Lastly, I will outline which *V. cholerae* strains I used during my thesis and what their advantages are to studying the T6SS of *V. cholerae*.

1-6.1 The T6SS gene clusters

The thirty-nine genes that encode the T6SS are distributed over four distinct clusters over the two chromosomes of *V. cholerae* (Figure 5) (Joshi et al., 2017). The large T6SS cluster contains twenty open reading frames (Pukatzki et al., 2007). This includes all the structural genes that encode proteins to make up the inner membrane complex, the outer sheath, the PAAR tip and one third of the VgrG trimers. Also, included is the gene, *vasH*, which encodes a regulator for the two auxiliary gene clusters (Kitaoka et al., 2011b; Pukatzki et al., 2007). Finally, the 3' end of the *vgrG* gene contains an effector domain, and the gene immediately downstream of the *vgrG* gene is an immunity gene (Brooks et al., 2013).

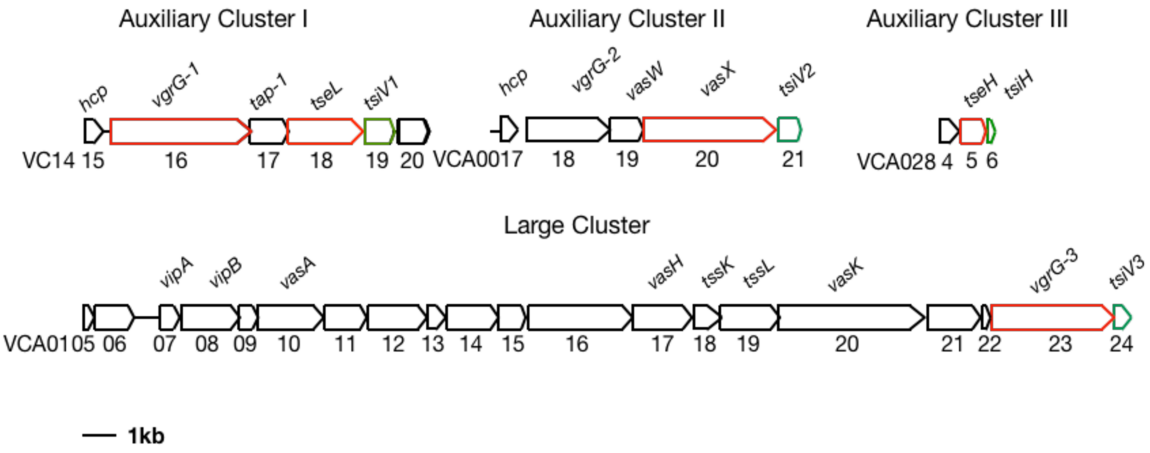

Figure 1-4. **Graphical depiction of the T6SS gene clusters (drawn to scale).** The gene names are indicated on top and the locus tags are indicated below the gene. Red represent effectors genes and green represent immunity genes.

In addition to the large cluster there are three auxiliary clusters. The first two auxiliary clusters follow the same organizational synteny and encode four genes (Miyata et al., 2013; Unterweger et al., 2014a). The first encodes a structural component. In auxiliary clusters 1 and 2, this is *hcp*. This is the gene that encodes Hcp, the protein making up the inner sheath of the T6SS that is secreted along with the effectors (MacIntyre et al., 2010). The next component is a *vgrG* gene. The next is an adaptor gene which encodes adaptor proteins that facilitates binding of the effector protein to the VgrG trimer (Unterweger et al., 2015). Following the adaptor is the effector gene, with its cognate immunity gene directly downstream (Dong et al., 2013). The third auxiliary cluster is

smaller, comprising of a structural PAAR gene, an effector, *tseH,* and an immunity gene, *tsiH.* (Altindis et al., 2015).

While structural T6SS components have >95% identity over 37 sequenced *V. cholerae* strains, effector module DNA sequences have <30% identity among the same strain set (Unterweger et al., 2014a). The DNA encoding the T6SS has a lower GC-content than surrounding regions, this implies that it is a genomic island, perhaps acquired through horizontal transfer (Unterweger et al., 2014a). Its similarity with the T4 phage suggests spread via transduction (Leiman et al., 2009). Further genetic differences are highlighted by GC-content divergence within the T6SS gene clusters itself, specifically between effector modules and core regions (Kirchberger et al., 2017a; Unterweger et al., 2015). Effector modules harbor a 6-13% lower GC-content than the core structural components indicating that these DNA sequences were acquired independently (Kirchberger et al., 2017a). This initial observation provoked the hypothesis that effector modules mobilize and are freely exchanged among *V. cholerae* strains. Together, this describes a T6SS in *V. cholerae* that is highly conserved in regions coding for the core structural components and assembly yet highly diverse in effector module sequences

1-6.2 Diversity in *V. cholerae* effectors

Diversity exists within *V. cholerae'*s T6SS effector both within a strain and amongst the species. Amongst different strains, *V. cholerae* secretes effectors with a wide variety of consequences. As an example, I will focus on the effectors secreted by the pandemic strains as they are the best characterized.

The pandemic *V. cholerae* strains secrete five effector proteins (Table 1). Three of these effectors, VgrG-3, TseL, and TseH, target bacteria (Altindis et al., 2015; Brooks et al., 2013; Dong et al., 2013). One of these effectors, VgrG-1, target eukaryotic cells (Pukatzki et al., 2007). The last effector, VasX, is unique and targets both eukaryotic and prokaryotic cells (Miyata et al., 2011, 2013). VgrG-3 is encoded in the large T6SS cluster, and contains both a structural component necessary for optimum secretion of the T6SS as well as a domain that degrades peptidoglycan (Brooks et al., 2013). This effector is covalently linked to the secretion system itself and is inhibited by TsiV3 (Brooks et al.,

2013). TseL is encoded in auxiliary cluster 1, and is an antibacterial effector with lipase activity (Dong et al., 2013; Unterweger et al., 2014a). TseL is a cargo effector, inhibited by TsiV1, that requires the help of an adaptor protein, Tap-1, to be loaded onto VgrG-1 so it can be secreted (Miyata et al., 2013; Unterweger et al., 2015). TseH is encoded in auxiliary cluster 3 and has activity as an amidase (Altindis et al., 2015). The exact delivery mechanism is unclear, but it is hypothesized to bind the PAAR-2 protein also encoded in the same gene cluster (Altindis et al., 2015). No toxic activity has been observed by this effector under natural conditions, although the enzyme is active and can kill *E. coli* when expressed in the periplasm and it can be inhibited by TsiH when it is also expressed in the periplasm (Altindis et al., 2015). VgrG-1 is similar to VgrG-3 as both effectors are delivered by the same mechanism, by being covalently linked to the secretion apparatus. However, the activity is different. VgrG-1 covalently links actin, a host protein that is necessary to create a cytoskeleton in eukaryotic cells (Pukatzki et al., 2007). VgrG-1 has been shown to kill both macrophage and amoeba (Pukatzki et al., 2006b). VasX is an effector that has been shown to target both eukaryotic and bacterial cells (Miyata et al., 2011, 2013). This is through the shared mechanism as a colicin, being able to form pores in the cell membranes indeterminately. VasX's mechanism of secretion is very similar to TseL it is aided by the adaptor VasW and loaded onto the T6SS through a direct interaction with VgrG-2 (Miyata et al., 2013). The effectors encoded by pandemic *V. cholerae* demonstrate the large diversity with which effectors act and how they are secreted.

Effector	Immunity	Loading Mechanism	Target	Reference
VgrG-1	-	Covalently linked	Eukaryotic -Actin	Pukatzki *et al.* (2006)
TseL	TsiV1	Cargo Adapter by Tap-1	Bacterial - Lipids	Dong *et al.* (2013)
VasX	TsiV2	Cargo Adapter by VasW	Cross Kingdom - Membranes	Miyata *et al.* (2014)
VgrG-3	TsiV3	Covalently linked	Bacterial - Peptidoglycan	*Brooks et al.* (2013)
TseH	TsiH	PAAR Associated	Bacterial - Peptidoglycan	*Dong et al.* (2016)

Table 1-1. **Effector modules from pandemic *V. cholerae.*** This table lists the effectors encoded by pandemic strains, V52, and 2740-80. The table list major characteristics such as immunity and adaptors.

Effector diversity also exists amongst strains. Two of the effectors appear to be either present or absent in different *V. cholerae* strains –the actin crosslinking domain of VgrG-1 and the *tseH* gene cluster (Unterweger et al., 2014, Santoreillo *et al.*, unpublished). In strains without the actin crosslinking domain, VgrG-1 serves only as a docking site for TseL and as a structural component (Kirchberger et al., 2017; Unterweger et al., 2014). In strains lacking the *tseH*, there is no replacement. The other three effectors – VasX, TseL and VgrG-3 – while encoded in all pandemic strains, have different effectors in their loci in non-pandemic strains. Although, there are exceptions where non-pandemic strains encode *vasX, tseL,* and/or *vgrG-3*, they are the exception (Kirchberger et al., 2017; Unterweger et al., 2014). For the most part, non-pandemic effectors have similar predicted functions but differ on an amino acid level by over 80%. In auxiliary cluster one, where *tseL* (A^1) and *tsiV1* (VC1418 and VC1419) is encoded, non-pandemic strains encode a different effector module that is also predicted to be a lipase (C^1) with a different activity (Unterweger et al., 2014). More diversity exists in auxiliary cluster two, where *vasX* and *tsiV2* (VCA0020 and VCA0021) are replaced by one of five alternative effector modules that have been identified so far (Kirchberger et al., 2017a). The most diversity exists within

the large cluster and within the 5' end of *vgrG-3* and tsiV3 (VCA0123 and VCA0124) where twelve different C-terminal extensions can be encoded for (Unterweger et al., 2014). This effector diversity results in 120 different combinations of strains each with a potentially diverse ability to compete in the environment and in the human host (Kostiuk et al., 2018). The consequences of this diversity is a major topic of discussion in my thesis and will be the primary focus of the remainder of the introduction.

1-6.3 *V. cholerae* compatibility groups

In 2014, our laboratory defined *V. cholerae* strains that could coexist as compatible, or belonging to the same compatibility group, and strains that could not coexist as being incompatible (Unterweger et al., 2014). This compatibility was determined to be to be entirely dependent on the T6SS (Unterweger et al., 2014). Further analysis demonstrated the sequence of the immunity genes – primarily those from the large cluster and the first two auxiliary clusters – dictated compatibility (Unterweger et al., 2014). Those that share all three immunity genes can coexist, while those that do not, will outcompete one another in a T6SS-dependent manner (Unterweger et al., 2014).

Taken together, these observations suggest that "compatibility rules" allow distinct strains of *V. cholerae* with identical effector modules to coexist, thereby giving rise to a unique self-recognition system. The effectors encoded by the strains are hypothesized to dictate which strain will outcompete the other. Conversely, *V. cholerae* strains expressing dissimilar effector/immunity pairs are unable to share a niche as one of the two strains will be excluded (Unterweger et al., 2014). Each *V. cholerae* strain examined to date encodes three distinct effector/immunity alleles within the three T6SS gene clusters. So far, we identified a total of nineteen effectors across the three clusters, but expect that number to increase as additional strain sequences become available (Kirchberger et al., 2017a). We assigned each module a letter as an identifier to distinguish strains able to coexist from those that compete against each other.

The format to express the compatibility group is three letters in series. The first letter refers to the immunity gene in auxiliary cluster one, the second to the immunity gene in auxiliary cluster two and the final letter is the immunity gene in the large cluster. As *V. cholerae* effector and immunity pairs appear to be restricted to one locus, a letter in the first position represents a different immunity gene than the same letter in the second or

third position. For example, El Tor pandemic *V. cholerae* belong to the AAA compatibility group (Unterweger et al., 2014). When referring to individual effectors, a superscript will be used to dictate which cluster the effector is from. For example A^1 refers to the A effector in auxiliary cluster one. Whereas, C^L refers to the C effector in the large cluster. Likewise, A^2 refers to VasX, the effector produced in auxiliary cluster 2.

Another important aspect of compatibility groups are so-called orphan immunity genes consisting of open reading frames that bear considerable homology to immunity genes but are not positioned directly downstream of a cognate effector (Kirchberger et al., 2017a; Kostiuk et al., 2018). All AAA-module strains harbor a single orphan immunity gene (VC1420) downstream of the tsiV1 immunity gene outside of the T6SS auxiliary cluster 1, yet other *V. cholerae* strains have several orphan immunity genes in long arrays following all three T6SS gene clusters (Kirchberger et al., 2017a). While it is not yet known if these purported genes are active and provide protection to other effector genes, RNAseq data from *V. cholerae* demonstrate that the orphan immunity gene downstream of *tsiV1* is transcribed along with the rest of the cluster when T6SS is induced (Scrudato and Blokesch, 2012). Additional immunity genes could offer a resistance mechanism for *V. cholerae* to effectors other than the ones they encode, providing a mechanism by which incompatible strains could coexist in a heterogeneous environmental niche (Kostiuk et al., 2018). Alternatively, these open reading frames – while once immunity genes, might have taken on a novel role.

The consequences of compatibility groups are far reaching and yet relatively unexplored. As the compatibility groups dictate which strains can coexist, that also dictates which strains can share genetic information. Belonging to the same compatibility groups therefore allow *V. cholerae* to share genetic traits. Indeed, virtually all strains belonging to the AAA compatibility group we examined shared the presence of the horizontally-acquired genetic element the Virulence Pathogenicity Island I (VPI-1) which is essential for pandemic spread (Unterweger et al., 2014a).

Despite this conservation of these virulence factors, membership to a compatibility group does not always correlate with their position on a phylogenetic tree (Kirchberger et al., 2017; Unterweger et al., 2014). Two independent studies have shown that while closely related strains can belong to different compatibility groups, strains far apart on the

phylogenetic tree can share effector modules (Kirchberger et al., 2017; Unterweger et al., 2014). This, in addition to the variation in GC content between effector modules and surrounding regions, led to the hypothesis that effector modules are freely exchanged (Thomas et al., 2017).

Membership to compatibility group could help define disease spread. In nature, complexes of *V. cholerae* that inhabit the same geographical area all belong to the same compatibility group. This indicates that those *V. cholerae* that live together will infect together (Kirchberger et al., 2016; Kostiuk et al., 2018). Furthermore, as the T6SS of *V. cholerae* has been shown to be active in the host, a co-infection between many compatibility groups could result in a bottleneck driven by the T6SS. As all pandemic strains belong to the AAA compatibility group which has been shown to be superior at killing both members of other compatibility groups and *E. coli*, this is a potential mechanism by which El Tor *V. cholerae* could dominate pandemics (Unterweger et al., 2012, 2014a).

Membership to a compatibility group dictates the outcome of competition, occupation of a niche, ability to participate in co-infections and the ability to share DNA (Kirchberger et al., 2016; Kostiuk et al., 2018; Unterweger et al., 2014a; Veening and Blokesch, 2017). Understanding how compatibility groups are acquired and maintained is critical to understanding *V. cholerae* biology. While the consequences of compatibility grouping are coming to light in environmental and laboratory conditions, the impact they have during colonization and pathogenesis remain unclear. However, the universality of the AAA compatibly group in pandemic strains suggests they are critical for *in-vivo* fitness.

1-6.4 Regulation of *V. cholerae's* T6SS

There has been a lot of research into the regulation of the T6SS of *V. cholerae,* including the environmental and host factors that control it, the regulatory network on a genetic level as well as which genes are coregulated with T6SS activity. Understanding the regulation of the T6SS in response to environmental signals and how its regulation interplays with other virulence factors/ bacterial functions can help give meaningful insight into the biological functions of the T6SS.

The T6SS of *V. cholerae* is tightly regulated and subject to distinct layers of regulation in different strains(Figure 6) (Bachmann et al., 2015; Bernardy et al., 2016; Dong and Mekalanos, 2012; Ishikawa et al., 2012; Kitaoka et al., 2011b; Metzger et al., 2016; Watve et al., 2015). Amongst pandemic *V. cholerae* strains, T6SS regulation is controlled by three principal transcriptional regulators: VasH, TfoY and TfoX (Kitaoka et al., 2011b; Metzger et al., 2016). The large cluster becomes transcriptionally activated first, by either TfoY or TfoX (Metzger et al., 2016). While both of these activators act on the large T6SS gene cluster, each also drives independent processes that dictate *V. cholerae'*s lifestyle. TfoX is activated in the presence of chitin and co-regulates chitin catabolism and DNA uptake, whereas TfoY's response to decreased cyclic-di-GMP levels in the cell encourages anti-eukaryotic behavior such as upregulation of motility and hemolysin production, while inhibiting cell attachment (Meibom et al., 2004; Metzger et al., 2016; Scrudato and Blokesch, 2012). These distinct pathways infer multiple roles for the T6SS based on the environment *V. cholerae* confronts regardless, both pathways result in the transcription of the large T6SS gene cluster, including the regulator, *vasH*. VasH is a sigma-54 dependent transcription factor that is enhanced by RpoN and is encoded in the large T6SS cluster that positively regulates the two auxiliary clusters essential for T6SS activity (Dong and Mekalanos, 2012; Kitaoka et al., 2011b). In addition to VasH, the quorum sensing-regulated transcription factor HapR - induced at high cell density - binds to *hcp-1* and *hcp-2* promoters and positively regulates the T6SS auxiliary clusters (Shao and Bassler, 2014; Zheng et al., 2010).

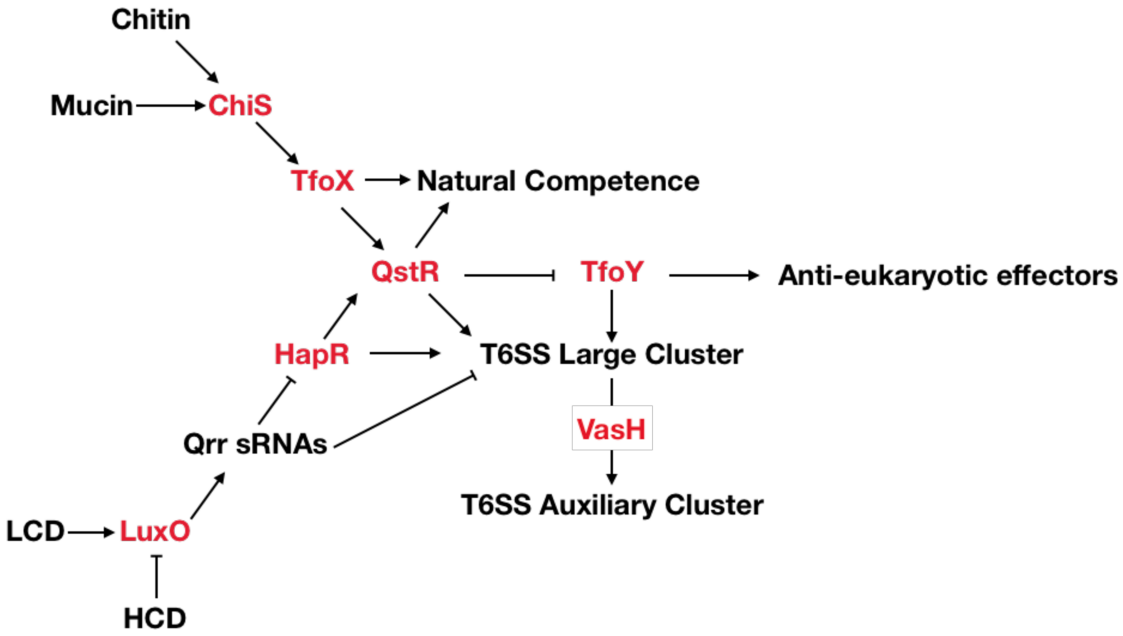

Figure 1-5. **Regulatory network of *V. cholerae* T6SS.** This map shows the genes involved in positively and negatively regulating the T6SS. Both genes (red) and classes if genes (black) are shown. HCD – high cell density and LCD – low cell density. See Section 1-6.4 for more details.

In *V. cholerae*, the T6SS is negatively regulated by sRNAs through two distinct mechanisms related to quorum sensing (Shao and Bassler, 2014). In response to low cell densities, LuxO is phosphorylated thereby producing quorum regulatory sRNAs. These small RNAs bind to and negatively regulate the 5' untranslated regions of the mRNA for *hapR* and the large T6SS cluster (Shao and Bassler, 2014). This is a two-pronged regulator silencing network that shuts down expression of auxiliary clusters through the downregulation of *hapR* and also downregulates the large cluster genes directly. Interestingly, this layer of regulation also exists in non-pandemic strains suggesting a conserved relationship between quorum sensing and the T6SS in this species (Shao and Bassler, 2014).

V. cholerae bacteria modulate T6SS activity in response to a wide variety of environmental cues; some of these function as "on/off" switches, while others modulate the intensity of the response. For example, mucin, chitin and high-osmolality have been shown to induce T6SS in a variety of toxigenic and non-toxigenic strains, while bile salts

and thiourea influence the magnitude of an already active T6SS (Bachmann et al., 2015; Borgeaud et al., 2015a; Dong et al., 2015; Ishikawa et al., 2012).

As a general rule, pandemic O1 strains appear to regulate T6SS expression differently than non-patient derived strains. One comprehensive study showed that a constitutively active T6SS under laboratory conditions is rare amongst clinical El Tor O1 strains (<15%), but common among environmentally derived strains (<90%) *(*Bernardy *et al.*, 2016). This correlates with *V. cholerae's* natural competence on chitin as more environmental than clinical strains incorporated exogenous DNA (33.3% vs 13.8%) (Bernardy et al., 2016). This profound regulatory difference might provide insights into how different sets of strains use the T6SS as it pertains to their individual lifestyles. Furthermore, the different regulatory cues that the strains respond to gives insight into where they use their T6SS.

1-6.5 *V. cholerae's* T6SS in the host

The majority of *V. cholerae* animal models have given insight into how the pathogen uses its T6SS. Early indication that the T6SS of *V. cholerae* is important *in vivo* came from expression studies in human volunteers (Lombardo et al., 2007). Using the sacB-based expression system IVET, T6SS genes, including *vgrG-1* and the Large Cluster were found to be induced *in-vivo* (Lombardo et al., 2007).

This observation has led to a large body of work finding the best *in-vivo* model to study various aspects of the T6SS. Not only have these studies attributed a variety of *in-vivo* roles to the T6SS, but they have added to our understanding of *V. cholerae* as a pathogen.

The infant mouse model was the first animal used to study the T6SS of *V. cholerae* – focusing on the anti-eukaryotic effectors. The effector VgrG-1 was shown to crosslink actin *in-vivo* and this observation was followed up with studies in the mouse gut (Ma and Mekalanos, 2010b). The authors found evidence of crosslinked actin in the mouse gut, as well as an increase in diarrhea and immune cell infiltration when the actin-crosslinking domain of *vgrG-1* was present (Ma and Mekalanos, 2010a). This inflammation was associated with an increase in *V. cholerae* colonization (Ma and Mekalanos, 2010b). In addition to studying the anti-eukaryotic effects of the *V. cholerae* T6SS, antibacterial

effectors have also been studied. The antibacterial effectors of the T6SS have been implicated in both inter and intraspecies competition (Bachmann et al., 2015; Zhao et al., 2018). In order to see an interspecies effect, the microbiome of the infant mouse had to be fortified with prey *E. coli* strains (Zhao et al., 2018). Interestingly, the killing of *E. coli* in the infant mouse caused an inflammatory response that not only increased the burden of *V. cholerae,* but also increased virulence factor production including cholera toxin (Zhao et al., 2018). Intraspecies competition has so far been reserved for two pandemic strains, one lacking their immunity genes (Bachmann et al., 2015). This observation implicates the T6SS as a way for incompatible *V. cholerae* strains to compete early in infection, potentially acting as a bottle neck for coinfections.

In the infant rabbit model, three major observations have been made. The first is that the T6SS is active under *in-vivo* conditions as shown through RNA-seq (Fu et al., 2013). This observation strengthens the role of the T6SS in the host. Secondly, this work has expanded on the findings that the T6SS can be used for intraspecies competition. This was accomplished by adding a conjugative plasmid to *V. cholerae* and counting events of conjugation *in-vivo* (Fu et al., 2018). This conjugation was prevented when one *V. cholerae* strain was T6SS-positive and the other was T6SS-negative (Fu et al., 2018). This indicates not only that the T6SS might be used to prevent certain types of horizontal gene transfer, but that the T6SS excludes incompatible strains when in contact. As *V. cholerae* forms microcolonies *in-vivo* that are essential for infection, it can be hypothesized that incompatible strains would not co-exist in microcolonies (Fu et al., 2018). Additionally, this work also indicated where the majority of *Vibrio-vibrio* interactions occur and therefore where the T6SS interspecies competition is likely to occur. The authors found that intraspecies competition is most likely to occur in the distal small intestine and cecum (Fu et al., 2013). By extension this suggests that interspecies competition with host resident microbes are more likely to occur in the proximal and middle small intestine (Fu et al., 2018). This work is relevant to both the study of the T6SS as well as the dynamics of *V. cholerae* in the host.

Most recently, the T6SS of *V. cholerae* was studied in the context of colonizing the zebrafish model of infection (Logan et al., 2018). The authors made the observation that *V. cholerae* with a constitutive T6SS could kill the commensal *Aeromonas veronii*,

removing it from the intestine of the zebrafish (Logan et al., 2018). However, upon further investigation it was shown that it was the actin-crosslinking domain and not the antibacterial effectors that were responsible for removing *A. veronni* from the host (Logan et al., 2018). This puzzled the researchers until they examined the contractile dynamics of the intestine. The actin crosslinking domain acts on the zebrafish intestine to increase contraction, thereby expelling the commensals. This is a unique example of an anti-eukaryotic effector having consequences on commensal members.

While there is a vast area of research on the consequences of the T6SS of *V. cholerae in-vivo*, there are still unresolved questions. The major three are addressed or are beginning to be addressed in my thesis. The first is the interaction of *V. cholerae* with a natural microbiome. As discussed earlier, it is difficult to investigate the interactions with the microbiome without a suitable model. Additionally, while contributions to the disease course have been investigated, the models have a major limitation as they are for sure short term infections only and so symptoms that arrive later in disease or host viability cannot be studied. Lastly, almost all studies to date have been focused on pandemic *V. cholerae* strains. This narrow examination of strains limits our knowledge of how the pandemic strains and non-pandemic strains interact within the host using their T6SSs. In order to study these aspects many different *V. cholerae* strains are necessary.

1-6.6 Choosing the appropriate *V. cholerae* strain for T6SS study

In this thesis there are many strains used to study various aspects of the T6SS and how it relates to the lifestyle of *V. cholerae.* This will be divided into two primary groups of strains: pandemic strains and non-pandemic strains (Table 2).

Effector	Serogroup/ pandemic	Compatibility Group	Activation Cue	Competence by Chitin	Chapter of Thesis
A1552	O1 El Tor	AAA	High Salt	+	2 & 4
C6706	O1 El Tor	AAA	Mouse & Fly	-	2 & 3
O395/NIH41/ CA401	O1 Classical	AAA	-	+	1 & 3
V52	O37	AAA	Constitutively Active	-	1,2,3 & 4
DL4215	O113	CEC	Constitutively Active	+	4
AM19226	O39	CDF	Constitutively Active	-	4
1587	O12	CDC	Constitutively Active	-	4

Table 1-2. **Summary of *V. cholerae* strains used in my thesis.**

For pandemic strains, I primarily used five strains. The quintessential El Tor pandemic strain, C6706, was used for all pandemic *in-vivo* work, both in the infant mouse and the *Drosophila melanogaster* model (Heidelberg et al., 2000). This is due to it being well established of having a host-activated T6SS (Zhao et al., 2018). Because of this feature, it is also the strain I used for studying the regulation behind the host-induction. Additionally, we have a transposon library for C6706. However, due to a mutation in LuxO, *V. cholerae* is not naturally competent on chitin. For studies involving the coregulation of the T6SS with natural competence, I used the El Tor strain A1552 as it has natural competence and the T6SS activated by chitin, or by the master regulator TfoX (Scrudato and Blokesch, 2012). For classical strains we used O395, CA401 and NIH41. All three strains were used in studies comparing the T6SS of classical strains with El Tor strains, and the O395 strain was used *in-vivo* as a comparison to El Tor strains.

In addition to the pandemic strains, I used four additional strains. The most frequently used is the O37 strain, V52. V52 has two primary advantages. The first is that, unlike pandemic *V. cholerae* strains, V52 has a constitutively active T6SS under laboratory conditions due to TfoY expression (MacIntyre et al., 2010; Metzger et al., 2016). The second is that V52 belongs to the AAA compatibility group – just like all pandemic strains

(Unterweger et al., 2014a). Next, DL4215 is an environmental isolate from the Rio Grande River in Texas, that like A1552 can be naturally transformed when grown on chitin (Chapter 5). Unlike A1552, however, DL4215 has an active T6SS under laboratory conditions (Unterweger et al., 2012). In addition to DL4215, we also examined AM19226 and 1587 as they are from different compatibility groups but also have active T6SSs under laboratory conditions (Unterweger et al., 2014b). AM19226 and 1587 are not naturally competent on chitin (Chapter 5).

1.7 Hypothesis and aims

Vibrio cholerae is a Gram-negative species that consists of over 200 serogroups; however, only one is responsible for the pandemic spread of the diarrheal disease cholera (Barua, 1992). The remaining serogroups represent non-pandemic strains displaying different degrees of pathogenicity. The O1 cholera serogroup has been responsible for the six historic cholera pandemics, as well as the ongoing seventh pandemic. The seventh-pandemic *V. cholerae* O1 El Tor biotype and the sixth pandemic O1 classical biotype evolved as distinct lineages and differ in the regulation and amounts of secreted cholera toxin, and carbohydrate metabolism among other biochemical properties (Barua, 1992). Another difference between El Tor pandemic strains, classical pandemic strains and non-pandemic strains is the sequences within their T6SS gene clusters (Miyata et al., 2010a). For my PhD thesis, I investigated how El Tor strains differ from classical and non-pandemic strains with respect to their ability to compete with other bacteria in microbial communities.

I focussed on the type VI secretion system (T6SS), a molecular syringe that Gram-negative bacteria use to deliver toxic effector proteins directly into neighbouring eukaryotic and prokaryotic cells. The bacterial toxins are deadly unless the recipient bacteria encode immunity proteins that sequester incoming effectors (Brooks et al., 2013; Dong et al., 2013; Miyata et al., 2013). Our lab recently demonstrated that pairs of *V. cholerae* strains encoding the same effector and immunity genes are compatible and are able to coexist. However, if two strains produce different effector and immunity proteins, they kill each other and are incompatible. All El Tor pandemic strains encode identical effector-immunity pairs and are compatible (Unterweger et al., 2014a). Non-pandemic strains do not share these effector-immunity pairs and are incompatible with El Tor strains as well as other non-

pandemic strains (Unterweger et al., 2014a). In contrast, classical pandemic strains have accumulated mutations in their T6SSs rendering them unable to compete.

In addition to the unique and conserved effectors, El Tor strains also tightly regulate their T6SS as it is not active under laboratory conditions but shows activity in the host. I **hypothesized that the effectors acquired by El Tor strains and their *in-vivo* activity allow enhanced competition compared to classical and non-pandemic strains.** In Chapter II of my thesis, I characterize a mechanism by which El Tor strains acquired their shared effector genes and compared their killing efficiencies to non-pandemic effectors. Chapter III explores mutations in structural T6SS components in classical *Vibrio cholerae* strains, and how they result in a dysfunctional system. In Chapter IV, I discuss how the host molecules mucin and bile regulate the T6SS *in-vivo*. In Chapter V, we investigated how an active T6SS of pandemic strains interact with the microbiome and how this interaction contributes to pathogenesis.

Chapter II: I examined how and why *V. cholerae* strains acquired the immune and effector combination they possess. I hypothesized that the effector modules are horizontally acquired, while allowing the retention of the original immunity gene. This feature allows the new strain to maintain compatibility with their sister strains while also acquiring a new effector. Through whole-genome comparison, we showed that a new effector can be acquired through conserved regions in the T6SS adaptor gene on the 5'-end, and domains of micro-homology on the 3'-end. Furthermore we showed, by competing genetically engineered strains, that the pandemic effector is dominant in T6SS-mediated competition when compared to the non-pandemic allele. These studies suggest that El Tor strains could have acquired the A effector through horizontal transfer, and that the A effector may have contributed to their fitness. This shows that pandemic strains are superior to environmental strains in respect to their T6SS effectors.

Chapter III: In chapter III I differentiate between the two clades of pandemic strains, classical and El Tor. Comparative genomic analysis between El Tor and classical strains, from both the 2nd and 6th cholera pandemics, was used to look for differences between the T6SS. Three mutations of interest were seen between the strains. The first, is a 12-bp deletion within *VCA0109,* a gene encoding an essential structural component that exists in both 2nd and 6th cholera pandemic strains. The second was a 16 base-pair deletion

in *vasK,* another essential structural component, that exists within 6th pandemic strains. The third was a single nucleotide polymorphism within the immunity gene, *tsiV1*. This mutation was only found in a subset of 6th pandemic classical strains. We then made these mutations in a *V. cholerae* strain with a constitutively active T6SS and saw that the two mutations in structural components disabled the T6SS. The mutation in the immunity gene resulted in a less efficient immunity gene and impaired competitive behaviour. Together, these results indicate that 2nd and 6th pandemic strains lacked a functional T6SS, and a subset of 6th pandemic strains lack the ability to fully defend a T6SS attack.

Chapter IV: To address the regulation of the T6SS in El Tor strains, we infected infant mice with *V. cholerae* by co-administering strains capable of engaging in T6SS-mediated killing with an isogenic strain lacking the immunity genes. These experiments suggested the presence of unknown factors that activate the T6SS and bacterial killing *in-vivo*. We identified mucin, the major glycoprotein in the small intestine, as a T6SS activator. In *in-vitro* experiments, we showed that mucin activated the T6SS of El Tor *V. cholerae.* Furthermore, we determined that bile salts could fine-tune the activity of the T6SS. The commensal metabolite deoxycholate reduced T6SS-killing by inhibiting assembly of the T6SS. In contrast, host-modified conjugated bile salts, such as taurocholate, enhanced T6SS killing. Additionally, we demonstrated the ability of the T6SS to be used *in vivo* between El Tor *V. cholerae* and incompatible environmental isolates to gain an advantage within the infant mouse model. Next, we sought to investigate the host-regulated system's ability to compete with the microbiota.

Chapter V: The consequences of a host-activated T6SS were explored using the *Drosophila melanogaster* model of cholera, as it houses a simple microbiome of five to seven commensal species. In collaboration with David Fast from the Foley lab in our department, we found that while El Tor strains were able to kill the fruit fly, classical strains were not. The T6SS contributes to the pathogenicity of El Tor *V. cholerae* in the fruit fly, and causes a significant reduction in lifespan. This T6SS-dependent pathogenicity was not observed in an animal devoid of a microbiome, suggesting bacteria-bacteria interactions are critical for virulence. We studied the consequences of this pathogenicity on the host through phenotypic assays and visually through TEM, and found that the El Tor T6SS negatively impacted host health. Through an RNA-seq study, as well as mutations in the

fly immune system, we were able to implicate the immune system as a mediator of the T6SS dependent effects. Finally, we isolated the specific bacteria-bacteria interaction responsible for this phenotype – that *V. cholerae* kills the Gram-negative commensal *Acetobacter pasteurianus* resulting in a decreased lifespan for *D. melanogaster.*

Together, this body of work demonstrates that key features of El Tor *V. cholerae's* T6SS, including regulation and effector specificity, contribute to superior bacterial competition over non-El Tor *V. cholerae* strains potentially providing a mechanism that contributed to the emergence of this seventh pandemic strain.

Chapter 2 :
Materials and Methods

Strains and culture conditions

Bacteria were grown in liquid culture in autoclaved Lysogeny broth (LB) (1% Bacto Tryptone (Biosciences), 0.5% Yeast extract (Sigma-Aldrirch), 0.5% NaCl) at 37ºC, or 30ºC for transformation experiments. Plates were prepared with LB broth supplemented with 1.5% agar. Liquid LB or plates were supplemented with antibiotics when required at the following concentrations: Streptomycin (100ug/ml), Rifampicin (50ug/ml), Kanamycin (50ug/ml), Ampicillin (100ug/ml). All bacteria stocks were stored in cryovials in 20% glycerol at -80 ºC.

All *Drosophila* commensal bacteria strains used in my thesis were isolated from wild-type *w1118* lab flies (Bloomington Drosophila Stock Center) from the Foley lab at the University of Alberta and are as follows: *Lactobacillus plantarum* KP (DDBJ/EMBL/GenBank chromosome 1 accession CP013749 and plasmids 1-3 for accession numbers CP013750, CP013751, and CP013752, respectively), *Lactobacillus brevis* EF (DDBJ/EMBL/GeneBank accession LPXV00000000), and *Acetobacter pasteurianus* AD (DDBJ/EMBL/GeneBank accession LPWU00000000) and are described in (Petkau et al., 2016a). *Lactobacillus* strains were grown in MRS broth (Sigma Lot: BCBS2861V) at 29°C and *Acetobacter pasteurianus* was grown in Mannitol broth (2.5% n-mannitol. 0.5% yeast extract, 0.3% peptone) 29°C with shaking at 200rpm. As indicated, bacteria were grown in the presence of 100 μg/ml streptomycin.

Primer design

Nucleotide sequences were acquired from NCBI database, or from our own sequencing efforts. Primers were designed manually. IDT's OligoAnalyzer tool determined the melting temperature and potential of primer-dimers. Restriction sites were added to the 5' end of primers when necessary. Primers were ordered from Integrated DNA Technologies (IDT; Coralville, IA, USA). Primers use for cloning are below, in Table 1.

Primer Name	Direction	Primer Sequence
Classical *vasK* A	F	AAGCTTGATATCGAATTCCTGCAGCCCGGGATGTGGAAATTCATTGTTGG
Classical *vasK* B	R	TCAATCAGGACAGATTCATCACCAATCAAACGAGTATGGG
Classical *vasK* C	F	CCCATACTCGTTTGATTGGTGATGAATCTGTCCTGATTGA
Classical *vasK* D	R	ATTAACCCTCACTAAAGGGAACAAAAGCTGTTAATAGAGTGTTTTAGACAG
Classical VCA0109 A	F	TTTATTGCTCTTACTATGCGTAAAGGC
Classical VCA0109 B	R	CATAGACATTCTTTGGATAAGGCAGC
Classical VCA0109 C	F	AGATCTCTCCGTGCGAATTAAATTGG
Classical VCA0109 D	F	CGTTTAACTCGCGTTCTGGTG
Classical VCA0109 E	R	CATAGACATTCTTTGGATAAGGCAGC

Table 2-1. Cloning PCR primers

Polymerase chain reaction (PCR)

PCR were reactions of 25µL or 50µL. 25µL were used for screening, whereas, if a downstream product was required 50µL reactions were made. TopTaq polymerase (Qiagen, Toronto, ON, Canada) lack proofreading activity was used for PCR reactions where downstream products were not important for cloning. Alternatively, Phusion polymerase (ThermoScientific, Waltham, MA, USA) or iProof polymerase (Bio-Rad, Hercules, CA, USA) was used for reactions if the product was needed downstream. For PCR off of genomic DNA, an overnight culture was resuspended in water at a 1 culture : 9 water ratio. The solution was boiled for 10 minutes and 3.5µL was used as template. When the template was a plasmid, 50ng of pure plasmid was used. The other components, as well as the PCR times and temperatures were chosen based on the manufactures recommendations with a melting temperature chosen 5ºC below the melting temperature of the primers (aim for 60ºC).

Agarose gel electrophoresis

Agarose gel electrophoresis was used with 0.8% agarose gels with Red Safe (1/20,000; iNtRON Biotechnology, Korea) added to the gel to visualize the DNA of the gel. Gels were run for 40 minutes at 110V. A geldoc system (Cell Biosciences) was used to visualize the DNA bands.

Gel extraction

I used the gel extraction kits from either TheromoScientific (ThermoScientific, Waltham, MA, USA) or FroogaBio (Toronto, ON, Canada). The manufacturer recommendations was used, however a 20µL volume of ddH_2O was used for elution. 1.8µL of the elute was used to determine the concentration of the yield using the NanoDrop (ThermoScientific, Waltham, MA, USA).

Preparation of electrocompetent V. cholerae

A small loop full of *V. cholerae* from a plate of bacteria after 5 hours growth at 37ºC is resuspended in pre-chilled 2mM CaCl2 and washed twice using a 4ºC centrifuge (10,000xg). Afterwards, the cells were resuspended in 50µL of 2mM CaCl2 and directly used for electroporation (Gonzales et al., 2013).

Transformations via electroporation

I added 5µL from the ligation reaction or purified plasmid to the competent cells prior to electroporation in a 2mm cuvette at 2.5V and 200 Ohms. The bacteria was allowed to recover for 1 hour at 37ºC in 1mL of LB. 100 µL bacteria was plated onto plates with appropriate antibiotics for the resistance conferred by the plasmid or insert.

Plasmid purification

Plasmids were purified from 4.5ml overnight culture using miniprep kits from ThermoScientific (Waltham, MA, USA) or FrogaBio (Toronto, ON, Canada). The manufacturer recommendations was used, however a 20µL volume of ddH_2O was used for elution.

Restriction digest

FastDigest restriction enzymes (ThermoFisher Scientific, Waltham, MA, USA) to release inserts from plasmids. 1µg of plasmid was digested in a final volume of 20µL 1µL of restriction enzyme was used a 2µL of digest buffer. The reaction was incubated at 37ºC for 1 hour. Digested vectors were treated with intestinal calf phosphatase (ThermoFisher Scientific, Waltham, MA, USA) for 5min at 37ºC to avoid self-ligation of the vector.

Sticky-end ligation

To ligate inserts into the vector pWM91, vector and insert were digested (Metcalf et al., 1996). The products were ligated using the T4 ligase (Thermo Scientific, Waltham, MA, USA). Vector and insert were mixed at a molar ratio of 1:3 with 50ng of vector and the T4 ligase instructions were used. The reaction was incubated at room temperature for one hour, followed by electroporation into *E. coli* DH5alpha lambda pir.

Purifying VrgG-3 and TsiV3

Recombinant VgrG-3 and TsiV3 constructs were purified from 4-liter expression cultures by nickel affinity. Briefly, the cell pellets were lysed in resuspension buffer (20 mM HEPES, 100 mM NaCl, pH 8) with 10 units of Dnase I (Fermentas) and complete protease inhibitor mixture (Roche Applied Science) using a French pressure cell (Thermo Scientific, French Press Cell Disruptor). Insoluble cellular debris were pelleted at 25,000xg, and the supernatant was filtered and applied to a HisTrap FF column equilibrated with binding buffer (20 mM HEPES, 500 mM NaCl, 20 mM imidazole, pH 8) on an AKTA basic FPLC system (GE Healthcare). Following three washes, the His-tagged proteins were eluted with a 20-ml gradient of 20–500 mM imidazole. Pure fractions were pooled and dialyzed against resuspension buffer to remove imidazole and decrease salinity.

Zymography

Peptidoglycan (PG) was isolated from *E. coli* MG1655. Briefly, four liters of volume of overnight culture was pelleted and resuspended in water to a density of 200 g/liter, then added dropwise to an equal volume of boiling 8% SDS. Constant watching of this mixture is important, and heat should be reduced if it starts boiling over. The mixture was boiled for 2 hours before ultracentrifugation at 100,000xg at room temperature to sediment PG. The pellet was washed with ddH_2O four times to remove SDS and then lyophilized to dryness to determine the yield. The crude PG preparation was mixed to 0.1% w/v in 12% SDS PAGE. Samples for zymography were prepared in 1M Laemmli buffer and electrophoresed at 200 V for 1 h. After electrophoresis, the gel was washed with water to remove SDS and then equilibrated in renaturation buffer (10 mM Tris-HCl, pH 7, 0.1%

Triton X-100). Fresh renaturation buffer was added, and the gel was incubated at 37 °C overnight with agitation. To visualize degraded PG, the gel was washed quickly three times with water and then stained with methylene blue stain (0.1% methylene blue, 0.01% KOH) for 3 h followed by water washing until bands were clearly visible. To assess the optimal buffer conditions for VgrG-3 degradation of PG, purified recombinant protein was run on a zymogram and incubated in variations of renaturation buffers.

Peptidoglycan degradation

Digestion of purified *E. coli* PG by VgrG-3C was monitored by mixing 10 ug of purified protein with 100 ug of PG in 100 µL of 20 mM HEPES, pH 6.8 in a 96-well plate then incubating at 37°C in an xMark microplate spectrophotometer (Bio-Rad) and measuring A595 over a 60 min period. Buffer alone served as negative control, whereas lysozyme was used as a positive control.

Lysis assay

Overnight cultures of *E. coli* TOP10 (Invitrogen) cells harboring the pBAD24-LS::*vgrG-3* plasmid or relevant controls were diluted to A600 1.0 in either LB 0.2% D-glucose (inhibiting) or LB 0.2% L-arabinose (inducing) and transferred to a 96-well plate. The A600 was measured in an xMark microplate spectrophotometer (Bio-Rad), and then the plate was incubated at 37°C on a vibrating shaker for 60 min, and the A600 was measured once more. The relative change in A600 was calculated as (A600 60 min x A600 0 min)/A600 0 min.

Chitin-dependent transformation

Overnight bacterial cultures grown at 30°C were sub-cultured 1:100 in LB broth. This was incubated while shaking for 2 hours at 30°C to an OD_{600} of 0.5-0.6. The culture is then spin down (10,000xg for 2 minutues) and resuspended in Instant Ocean with 100x vitamins(Gibco, MEM vitamin solution 100x, 11120-037). Add 500µL of the resuspended culture to an Eppendorf tube that contains 100mg of autoclaved chitin flakes (Sigma catalog number C9213) supplemented with 500µL of instant ocean. This was incubated statically for 16 hours at 30°C. To transform the bacteria, 2ug of genomic DNA (isolated

from Gene Elute Bacterial Genome DNA Kit) was added into the Eppendorf tube. This was incubated statically for 16 hours at 30°C. Cells were removed from chitin by vortexing the bacteria for 30 seconds. To isolate the successful transformants, serial dilutions of the supernatant were made into PBS and plated on appropriate antibiotics – one for transformants (usually kanamycin) and the other for total bacteria. Lastly, the transformation efficiency was calculated by dividing the number of transformants by the total number of bacteria (Meibom et al., 2005).

Chitin-independent transformation

Overnight bacterial cultures of A1552 or DL4215 overexpressing *tFoX* on the mini-Tn7 transposon were grown at 30°C and were subcultured 1:10 supplemented with 0.02% arabinose to induce the expression of *tFoX* (Scrudato and Blokesch, 2012). To induce expression, the bacteria was grown for 2 hours at 30ºC while shaking to an OD_{600} of 1. Next, 1µg of gDNA (isolated from Gene Elute Bacterial Genome DNA Kit) was added to 0.5mL of the bacteria overexpressing *tFoX* to result in uptake of the DNA over a 5 hour incubation while shaking horizontally at 30°C. To isolate the successful transformants, serial dilutions of the supernatant were made into PBS and plated on appropriate antibiotics – one for transformants (usually kanamycin) and the other for total bacteria. Lastly, the transformation efficiency was calculated by dividing the number of transformants by the total number of bacteria (Meibom et al., 2005).

Sequencing and bioinformatic analysis of hybrid DL4215

Following chitin dependent transformation of T6SS genes into *V. cholerae* DL4215, the genomic DNA was isolated (Gene Elute Bacterial Genome DNA Kit). Genomic DNA was sent for sequencing at the University of Alberta TAGC sequencing core facility. The library was constructed using the Nextera kits, and were sequenced using Illumina paired-read sequencing on a MiSeq platform. Returned reads were evaluated using software in the Geneious (Version 11.0.2) software package. First, the reads were trimmed and were mapped to reference using the Geneious Mapper to both the genomes of DL4215 and C6706. Regions mapping C6706 were scored as being acquired from the

C6706 gDNA , whereas genomic regions not mapped to DL4215 were scored as being lost by DL4215.

Identification of recombination between compatibility groups

Following chitin-independent transformation of the linear "A^1 module" marked with a kanamycin cassette, the genomic DNA was isolated (Gene Elute Bacterial Genome DNA Kit). Genomic DNA was sent for sequencing at the University of Alberta TAGC sequencing core facility. Returned reads were evaluated using software in the Geneious (Version 11.0.2) software package (Kearse et al., 2012). First, the reads were trimmed with an error probability of 0.05 and then mapped to reference using the Geneious Mapper to both the auxiliary cluster one from DL4215 and A1552, including a region of 2kb on either side. The reads that mapped to either gene cluster were then combined and used to create one contig through the Geneious de-novo assembly function. The resulting contigs were aligned using the Muscle Alignment tool.

Competition assays

Bacterial strains were grown overnight in regular LB without antibiotics, unless otherwise indicated. The bacteria were then concentrated 10x to $5x10^8$ of each bacteria (pelleting 1mL of bacteria and resuspending it into 100µL LB). The bacteria were then mixed at 1:1 ratio, unless indicated otherwise. Twenty-five microliters of the mixed bacterial culture was spotted onto prewarmed LB agar. Prewarmed LB agar was done by leaving the lids ajar at 37 °C for one hour. The incubation was left at 37°C for 4 hours, unless indicated otherwise. Bacterial spots were harvested into 1mL LB and vortexed for 30 seconds. The surviving prey and predator were measured by serial dilution and selective growth on agar containing antibiotics to select for the individual bacteria.

Construction of PA1849 genome

Intestinal sample was acquired from the Mutter Museum of the College of Physicians in Philadelphia, PA, USA. Using the MycoArray (now Arbor Biosciences) MyBaits technology, the sample was enriched for genes from the *V. cholerae* genome as

well as additionally for the T6SS of *V. cholerae* and libraries were constructed using Illumina Nextera Kits before sequencing on the Illumina platform.

Raw PA1849 FASTQ files were QC validated with FASTX-Toolkit (v0.0.14) to assess Phred quality score and nucleotide distribution over reads (Andrews, 2010). Satisfactory files were trimmed using cutadapt (v1.16). Adaptors were removed from paired end read files and ends were trimmed with a Phred quality score cutoff of 20 (Bolger et al., 2014). Reads below a minimum length cutoff of 25 nucleotides were removed. Trimmed paired end FASTQ files were aligned to a reference FASTA with the Burrows-Wheeler Aligner (bwa v0.7.17) MEM algorithm. Reference FASTA files were constructed by concatenating genomic islands extracted from N16961 (RefSeq NC_002505.1, NC_002506.1) or O395 (PacBio sequence of laboratory stock) with 100 nucleotide spacers between each region (Li and Durbin, 2009). Generated SAM files were sorted and marked for duplicates with Picard Tools (v2.17.11) to generate sorted, unique BAM files (Li et al., 2009). BAM files were indexed with Picard Tools (Walker et al., 2014). Variants were called against the constructed reference FASTA and consensus sequences were generated with Pilon (v1.22) (Walker et al., 2014). PA1849 consensus sequences were aligned to N16961 and O395 reference sequences using the progressiveMauve algorithm in Geneious (v10.0.9) assuming co-linear genomes (Darling et al., 2010). Genome coverage BED files were generated from sorted, unique BAM files with bedtools (v2.27.1), and coverage plots were generated using the ggplot2 package (v2.0.0) in R (v3.3.2) (Quinlan and Hall, 2010).

Allelic exchange in V. cholerae

Allelic exchange was used to knock out, or knock in genes (Metcalf et al., 1996). A construct was created that contains 750 base pairs of overlapping DNA on either side for recombination. In between the overlap was either a scar of 30bp of the gene to knockout, or the gene to be inserted. This construct was ligated into the suicide vector, pWM91. Six primers (A-F) were used to make and verify this construct. A is a forward primer than binds between 750 and 800 base pairs upstream of the target gene. D is a reverse primer binds between 750 and 800 base pairs downstream of the target gene. Both primers contain the same restriction site. If the goal is to delete the target gene, C is a primer that is complimentary to the 4 nucleotides upstream the target gene, followed by the first 15

nucleotides of the target gene and the last 15 nucleotides of the target gene, and ends with the 4 nucleotides downstream of the gene of interest. The B primer is a reverse complement of the C primer. E and F primers are outside of the A and D primers and function to screen knock-outs.

First, two PCRs with primers A-B and C-D make the arms. Second, the two arms are merged through overlapping PCR, making the A-D fragment. The construct is then ligated into pWM91. This is then transformed into *E. coli* DH5α λpir, and then finally into *E. coli* SM10 λpir.

Mating and allelic exchange

In short, pWM91 with the knock out or knock in construct allows allelic exchange through two rounds of selection. After conjugation into the *V. cholerae* strain, the first round of selection is the incorporation of pWM91 into the genome of *V. cholerae.* This is done by mating the plasmid in, and selecting on ampicillin and an antibiotic that *V. cholerae* is resistant to. The second round of selection is the selection for the "cross-out" This selection is the removal of the pWM91 plasmid while the retention of the insert to either exchange alleles or delete the target gene. This selection works as the pWM91 plasmid encodes a *sacB* gene that metabolizes sucrose into a toxic byproduct preventing growth on chitin.

First, to conjugate pWM91 into the *V. cholerae* strain, the initial selection is mating *E. coli* SM10 λpir with the *V. cholerae* strain. Grow both strains overnight in lawn on LB agar plates – with appropriate antibiotics. Next, to mix the two bacteria , harvest half a plate of each bacteria and mix them on a LB agar plate without selection. After 6 hours, resuspend the bacteria into LB and make serial dilutions. Plate these dilutions on LB agar plates with 2 antibiotics – ampicillin and an antibiotic to select for *V. cholerae* while killing *E. coli.* This is streptomycin or rifampicin. Four colonies are picked from these plates and inoculated in 1mL of LB without selection. Four hours later these bacteria are serially diluted onto sucrose plates (1% tryptone, 0.5% yeast, 10% sucrose, 2% agar). These plates must be left at 18-20°C for two days. Bacteria encoding the plasmid, and by extension *sacB* will be unable to grow on sucrose through metabolizing it into a toxic byproduct. 94 colonies are picked from the sucrose plates and colony PCR is performed with the E and F

primers. Colonies with the deletion band, as well as susceptibility to ampicillin likely have the knockout. The final test is to sequence the scar to make sure no point-mutation were accumulated.

Infant mice experiments

To determine if T6SS-mediated killing happens *in vivo*, we conducted animal experiments using the suckling mouse model for cholera (Klose, 2000). 5-day old mice were inoculated intragastrically with a 1:1 mix of a lacZ-positive and lacZ-negative strain at a total number of 10^9 bacteria/50μL Serial dilutions of the input mix were prepared to determine the exact number of bacteria by CFU count. The mice were kept over-night and sacrificed to remove the small intestine. The tissue was resuspended in PBS and homogenized. Serial dilutions of the homogenate were prepared and plated onto LB plates supplemented with streptomycin and X-Gal (40ug/ml) to
determine the ratio of bacteria that colonized the small intestine.

For the experiments between C6706 and the environmental strains was performed so the total input of bacteria was 10^8 of 10^9 as mortality of the mice was deemed too great. Instead of X-gal, antibiotics were used to distinguish between the strains. The experiment was approved by the respective Ethics Committee at the University of Alberta. . In parallel, this experiment was performed *in vitro* by adding 50 μL of *V. cholerae* mixture (in 2.5% sodium bicarbonate buffer) to 5 mL LB. Cultures tubes were rolled overnight at 37°C. Serial dilutions of the *in-vitro* and *in-vivo* samples, and the bacterial inoculum, were plated on LB agar plates supplemented with Sm and 5-bromo-4-chloro-3-indolyl-β-D-galactopyranoside (X-gal) to count predator and prey strains. The competitive index was calculated by taking the input ratio (mutant/wild-type) and dividing it by the output ratio (mutant/wild-type).

Mucin column assays

Columns contained 500 μl of 3% (wt/vol) bovine submaxillary mucins (Sigma, St. Louis MO) or 3% (wt/vol) of Difco gelatin (BD, Mississauga ON) in Krebs-Ringer Tris buffer (7.5g of NaCl, 0.383g of KCl, 0.318g of $MgSO_4$ and 0.305g of $CaCl_2$ in 1 litre of water). Columns were allowed to settle for 1 h at room temperature. For viability tests,

columns were prepared in 1.5 ml reaction tubes. Approximately 1×10^8 mid-logarithmic phase bacteria (20 µL) were loaded on top of each column and incubated for 1 h or 2 h at 37°C. One hour after adding supplementing bile acids/amino acids, colony-forming units (CFUs) were determined by plating serial dilutions on LB agar plates with appropriate antibiotics. For killing tests, columns were prepared in 1.5 ml reaction tubes. Indicated predator and prey strains were loaded on top of each column at a 10:1 ratio and incubated for 2 h at 37°C. CFUs/ml were determined by plating serial dilutions on LB agar plates with appropriate antibiotics.

Bile salt competition assays

Competition assays were performed as above. Sodium deoxycholate, sodium cholate, taurodeoxycholate, glycodeoxycholate, taurocholate, glycocholate, and taurine were obtained from Sigma (St. Louis MO). Glycine was obtained from Thermo Fisher Scientific (Waltham MA). Difco™ Bile Salts No.3 was obtained from BD (Mississauga ON).

qPCR

Total RNA was extracted using the TRizol reagent (Invitrogen) according to the manufacturer's instructions. RNA concentrations were determined using a NanoDrop spectrophotometer (Thermo Scientific). 1µg of RNA from each sample was treated with DNase I (Invitrogen), and transcribed into cDNA using the SuperScript III Reverse Transcriptase (Invitrogen). Quantitative real-time PCR (qPCR) was performed with SensiFAST SYBR No-ROX Kit (FroggaBio), using the CFX96 Real-Time System (Biorad). Thermocycling parameters were as follows: 95°C for 2 min, followed by 40 cycles of 95°C for 15 s and 60°C for 1 min, followed by a melting curve. Primers against the different genes of interest were designed using the PrimerQuest software from Integrated DNA Technologies (IDT). Primers were tested for performance in qPCR with a cDNA concentration gradient, and those with slopes between −3.3 and −3.7, efficiency of ∼1.0, and R^2 of ∼1.0 were used in the qPCR studies (primer sequences used in the study are summarized in Table 2). The expression levels of the different targets in relation to the endogenous 16S rRNA gene control was determined by the $2^{-\Delta\Delta CT}$ method using the CFX

Manager Software (Biorad). The relative quantification (RQ) values of all samples were normalized against the expression of the 16S control for each target.

Target	Direction	Sequence
16S rRNA gene	F	GTG TAG CGG TGA AAT GCG TAG AG
	R	GCG TGG ACT ACC AGG GTA TCT AAT
hcp	F	TGT GAA ATG CCA CAC TGC CAA GAC
	R	GCG TTA ACG TGG TCC CAA GTG ATT
tseL	F	GTT AGA GCT AGA GTT TCG GAG TG
	R	GTG GTT TGC GTG TAT GTG TTA G
vasX	F	GAG TCA GAA ACT GGG TGG ATT AG
	R	GTG CGA CCT TAT AGC GGA TAT T
vgrG-3	F	CTC GTG GTA CAA GCC AAT CA
	R	AGT GAT GTG AGC GGG AAT AAG
vasH	F	TAT CTG CCA CAC AGC TCA ATC
	R	CAA GGT GAT CGG ATA CTG GAA TAG

Table 2-2. qPCR primers.

Growth curves

Overnight cultures of *V. cholerae* were diluted 1:100 in plain LB broth or LB supplemented with various concentrations of deoxycholic acid, glycine or taurine. OD600 readings were recorded every hour. The resulting OD600 was plotted versus time, and the linear portion of the graph was used to calculate a slope over the linear portion by dividing the change in optical density by the duration of the linear portion (Provenzano and Klose, 2000). This slope was then compared to the bacteria's slope when grown in plain LB to determine its relative growth rate

Western Blot

Overnight cultures of indicated bacterial strains were diluted in LB broth supplemented as indicated and grown to mid-logarithmic phase (OD_{600} ~ 0.6). Samples were subjected to SDS-PAGE and analyzed by western blotting using a mouse monoclonal antibody against DnaK (1:15000) (Stressgen Bioreagents, Victoria BC) (Sigma, St. Louis MO), or a rabbit polyclonal antibody against Hcp (1:500). For detection, secondary antibodies goat anti-rabbit-horseradish peroxidase and goat anti-mouse-horseradish peroxidase were used (Santa Cruz Biotechnology, Santa Cruz CA).

Microscopy to determine T6SS activity

Bacteria for the microscopy was similar to for a T6SS competition assay. To visualize the T6SS, the *vipA* gene of 2740-80 was tagged with *sfGFP*. *V. cholerae* was grown on plates overnight on LB agar plates either supplemented with DOC, taurine, or cholate as a control to influence the magnitude of the T6SS. Next, the bacteria were suspended in LB containing the bile salts at an OD_{600} of 1.0. Instead of spotting the bacteria on a LB-agar plate, the bacteria was spotted onto a 1% agarose pad, as it has a lower optical density and left to settle on this pad for 30 minutes so they are resting on the surface. After this incubation, the cells were imaged for ten minutes using the Super Resolution OMX microscope. Three frames were chosen at random and the number of extended T6SS tubes were counted, as well as the total number of cells. The activity of the T6SS was judged based on the number of T6SS tubes observed over the course of 100 bacteria.

Fly husbandry

All experiments were performed with virgin female flies. w^{1118} flies were used as wild type. The *imd* $^{-/-}$ (*imd[*Ey08573) flies have previously been described (Buchon et al., 2010a). Flies were raised on standard corn meal medium (Nutri-Fly Bloomington Formulation, Genesse Scientific). Germ-free flies were generated by raising adult flies on autoclaved standard media supplemented with an antibiotic solution (100 µg/mL ampicillin, 100 µg/ml metronidazole, 40 µg/mL vancomycin dissolved in 50% ethanol and 100 µg/mL Neomycin dissolved in water) to eliminate the microbiome from adult flies. CR flies were raised on autoclaved standard cornmeal medium.

V. cholerae infection of the fly

Virgin female flies were separated from male flies after eclosion and placed on autoclaved standard Bloomington food for 5 days at 29°C. Flies were starved 2 hours prior to infection. Ten flies were then placed in a vial containing a cotton plug soaked with *V. cholerae* (OD_{600} of 0.125) in groups of 5 per experimental group, resulting in 50 flies for each survival curve. Dead flies were counted every 8hours for the first 100 hours, and every 24 hours thereafter.

Generation of gnotobiotic Drosophila

Virgin females were raised on selective medium for 5 days at 29° C. On day 5 of antibiotic treatment, a fly from each group to be mono/ploy-associated was homogenized in MRS broth and plated on MRS and GYC agar plates to ensure eradication of pre-existing microbes. Flies were starved in sterile empty vials for 2 hours prior to bacterial association. Lab isolate *Acetobacter pasteuranius* was grown in Mannitol broth at 29°C with shaking 2 days prior to association. Lab isolates *Lactobacillus brevis* and *Lactobacillus plantarum* were grown in MRS broth at 29°C 1 day prior to association. For mono-associations, the OD_{600} of bacteria liquid cultures was measured and then the culture was spun down and re-suspended in in 5% sucrose in PBS to final OD_{600} of 50 For poly-associations, bacterial cultures of *Ap, Lb,* and *Lp* were prepared to an OD_{600} of 50 in 5% sucrose in PBS as described above. The bacterial cultures were then mixed at a 1:1:1 ratio. For all bacterial associations, twelve flies/vial were associated with 1mL of bacterial suspension on autoclaved cotton plugs. Flies were fed the bacteria sucrose suspension for 16 hours at 29°C and then kept on autoclaved food for 5 days prior to infection. CR and GF flies were given mock associations of 1ml of 5% sucrose in PBS for 16 hours at 29°C. To ensure mono-association or GF conditions, respective flies were homogenized in MRS broth and plated on MRS or GYC agar plates.

Fly Fecal Assays

Flies were infected as described above except that the infection culture contained Erioglaucine disodium salt (0.1%). After 24 hours of infection, flies were placed in a petri dish lined with a filter paper. The number of new blue spots were counted every hour. After 4 hours, the filter paper was imaged and the size of the spots was calculated with CellProfiler (3.0.0, Broad Institute).

V. cholerae shedding assay.

Flies were infected as above. After a 24-hour infection, individual flies were placed in a 96 well plate where each well had been lined with filter paper soaked in PBS + 5% sucrose. After 4 hours, the filter paper was vortexed vigorously for 15 seconds in 1mL of

LB and serial dilutions were made on LB + Streptomycin. CFUs were counted the next day.

Transmission Electron Microscopy

Flies were washed with 95% ethanol and dissected into PBS. Posterior midguts were immediately excised and placed into fixative (3% paraformaldehyde + 3% glutaraldehyde). Fixation preparation, contrasting sectioning, sectioning, and visualization were performed at the Faculty of Medicine and Dentistry Imaging Core at the University of Alberta. Midgut sections were visualized with Hitachi H-7650 transmission electron microscope at 60Kv in high contrast mode.

Colony forming units per fly

At indicated time points 25 flies per infection group were collected and placed into successive solutions of 20% bleach, distilled water, 70% ethanol, distilled water to surface sterilize and rinse flies respectively. These 25 flies were then randomly divided into groups of 5 and mechanically homogenized in LB broth. Fly homogenate was then diluted in serial dilutions in a 96 well plate and 10μL spots were then plated on either MRS agar (to select for *Lactobacillius*) GYC agar (to select for *Acetobacter*) and LB agar supplemented with 100 μg/ml streptomycin (to select for *Vibrio cholerae*).

RNAseq of intestinal progenitor cells

To isolate stem cells for RNAseq, first the fly guts were dissected. The flies used were w^{1118} esg^{ts}*-GFP* fly line that expresses GFP in intestinal progenitor cells through the escargot transcription factor. Dissected guts are placed in a PBS solution with 4mg/mL Elastase to aid in dissociation of the cells from the gut along with mechanical disruption by pipetting up and down. Next, we spun down the mixture to pellet the cells. The cells were washed with PBS. Next, the cells were run through the Attune NxT flow cytometer to isolate GFP position cells. The cells were collected directly into Trizol and RNA was isolated by manufactures instructions.

The RNA was sent for library preparation and RNA sequencing at the sequencing facility in the Lunenfeld-Tanenbaum research institute. PolyA selection was used to isolate

eukaroyic RNA reads, and the mRNA was placed on a HiSeq3000 lane. The resulting reads were analyzed by the following pipeline. First, the reads were analyzed for quality by FastQC (Andrews, 2010). Next, the reads were trimmed using Trimmomatic and the reads were aligned to the *Drosophila melanogaster* genome (bdgp6_tran) using Hisat2 (Bolger et al., 2014; Kim et al., 2016). Samtools was used to convert, sort and index the resulting files (Li et al., 2009). Next, reads were counted using RsubREAD (Chen, Lun, & Smyth, 2005.). EdgeR was used to generate a PCA plot and normalize the counts, and provide p-values for analysis (Chen et al., 2006).

Chapter 3: Pandemic strains encode a horizontally acquired unique compatibility group

All figures are the work of Benjamin Kostiuk

Figures 1-3 were published in :

Brooks, T.M., Unterweger, D., Bachmann, V., Kostiuk, B., and Pukatzki, S. (2013). Lytic activity of the Vibrio cholerae type VI secretion toxin VgrG-3 is inhibited by the antitoxin TsaB. J. Biol. Chem. *288*, 7618–7625.

Figures in the above paper which I did not perform the majority of the work for will be referenced rather than having the figures shown.

3-1 Introduction

V. cholerae's T6SS-dependent competition is important for bacterial competition on chitin and in the host intestine (Borgeaud et al., 2015b; Zhao et al., 2018). There is evidence that this competition is directed at both *V. cholerae* strains and commensal/environmental bacteria of different species (Fu et al., 2018; Zhao et al., 2018). Our lab showed that while some *V. cholerae* strains were able to coexist, others were not (Unterweger et al., 2014a). This difference was due to the compatibility group of the *V. cholerae* strain, the combination of effector and immunity genes that are encoded. All El Tor pandemic strains are able to coexist as they share the AAA compatibility group (Kirchberger et al., 2017b; Unterweger et al., 2014a). "AAA" indicates that the strain encodes *tseL* in auxiliary cluster 1, *vasX* in auxiliary cluster 2, and *vgrG-3* in the main cluster. When referring to an A effector, the subscript will indicate which cluster I am referring to A^1 for an A in auxiliary cluster 1, A^2 for an A auxiliary cluster 2 and A^M for an A effector in the main cluster. These shared effector modules may be yet another advantage of the T6SS of El Tor strains. We have observed dominance of AAA strains in competition assays, where all other studied compatibility groups are killed by V52 – an AAA strain with a constitutively active T6SS (Unterweger et al., 2014a). However, these studies do not account for differences beyond the different compatibility groups such as the strains also being extremely different on a genetic and phenotypic level. Additionally, the strains could differ at the level of T6SS expression, so it is incomplete to attribute the competition difference to simply the presence or absence of effectors.

V. cholerae is naturally competent on chitin, through the expression of *tfoX,* allowing DNA to be taken up into the bacteria and recombined into the *V. cholerae* genome (Borgeaud et al., 2015b; Thomas et al., 2017). Through this mechanism, it is postulated that compatibility groups can be horizontally acquired through recombination (Thomas et al., 2017). This observation was first made in our lab by the presence of a conserved 99-bp

stretch of DNA within the T6SS adaptor genes (*tap-1)* that is shared with all sequenced *V. cholerae* strains (Unterweger et al., 2015). *tap-1* is encoded between the structural components of auxiliary cluster 1 (*hcp-1* and *vgrG-1)* and the effector module, *tseL* and *tsiV1*. Another piece of evidence that the genes are horizontally exchanged, is that there is no correlation between effector/immunity repertoire and the position on the phylogenetic tree (Kirchberger et al., 2017b; Unterweger et al., 2014a). Lastly, is the orphan immunity gene Orphan immunity genes are immunity genes encoded by *V. cholerae* that do not have a cognate effector (Kirchberger et al., 2017b). This suggests horizontal transfer, as the previously encoded DNA still remains, the orphan immunity gene is encoded directly after *tsiV1*. Although orphan immunity genes are not known to be active, they are expressed with the rest of the T6SS gene cluster on chitin (Scrudato and Blokesch, 2012). Interestingly, El Tor strains despite being AAA, have a C immunity gene in auxiliary cluster one as an orphan immunity gene (Kirchberger et al., 2017b). This observation indicates that they might have once had a C effector in that locus, and provides insight into the mechanism of exchange. There is an advantage to switching effectors while maintaining the original immunity gene. When a bacterium picks up a new effector, they are likely in the minority and keeping the original immunity gene prevents them from being immediately killed by their sister bacteria.

A recent study explored the concept of compatibility group switching on chitin (Thomas et al., 2017). They demonstrated that when pandemic strains acquired effectors from environmental strains, they were able to outcompete their parental strain. This is a different result than we have seen as we found the pandemic effectors to be superior in kin strains, however there are differences between our studies. The biggest difference is the source of transferred DNA. The Hammer lab used genomic DNA to enable the exchange of effectors, which could have also facilitated the exchange of other factors that could be responsible for the advantage (Thomas et al., 2017). Additionally, while the researchers did a thorough job comparing the competitive behaviour of their hybrid strains, they did not investigate the mechanism of horizontal gene transfer.

Altogether, we hypothesize that El Tor *V. cholerae* strains acquired *tseL* (A^1) through recombination within *tap-1* while retaining their original C immunity gene and that the acquired AAA effectors are superior to those that exist in the environment. In this chapter,

I biochemically dissect one of the effectors encoded by El Tor strains, VgrG3 (A^M), demonstrate the ability of T6SS genes to be acquired by incompatible bacteria and begin to uncover the mechanism of effector module exchange. Finally, I demonstrate the dominance of AAA effectors over select environmental counterparts.

3-2 VgrG-3 is a peptidoglycan degrading effector that is inhibited by TsiV3

To study the antibacterial activity of VrgG-3 I took a biochemical approach and purified VgrG-3, the C-terminus of VgrG-3 and its cognate immunity TsiV3. These were purified by expressing the proteins with a 6x His tag in *E. coli* BL21DE3*, after expression conditions were found a full-scale expression was done. The constructs were purified by nickel affinity and eluted with increasing concentrations of imidazole. The purified proteins could then be used for various downstream assays (Brooks et al., 2013).

As bioinformatics analysis suggests that the C-termini of VgrG3 contains a peptidoglycan-degrading domain, we performed zymography to look for peptidoglycan degrading activity (Brooks et al., 2013). A zymogram is an SDS-PAGE gel that contains purified peptidoglycan (Strating and Clarke, 2001). The gel was run so the gel separates the protein based on size. After this, the SDS was allowed to diffuse out of the gel by washing in water. Next, the gel was placed in a buffer that promotes enzymatic activity for 24 hours at 37C. The gels were then stained with methylene blue to stain the peptidoglycan blue. Any area that does not stain blue had the peptidoglycan degraded (Strating and Clarke, 2001).

I ran the supernatant of V52, V52Δ*vgrG-3*, recombinant VgrG-3, recombinant C-terminal VgrG-3 as well as another T6SS effector as a control – recombinant VasX – on an acrylamide gel impregnated with peptidoglycan (Figure 1A,B). I saw that V52's supernatant was able to degrade peptidoglycan at the size correlating with the C-terminus of VgrG-3, 115kDa (Figure 1A). When *vgrG-3* was deleted, there was no peptidoglycan degrading activity. This suggests that VgrG-3 is the sole enzyme in the supernatant that degrades peptidoglycan (Figure 1A). Recombinant VgrG-3 (115kDa) and the recombinant C-terminus (30kDa) both caused peptidoglycan clearing, further confirming the enzymes ability to degrade peptidoglycan (Figure 1B).

I then repeated this zymogram but incubated the gel in different buffers during the enzymatic phase, to gain an understanding of the conditions needed for optimum enzymatic function (Figure 2AB). I tested a variety of divalent ions, and pHs (Figure 2AB). I found that that between a pH 5 and 9, the enzymatic activity was strongest, as well as in the presence of $CaCl_2$ (Figure 2AB). In contrast, the activity was inhibited by other metals, such as zinc, and at the basic pH of 10 (Figure 2AB). The range of pHs where the enzyme is active suggests the T6SS effector could be active in the host.

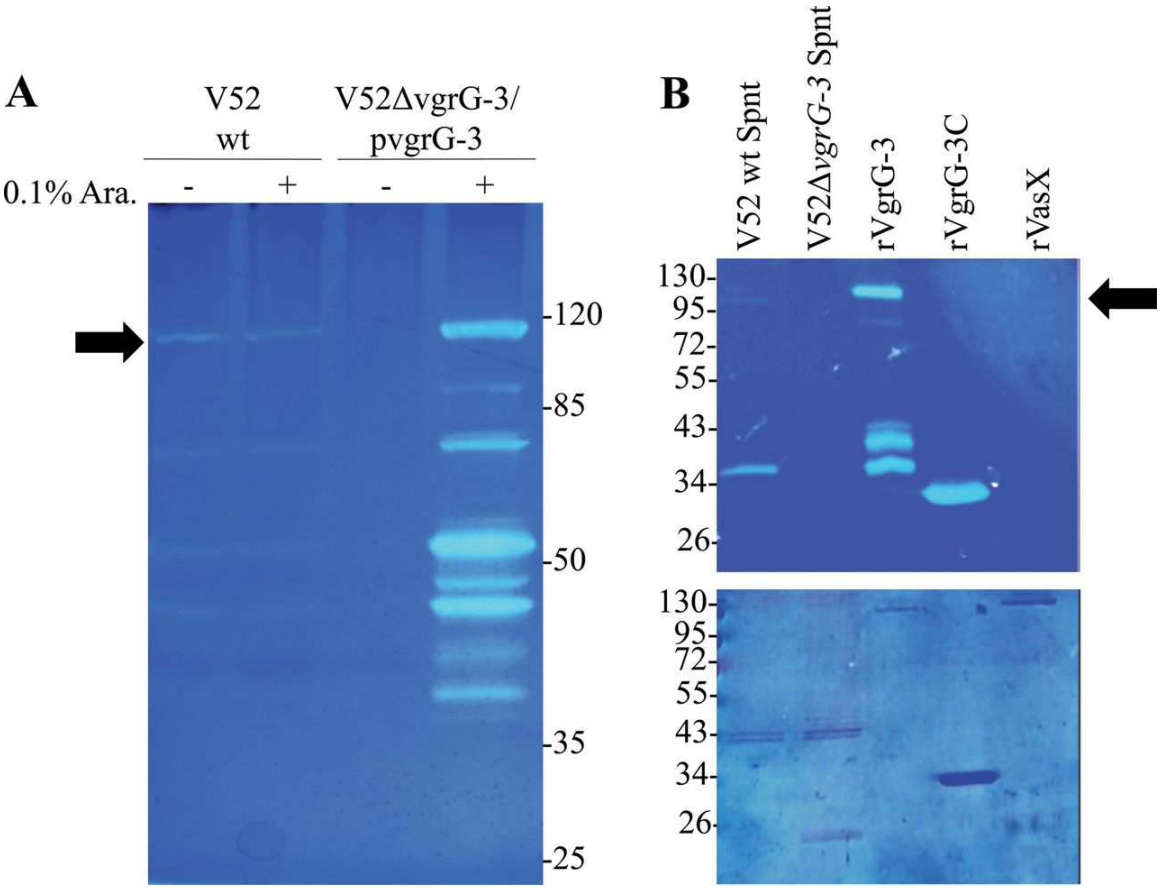

Figure 3-1. **VgrG-3 degrades peptidoglycan**. (**A)** Total cell lysates of V52 wild type (wt), and V52Δ*vgrG-3/pvgrG-3* under inducing and non-inducing conditions (+/- 0.1% arabinose (Ara.)) were analyzed for peptidoglycan degradation by zymography. Protein samples were run on SDS-PAGE containing 0.1% *E. coli* peptidoglycan and stained with methylene blue to visualize zones of clearing (left panel). The arrow indicates the molecular weight of VgrG-3. (**B)** zymogram analysis of culture supernatants and of purified VgrG-3 constructs and analyzed by zymography as described in A (right panel). The arrow indicates a VgrG-3 degradation product with lytic activity.

To measure peptidoglycan degradation in another way, we added 10ug of purified recombinant C-terminal VgrG-3 to 2mg of purified peptidoglycan. Over 50 minutes, there was a 40% reduction in optical density of the peptidoglycan indicating degradation of peptidoglycan (Figure 3A). This was similar levels seen when this assay was performed with lysozyme (Figure 3A). To test the ability of TsiV3 to act as the immunity protein, we coincubated the immunity protein with VgrG-3 before adding the protein mixture to the peptidoglycan. With both effector and immunity protein present we saw an intermediate reduction in optical density, approximately 25%, indicating that the immunity protein reduced the peptidoglycan degradation. Importantly, neither buffer alone nor immunity protein alone caused a change in optical density. This demonstrates that TsiV3 acts as an immunity protein to VgrG-3.

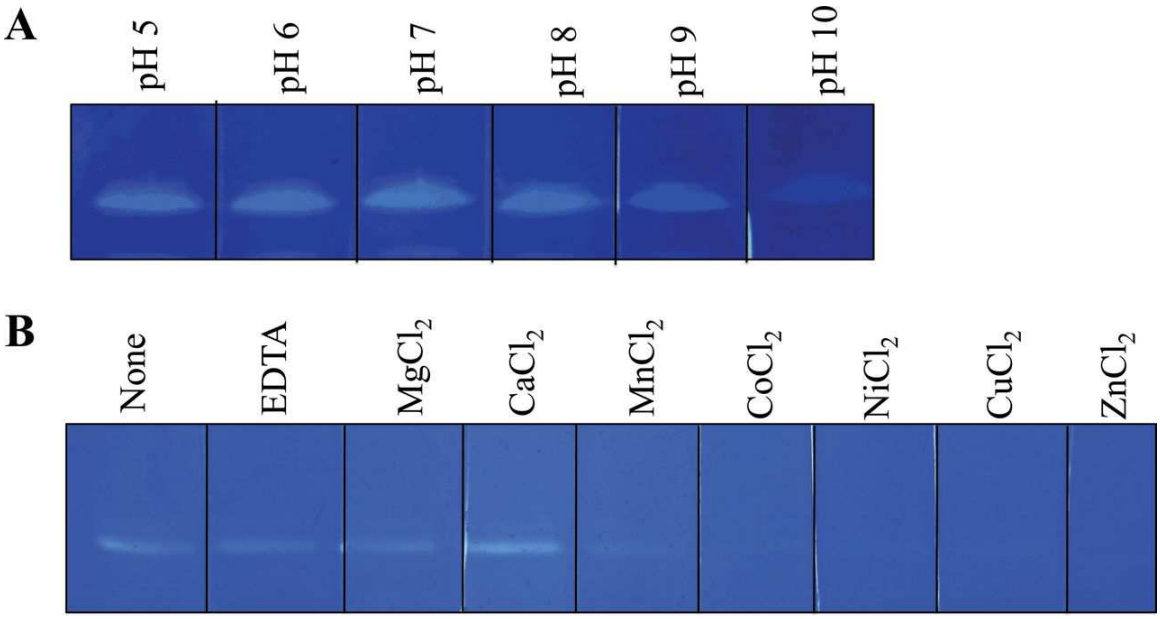

Figure 3-2 . **Zymogram analysis demonstrating the effects of pH and divalent cations on lytic activity of VgrG-3C**. (A) VgrG-3C within a SDS polyacrylamide gel containing 0.1% (w/v) E. coli peptidoglycan was renatured in 25 mM Tris, pH 7.0, 0.1% Triton X-100 with the indicated additive at a concentration of 10 mM. (B)The atomic number of the divalent cations increases from left to right.

Next, we investigated if the activity identified above was capable of causing cell death in *E. coli.* To perform this assay, we suspended a mid-log culture of *E. coli* in Tris-HCl and added the same purified proteins as the previous assay and measured the decrease in optical density as a measure of cell lysis (Figure 3B). Under natural T6SS conditions,

the T6SS sheath is responsible for delivering the toxins to the inner membrane. To mimic that in this assay, we treated *E. coli* with Polymyxin B to permeate the outer membrane,

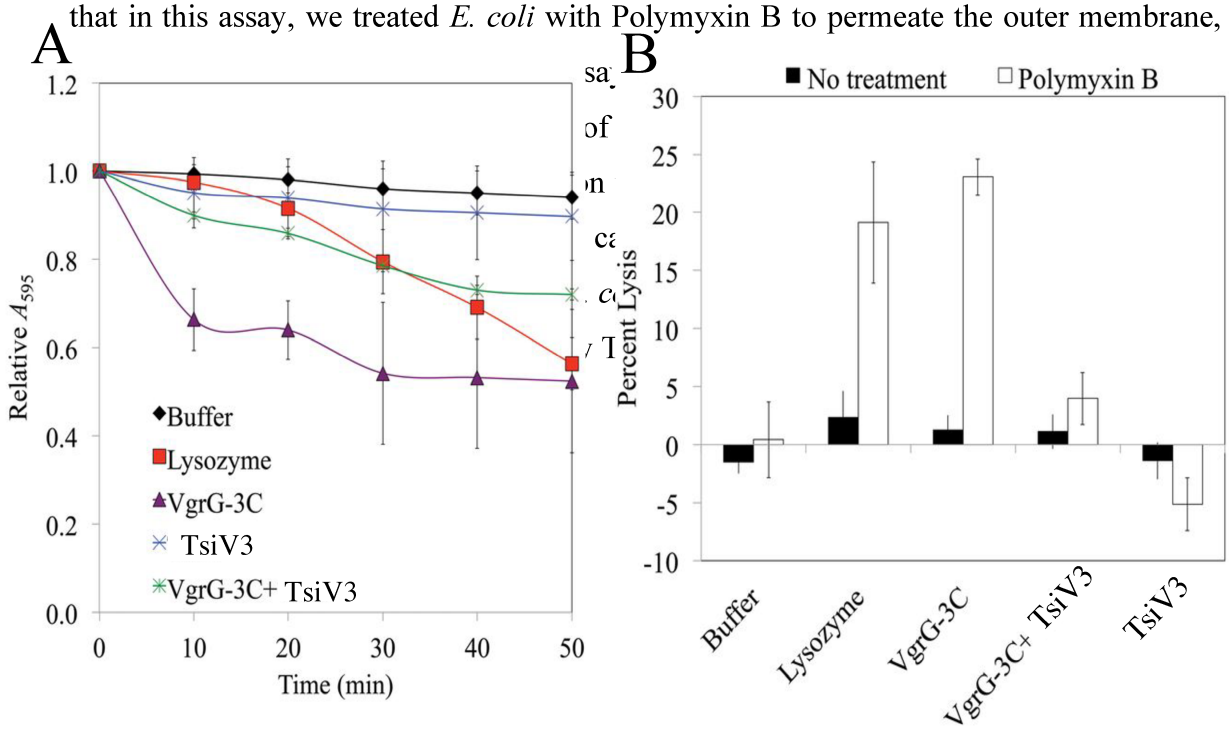

Figure 3-3. **Addition of exogenous VgrG-3 C-terminal domain (VgrG-3C) leads to lysis of *E. coli* in the presence of polymyxin B and degradation of PG**. **(A)** 10 ug of purified recombinant VgrG-3C or TsiV3 were added to 2 mg *E. coli* peptidoglycan and the A600 was monitored over 50 min in a microplate reader at 37 °C. For VgrG-3C TsiV3, 10 g of each protein were mixed together and incubated on ice for 10 min prior to adding to the substrate. Bars represent the standard error of six data points from two experiments. **(B)** mid-logarithmic phase *E. coli* were resuspended in 20 mM Tris-HCl, pH 7.0, and incubated with purified proteins, and the A600 was measured at 0 and 5 min. Permeabilization of the outer membrane with 40 grams/ml polymyxin B led to lysis in the presence of lysozyme or VgrG-3C. Preincubation of VgrG-3C with a 3-fold molar excess of the immunity protein TsiV3 for 10 min on ice protects against this effect. Results represent the average of four independent experiments each performed in duplicate. Bars represent the standard error of all data points.

3-3 T6SS and non-T6SS genes can be horizontally acquired without preference

El Tor *V. cholerae* strains become competent when grown on chitin. This has been shown many ways, but traditionally, an antibiotic cassette (in our case kanamycin) is integrated into a defined locus in the genome, and that genome is purified and "fed" to *V. cholerae* grown on chitin. *V. cholerae* is then able to be transformed on chitin at a frequency of 10^{-4}. We hypothesize that T6SS genes can also be exchanged in such a manner. To do this, we isolated 1ug gDNA from our C6706 transposon library, specifically 3 strains of C6706 with a transposon in one of *tseL tsiV2* or *clpV*. These were chosen because they are spread amongst all three T6SS gene clusters, and contain an effector, immunity and structural gene component. After feeding this DNA to A1552 – which is highly related to C6706 –grown on chitin, the kanamycin cassette was picked up in all cases at relatively equal frequencies, between $8.5x10^{-5}$ to $1.0x10^{-4}$ (Table 1). This demonstrates that T6SS components can be acquired via chitin mediated natural competence and that all clusters and T6SS components appear to be acquired at equal rates (Table 1).

Recipient	Donor DNA	T6SS Gene Name	Transformation Frequency	Standard Deviation
A1552	C6706	*clpV*	1×10^{-4}	2.2×10^{-5}
A1552	C6706	*tseL*	8.5×10^{-5}	2.6×10^{-5}
A1552	C6706	*tsiV2*	8.7×10^{-5}	2.7×10^{-5}
A1552	C6706	*malT*	2.9×10^{-5}	3.0×10^{-5}
A1552	C6706	*tcpI*	7.3×10^{-5}	3.4×10^{-5}
A1552	C6706	VCA0419	8.8×10^{-5}	3.5×10^{-5}
A1552	No DNA	-	0	0

Table 3-1. **Recombination efficiency of type-six and non-type-six genes in naturally competent A1552.** A1552 was grown on chitin resuspended in DASW for 24 hours, before 1ug of gDNA marked with a kanamycin cassette was added. After an additional 24 hours, the mixture was plated on kanamycin + rifampicin plates to look for transformants and rifampicin plates to look for the total bacteria. A transformation efficiency was calculated by dividing the transformants by the total number of bacteria. Three genomes with kanamycin cassetes in T6SS genes (*clpV, tseL* and *tsiV2)* were chosen as they are each in a different T6SS gene cluster. The three non-T6SS genes were chosen (*malT, tcpI,* and

VCA0419) as they were matched in GC% content, length and chromosome with one of the T6SS genes.

Next, we looked to see if there was a difference between rates of acquisition for T6SS genes and non-T6SS genes. As we hypothesized that T6SS module exchange follows T6SS-dependent release of gDNA, we thought there might be a mechanism in place that facilitates T6SS genes specifically. To investigate this, we picked genes to match the T6SS genes' characteristics, specifically genes of a similar length, a similar GC content and on the same chromosome. Both T6SS and non-T6SS genes showed similar transformation and recombination rates (Table 1), indicating it is unlikely that there is a preference for acquiring T6SS genes over non-T6SS genes

Next, we tested a 100-fold range of gDNA. Our rationale was that 1ug/mL might be saturating the system and any difference in the rates of acquisition might be masked by the over-availability of DNA. To that end, we used 1ug/mL, 0.5ug/mL, 0.33ug/mL and 0.11 ug/mL. While we did see a dose dependent effect on the concentration of DNA, indicating that the concentration of DNA is rate limiting, we did not see a difference between *tsiV2* or three matched genes, substantiating that there might not be a preference in acquisition (Figure 4).

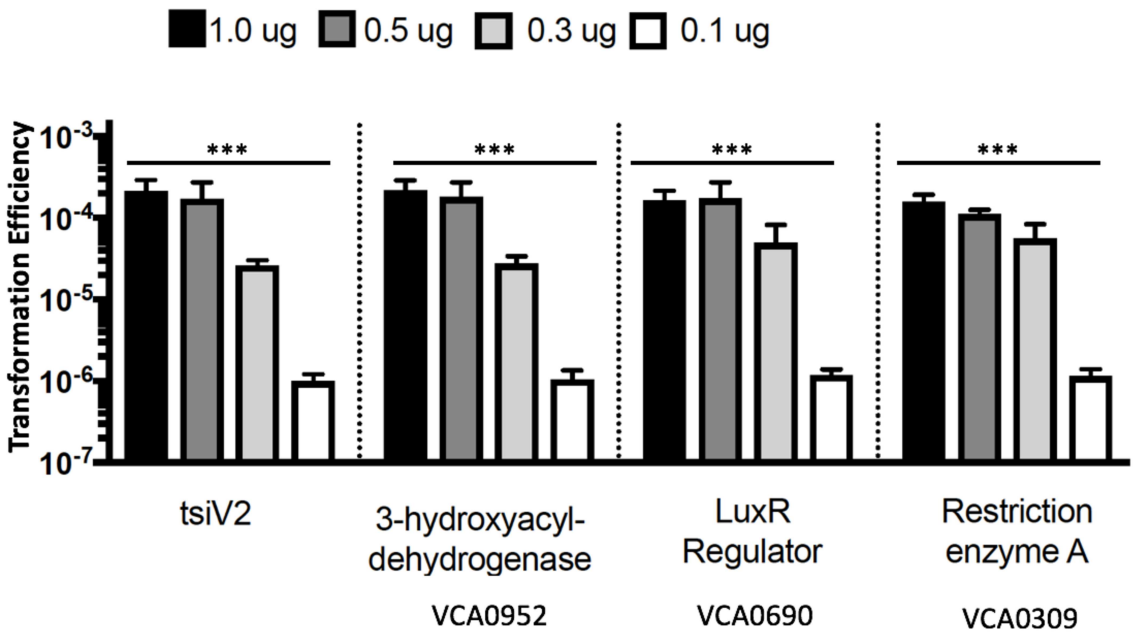

Figure 3-4. **Recombination efficiency of type-six and non-type-six genes in naturally competent A1552 at a variety of concentrations.** A1552 was grown on chitin resuspended in DASW for 24 hours, before 1ug of gDNA marked with a kanamycin cassette was added. After an additional 24 hours, the mixed was plated on kanamycin + rifampicin plates to look for transformants and rifampicin plates to look for the total surviving bacteria. A transformation efficiency was calculated by dividing the transformants by the total number of bacteria. One T6SS gene, *tsiV2,* was used with three genes (VCA0952, VCA0690 and VCA0309) for comparisons at a similar length and GC%. *** represents a p-value of < 0.001. Means are shown of 6 replicates over 3 experiments.

All of the studies of natural competence in *V. cholerae* have specifically looked at El Tor strains, so we decided to extend this to investigate classical and environmental strains. While AM19226 and the classical O395 were not able to acquire DNA through chitin-mediated transformation, we found one environmental strain, DL4215, that was able to acquire foreign DNA. Although a small sample size, DL4215 acquired foreign DNA to a significantly lesser extent than A1552, integrating the kanamycin module at around 100x less efficiency (Figure 5). Testing more isolates is critical to determining if this difference is a common theme between El Tor and environmental isolates.

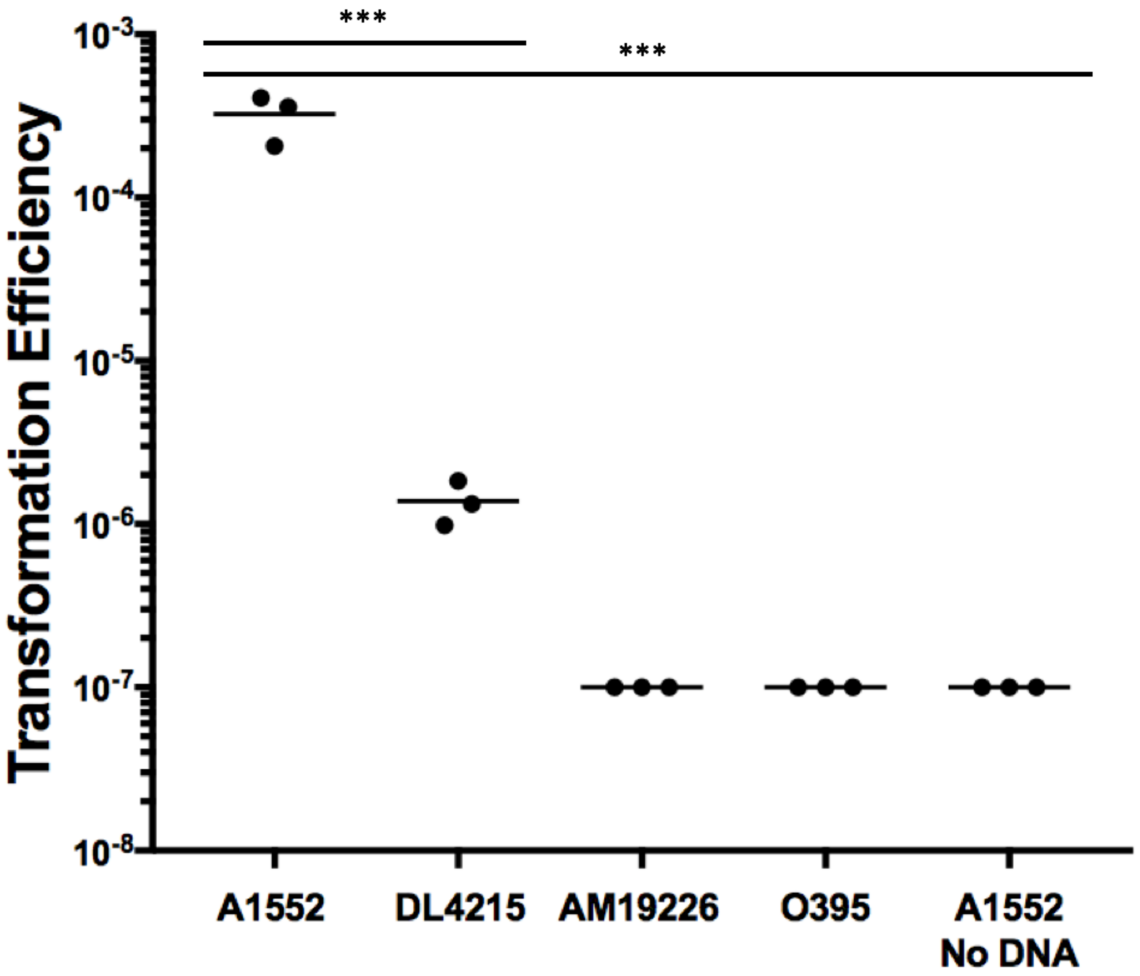

Figure 3-5. **Only a subset of *V. cholerae* strains are naturally competent on chitin.** A1552, DL4215, AM19226 and O395, were grown on chitin, resuspended in DASW for 24 hours, before 1μg of genomic DNA marked with a kanamycin cassette was added. After an additional 24 hours, the mixed was plated on kanamycin + rifampicin plates to look for transformants and rifampicin plates to enumerate for the total surviving bacteria. A transformation efficiency was calculated by dividing the transformants by the total number of bacteria. *** represents a p-value of < 0.001. Means are shown of 3 replicates over 1 experiments.

We envision scenarios where there is pressure for *V. cholerae* to acquire new modules when growing on chitin. We hypothesized that the pressure to acquire a T6SS module could result in also picking up other DNA without any pressure. This could be a unique mechanism where virulence factors are disseminated amongst strains. To test this hypothesis, we used kanamycin-cassette marked immunity genes from the El Tor strain C6706 to simulate the need for acquiring a new effector module. To model the potential flow of virulence factors from El Tor to environmental *V. cholerae,* we fed this DNA to

DL4215. We took successful transformants from four different reactions and isolated gDNA. We then sequenced the genomes on the Illumina platform. In all cases, the entire T6SS gene cluster was exchanged, not just the immunity gene. In addition to a T6SS gene cluster, 86% of transformants also acquired at least another gene cluster. In Figure 6, I show six representative chromosomes demonstrating transferred genes. In the red box is the Large T6SS gene cluster. Included in these gene transfers were genes encoding proteins necessary for motility, a known virulence factor in *V. cholerae* (Figure 6). This implicates a pressure for T6SS horizontal gene transfer event results in the transfer of other genes, including genes important in virulence.

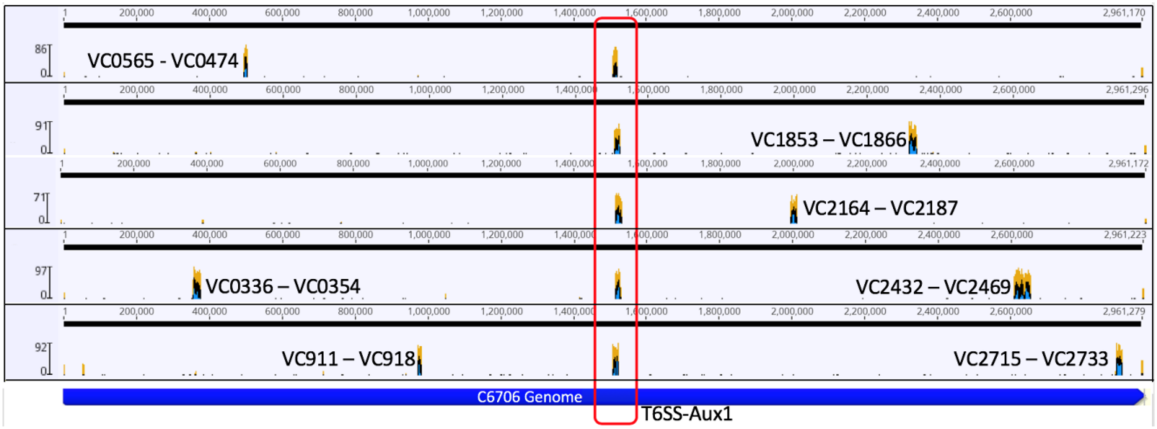

Figure 3-6. **Entire T6SS large cluster and non-T6SS gene clusters are transferred via natural transformation.** DL4215 was grown on chitin resuspended in DASW for 24 hours, before 1ug of gDNA marked with a kanamycin cassette in the orphan immunity gene (VC1420) was added. After an additional 24 hours, the mixed was plated on kanamycin + rifampicin plates to look for transformants and rifampicin plates to look for the total surviving bacteria. A transformation efficiency was calculated by dividing the transformants by the total number of bacteria. Transformants from 4 independent reactions were sequenced. The reads from the DL4215:: VC1420 hybrids were ran against the A1552 genome. Reads that matched to the A1552 genome were picked up by DL4215. Five genomes are shown.

Altogether, these data suggest that genetic exchange of T6SS and non-T6SS dependent genes is unbiased. Furthermore, using antibiotics to pressure *V. cholerae* to switch compatibility groups results in acquiring other virulence genes. This presents a novel mechanism for the diversification of *V. cholerae* and the flow of virulence factors.

3-3 Module exchange can occur through recombination within *tap-1*

To test our hypothesis of module exchange occurring with the 99-bp region, we next examined the ability of the *tap-1* to serve as the site of recombination. There are two main advantages for recombination to occur within a 99-basepair region of *tap-1*. First, this region is conserved amongst all sequenced *V. cholerae* strains (Unterweger et al., 2014a). This allows the same site to be used for recombining different effectors regardless of how different the surrounding regions are. Secondly, the region is downstream of *vgrG-1*. VgrG-1 is a structural T6SS protein whose sequence varies between strains. As VgrG proteins help make up the tip of the T6SS apparatus, there is likely evolutionary pressure to keeping the sequence consistent and to not tolerate changes (Unterweger et al., 2015). However, the *vgrG* sequences differ for strains, giving rise to our hypothesis that strains would not tolerate exchange in that region (Unterweger et al., 2015). Additionally, some *V. cholerae* strains have a *vgrG-1* gene that also encodes a T6SS effector that is covalently linked (Unterweger et al., 2014a). Switching out T6SS modules downstream of *vgrG-1* allows the VgrG-1 protein to remain unchanged for structural and enzymatic reasons. Previous work suggests that the evolutionary precursor to the AAA effector module set is the CAA effector module set (Kirchberger et al., 2017b). We tested our hypothesis that *tap-1* could be used as a site of recombination for switching the C^1 to the A^1 effector module. The A^1 effector (TseL) has been demonstrated by a blast-p search to be a class 3 lipase (Unterweger et al., 2014a). The C^1 effector is also predicted to have a lipase activity, however is a different class, containing a DUF2235 domain. It has been previously shown in *Pseudomonas aeruginosa* that many different lipases can be secreted by the T6SS (Russell et al., 2013b).

To test this hypothesis, we constructed a version of the A-module that encoded a kanamycin cassette in between the adaptor and the effector gene. This linear piece of DNA was provided to DL4215 overexpressing Tfox to induce competence. Recombinants were selected for on kanamycin, and 42 colonies over four independent reactions were sequenced. To determine the hybrid effector module sequence, we took the reads from the Illumina sequencing and ran them against the A and C modules separately, we then combined the reads that matched either module and performed a de-novo assembly using Geneious Software. The resulting contiguous DNA was aligned to both the A and C modules. The same pipeline was used for all 42 sequences. We found that in all cases, the

A effector was acquired at the loss of the C effector. However, in the majority of the cases, 40 out of 42 (>95%), the recombination occurred within *vgrG-1* and not within *tap-1*. However, in the remaining ~5%, recombination occurred in the conserved 99-base pair region in *tap-1*, leaving the original *vgrG-1* gene intact (Figure 7). This demonstrates that the 99-base pair region within *tap-1* gene can be used for recombination.

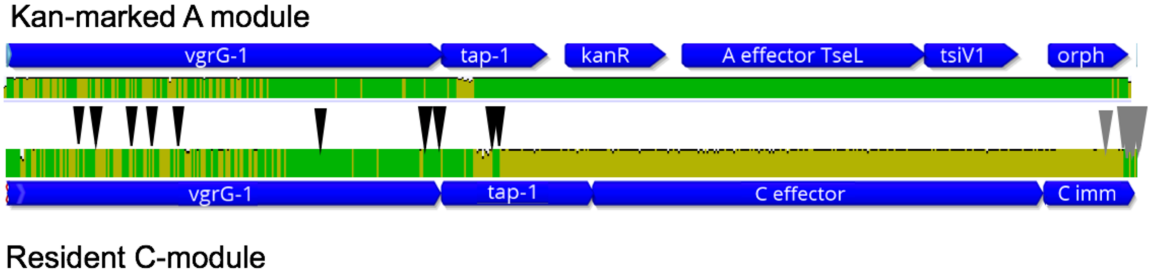

Figure 2-7: **Defined recombination events permit exchange of T6SS modules.** Host strain DL4215 (CEC) was transformed with a kanamycin-marked A^1 module. Transformant DNA was isolated and sequenced on an Illumina NovaSeq platform. Paired-reads (150 cycles) were de-novo assembled and annotated. The results of a sliding-window analysis (with a window size of 10 nucleotides) in which the auxiliary T6SS cluster 1 of five transformants were aligned and compared to the host cluster and the marked A-module is indicated as average percent of nucleotide identity: 100% identity (green bars), at least 30% identity (yellow bars) and less than 30% identity (red bars). Recombination events are indicated by triangles (upstream events in black and downstream events in grey).

Another hypothesis we were testing with this experiment was if the retention of the original immunity gene was possible, to produce an orphan immunity gene. Retention of the original immunity gene has presumed to be witnessed several times in nature based on phylogenetic analysis (Kirchberger et al., 2017b). Homology facilitated illegitimate recombination (HFIR) is a potential mechanism that could be employed to obtain a new effector module while retaining the original immunity gene (de Vries and Wackernagel, 2002, 2002). This mechanism describes recombination where one side of the incoming DNA has a short arm of homology (20-100 base pairs) and the other side has a short stretch of microhomology (2-6 base pairs). The homology, in this case within *tap-1*, must be a minimum of 20 base pairs which is satisfied by the 99 base pairs that can be used for recombination. As HFIR occurs at a frequency of 1:1000 when compared to homologous recombination, these experiments will need to be redesigned with a selective pressure to retain the original immunity gene (de Vries and Wackernagel, 2002). After a dissection of

the mechanism of module transfer, in the next section I will look at the consequence of module transfer in the same genetic background.

3-4 Pandemic strains equipped with non-pandemic "C" effector are less competitive than their parental strain

Previous studies evaluating the role of the T6SS and specific effector modules in competition have been limited by the large diversity in strain backgrounds that these studies are often performed in (Unterweger et al., 2014a). For example, it is well characterized that different *V. cholerae* strains secrete varying amounts of Hcp, even when fully activated (Unterweger et al., 2012). Additionally, strain differences could exist that confer immunity protein independent protection from T6SS attacks, such as thicker peptidoglycan or a capsule (Toska et al., 2018). Lastly, any growth rate differences between strains could mask important T6SS phenotypes (Borenstein et al., 2015).

To examine the importance of specific effector modules, we decided to equip a pandemic strain, normally encoding the "A^1" effector, with the historical "C^1" effector in auxiliary cluster one (Kirchberger et al., 2017b). This is an important comparison, because A^1 and C^1 are the only two effectors that are encoded in auxiliary cluster one, and all pandemic strains encode the A^1 effector and the majority of environmental strains encode the C^1 effector. We hypothesize that the historical CAA pandemic strains acquired the A effector to make them more competitive. We grew the pandemic strain, A1552, on chitin to induce natural competence and provided the C-module as linear DNA, marked with a kanamycin cassette for selection purposes. We then sequenced the strain to confirm the switch between the C and the A-modules.

Now that we had both a CAA and AAA in the same strain background, we were able to compare their competitive profiles. First, we performed a competition assay between either the CAA or AAA strain and *E. coli*. These experiments were performed under high salt to activate the T6SS of A1552. To determine which strain was more competitive we calculated the competitive index, this is the number of surviving prey divided by the number of surviving $A1552_{AAA}$ or $A1552_{CAA}$. This experiment demonstrated the difference in killing between the A and the C effector, we saw 2 logs of killing between

AAA and *E. coli* and ~1.5 logs of killing between CAA and *E. coli* (Figure 8). This difference indicates that the A effector is more efficient at killing *E. coli* than the C effector.

After looking at interspecific competition we turned to *Vibrio-vibrio* killing and examined the CAA and AAA strains ability to compete with A encoding strains C6706 and V52. We competed the CAA and AAA A1552 strains against C6706 to demonstrate whether or not the C effector is effective. C6706 does not have an active T6SS under laboratory conditions and does not produce an immunity protein against the C-effector. $A1552_{AAA}$ was able to coexist with C6706 as they are compatible whereas $A1552_{CAA}$ outcompeted C6706 by half a log (Figure 8). This also demonstrates that the $A1552_{CAA}$ strain, while able to outcompete C6706 under non-inducing conditions, would not benefit from the ability to share resources with the pandemic strains and would not be able to coinfect. This demonstrates an advantage for all pandemic strains to encode the same compatibility group.

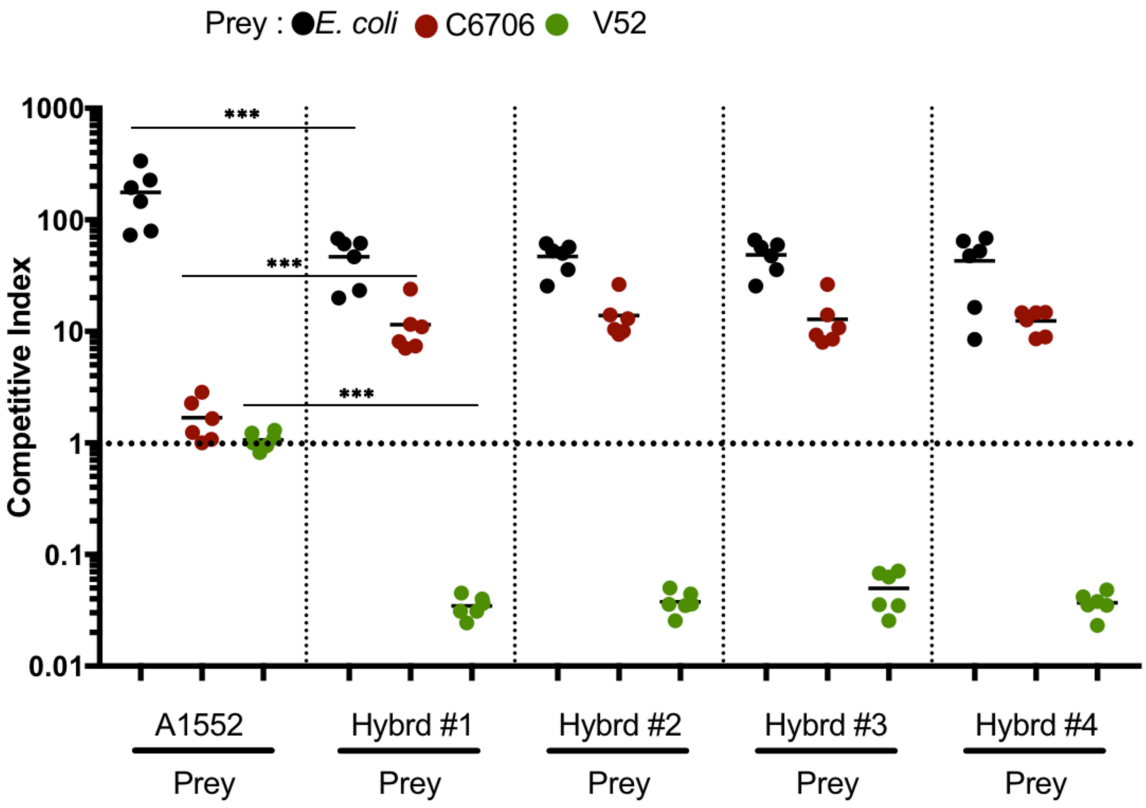

Figure 3-8. **$A1552_{CAA}$ is incompatible with the AAA pandemic compatibility group.** $A1552_{AAA}$ and four independent $A1552_{CAA}$ hybrids were placed in competition assays with *E. coli* and the AAA strains V52 and C6706. Competition assays were performed on 340mM NaCl LB agar plates for 24 hours at 37°C. Bacterial spots were resuspended,

serially diluted, and plated on selective media to determine the number of surviving prey. The number of surviving prey was divided by the number of surviving A1552/hybrid and presented as a competitive index. *** represents a p-value of < 0.001. Means are shown of 6 replicates over 3 experiments.

Subsequently, we put $A1552_{AAA}$ and $A1552_{CAA}$ in competition with V52 to simulate competition between the two A1552 strains and a pandemic strain with an active T6SS. In this case $A1552_{AAA}$ was able to coexist with V52, demonstrating an advantage for the AAA compatibility group. In direct contrast, $A1552_{CAA}$ was outcompeted by V52 by 3-logs.Together, this demonstrates the advantage of having an AAA module set when interacting with pandemic strains.

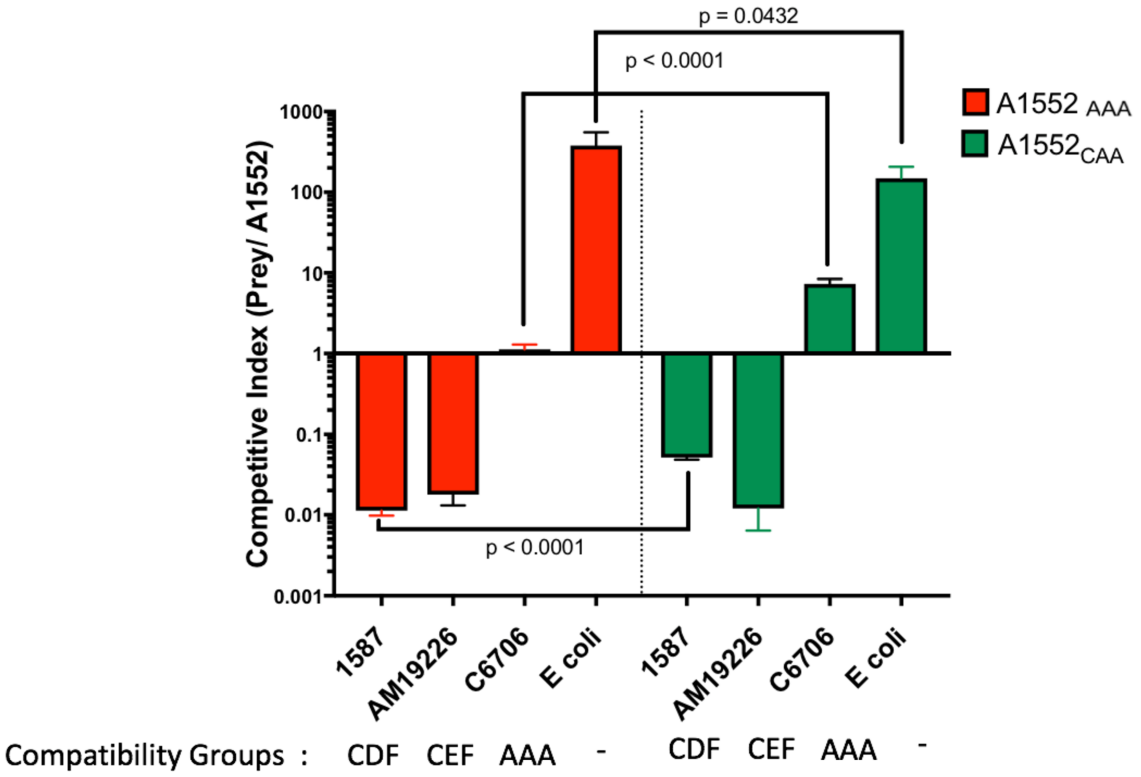

Figure 3-9. **Encoding the C or A effector changes the competitive behavior of A1552.** $A1552_{AAA}$ and $A1552_{CAA}$ hybrids were placed in competition assays with *E. coli* and environmental strains AM19226 and 1587. Competition assays were performed on 340mM NaCl LB agar plates for 24 hours at 37ºC. Bacterial spots were resuspended, serially diluted, and plated on selective media to determine the number of surviving prey. The number of surviving prey was divided by the number of surviving A1552/hybrid and presented as a competitive index. Means are shown of 6 replicates over 3 experiments.

After looking at interactions with pandemic strains, we put $A1552_{AAA}$ and $A1552_{CAA}$ in competition with environmental strains that encoded the C effector, instead (Figure 9). Because we performed these killing assays on high salt, the T6SS secretion system of A1552 is active, but not as active as strains that have the system constitutively activated under laboratory conditions. Therefore, in these scenarios we hypothesize that the C^1 effector will prove advantageous. In killing assays between $A1552_{AAA}$ or $A1552_{CAA}$ with the environmental strains AM19226, 1587 or DL4215 we found that while both strains were outcompeted, $A1552_{AAA}$ was outcompeted to a greater extent when against 1587 by an additional half of a log (Figure 9). AM19226, 1587 and DL4215 are all environmental strains lacking cholera toxin, but lack the ability to colonize the infant mouse. Again in this experiment, $A1552_{AAA}$ was able to kill *E. coli* to a greater extent than $A1552_{CAA}$. Finally, to directly test $A1552_{AAA}$ and $A1552_{CAA}$ against one another, we performed a competition assay and selected for just the $A1552_{CAA}$ strain on kanamycin (Figure 10). We saw a 10-fold reduction in $A1552_{CAA}$ indicating that the A effector is superior to the C effector against both *E. coli* and pandemic *V. cholerae*. This demonstrates that while it appears that the A effector is more efficient at killing than the C^1 effector, effector exchange may be more about dictating what group of strains *V. cholerae* can coexist with, more-so than acquiring effectors that are more efficient killers. For example, there are other factors that determine a strains competitive behavior beyond the effectors it contains. Additionally, there could be environments were one set of effectors would be more effective than in other environments. Therefore even encoding the more effective effectors does not guarantee that a strain will outcompete another. In these cases, favouring cooperation might be the best for survival.

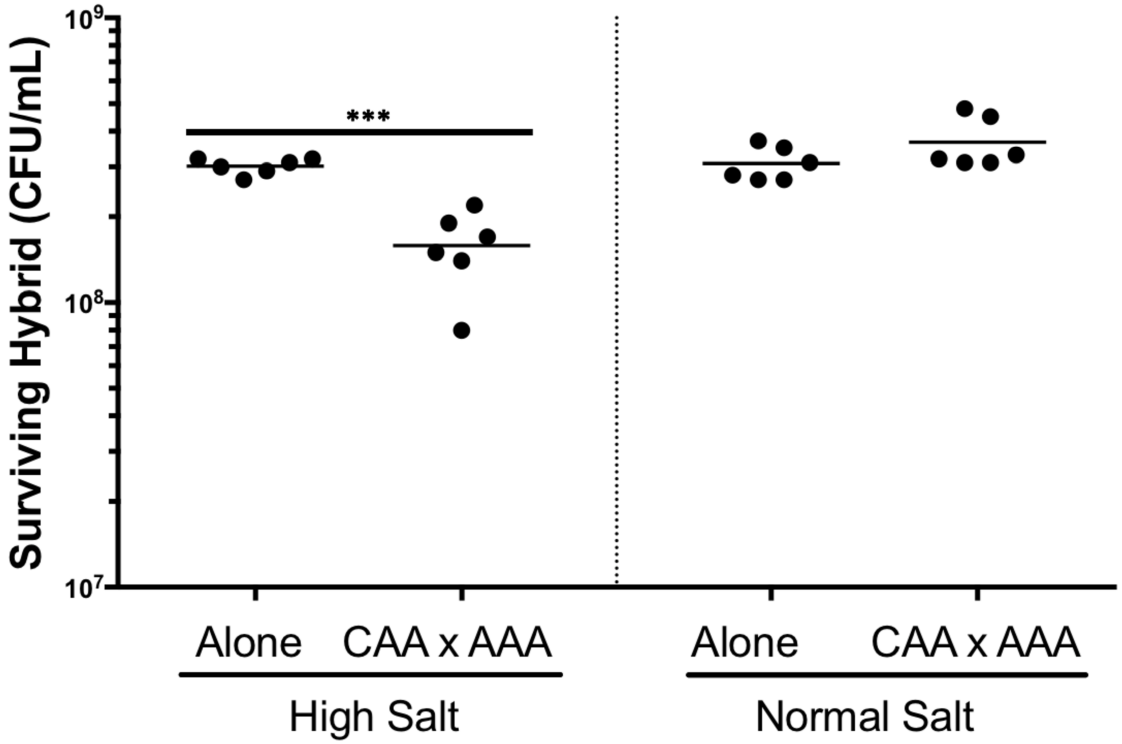

Figure 3-10. **$A1552_{AAA}$ outcompetes $A1552_{CAA}$ in a T6SS-dependent manner.** $A1552_{AAA}$ and $A1552_{CAA}$ hybrids were placed in competition assays with one another. Competition assays were performed on 340 mM NaCl (high salt) or 80 mM NaCl (low salt) LB agar plates for 24 hours at 37°C. Bacterial spots were resuspended, serially diluted, and plated on selective media to determine the number of surviving prey. The number of surviving $A1552_{CAA}$ was calculated by plating on kanamycin plates. *** represents a p-value of < 0.001. Means are shown of 6 replicates over 3 experiments.

3-5 Non-pandemic strains equipped with TseL (A^1) or VgrG3 (A^M) are more competitive than their parental strain

Lastly, we wanted to test the consequences of the alternative, where an environmental strain is equipped with effectors from the pandemic AAA compatibility group. When we reverted $A1552_{AAA}$ back to the presumed historical $A1552_{CAA}$ we saw a change in competitive behavior. While $A1552_{CAA}$ generally did become less competitive, it became more competitive amongst environmental strains, changing the potential tropism of strains it could interact with. We next decided to examine if the opposite was true – does an environmental strain acquiring pandemic effectors gain a boost in competitive behavior.

Throughout our studies to look for genetic recombination, we generated two DL4215 hybrid strains: $DL4215_{AEC}$ and $DL4215_{CEA}$ as well as the parental strain,

DL4215$_{CEC}$. First, to compare the competitive behavior of the hybrid strains with the parental, we performed killing assays. As reported recently, closely related strains need extended killing assay times to fully see a phenotype (Thomas et al., 2017). To compare the hybrid strains with the parental strains, we performed killing assays over 24 hours. We saw that in both cases, the hybrids – either DL4215$_{AEC}$ or DL4215$_{CEA}$ – the hybrid strain outcompeted the parental strain by 1000-fold and 500-fold respectively (Figure 11AB) over 24 hours. This suggests that when competing sister strains against one another with different T6SS effectors, the pandemic effectors are superior.

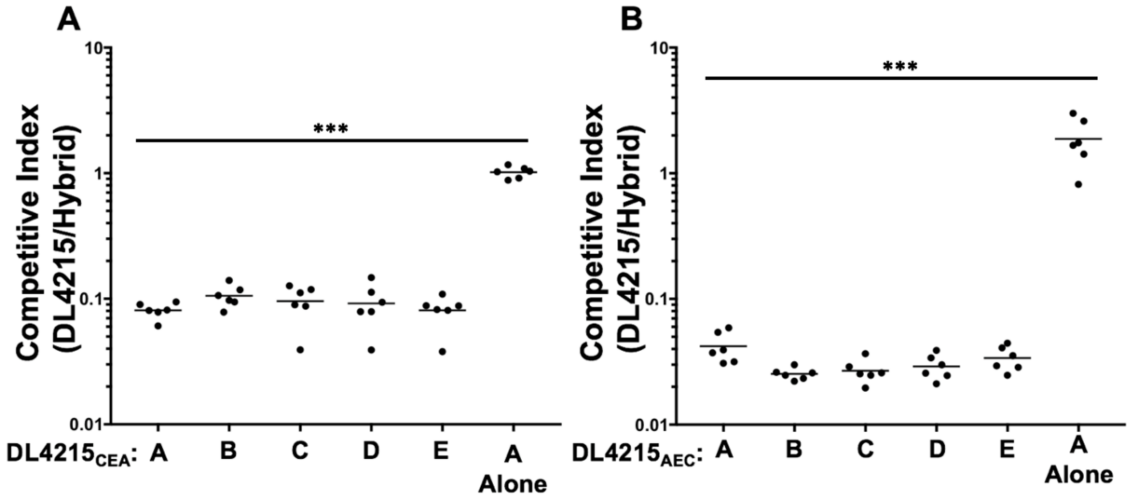

Figure 3-11. **DL4215$_{CEA}$ and DL4215$_{AEC}$ outcompete wildtype DL4215$_{CEC}$.** DL4215$_{CEA}$ and DL4215$_{AEC}$ hybrids were placed in competition assays with DL4215$_{CEC}$. Competition assays for 24 hours at 37^{o}C. The number of surviving DL4215 hybrids were selected by plating on streptomycin plates and DL4215 wild-type was selected for by plating on rifampicin plates. *** represents a p-value of < 0.001. Means are shown of 6 replicates over 3 experiments.

Altogether, these data suggests that *V. cholerae* can acquire new effector modules, without mutating their *vgrG* gene with the consequences of differing competitive behavior and the ability to interact with different strains. Mutating the *vgrG* could result in loss of anti-eukaryotic activity or incompatible structural changes reducing T6SS efficiency. In the case of pandemic strains, they may have acquired/retained the same effector modules because they are superior killers and it allows them to coexist, giving them advantages during infection or in the environment.

3-6 Discussion

Within bacterial communities, *V. cholerae* can protect against T6SS-mediated attacks. *V. cholerae* synthesizes immunity proteins that sequester cognate T6SS effectors expressed by sister cells (Dong et al., 2013; Unterweger et al., 2014a). Immunity proteins that protect cells from effector alleles of kin cells are ineffective against effectors encoded by alleles of non-kin bacteria belonging to the same species. Taken together, these observations suggest that "compatibility rules" allow distinct strains of *V. cholerae* with identical effector modules to coexist, thereby giving rise to a unique self-recognition system (Unterweger et al., 2014a). Conversely, *V. cholerae* strains expressing dissimilar effector/immunity pairs are unable to share a niche as one of the two strains will be excluded (Thomas et al., 2017; Unterweger et al., 2012, 2014a). Each *V. cholerae* strain examined to date encodes three distinct effector/immunity alleles within the three T6SS gene clusters. So far, we identified a total of nineteen effectors across the three clusters, but expect that number to increase as additional strain sequences become available (Kirchberger et al., 2017a). Experimental and bioinformatic evidence suggests that these modules can be freely exchanged between *V. cholerae* strains (Borgeaud et al., 2015b; Kirchberger et al., 2017a; Thomas et al., 2017; Unterweger et al., 2014a, 2015). Interestingly, all pandemic *V. cholerae* strains encode the same three effector modules – termed AAA (Unterweger et al., 2014a). Furthermore, our experiments demonstrated the AAA effector/immunity allele pair to be by far the most effective at killing non-kin *V. cholerae* (Unterweger et al., 2012, 2014a). However, these experiments were limited by the fact that different strain backgrounds were used, and it cannot be ruled out that differences in T6SS expression, turnover or natural resistance were conflating factors.

In this study, we primarily focused on auxiliary cluster one and the two effectors, A^1 found in pandemic strains and C^1 found in the majority of environmental strains (Kirchberger et al., 2017a). We then either equipped pandemic strains with C^1 or non-pandemic *V. cholerae* strains with A^1. This allowed us to compare the competitive behavior of *V. cholerae* in the same strain background, so all that is different is the effector module. Aligned with our hypothesis, the pandemic effectors A^1 and A^M were found superior in competition assays within the same background (Figure 3.10-11). This held true against *E. coli, V. cholerae* without a T6SS and directly between the two strains (Figure 3.10-11).

Collectively, these results suggest that pandemic strains exclude non-pandemic strains through their superior T6SS effector modules. The only exception to this rule is that A1552$_{AAA}$ and A1552$_{CAA}$ were both outcompeted by environmental strains (Figure 3.9). We hypothesize that this is because those environmental strains have a more active T6SS than A1552 grown on high salt – which does not secrete Hcp to the same degree (Metzger et al., 2016). However, A1552$_{CAA}$ performed better than A1552$_{AAA}$. We hypothesize that this is because the C^1-immunity gene gives protection that elsewise would not be there. This indicates a model where having the same immunity genes as the strain expressing their T6SS to the highest degree will provide an advantage. However, all other things being equal A^1 is more effective at killing than C^1. Similarly, we performed the same experiments with the converse – giving the effectors of pandemic strains to the environmental strain, DL4215$_{CEC}$. To this end, we made DL4215$_{AEC}$ and DL4215$_{CEA}$ and found similar to the previous hybrids that the pandemic effectors gave a competitive advantage (Figure 2.11).

This notion of compatibility groups was recently expanded upon by an in-depth study examining over 400 *V. cholerae* strains isolated from five different locations within Oyster Pond, MA, USA. Kirchberger *et al.* found that *V. cholerae* isolated from the same collection site all shared the same compatibility group, yet compatibility groups were distinct across different sites (Kirchberger et al., 2016). The authors hypothesized that homogeneity of *V. cholerae* at any given site is driven by the T6SS, resulting in incompatible strains being excluded.

Another important aspect of compatibility groups are orphan immunity genes consisting of open reading frames that bear considerable homology to immunity genes but are not positioned directly downstream of a cognate effector but still exist within a given T6SS gene cluster (Kirchberger et al., 2017a). All AAA-module strains harbor a single orphan immunity gene downstream of the *tsiV1* immunity gene outside of the T6SS auxiliary cluster 1, yet other *V. cholerae* strains have several orphan immunity genes in long arrays following all three T6SS gene clusters (Kirchberger et al., 2017a). While it is not yet known if these purported genes are active and provide protection to other effector genes, RNAseq data from *V. cholerae* demonstrate that the orphan immunity gene downstream of *tsiV1* is activated along with the rest of the cluster when T6SS is induced through *tfoX* overexpression (Borgeaud et al., 2015b). Additional immunity genes could

offer a resistance mechanism for *V. cholerae* to effectors other than the ones they encode, providing a mechanism by which incompatible strains could coexist in a heterogeneous environmental niche. Therefore, ideal genetic exchange of effector modules would be where the immunity gene is retained.

Another aspect of an ideal module exchange is for the recombination to occur within tap-1. This provides two advantages. The first being that within *tap-1* there is a conserved 99-bp region amongst all sequenced *V. cholerae* strains (Unterweger et al., 2015). Maintaining this region is important for subsequent acquisitions. Secondly, this region is downstream of the *vgrG-1* gene and therefore using this region for recombination allows *vgrG-1* to be maintained. As VgrG-1 is a multidomain protein with both structural and potentially enzymatic activity, it might not be beneficial to exchange that gene. However, our experiments show that only 5% of recombination occurred in this 99-base pair region. I hypothesize that the advantages of this relatively rare event is advantageous and will therefore be the most fit on chitin and in the host – outcompeting the 95% of recombination events. However, this must be further tested.

Therefore, ideal module exchange has two features, recombination between homologous regions on the 5' side within *tap-1* of the two modules and non-homologous recombination between the incoming immunity gene and the region between the host effector and immunity gene. HFIR is a rare recombination event that satisfies both of those conditions (de Vries and Wackernagel, 2002). When looking for HFIR, we found that the first condition – homologous recombination within *tap-1* occurred at a high frequency (42/46 screen hybrids). The second condition was not satisfied, and the immunity gene was not retained. HFIR is a rare event, occurring at a rate of 1/1000 compared to homologous recombination (Meier and Wackernagel, 2003). Therefore, repeating this experiment with a selective pressure for the retention of the original immunity gene. This could come in the form of expressing the original effector off of a plasmid, therefore, recombination without the retention of the original immunity gene would result in bacterial death.

Co-regulation of T6SS and natural competence invites an intriguing hypothesis whereby T6SS mediated killing causes release of extracellular prey DNA (eDNA), which could then be acquired by the predator strains (Borgeaud et al., 2015b). When there is a selective pressure to switch T6SS effector modules, this could result in the acquisition of

potentially any gene including new virulence factors. To test this hypothesis, we labelled T6SS modules with an antibiotic resistance cassette and sequenced the genome of the hybrids. We found that indeed other genes, including virulence factors were transferred (Figure 6).

Altogether, this chapter examines the consequences of the diversification of the T6SS and the mechanism behind the acquisition of new effector modules. Specifically, the AAA module set of pandemic *V. cholerae* strains was shown to be superior to the effectors encoded by environmental strains. This shows that exchanging effectors can change the competitiveness of *V. cholerae.* Another consequence of exchanging effectors is the ability to pick up other DNA at the same time. This can change the pathogenesis of *V. cholerae* through the acquisition of new virulence traits. Lastly, we looked at the mechanism of effector module exchange, and hypothesized it occurs through HFIR. We showed that the 93-bp region in *tap-1* satisfies the "homology facilitated" component of HFIR, and bioinformatic analysis suggests that illegitimate recombination readily occurs. Diversification following T6SS mediated killing illustrates an important mechanism of *V. cholerae* evolution.

Chapter 4

T6SS mutations in 2nd and 6th pandemic *V. cholerae* result in a competitive disadvantage

Figure 1 was made by Francis Santoriello

All other Figures are the work of Benjamin Kostiuk

4-1 Introduction

There have been 7 reported pandemics in the modern history of cholera; however, the disease is likely much older. Cholera outbreaks date back to 600BC as reported by early Greek and Roman physicians (Barua, 1992). The pandemics have been predominatly caused by the O1 serogroup; however, the strains responsible for pandemic cholera have changed dramatically since the first pandemic began in 1817 (Barua, 1992; Kitaoka et al., 2011a). The study of how pandemic strains evolved is hampered by the lack of sequence information. The majority of sequences are from strains of the 6th pandemic (classical strains, 1899 – 1923) and the ongoing 7th pandemic (El Tor strains, 1963 – today).

Many studies address the differences between these two biotypes (Jonson et al., 1989; Nair et al., 2002; Richardson et al., 1986; Takeya et al., 1981; Yoon and Mekalanos, 2006). The seventh pandemic *V. cholerae* O1 El Tor biotype and the sixth pandemic O1 classical biotype evolved as distinct lineages and differ not only in the regulation and amounts of secreted cholera toxin, but also in carbohydrate metabolism among other properties such as differences in the temporal expression of TcpP, increased biofilm production in El Tor, and increased motility in El Tor strains (Beyhan et al., 2006; Jonson et al., 1990; Takeya et al., 1981; Yoon and Mekalanos, 2006). Another difference was noted in the T6SS of classical strains, as a premature stop codon exists in *vasK*, a gene in the large T6SS cluster encoding an inner membrane protein (Ma et al., 2009; Miyata et al., 2010b). Despite the differences between the T6SS gene cluster, all pandemic strains share the same immunity genes and therefore are in the same compatibility group. Compatibility groups are the set of immunity genes that the strain encodes. Each immunity gene is given a letter, pandemic strains are a part of the AAA compatibility group. It is unknown which of these differences between the two biotypes results in the different pathology of disease. When the El Tor strains emerged in 1963, cholera disease symptoms and progression changed; compared to a classical infection, El Tor cholera has a greater likelihood of being mild or asymptomatic, resulting in less hospitalizations and a longer period where the bacteria are shed – up to five days for El Tor and only 1.5 days for classical infections (Bart et al., 1970; Khan and Shahidullah, 1980; Niyogi, 1979; Oseasohn et al., 1966; Woodward and Mosley, 1972). This increased time of excretion might be beneficial to the pathogen as it allows increased dissemination (Woodward and Mosley, 1972). Additionally, *V. cholerae* bacteria shed

from the human host are hyper-infectious (Merrell et al., 2002a). Therefore, an extended period of excretion in addition to their hyper-infectivity promote dissemination in an additive manner. Despite multiple differences between the biotypes, it is unknown how the El Tor strains from the 7th pandemic replaced the classical strains as the cause of the current cholera pandemic globally.

A preserved intestine from a cholera patient from 1849 is part of the Mutter Museum collection in Philadelphia (Devault et al., 2014). This strain was collected by Dr. John Neil during the Philadelphia second-pandemic cholera outbreak of 1849 (Devault et al., 2014). This medical specimen has the potential to give us invaluable insights into the 2nd cholera pandemic and allows us to better track the evolution of *V. cholerae* throughout the pandemics. We hypothesize that the 7th pandemic strains are more competitive than the strains responsible for previous pandemics, contributing to the replacement of 6th pandemic strains.

In this chapter, I will continue on the assumption that the 2nd pandemic strain PA1849 is representative of the 2nd pandemic. I will focus on how the competitive behavior of *V. cholerae* has changed from strains from the 2nd pandemic to strains from the 6th and 7th pandemics. This project started with resequencing the 2nd-pandemic *V. cholerae* strain PA1849, and comparing the T6SS gene clusters. Next, I introduced mutations from the 2nd and 6th pandemic strains into the genome of V52, a *V. cholerae* strain with a constitutively active T6SS, allowing us to infer the competitive behaviour of previous pandemic strains mutations. We found that 2nd and 6th pandemic strains were unable to use their T6SSs as means of competition, and that a subset of 6th pandemic strains are unable to defend themselves against a T6SS attack.

3-2 2nd and 6th pandemic strains carry mutations in the T6SS structural genes

In 2014, Devault *et al.* published the partial genome of the 2nd cholera pandemic strain PA1849 isolated from an intestine preserved in the Mutter Museum in Philadelphia. Unfortunately, this sequencing effort did not give a clear picture of the T6SS gene clusters, with some areas having no coverage, and other areas having insufficient coverage to call SNPs with confidence. Since then, new developments in sequencing technologies and another sample from the museum allowed us to resequence the genome. Additionally, we

designed booster probes specific to the T6SS gene clusters to enrich these areas and ensure adequate coverage. This approach provided us with an average coverage across the T6SS gene clusters of ~10,000 (Figure 4-1).

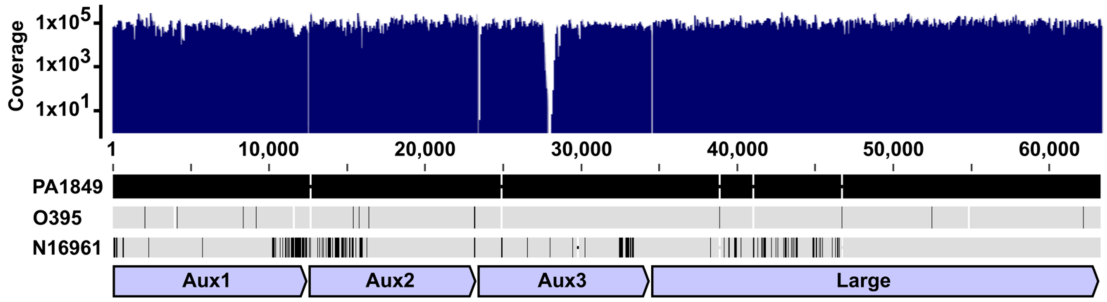

Figure 4-1. Construction of the T6SS gene clusters of PA1849. A sample of intestine was obtained from the Mutter museum in Philadelphia. MyBaits was used to enrich the T6SS gene clusters. Next, it was sequenced through the Illumina platform. These reads were then mapped to a representative from the 6th pandemic (O395) and a representative from the 7th pandemic (N16961). On top is a logarithmic graph showing the number of reads on the y-axis and on the x-axis the position in the genome. In the bottom, SNPs and INDELS are highlighted through the use of a black line. Homology is represented by a grey line.

Variants were compared against the constructed reference suquence and consensus sequences were generated with Pilon (Walker et al., 2014). The consensus sequence of PA1849 was then compared to the 2nd pandemic strain PA1849, the 6th pandemic strains O395 and CA401, and the 7th pandemic strain C6706. We found the structural components to be highly similar with a few important mutations (Figure 4-2). As we knew the T6SS of C6706 is functional (Bachmann et al., 2015; Dong et al., 2013), we inferred that major insertions, deletions and SNPs from those sequences should be investigated as potentially disabling.

First, we noticed that the 6th-pandemic strains shared a 16 base-pair deletion in the first third of *vasK* in common. *vasK* encodes the inner membrane protein VasK critical to T6SS activity; a *vasK* deletion is often used as a negative control for T6SS activity (Figure 4-1A) (Ma et al., 2009). The 16 base-pair deletion causes a stop codon (TGG) 171 amino acids into the protein and likely abolishes T6SS activity. Interestingly, the 2nd pandemic strain does not have this deletion and so the *vasK*-deletion, if *vasK* was functional in contemporary 2nd pandemic strains, occurred in strains sometime between the 2nd and 6th pandemic (Figure 4-2A).

Despite this difference between the 2nd and 6th pandemic strains, the O395 and PA1849 shared a 12-base-pair deletion in *VCA0109* (Figure 4-2B). *VCA0109* encodes a protein that is poorly studied. It is known to be an essential gene for T6SS activity in *V. cholerae* and *P. aeruginosa* (Lossi et al., 2011; Zheng et al., 2011). VCA0109 is thought to be a mediator of protein-protein interactions between the inner membrane complex and the VipA/B tube (Lossi et al., 2011). However, this deletion is in-frame. Interestingly, this deletion removes four amino acids (valine-luecine-valine-arginine) in the middle of a B-barrel which could influence protein folding (Figure 4-3).

Together, we were able to reconstruct the T6SS gene clusters of PA1849 and compare it with the gene clusters of 6th and 7th pandemic strains. This provides us with a basis for exploring whether the 2nd and 6th pandemic strains encoded a functional T6SS.

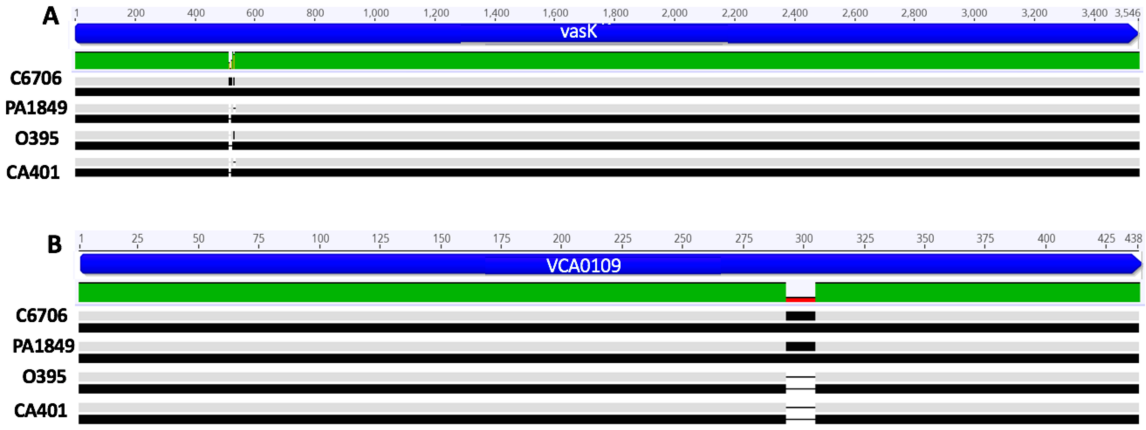

Figure 4-2. **Comparison of *VCA0109* and *vasK* between 2nd, 6th and 7th pandemic strains.** Using Geneious' Muscle multi-alignment tool the *vasK* (A) and *VCA0109* (B) from the large T6SS cluster of C6706, PA1849, O395 and CA401. The bar at the top represents % identity. A green bar represents 100% identity, a yellow bar represents an identity between 30 and 99%, a red bar represents identity between 1 and 29% and no bar represents 0% identity.

4-3 The 2nd and 6th pandemic strains were unable to compete with their T6SSs

After taking a genomic approach to resolve the differences between the T6SSs of representative strains for three pandemics, we evaluated T6SS function by introducing the mutations found in PA1849 into the chromosome of V52. We used V52 as the host strain for two primary reasons. One, V52 employs a constitutive T6SS activity under laboratory conditions, allowing us to determine if the mutations found in PA1849 interfere with T6SS activity (MacIntyre et al., 2010). Secondly, V52 has a 99.3% amino acid identity with T6SS

structural components of 7th pandemic (Unterweger et al., 2014a). This conservation with El Tor strains allows us to isolate unique mutations from the 2nd and 6th pandemic strains and compare them to El Tor strains.

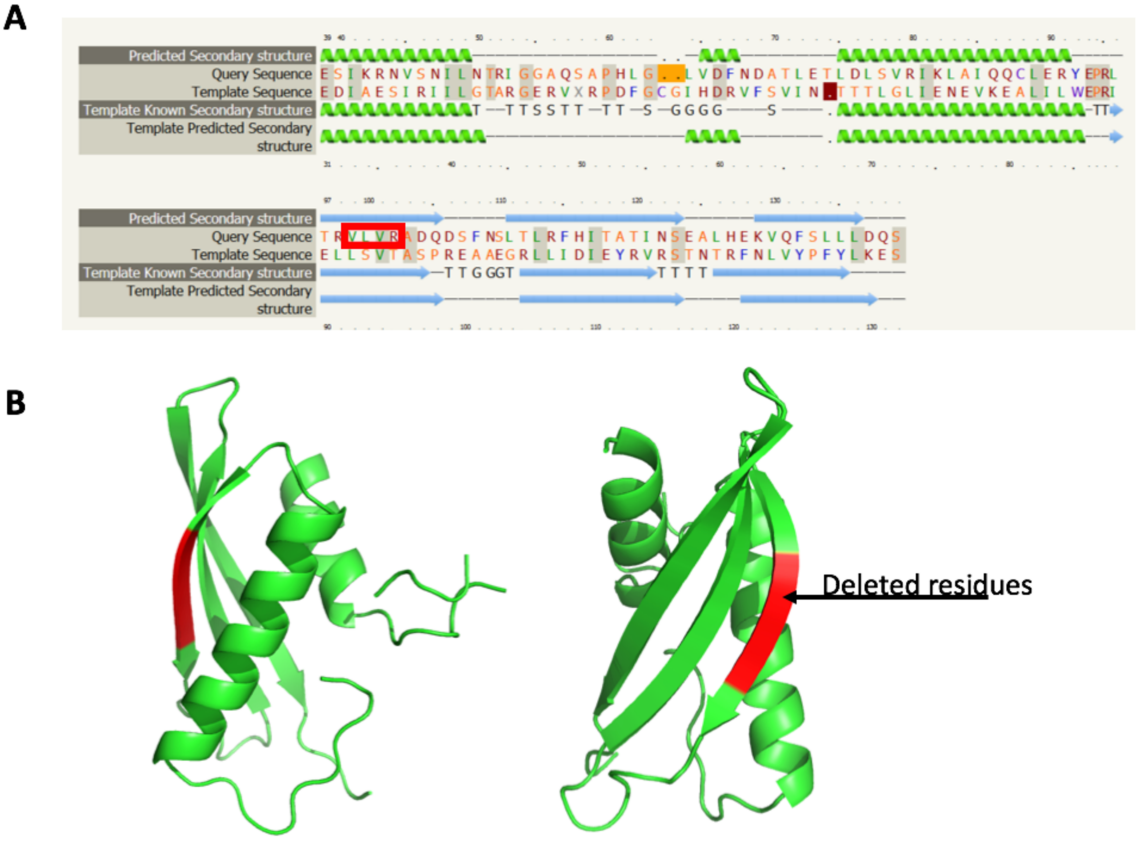

Figure 4-3. **PHYRE2 analysis of VCA0109.** The protein sequence from C6706's VCA0109 was submitted for PHYRE2 analysis to predict for secondary and tertiary structure. Due to high sequence homology with the GP-27 like lysozyme, this model came with 97% confidence. (A) Represents the amino acid sequence of the query (VCA0109) and of the template. Beneath and above the sequence is the secondary structure. A green spiral represents alpha helices and blue arrows represent beta sheets. The red box is on the 4 amino acids that are deleted in 2nd and 6th pandemic strains. (B) A 3-dimensional representation of VCA0109 with the 4-amino acids deleted in 2nd and 6th pandemic strains labelled in red.

Using Gibson cloning, we generated constructs encoding the *vasK* from 6th pandemic classical strains, and *VCA0109* from 2nd and 6th pandemic strains into pWM91 – a suicide vector frequently used for allelic exchange (Metcalf et al., 1996). After mating these plasmids into V52 and screening for the clones with the deletion, we used them in competition assays with *E. coli* to measure the magnitude of T6SS activity. V52 kills *E.*

coli approximately 3 logs under wildtype conditions (Figure 4). V52 equipped with *vasK* from the 6th pandemic strains lacked all T6SS activity and did not reduce *E. coli* viability (Figure 4). This mutation in *vasK* is a stop codon 32% into the protein, resulting in a truncated protein unlikely to function (Figure 4-3). Interestingly, the 12-bp deletion in *VCA0109* present in 2nd and 6th pandemic strains also completely removed T6SS activity from V52, causing none of the 3-logs of killing seen by wildtype V52 (Figure 4). This deletion, although in-frame, is located in a fold that could disrupt important secondary structure (Figure 2A-C). Together these results indicate that a single mutation in 2nd pandemic strains is responsible for disabling their T6SS. 6th pandemic strains accumulated a second mutation in *vasK* further disabling the T6SS.

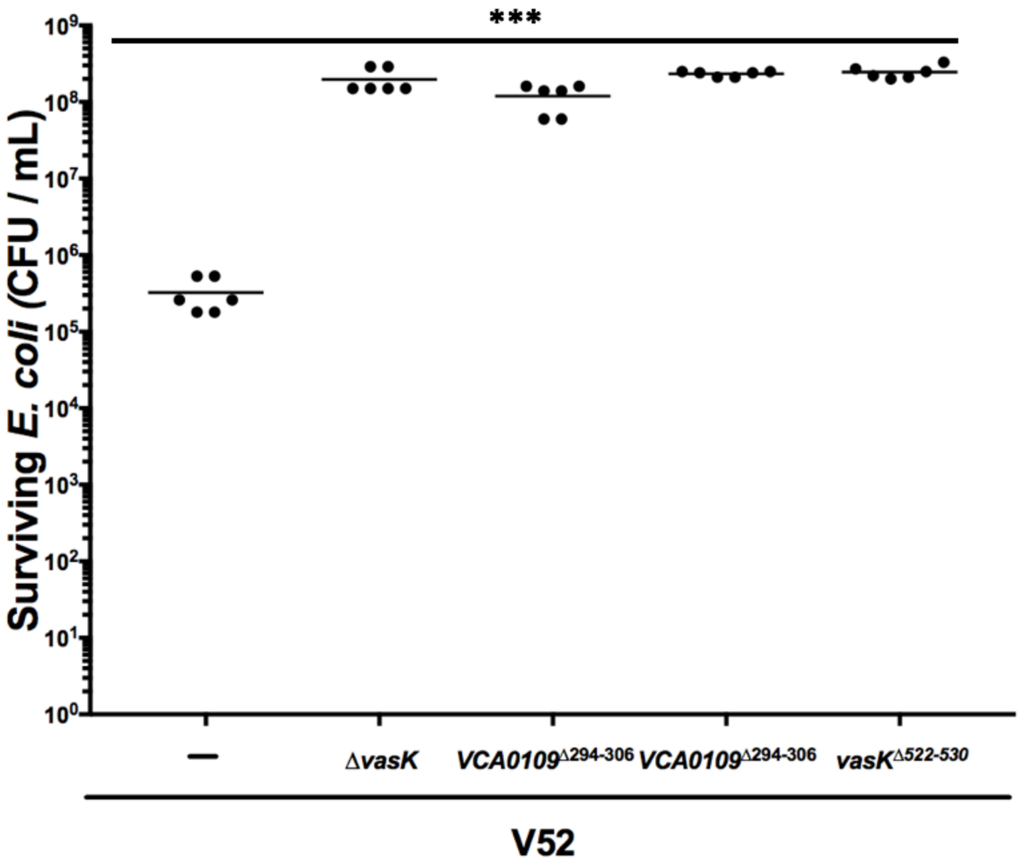

Figure 4-4. **Mutations found within classical pandemic strains disable the T6SS.** A deletion within *VCA0109* that is present in 2nd and 6th pandemic strains, or a deletion in *vasK* found in 6th pandemic strains were made in V52. These strains were placed in a killing assay against *E. coli* MG1655 to screen for an active or inactive T6SS. Wildtype V52 was used as a positive control, and V52Δ*vasK* was used as a negative control. Killing assays

were performed for 4 hours at 37C. *** represents a p-value of < 0.001. Means are shown of 6 replicates over 3 experiments.

4-3 The 2nd pandemic strain PA1849 is immunocompetent whereas a subset of 6th pandemic strains are not

Previously, our lab compared the immunity genes on a genetic level between *V. cholerae* strains and found that they belonged in different compatibility groups (Unterweger et al., 2014a). We noticed that most AAA strains shared the identical immunity gene, *tsiV1*, yet some classical strains encode conserved SNPs. Interestingly, a subset of 6th pandemic strains all encoded an amino acid substitution at position 163 from an isoleucine to a phenylalanine. Although these strains belong to the AAA compatibility group, the strains were shown to be sensitive to a T6SS-dependent attack from V52 – another AAA strain (Unterweger et al., 2018). To investigate this, I made a plasmid that expressed either of the two isoforms of *tsiV1*. The strain expressing the phenylalanine copy of TsiV1 had its viability reduced by ~1.8 fold when exposed to V52 for four hours (Figure 5). At 24 hours of competition, this phenotype was extended to a 12-fold loss in bacterial numbers demonstrating that the inferiority of the immunity gene is exposed after increased exposure to T6SS attacks (Figure 5).

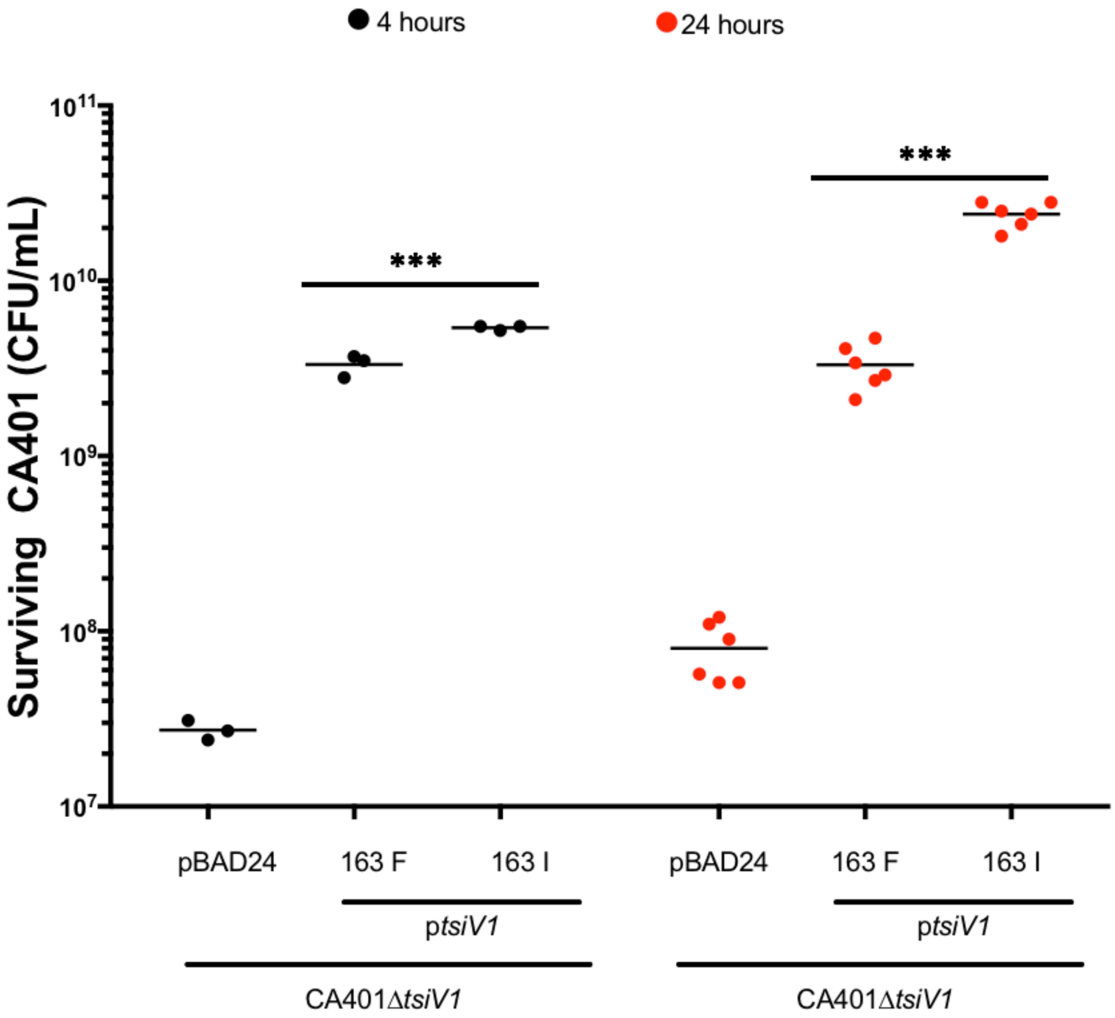

Figure 4-6. **Mutations found within a subset of 6th pandemic classical strain's *tsiV1* reduce immunity.** A SNP within *tsiV1* that is present within a subset of 6th pandemic strains (163F) or the 7th pandemic version of $tsiV1_{163I}$ was provided on a plasmid to CA401 lacking *tsiV1*. V52 was used as a predator against these strains to test the effectiveness of the immunity protein. $TsiV1_{163I}$ was used as a control for no killing and a plasmid alone control was used as a positive control for killing. Killing assays were performed for 4 hours at 37C. *** represents a p-value of < 0.001. Means are shown of 6 replicates over 3 experiments.

Through genomic comparison of the immunity genes encoded by PA1849, we see no differences on the genetic level, suggesting that this strain would have been fully immune competent (Figure 4-6). This is interesting as it shows the potential and partial degradation of the immunity gene occurred in a subset of *V. cholerae* strains sometime between the 2nd and 6th pandemic.

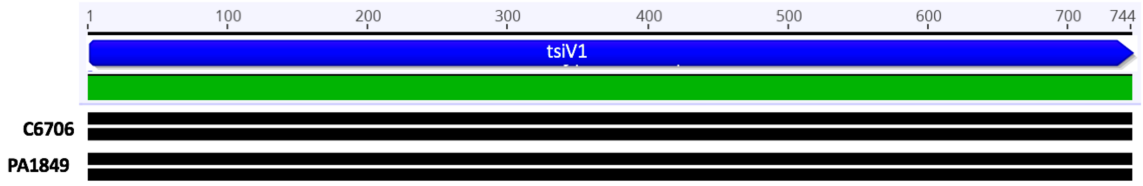

Figure 4-6. PA1849 encodes a functional *tsiV1* allele. Using Geneious' Muscle alignment tool tsiV1 of C6706 and PA1849 were compared. The bar at the top represents % identity. A green bar represents 100% identity.

In conclusion, while focusing on the evolution of the immunity gene *tsiV,* we demonstrate it has changed throughout the pandemics of *V. cholerae* from being fully competent in the 2nd pandemic, to partially losing that protection in a subset of 6th pandemic strains before being replaced by the fully competent allele once again in the 7th pandemic. The 6th pandemic immunity gene could have been a contributing factor to its replacement as prolonged exposure to a fully competent AAA T6SS results in a large amount of killing by El Tor strains.

4-5 Discussion

I propose a model for the degradation of the T6SS gene cluster between the 2nd and 6th pandemic, and the decrease in competitiveness that occurred between the pandemics. In this model, the emergence of El Tor strains represents pandemics with an ability to engage in T6SS competition in a tightly regulated fashion. Recently isolated El Tor strains have evolved a constitutively active T6SS, inferring it has an increasingly important role (Zhao et al., 2018). This observation suggests that pandemic strains have shifted from being T6SS-negative to -positive to -constitutively active as seen in Haiti El Tor strains. Haiti pandemic strains represent an anomaly in the 7th pandemic as *V. cholerae* was introduced from a small subset of clones from an aids worker from Nepal (Moore et al., 2014). Therefore, at least in this environment, there must have been an evolutionary advantage to move to a more competitive state.

Despite these hypotheses, one question remains unanswered: How were classical strains so successful as the cause of pandemic cholera without using the T6SS as the means of competition? One explanation is that classical strains employ an alternative mechanism to outcompete microbial competitors in the gut. The increased cholera toxin production by

classical strains, compared to El Tor cholera toxin production, could do a more efficient job of clearing the commensals in the mucus layer through violent episodes of diarrhea (Kaper et al., 1995). Cholera diarrhea has been shown to carry other commensals and pathogens other than *V. cholerae* (Begum et al., 2018; Monira et al., 2013). Other studies show a drastic shift in the population of the microbiota indicating that some bacteria have been removed (David et al., 2015; Hsiao et al., 2014). Cholera diarrheal mechanism of action works by causing an electrolyte imbalance across the intestinal layer (Holmgren, 1981). This causes water to rush into the lumen of the small intestine and upwards of 20 litres of diarrhea is released daily (Ali et al., 2012). This diarrhea also removes the mucus layer from the intestine which would likely remove a vast majority of commensal bacteria from the intestine (Alexakis, 2017). Therefore, excess cholera toxin production could be an auxiliary mechanism to the T6SS to remove commensal bacteria from the gut.

A dysfunctional VasK stops production of the T6SS assembly of both the inner and outer tube (Vettiger et al., 2017b). Not employing an active T6SS might offer some advantages. The T6SS costs the bacteria upwards of 750,000 molecules of ATP (80 amoles) per assembly and disassembly of a single sheath (Basler, 2015). The energy intensive component of T6SS activity is the disassembly of the T6SS outer sheath by ClpV. ClpV is an unfoldase necessary to unfold the 1500 VipA/B subunits (Basler, 2015). This is equivalent to the energy from ~20,000 molecules of glucose. Another potential disadvantage of an active T6SS is immunogenicity. Not secreting T6SS proteins will result in a less immunogenic infection and less immune invasion (Ma and Mekalanos, 2010a; Mougous et al., 2006). Additionally, some T6SS competitors do not engage in T6SS competition unless provoked (Basler et al., 2013). Therefore, not producing the T6SS has the advantage of causing a lower response of anti-prokaryotic activities of other bacteria. Other *V. cholerae* strains, including El Tor strains have developed a different strategy to reduce the cost of the T6SS. Instead of disabling mutations, the T6SS is subjected to differential regulation (Miyata et al., 2013). The T6SS appears to only be activated by chitin or mucin (Bachmann et al., 2015; Borgeaud et al., 2015a; Veening and Blokesch, 2017). Under non-inducing conditions, the immunity genes are still produced by a separate promoter located in the 3' region of the effector gene located immediately upstream of the immunity gene (Miyata et al., 2013). This dual regulation provides the bacteria with a

mechanism to not attack with the T6SS whilst still being able to defend (Miyata et al., 2013).

However, there are many advantages to having an active T6SS, that are not limited to the following examples. One advantage is the ability to use anti-eukaryotic effectors. Two anti-eukaryotic effectors have been described in *V. cholerae,* both are utilized by all El Tor strains (Miyata et al., 2011; Pukatzki et al., 2007). One is the C-terminal extension of VgrG-1 (Ma and Mekalanos, 2010a; Pukatzki et al., 2007) and the other is VasX, a cross kingdom effector (Miyata et al., 2011). Both have been shown to have activity against macrophage and the amoeba *Dictyostelium discoideum*. Another advantage is the ability to resist conjugation. In experiments performed with *Pseudomonas aeruginosa,* the bacteria were able to resist conjugation in a T6SS dependent manner (Ho et al., 2013). The T6SS kills cells coming in contact with it attempting to inject potentially parasitic DNA through the T4SS. Additionally, *V. cholerae* with an active T6SS has the increased ability to not only compete within its own species, but also with other Gram-negative bacteria, both commensals and other pathogens (Bernardy et al., 2016; MacIntyre et al., 2010; Unterweger et al., 2012, 2014a). This has been shown under laboratory conditions, on chitin and in the mouse intestine (Bachmann et al., 2015; Borgeaud et al., 2015a; Zhao et al., 2018). Lastly, is the DNA released from the T6SS attack. When cells lyse in a T6SS dependent manner, they release their DNA into the environment (Borgeaud et al., 2015a). This DNA can be used for nutrients, as well as for genetic diversity (Veening and Blokesch, 2017). Genetic exchange following a T6SS mediated attack has been demonstrated (Borgeaud et al., 2015a; Thomas et al., 2017). Ultimately, we propose that the advantages outweigh the disadvantages for El Tor *V. cholerae* strains.

It is unknown what changed to make a previously inactive T6SS important for infection. However, the disease, cholera, has changed. From a shorter, severe disease to a longer lasting disease with a larger window for dissemination (Woodward and Mosley, 1972). It is hypothesized that lower production of cholera toxin might account for the reduced disease symptoms (Kaper et al., 1995). It is possible that the T6SS extends the duration of the disease cholera by keeping the commensal bacteria from reclaiming their niche (Sana et al., 2016b). Interestingly, a new variant of Haitian El Tor strains are emerging that not only has a constitutively active T6SS, but also has classical cholera toxin

production, potentially making them the most competitive *V. cholerae* strains (Son et al., 2011; Zhao et al., 2018). Alternatively, the T6SS might have become more important due to different environmental competitors, a changing microbiome or increasing intraspecific competition

I consider T6SS competition to have two separate facets, the first is the ability to engage in T6SS competition and the second is the ability to defend against a T6SS-dependent attack. In this chapter, I looked at three different groups of pandemic strains – from the 2nd pandemic, and two groups from the 6th pandemic, one with the phenylalanine isoform of TsiV1 and one with the isoleucine isoform of TsiV1 (Table 1) (Unterweger et al., 2018).

Strain Name	Year of Isolation	Country of Isolation	TsiV1 status	Source
PA1849	1849	U.S.A	Isoleucine	(Devault, 2014)
NIH41	1940	India	Isoleucine	John Mekalanos (Harvard Medical School, Boston, MA, USA)
CA401	1953	India	Phenylalanine	Shelley Paine (University of Texas at Austin)
O395	1965	India	Phenylalanine	John Mekalanos (Harvard Medical School, Boston, MA, USA)
A76	1982	Bangladesh	Isoleucine	(Mutreja, 2011)
A389	1987	Bangladesh	Isoleucine	(Mutreja, 2011)
C6706	1993	Peru	Isoleucine	(Thelin and Taylor, 1996)

Table 4-1. **Pandemic strains discussed in this chapter**. The strains are ordered in ascending order of date isolated. The table also gives information on the country of isolation, the immune status and the source of the strain. The isoleucine TsiV1 is a fully competent immunity protein and phenylalanine is the defective copy.

I decided to complete this study by introducing mutations found on the pandemic strains in the strain V52, that has a constitutively active T6SS (Bachmann et al., 2015; Ishikawa et al., 2012; MacIntyre et al., 2010; Metzger et al., 2016). This allows a system to be developed where we can isolate individual mutations by introducing them in the

chromosome of V52 to mimic aspects of the T6SSs of the 2nd and 6th pandemics. Due to mutations in *VCA0109* and *vasK,* 6th pandemic strains are rendered without T6SS activity. Via the same mutation in *VCA0109*, 2nd pandemic strains also do not have T6SS activity (Figure 3). Both of these genes are essential to T6SS activity in *V. cholerae* (Zheng et al., 2011). The mutation in *VCA0109* is a 12 base-pair deletion resulting in the deletion of the amino acids, Valine-Leucine-Valine-Arginine (Figure 3A). PHYRE2 modelling predicts that these four amino acids are a part of a beta-barrel (Figure 3B) (Kelley et al., 2015). Removal of these amino acids likely destroys this secondary structure. Additionally, these four amino acids are located 4 amino acids downstream from a glutamate residue critical for function (Figure 3A) (Lossi et al., 2011). As the mutation in *vasK* is a 16-bp frameshift mutation it is a little easier to interpret. This mutation causes a premature stop codon and likely makes a non-functional protein.

The sudden change in the structural components of the T6SS could explain the new disease course of strains from the 7th pandemic , but it does not explain how the 6th pandemic strains were replaced by El Tor *V. cholerae*. The replacement of pandemics could also be in part T6SS dependent, specifically due to the difference within *tsiV1* between the 6th and 2nd pandemics. A subset of 6th pandemic strains encode a SNP in the immunity gene, *tsiV1*. This SNP causes an amino acid mutation position 163. The 2nd and 7th pandemic *tsiV1* has an isoleucine, which provides full protection to TseL, while a subset of 6th pandemic strains has a phenylalanine at that position and does not provide full protection. This results in a ~10-fold disadvantage over a 24-hour period (Figure 5). This provides a potential mechanism whereby the 7th pandemic strains might have replaced the 6th pandemic strains. Interestingly, 6th pandemic strains isolated after the emergence of El Tor strains had a completely functional TsiV1 (Table 1). This suggests that through a mistake in the polymerase or horizontal gene transfer, 6th pandemics must have repaired their immunity gene to extend their prevalence.

The loss of T6SS activity in the 2nd pandemic, or before, might have been advantageous at the time; however, if this hypothesis is correct it would have ultimately led to its demise. A constantly active T6SS gives evolutionary pressure to retain the immunity genes, and so sometime before or during the 2nd pandemic this pressure was lost,

and subsequently the immunity gene was degraded, allowing a T6SS-active pandemic strain the ability to kill the 6th pandemic strains (Figure 6).

In conclusion, our results suggest that classical *V. cholerae* strains that lack the ability to attack and to defend themselves are weak microbial competitors compared to El Tor strains. New El Tor variants are able to constitutively produce the T6SS and make the classical levels of cholrea toxin. The difference in microbial competitiveness could have been a contributing factor that played into the replacement of pandemic strains, with the competitive El Tor biotype being able to outcompete the classical biotype.

Chapter 5: The T6SS of El Tor *V. cholerae* is tightly regulated by *in-vivo* host factors

Figures 1, 2 3, 5, 6, 7, 8, 9 are published in:

Bachmann, V.*, **Kostiuk, B.***, Unterweger, D., Diaz-Satizabal, L., Ogg, O., and Pukatzki, S.: Bile Salts Modulate the Mucin-Activated Type VI Secretion System of Pandemic *Vibrio cholerae*, *PLoS Neglected Tropical Disease*s 2015

*Authors contributed equally

Figures 2-7 were performed soley by Ben Kostiuk

Experiments to generate data for Figure 1 were performed in collaboration with Dr. Daniel Unterweger.
Experiments to generate data for Figure 8A were performed by Dr. Verena Bachmann.

Experiments to generate data for Figure 9AB were performed in collaboration with Laura Diaz-Satizabal.

Experiments to generate data for Figure 10AB was performed in collaboration with Ashley Wagner

Experiments to generate data for Figure 10C were performed in collaboration with Dr. Stefan Pukatzki.

When referencing data from the manuscript that I was not directly involved in, I will cite (Bachmann et al., 2015)

5-1 Introduction

Upon entering a human host, a bacterial pathogen is vastly outnumbered by both eukaryotic and prokaryotic cells. Pathogens, including the cholera-causing bacterium *Vibrio cholerae*, overcome this numerical disadvantage with strategies to either avoid or fight the host immune system and microbiota (MacIntyre et al., 2010; Pukatzki et al., 2006a).

The small intestine is full of regulatory molecules that bacteria use as signals to control gene expression and coordinate cellular activity. For *V. cholerae* this exposure to host regulatory cues begins in the stomach as the bacteria must adapt to a high acid environment (Merrell and Camilli, 2002; Merrell et al., 2002b). When *V. cholerae* enters the small intestine the environment changes to include a greatly reduced oxygen concentration, a plethora of bile salts, a complex mucin layer, and other bacterial species and metabolites (Begley et al., 2005; Bhowmick et al., 2008; Gunn, 2000; Hsiao et al., 2014; Hung and Mekalanos, 2005; Marteyn et al., 2010).

V. cholerae's type-six secretion system is used to outcompeting prokaryotic and eukaryotic competitors in the environment and human host. Although all *V. cholerae* strains sequenced to date carry the genetic information for the T6SS, not all *V. cholerae* strains have an active T6SS under laboratory conditions (MacIntyre et al., 2010). For example, while the O37 serogroup strain V52 (isolated from a cholera patient in the Republic of the Sudan in 1964) has an active T6SS under laboratory conditions, pandemic *V. cholerae* strains, like the O1 serogroup strain C6706 from Peru, do not express T6SS genes under the same setting (Shao and Bassler, 2014). It is hypothesized that V52's constitutively active T6SS comes from misregulation of the regulator tFoY (Metzger et al., 2016). Zheng *et al.* showed that the T6SS of C6706 is repressed at low cell densities due to the activity of the quorum-sensing regulator LuxO and the transcriptional repressor TsrA (Zheng et al., 2010). At low cell densities, LuxO is phosphorylated and contributes to the generation of small RNAs. These small RNAs specifically bind mRNA transcripts of the large T6SS cluster, thereby inhibiting the translation of important T6SS structural genes and activators. At high cell density, an unphosphorylated LuxO allows activation of the T6SS in pandemic strains when *tsrA* is disrupted (Zheng et al., 2010). This

permits bacterial cells to engage in T6SS-mediated virulence, indicating that high density is critical for expression of the T6SS pandemic *V. cholerae*. The ability to genetically activate the T6SS through *luxO* and *tsrA* deletions establishes that pandemic strains have evolved mechanisms to tightly control a fully functional T6SS (Shao and Bassler, 2014; Zheng et al., 2010).

Experimental evidence suggests that pandemic *V. cholerae* strains de-repress T6SS gene expression during infection of the small intestine of infant mice, rabbits and humans (Fu et al., 2018; Lombardo et al., 2007; Zhao et al., 2018). More recently, *V. cholerae* was shown to engage in T6SS-mediated killing in infant rabbits (Fu et al., 2013, 2018). The biological significance of *in-vivo* T6SS de-repression is beginning to be addressed. *In-vivo,* the T6SS has been implicated in *Vibrio-vibrio* competition, competition with commensals, increased inflammation, increased colonization, and increased expression of other virulence factors (Fast et al., 2018; Fu et al., 2018; Ma and Mekalanos, 2010b; Zhao et al., 2018).

Our laboratory and others observed that the type six secretion system is active *in-vivo,* and given the prevalence of mucin *in-vivo*, in this chapter I explore the role of mucin in T6SS activation. Our experiments revealed that *V. cholerae* C6706 is involved in intraspecific competition inside the infant mouse. We found that the family of glycoproteins that make up the mucus lining, mucins, are responsible for the de-repression of the T6SS, and that bile salts are utilized to modulate T6SS activity either negatively or positively. As the composition of bile is heavily influenced by the spatial location in the gut and by the microbiome, we attempted to gain an understanding of where in the intestines the T6SS is used. Finally, we demonstrate the importance of the T6SS during coinfections with El Tor *V. cholerae* and incompatible environmental isolates.

5-2 The T6SS of *V. cholerae* participates in bacterial killing in the infant mouse

I wanted to understand how the complex array of regulatory cues in the host intestine impacted the type six secretion system. The T6SS of El Tor *V. cholerae* is inactive under laboratory conditions yet is genetically identical to the T6SS of strains that are constitutively active (Miyata et al., 2010b). We therefore reasoned that the El Tor T6SS is tightly regulated and may be only utilized under inducing conditions. To understand the

regulatory cues, we used the El Tor strain C6706 and created a system that resulted in cell death when the T6SS was activated. Specifically, we constructed a strain of C6706 with all three of its immunity genes deleted (C6706Δ*lacZ*Δ*tsiV1-3)*. This strain is unable to grow if the bacterium engages in T6SS mediated competition as the bacterium would be susceptible to T6SS attack and die.

To determine if the T6SS is active in our infant mouse model for cholera, we used combinations of C6706, C6706ΔlacZ, C6706ΔlacZΔvasK, C6706ΔlacZΔtsiV1-3 and C6706ΔvasKΔtsiv1-3. Strains lacking vasK are important controls as they are unable to use their T6SS and therefore any phenotype we see between these strains and vasK-positive strains can be attributed to the T6SS. The presence or absence of lacZ is simply used as a means to differentiate between the two strains in a blue-white screen. Finally, the lack of tsiV1-3 indicates the strain is susceptible to the T6SS attack. To perform these experiments, we infected 3-5 day old infant mice with $5x10^8$ of two strains. The bacteria were resuspended in a 2.5% bicarbonate solution to buffer the stomach acid and increase bacterial titres reaching the small intestine (Fu et al., 2013). The mice were infected for 16 hours, the animals were euthanized and small intestines were homogenized in PBS, diluted and spread on plates containing streptomycin (to select for V. cholerae) and X-gal (a substrate for LacZ that is the basis of the blue-white screen). Concurrent to the infection, the same strains and titres were inoculated into 5mL of LB as an *in-vitro* control. Therefore any difference between the two strains can be attributed to the T6SS.

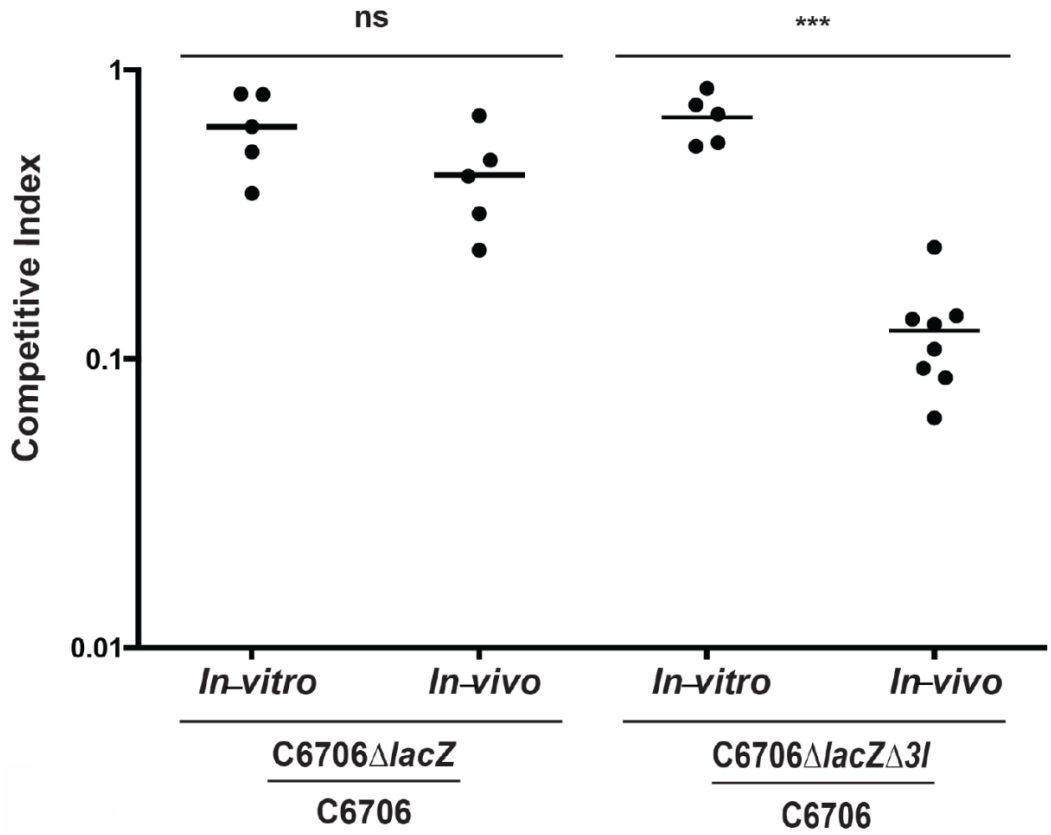

Figure 5-1. **The T6SS of *V. cholerae* is functional *in vivo*.** The T6SS of *V. cholerae* O1 strain C6706 is active in the infant mouse model of infection. *V. cholerae* C6706, C6706Δ*lacZ*, and C6706*ΔlacZΔtsiV1-3* were mixed in pairwise combinations and administered to the infant mouse as mixtures via oral gavage. As an *in-vitro* control, 2 mL LB were inoculated with the same bacterial mixtures and grown overnight at 37°C. After a 16-h incubation, the mice were sacrificed and their small intestines were harvested and plated on X-gal plates to count surviving bacteria. The competitive index of the two competing strains is shown on the *y*-axis. Horizontal bars represent the arithmetic mean of one experiment performed with a minimum of 5 mice in each group. Stars indicate statistical significance (unpaired two-tailed Student's *t*-test), with *** $p < 0.0005$, ns = not significant.

When C6706 was coinfected with C6706Δ*lacZ*Δ*tsiV1-3*, there was an approximate 10-fold reduction in C6706Δ*lacZ*Δ*tsiV1-3* compared to C6706 as measured by competitive index (Figure 5-1). Importantly, this difference was not seen when the experiment was performed in liquid LB, by making a 1:50 dilution of overnight culture and rotating it at 200rpm for 16 hours at 37^{o}C (Figure 1). As controls, C6706 and C6706Δ*lacZ* remained at a 1:1 ratio both *in-vivo* and *in-vitro* (Figure 1). Additionally, C6706Δ*lacZ*Δ*vasK* and C6706Δ*vasK*Δ*tsiV1-3* also remained at a 1:1 ratio (Figure 2A). Finally, the reduction of

C6706Δ*lacZ*Δ*tsiV1-3* was due to TS66-dependent killing and not reduced bacteria division rates, because we saw no reduction of C6706Δ*lacZ*Δ*tsiV1-3* bacterial counts when co-cultured with T6SS-inactive strains (Figure 2B). Together, these results demonstrate that T6SS is active *in-vivo* and that the bacterial density in the small intestine is sufficient to observe T6SS-dependent killing. Furthermore, our experiments suggest that the T6SS might be most important for interspecific competition in the infant mouse model of cholera and not for colonization.

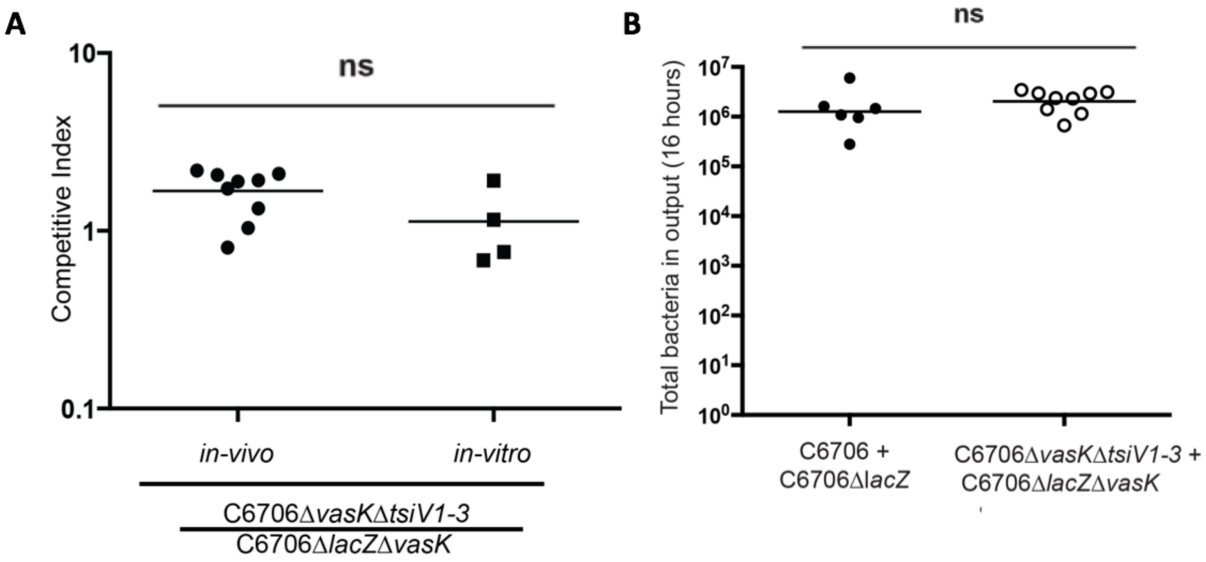

Figure 5-2 **The T6SS is not necessary for colonization of the infant mouse (A)** The T6SS of *V. cholerae* O1 strain C6706 is not required to grow to high titers in the small intestine of infant mice. We mixed *V. cholerae* C6706 with C6706Δ*lacZ*, or C6706*ΔlacZΔvasK* with C6706*ΔtsiV1-3ΔlacZ* and administered the mixtures to the infant mouse via oral gavage. As an *in-vitro* control, we added strain mixtures to 2 mL LB to be grown overnight at 37°C. After a 16-h incubation, the mice were sacrificed, their small intestines were harvested and plated on X-gal plates to count the total numbers of surviving bacteria. **(B)** The T6SS of *V. cholerae* O1 strain C6706 is not involved in the colonization of the infant mouse model of infection. We mixed *V. cholerae*C6706*ΔlacZΔvasK* and C6706*ΔvasKΔtsiV1-3* and administered to the infant mouse via oral gavage. As an *in-vitro* control, we added strain mixtures to 2 mL LB to be grown overnight at 37°C. After a 16-h incubation, the mice were sacrificed, their small intestines were harvested and plated on X-gal plates to count surviving bacteria The competitive index of the two competing strains is shown on the *y*-axis. Horizontal bars represent the geometric mean of one experiment performed with a minimum of 6 mice in each group. A Student's *t*-test was performed for significance with ns representing no significance.

5-3 Mucin allows pandemic strains to utilize their T6SS

Having discovered that the T6SS of C6706 is activated in mouse intestines, I sought to investigate the cues within the host responsible for T6SS activation. We investigated three major factors of the intestine that we proposed could affect the activation of the T6SS; mucin, bile, and anaerobic environments. Competition assays were used as a readout for an activated T6SS. A competition assay in this context is an assay where two bacterial strains are combined, one *V. cholerae* with a prey strain of *E. coli*, on an agar plate for four hours and then I would enumerate the surviving *E. coli.* By changing the environment of the competition assay, we can isolate the environmental characteristics that affect the T6SS by changes in surviving *E. coli*. Removing oxygen does not activate the T6SS of C6706, as evidenced by competition assays performed in an anaerobic chamber. We also performed a control experiment to ensure that our anaerobic conditions did not reduce T6SS activity; specifically we mixed the T6SS active strain V52 with *E. coli*. Since anaerobic conditions did not alter T6SS activity of V52, we concluded that T6SS activity could occur under the anaerobic conditions of the gut (Bachmann et al., 2015). Next, a crude preparation of bile from the gut of an ox was supplemented into the LB agar plate at various concentrations (Bachmann et al., 2015). While ox bile had no activity on the T6SS of C6706 at a range of concentrations, at high concentrations, bile inhibited the T6SS of V52 (Bachmann et al., 2015). This indicates that components of bile can influence the activity of T6SS. This further implicates a possible *in-vivo* role of the T6SS of *V. cholerae*.

Lastly, we tested the ability of mucin to activate the T6SS of *V. cholerae*. To perform these experiments, I prepared 2% mucin columns in Eppendorf tubes dissolved in Krebs-Ringer Tris buffer (KRT). 10^8 *V. cholerae* were placed on top of the mucin column. As a control, gelatin was used to resemble the consistency of mucin. To test for activation, we used the strains C6706, C6706Δ*tsiv1-3*, and C6706Δ*vasK*Δ*tsiv1-3*. The rationale for this experiment is that if the T6SS is activated, the bacteria will start attacking their sister cells. While C6706 and C6706Δ*vasK*Δ*tsiv1-3* levels remained at the inoculated level there was a ~10 fold decrease in the number of C6706Δ*tsiv1-3* bacteria, indicating that they failed to protect themselves from T6SS mediated attack (Figure 3). In the case of the wild-type C6706, we hypothesized the bacteria survived as they encode the immunity genes.

However, C6706Δ*tsiv1-3* attacked their sister cells and succumbed to the toxins therefore decreasing in bacterial numbers. As the final T6SS control, C6706Δ*vasK*Δ*tsiv1-3* does not secrete T6SS toxins and therefore did not kill one another. The results implicated mucin as the likely *in-vivo* activator of the T6SS.

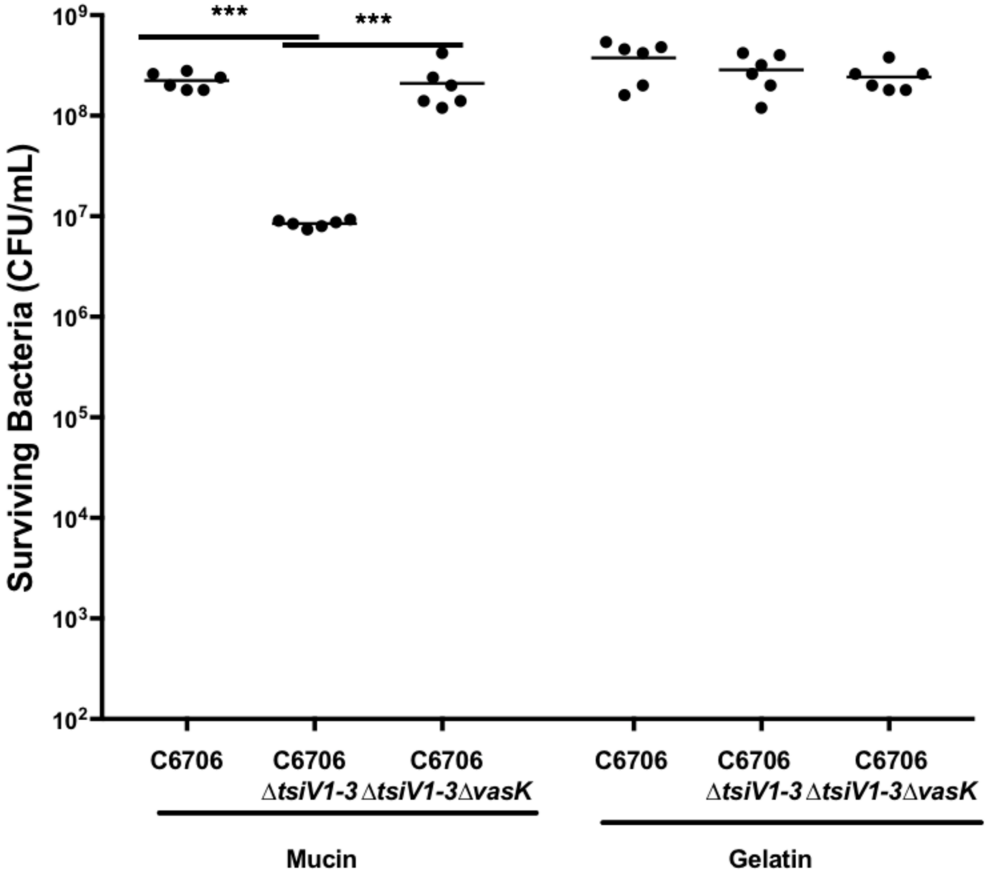

Figure 5-3. ***V. cholerae* O1 C6706 have an activated T6SS in the presence of mucins.** **(A)** Survival assay of *V. cholerae* C6706 mutants on mucins. 1×10^8 *V. cholerae* C6706, C6706Δ*tsiV1–3* (lacking all three immunity genes), or C6706Δ*tsiV1–3*Δ*vasK* (lacking all three immunity genes and the T6SS gene *vasK*) were loaded separately on columns containing 3% mucins or **(B)** 3% gelatin. After incubation for 2 h at 37°C, eluents were collected, and serial dilutions were plated on selective LB agar plates. Surviving numbers of *V. cholerae* bacteria were plotted as CFUs. Means are shown of 6 replicates over 3 experiments. Stars indicate statistical significance (unpaired two-tailed Student's *t*-test), with *** $p < 0.001$.

Mucins are a class of glycoproteins that are the primary constituents of mucus that lines the entire digestive and respiratory tract of mammals (Turner, 2009). Mucins are a diverse group of proteins that carry a variety of functions. Some mucins remain attached to the cell

surface while others are secreted (Perez-Vilar and Hill, 1999). Mucus functions to aid in digestion, protect the intestines from pathogens and house commensal bacteria (Turner, 2009). Mucus acts as a cue to *V. cholerae* to upregulate genes involved in motility for the pathogen (Bhowmick et al., 2008; Liu et al., 2008). I rationalized that *V. cholerae* interacting with mucus coupled with turning on an antibacterial system will aid in the colonization of the pathogen.

However, there are several components of mucus that could activate the T6SS. I attempted to biochemically dissect the component or components of mucus that are responsible for this activation. The first logical component to test was the proteins themselves, however, due to the nature of mucins – being glycosylated on approximately every third amino acid – makes it incompatible with proteases and glycosylases/neuraminidases (Perez-Vilar and Hill, 1999).

This complexity made the dissection of the activating compound difficult. One theme that remained consistent was that I was unable to dialyze out the T6SS de-repressing compound even at a pore size of 100kDa (Figure 4A). This indicates that the activating molecule is very large or attached to the protein. A sugar attached to the protein backbone of mucin fits this description. Sugars are often used as regulatory cues for *V. cholerae* (Meibom et al., 2005). However, the major mucin-based sugar, N-acetyl neuraminic acid, yielded no de-repression of the T6SS (Figure 4B). Next, I looked to investigate the inhibitory effects of crude ox bile.

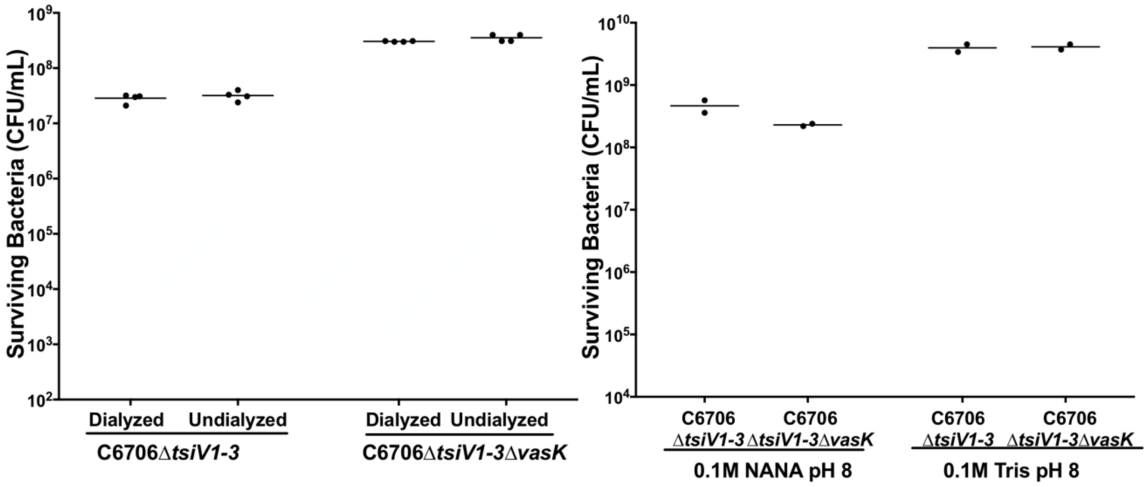

Figure 5-4. **Dissecting the component of mucin to activate the T6SS of *V. cholerae*** **(A)** 1 × 10^8 *V. cholerae* C6706, C6706Δ*tsiV1–3* (lacking all three immunity genes), or C6706Δ*tsiV1–3*Δ*vasK* (lacking all three immunity genes and the T6SS gene *vasK*) were

loaded separately on columns containing 3% mucin or 3% dialyzed mucin (100kDa pore size). After incubation for 2 h at 37°C, eluents were collected, and serial dilutions were plated on selective LB agar plates. Surviving numbers of *V. cholerae* bacteria were plotted as CFUs. Data represent values of two independent experiments done in duplicate with a line at the arithmetic mean. **(B)** The same experiment as in (A), however, instead of mucin, to investigate the major mucin sugar, we used 0.1M n-acetylneuraminic acid Tris solution as the medium. As a negative control for the sugar, a Tris solution alone was used. Means are shown of 4 replicates over 2 experiments.

5-4 Specific bile salts can enhance or decrease T6SS killing

Bile acid is the major component of bile, along with cholesterol and other fats. Primary bile acids are a collection of molecules synthesized by the liver and secreted into the intestine to aid in the digestion of lipids. Primary bile acids largely include cholic acid (CA), a derivative of cholesterol, as well as cholic acid conjugated to glycine (gly) or taurine (tau) – resulting in glycocholic (GC) and taurocholic acid (TC), respectively (Begley et al., 2005). As bile transverses the small intestine, commensal bacteria metabolize the bile salts, by removing the glycine and taurine or through dehydroxylation, resulting in deoxycholic acid (DOC), glycodeoxcycholic acid (GD) or taurodeoxcyholic acid (TD). The dehydroxylated bile acids are termed secondary bile acids, and are less lipophilic, and are thereby able to be reabsorbed by the large intestine so they can be hydroxylated by the liver and enter the small intestine once again (Begley et al., 2005). This enterohepatic recycling pathway is summarized in figure 5. In addition to its role as a regulatory cue, aiding in digestion, bile acids are also antibacterial. Therefore, pathogenic bacteria not only need to develop mechanisms to resist bile salt but also to use it as a signal (Bina et al., 2008; Gunn, 2000).

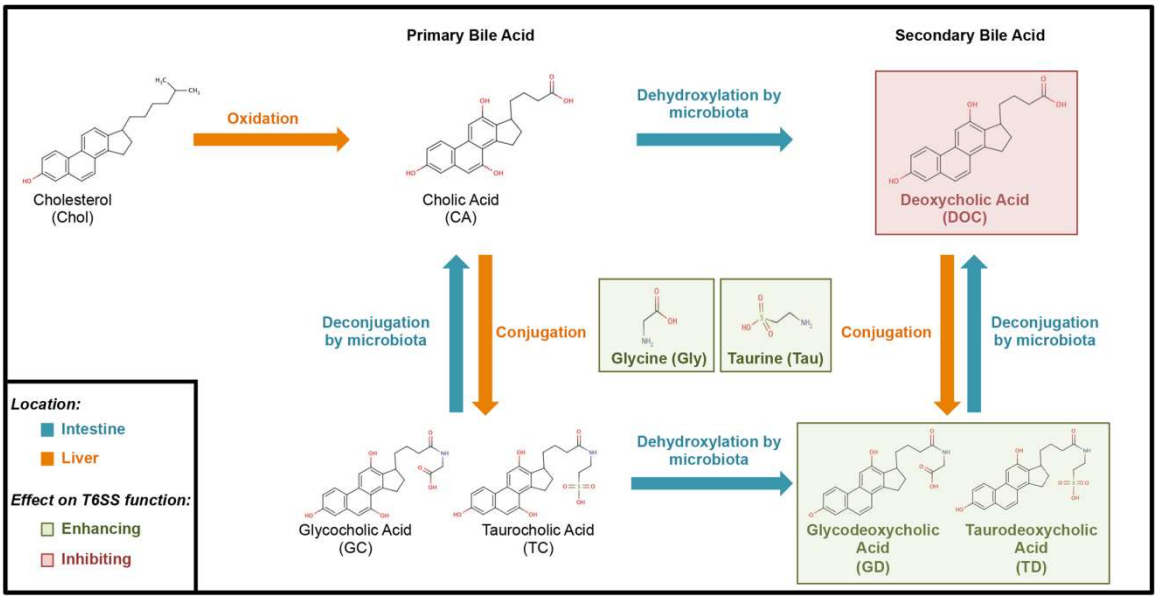

Figure 5-5. **Bile acid metabolism.** In the liver (orange arrows), cholesterol is enzymatically converted to primary bile acids such as cholic acid. After conjugation of taurine or glycine to cholic acid by hepatocytes, the resulting glycocholic acid or taurocholic acid are stored in the gall bladder until released into the small intestine in response to food ingestion. In the small intestine (blue arrows), several commensals deconjugate and/or dehydroxylate bile acids, producing unconjugated deoxycholic acid and cholic acid. Alternatively, glycholic acid or taurocholic acid can be dehydroxylated to the conjugated secondary bile acids glycodeoxycholic acid or taurodeoxycholic acid. In a process called enterohepatic circulation, unconjugated bile acids are excreted with the feces or reabsorbed from the ileum back into the liver. Depending on the types of microbiota and nutrition ingested, bile acid composition may vary throughout the intestines. Therefore, the inhibitory effect identified in this study (red) of deoxycholic acid and the enhancing effect (green) of glycodeoxycholic acid or taurodeoxycholic acid on the T6SS of *V. cholerae* may vary depending on the microbiota present.

Because the composition of bile is dependent on the microbial composition of the gut it varies in different spatial locations, it is often used as a cue for bacteria to determine their spatial environment (Hay and Zhu, 2015; Hung and Mekalanos, 2005). For *V. cholerae*, bile salts have been implicated in many different cellular processes. For example, components of bile have been linked to biofilm formation and dispersal, cholera toxin production and motility (Gupta and Chowdhury, 1997; Hay and Zhu, 2015; Hung and Mekalanos, 2005). To determine the components of bile that are responsible for the decrease in T6SS activity, I prepared LB agar plates supplemented with either 1.2mM of CA, DOC, GD, TD, glycine or taurine. On these plates we performed competition assays between either V52, V52Δ*vasK* and *E. coli*. We were then able to enumerate surviving *E.*

coli and compare the degree of killing versus a control plate lacking bile salts, allowing us to determine the effect that the individual components had on T6SS activity. Surprisingly, we found that while CA did not affect the numbers of *E. coli* killed, GD, TD, glycine and taurine increased T6SS dependent killing by approximately 10-fold (Figure 6). These phenomena are in direct contrast with the effect of a crude bile prep. The bile salt DOC caused a large reduction in T6SS-dependent killing (Figure 6). DOC is a bile salt produced during metabolism by commensal bacteria, where it is both deconjugated and dehydroxylated (Begley et al., 2005). This invokes an intriguing model where commensal bacteria metabolize bile salts to decrease the activity of an antibacterial system. To investigate whether the increased killing in the presence of glycine was a general effect of amino acid supplementation or specific to bile, we included two amino acids – phenylalanine and alanine in our killing assays and observed no enhancing effects of the T6SS (Figure 6). In fact, we saw a statistically significant reduction in killing that we hypothesize to not be biologically relevant due to the small magnitude. Interestingly, GD and TD stimulated the V52 T6SS at levels similar to unconjugated glycine and taurine (Figure 6). When DOC was supplied in combination with either free glycine or taurine, an intermediate repression of T6SS activity was observed (Figure 6). The reduction in T6SS was reduced from 12-fold to 6-fold. This suggests that the carboxylic acid group on deoxycholic acid (to which glycine and taurine are conjugated) may be important for inhibition of the T6SS of *V. cholerae*.

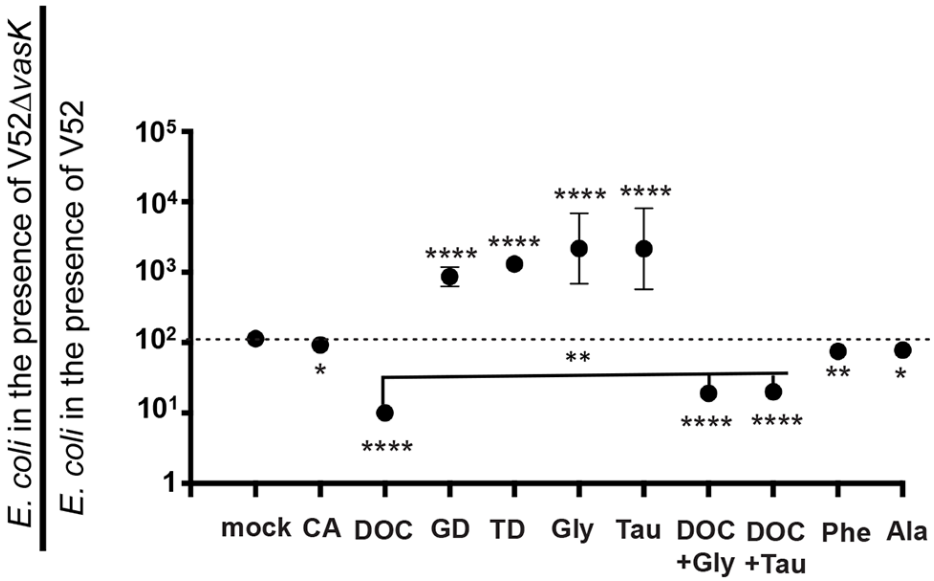

Figure 5-6**. Bile salts influence T6SS function.** Individual bile acids affect the T6SS of *V. cholerae* V52. Predator *V. cholerae* V52 or V52Δ*vasK* were mixed at a 10:1 ratio with prey *E. coli* MG1655 and spotted on LB agar plates supplemented with 1.2 mM cholic acid (CA), glycocholic acid (GC), taurocholic acid (TC), deoxycholic acid (DOC), glycodeoxycholic acid (GD), taurodeoxycholic acid (TD), glycine (Gly), or taurine (Tau) for 4 h at 37°C. CFUs were counted after incubation of serial dilutions of eluent on LB agar plates overnight. The killing index was calculated by the ratio of surviving prey in the presence of V52 versus attenuated V52. The graph gives mean values ± SD of two experiments done in duplicate. A Student's *t*-test was performed for significance, with *$p<$ 0.05, ** $p < 0.005$, *** $p < 0.0005$, **** $p < 0.0001$.

DOC downregulating the T6SS is not unique to *V. cholerae.* In the Gram-negative intestinal pathogen *Campylobacter jejuni* DOC downregulated the T6SS, however it was killing the bacteria through selective T6SS-dependent toxicity rather than through a regulatory mechanism (Lertpiriyapong et al., 2012). When the T6SS was active, pores are made in the outer-membrane of the bacteria where the T6SS tube is ejected. Through this pore, the authors suggest that DOC diffuses in and is cytotoxic (Lertpiriyapong et al., 2012). We tested whether this was the case for *V. cholerae* as well. I found no difference in growth rate between V52 and V52Δ*vasK* at a variety of concentrations of DOC. However, in liquid culture, the growth rate of V52 and V52Δ*vasK* was severely (by 10-fold), but equally, reduced at higher concentrations (Figure 7A). This was not an observation we had made on agar plates where T6SS competition assays were performed (Figure 7B). Together, this suggests that DOC does not regulate the T6SS of *V. cholerae* through T6SS-dependent toxicity.

To rule out the potential that the bile salts are toxic or enhance the growth of either *V. cholerae* or *E. coli* on the agar plates, the strains were plated individually; no growth defect was found at a variety of concentrations for glycine, taurine or DOC (Figure 7BC). Concurrently, we tested T6SS-dependent killing and found that DOC, glycine and taurine work on the T6SS in a dose-dependent manner (Figure 7BC).

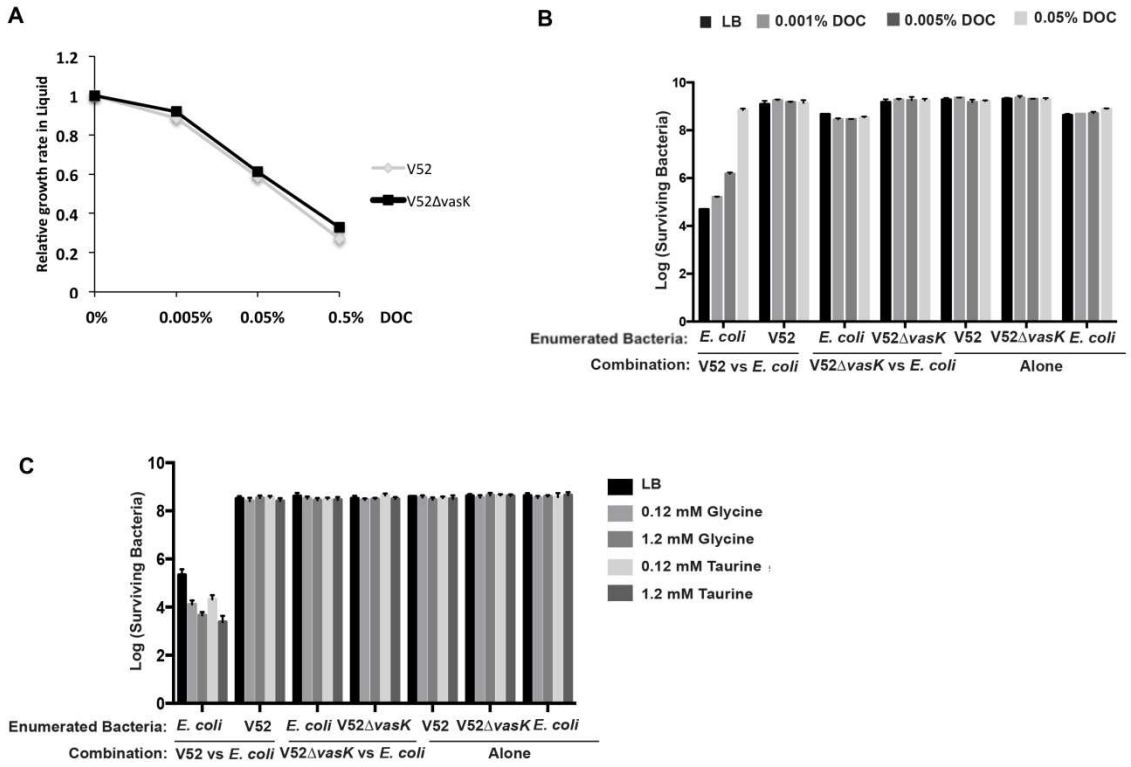

Figure 5-7. **Deoxycholic acid (DOC), glycine and taurine affect the T6SS of *V. cholerae*. (A)** Growth curves of V52 and V52Δ*vasK* in various concentrations of DOC. A 1:100 dilution of overnight culture was made in LB, LB + 0.005% DOC, LB + 0.05% DOC and LB + 0.5% DOC. OD_{600} values were measured for both *V. cholerae* strains under these four concentrations every 30 min for 6 h. The slope of each growth curve was calculated for mid-log bacteria. The slopes of the growth curves in LB + DOC were compared to the slopes in LB alone and the ratios were plotted. **(B)** Killing assays in the presence of various concentrations of DOC. *V. cholerae* V52 or V52Δ*vasK* were mixed at a 10:1 ratio with *E. coli* MG1655 and employed in a killing assay with *E. coli* MG1655 as prey. Surviving numbers of *E. coli* are plotted on the y-axis. Bars show mean values ± SD of two independent experiments done in duplicate. **(C)** Killing assays in the presence of various concentrations of taurine and glycine. *V. cholerae* V52 or V52Δ*vasK* were mixed at a 10:1 ratio with *E. coli* MG1655 and employed in a killing assay with *E. coli* MG1655 as prey. Surviving numbers of *E. coli* are plotted on the graph. Bars show mean values ± SD of two independent experiments done in duplicate.

We next investigated if these phenomena held true for C6706. This strain requires de-repression of the T6SS by mucin, so we tested the ability of bile salts to modulate the activity by supplementing the mucin with bile salts. We used the same strains as in previous mucin experiments, C6706 and C6706Δ*tsiV1-3*, to determine the extent of T6SS activation. In this case a ratio was made between survival on mucin columns and survival on mucin

columns supplemented with bile salts to calculate modulation. Indeed, we saw increased killing of sister cells with glycine and taurine by five-fold and reduced killing with DOC by three-fold (Figure 8A). This matches our results with V52. The exception is that for C6706, GD and TD did not increase killing (Figure 8A). It could be that these bile salts have a minor effect, and that C6706 is less able to respond to bile salts, or perhaps some bile salts are present in the crude mucin mix and their effect is already accounted for. To confirm that these effects were mucin-dependent, we performed growth curves with C6706 and C6706Δ*tsiV1-3* in the presence of the bile salts without any mucin. Aligned with the hypothesis that this is a T6SS dependent effect brought on by mucin, we saw no difference in the growth rate when comparing the two strains (Figure 8B).

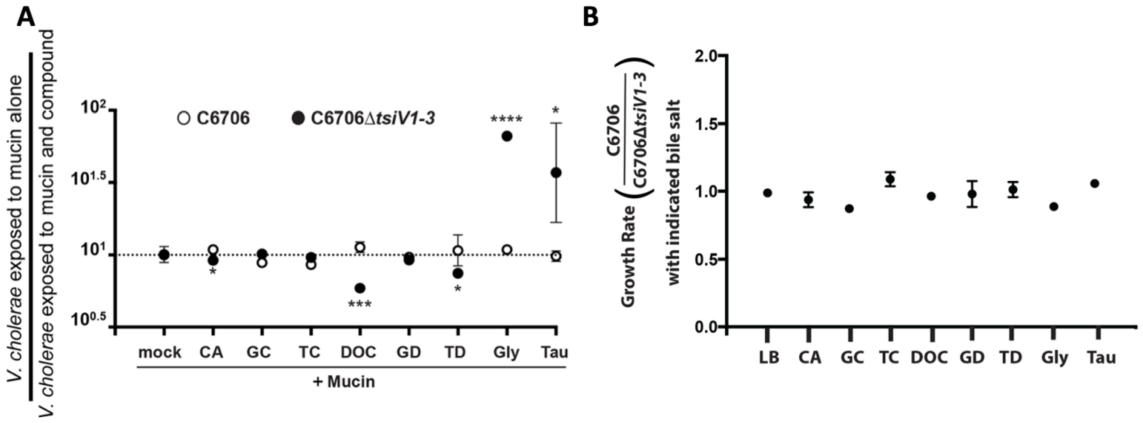

Figure 5-8. **Bile salts modulate a mucin activated T6SS. (A)** Bile acids affect a mucin-activated T6SS of *V. cholerae* C6706. 1 × 10^8 *V. cholerae* C6706 or C6706Δ*tsiV1–3* were loaded separately on columns containing 3% mucins. After incubation for 1 h at 37°C, either cholic acid (CA), glycocholic acid (GC), taurocholic acid (TC), deoxycholic acid (DOC), taurodeoxycholic acid (TD), glycodeoxycholic acid (GD), glycine (Gly), or taurine (Tau) were added to the mucin columns at a final concentration of 1.2 mM each. After incubation for 2 h at 37°C, cells were collected, serial dilutions were plated on LB agar plates, and surviving numbers of C6706 or C6706Δ*tsiV1–3* were plotted. Bars show mean values ± SD of two independent experiments done in duplicate. **(B)** Growth curves of C6706 and C6706Δ*tsiV1-3* in various bile salts. A 1:100 dilution of overnight culture was made in LB, and LB with cholic acid (CA), glycholic acid (GC), taurocholic acid (TC), deoxycholic acid (DOC), glycodeoxycholic acid (GD), taurodeoxycholic acid (TD) glycine (Gly) or taurine (Tau). OD_{600} values were measured for both *V. cholerae* mutants under these conditions every 60 min for 4h. The slope of each growth curve was calculated for mid-log bacteria. The slope of C6706 was divided by C6706Δ*tsiV1-3* and plotted.

Next, we sought to investigate the regulatory mechanism behind the bile salt dependent inhibition and enhancement of T6SS activity. To do so, we performed qRTPCR

on V52 grown in the presence of DOC, glycine, taurine, DOC plus glycine or DOC plus taurine and looked at the expression of an essential T6SS gene. We used the transcript of *hcp* as a readout for T6SS activity. None of the compounds had an effect on *hcp* expression (Figure 9A). As *hcp* is only found in the auxiliary T6SS gene clusters, we looked at the ability of DOC to affect the gene expression of effector genes as well as the master regulator in the large T6SS gene cluster. To do this, we looked at *tseL, vasX, vgrG,* and *vasH* and saw no decrease in gene expression (Figure 9B). To examine if the regulation was occurring on the protein level, we performed the same experiments (using the same samples for the qRTPCR and killing assays) but did Western blot analysis for Hcp. Again, we saw no appreciable difference in Hcp levels in the pellet of the bacteria (Figure 9C).

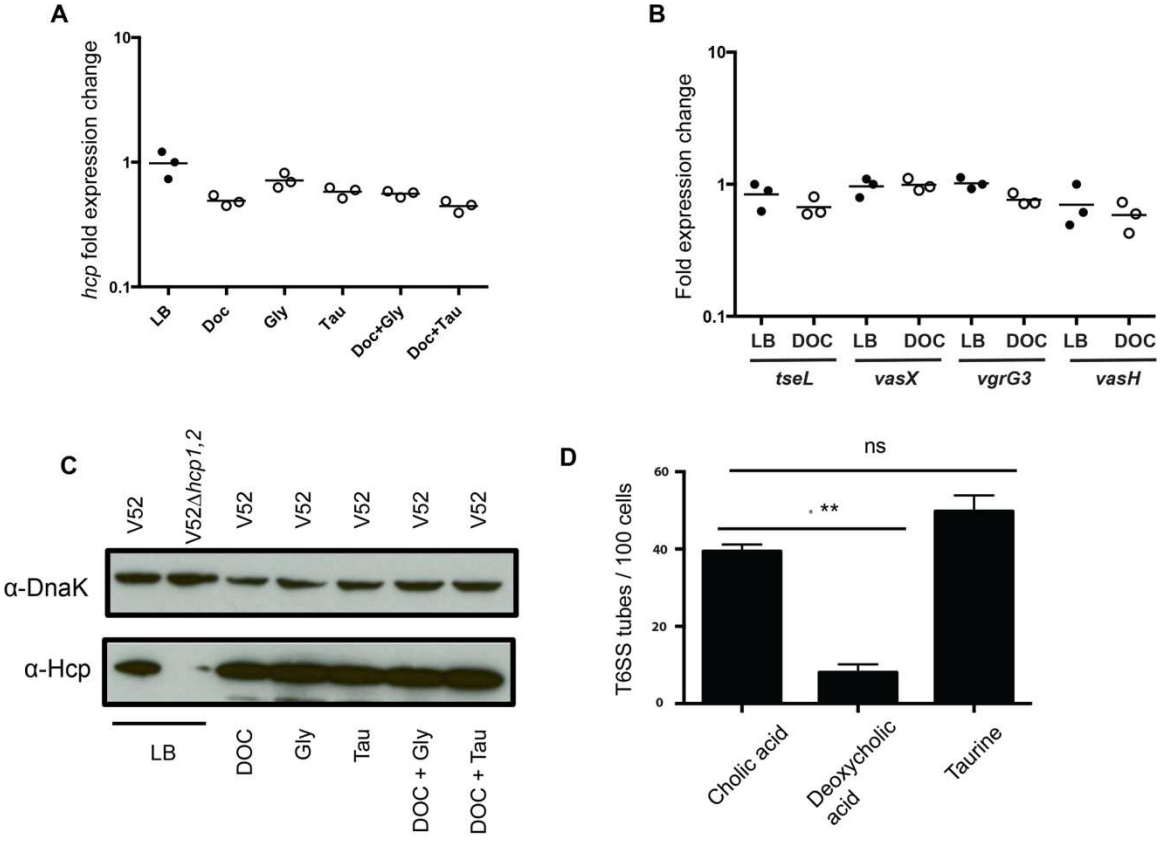

Figure 5-9. **Deoxycholic acid regulates tube formation. (A)** Bile salts do not affect the transcription of *hcp* in V52. V52 was incubated for two hours with 1.2 mM deoxycholic acid, glycine, taurine and combinations of the three. RNA was then isolated, converted to cDNA, quantified using qPCR, and compared to 16S rRNA gene. Experiments were performed in triplicates and normalized to the LB control. **(B)** Deoxycholic acid does not affect the transcription of *tseL*, *vasX*, *vgrG3*, *vasH* in V52. V52 was incubated with 1.2 mM deoxycholic acid for two hours. RNA was isolated, converted to cDNA and quantified using qPCR. Experiments were performed in triplicates and normalized to the LB

control. **(C)** Bile salts do not affect Hcp-2 levels in V52. V52 was incubated with 1.2 mM deoxycholic acid, glycine, taurine and combinations of the three for two hours. Bacteria were harvested and western blot analysis was performed using antibodies for Hcp-2 and DnaK. **(D)** Deoxycholic acid affects the ability of the T6SS to form tubes. *V. cholerae* 2740–80 with a sfGFP labeled *vipA* was incubated with 1.2 mM cholate (negative control), deoxycholic acid or taurine for thirty minutes. After this incubation, the cells were imaged for ten minutes using the Super Resolution OMX microscope. Three frames were chosen and the number of extended T6SS tubes were counted. A Student's *t*-test was performed for significance, with ** $p < 0.005$; ns is no significance.

As we were unable to see a difference on the transcript or protein level, we thought it best to visualize the T6SS using microscopy to determine if we could directly see a difference. We tagged the outer sheath protein, VipA, with a sfGFP protein in the *V. cholerae* strain 2740-80. This is a technique widely used to measure T6SS dynamics in a living bacteria (Basler et al., 2013; Borgeaud et al., 2015a; Vettiger et al., 2017a). I grew the bacteria in liquid media containing LB supplemented with 1.2mM of CA, DOC or taurine. I then placed the bacteria on agarose pads and prepared them for microscopy on a Super Resolution OMX microscope and imaged every 30 seconds for 10 minutes.

The images were then analyzed by randomly choosing three images per experimental group and counting not only the bacterial cells but also the T6SS rods. In the cholate control, we counted just under 40 T6SS tubes per 100 bacterial cells (Figure 9D). This dropped 13-fold when the bacteria were grown under the presence of DOC (Figure 9D). When the bacteria were grown in the presence of taurine there appeared to be increased number of T6SS tubes, however, this difference proved statistically insignificant (Figure 9D). We hypothesize that deoxycholic acid regulates the T6SS by destabilizing the macromolecular tube complex, which prevents delivery of toxic effectors to neighboring cells.

Together, these data suggest that the repression on the T6SS of *V. cholerae* is relieved *in-vivo*, and that the spatial composition of bile has the ability to influence the magnitude of T6SS activity. However, we have yet to ascribe a T6SS role. While T6SS-dependent killing was observed in the infant mouse, we saw no advantage between T6SS-positive and T6SS-negative strains, indicating that at least in this model, there was no advantage between encoding the T6SS or not when both *V. cholerae* strains encoded the immunity genes (Figure 2B). This suggested that the T6SS might not be important for

interacting with the undeveloped microbiome of infant mouse. Instead, we turned to look at intraspecific competition.

5-5 The T6SS of pandemic *V. cholerae* is used for intraspecific competition in the infant mouse

To explore the role of the T6SS of El Tor *V. cholerae* in competition with non-pandemic strains, we performed infections with C6706 or C6706Δ*vasK* and three environmental isolates that did not share the AAA compatibility group but were able to successfully colonize the infant mouse (Unterweger et al., 2012, 2014a). C6706 or C6706Δ*vasK* was marked with a transposon encoding a kanamycin resistance cassette, DL4212, DL2114, and DL4211 were marked with transposons encoding chloramphenicol, trimethoprim and spectinomycin, respectively. After 16 hours of infection, the mice were sacrificed. We looked specifically at the proximal 1cm of the small intestine to test our hypothesis that the T6SS is important at early timepoints in infection. Each were plated onto plates with the four antibiotics to look for the difference in colonization over the tissue and the effect of the T6SS. In these tissues, we saw a complete removal of DL4212 and DL2114 in a T6SS dependent manner (figure 10A). Perhaps more interesting is the observation that C6706 numbers were approximately 10-fold higher than C6706Δ*vasK* in tissues where we presume killing occurred (Figure 10B). The killing of the DL2114 and DL4212 *in-vivo* matched *in-vitro* data using V52 as the predator against these strains *in-vitro* (Figure 10C). We saw that, when enabled with a T6SS, V52 outcompeted the DL strains by between 10 and 1000 times. This phenotype was reversed when V52 was not equipped with the T6SS. This matches the literature that suggests that T6SS mediated killing creates a favourable environment for the proliferation of *V. cholerae* (Zhao et al., 2018). These results invite intriguing hypotheses whereby toxigenic *V. cholerae* strains use their T6SS to exclude non-toxigenic *V. cholerae* strains in early spatial areas during infection.

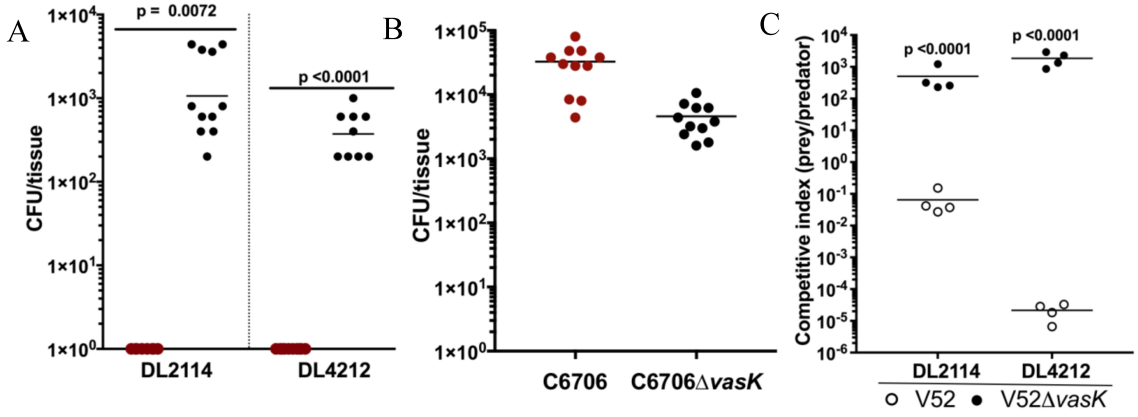

Figure 5-10. **Toxigenic El Tor exclude nontoxigenic strains. (A)** Co-infections with nontoxigenic and toxigenic strains. After 16 hours post infection (hpi), the proximal quarter of the small intestine was removed. Total colony-forming units of DL strains are plotted in the presence of C6706 (red circles on x-axis) or C6706Δ*vasK* (black circles). **(B)** Total colony-forming units o of C6706 (red circles on x-axis) or C6706Δ*vasK* in the same experiment as (A) **(C)** Nontoxigenic DL strains were competed against V52 or V52Δ*vasK*. The competitive index was calculated by dividing surviving prey by surviving predator. P-values from Student T-test are indicated.

5-6 Discussion

The marine bacterium *V. cholerae* thrives in a wide variety of environments and has evolved mechanisms to sense cues that control host colonization and virulence factors in a spatiotemporal fashion. For example the bile salt cholate acts as a cue to form biofilms, whereas the bile salt taurocholate acts as a signal for biofilm dispersal (Hay and Zhu, 2015; Hung et al., 2006). Additionally, some bile salts are known to increase cholera toxin production, while others decrease it (Gupta and Chowdhury, 1997; Hung and Mekalanos, 2005). Bile also has been shown to increase motility of *V. cholerae* (Gupta and Chowdhury, 1997). Not all the actions of bile act on gene regulation. Bile has been shown to reduce the binding of cholera toxin to G_{M1} gangliosides, the receptor on epithelial cells that facilitates cholera toxin internalization (Chatterjee and Chowdhury, 2008). Additionally, bile has antibacterial properties that *V. cholerae* must expel in order to survive (Bina and Mekalanos, 2001; Bina et al., 2008). This demonstrates that the physical properties of bile, as well as its regulatory properties allow it to control the pathogen. The later appears to be true for bile reducing T6SS activity. Mucin is also a major regulator of *V. cholerae*, as mucin causes the overexpression of the protease HapA (Silva et al., 2003).

HapA is necessary for motility through mucin and subsequent virulence (Silva et al., 2003). Here, we add these regulatory cues to another virulence factor – the T6SS.

Together with the recent findings from other research groups, our *in-vivo* experiments demonstrate the T6SS activation of pandemic *V cholerae* strains *in-vivo* (Fu et al., 2018; Zhao et al., 2018). However, the host factors responsible for *in-vivo* activation of T6SS for pandemic strains were previously unknown. Our finding that the T6SS is functional under anaerobic conditions prompted us to identify host cues for T6SS activation and to investigate the role of anaerobic commensal bacteria in regulating the T6SS (Bachmann et al., 2015). We found that mucins activate the T6SS and that this activation can further be modulated by bile acids which are under the metabolic control of commensal bacteria (Figure 8A). This provides new insights into the complex regulation of the T6SS *in vivo*. We hypothesize that the activated T6SS is used by *V. cholerae* to counteract host defense cells, such as macrophage, and to compete with other bacteria for nutrients and space during infection of the host small intestine. These other bacteria could be commensals, other pathogens, or members of the same species (Figure 10AD) (Fu et al., 2018; Zhao et al., 2018).

Our experiments between the El Tor pandemic C6706 and the environmental isolates show that pandemic strains may utilize their T6SS to outcompete environmental strains that do not productively contribute to infection (Figure 10). These experiments help us understand a conceptual paradox of cholera that infections are clonal (Ali et al., 2011; Dixit et al., 2014; Domman et al., 2018) despite the observation that aquatic environments contain a diverse population of cholera toxin producing and non-producing *V. cholerae* (Dutta et al., 2013a; Faruque et al., 2003b). Strains not producing cholera toxin would be predicted to cheat, by benefiting from cholera toxin and amplifying alongside the more pathogenic strains. However, this does not occur, and when cholera toxin producing strains bloom, non-toxigenic strains are greatly reduced (Faruque et al., 2004). When Faruque *et al.* collected 129 water samples from six environmental sites, they found that only 2.3% of culturable *V. cholerae* were toxigenic – likely El Tol strains. However, when those water samples were introduced into the infant rabbit, the proportion shifted and there was a 30-fold increase in toxigenic strains in the intestines. This amplification is despite the observation that most of the non-toxigenic strains were able to colonize the gut (Faruque

et al., 2004). This observation is supported by another finding that while non-toxigenic strains often in patients where non-toxigenic strains are present, there is a high proportion (37%) of multiple serogroups being present (Dutta et al., 2013b). However, when an O1 or O139 strain is present, non-toxigenic strains appear to be absent (Dutta et al., 2013b). While no mechanism has been explored, our data suggests the T6SS contributes to this clonal domination of El Tor strains. Differences between El Tor and environmental T6SSs include regulation as well as the repertoire of effectors (which will be explored in chapter 5).

Different *V. cholerae* strains regulate their T6SS differently (Kitaoka et al., 2011b; Metzger et al., 2016). V52 employs a constitutively active T6SS, whereas C6706 has a repressed T6SS that is activated *in vivo* (Figure 1) (MacIntyre et al., 2010). This is reflected by different regulatory paths for the T6SS (Metzger et al., 2016). Diversity of T6SS regulation among *V. cholerae* strains might indicate a diversity of biological function between pandemic strains and those associated with smaller outbreaks and the differential role the T6SS might have in the host versus the environment. T6SS regulators are likely utilized differently in V52 and C6706. Three direct regulators of the T6SS have been identified, VasH, TfoX, and TfoY (Kitaoka et al., 2011b; Metzger et al., 2016). Both TfoX, and TfoY appear to work by activating the large cluster, so that VasH can drive transcription of the auxiliary clusters (Metzger et al., 2016). TfoX has been shown to be activated for growth on chitin, and coregulates the T6SS and natural competence (Borgeaud et al., 2015b). The environmental cues that govern TfoY regulation are unknown, but as TfoX is regulated by environmental cues, perhaps TfoY is regulated by *in-vivo* cues, such as bile and mucin.

C6706 and other pandemic strains have a T6SS that is repressed under laboratory conditions and potentially in other stages of the lifecycle (Kostiuk et al., 2018). However, as shown recently for chitin and now for mucins, El Tor *V. cholerae* strains can de-repress their T6SS to compete within their species and with other prokaryotes. *V. cholerae* is often introduced to the human host by the ingestion of contaminated water, thus multiple strains may launch an infection (Figure 2) (Borgeaud et al., 2015b). Activation of the T6SS in pandemic strains by mucins may allow the pandemic *V. cholerae* to kill

competing *V. cholerae* strains to become the dominant agent of infection. This is demonstrated in figure 10.

Our findings suggest that products of bile acid metabolism by commensal bacteria have roles in regulating *V. cholerae* virulence factors. Such effects would be expected to differ among human hosts depending on host microbiota composition. Hsaio *et al*. recently shed light on how members of the microbiota modulate *V. cholerae* infection (Hsiao et al., 2014). They showed that different members of the human microbiota were able to prevent *V. cholerae* infection. Our findings identified additional members of the human microbiota that can prevent the T6SS, giving potential to develop host-based therapies that minimize the effects of a *V. cholerae* infection by removing T6SS activity (Bachmann et al., 2015).

There is precedence for a role for bile manipulation in controlling pathogens. Fecal microbiota transplantation was recently proposed to prevent recurrence of *C. difficile* infection by correcting bile acid metabolism (Weingarden et al., 2014). Thus, experimental support is emerging for the idea that the host microbiota composition determines the course of *C. difficile* infection (Buffie & Pamer, 2013; Willing, Vacharaksa, Croxen, Thanachayanont, & Finlay, 2011). Furthermore, modification of bile by commensal bacteria might help the microbiota adapt to defend itself against pathogenic bacteria. Alternatively, as the commensal organisms that dehydroxylate bile are mainly colonic, *V. cholerae* may utilize bile salts as a spatial signal such that it recognizes deoxycholic acid as a signal to turn off its T6SS in the colon before being released into the environment. Locations in the gut where bile-deconjugating and-dehydroxylating commensals are absent may result in *V. cholerae* bacteria having a higher T6SS activity than in locations where these commensal species are present. Therefore, preventive alteration of the microbiota, through the addition of *Bifidobacterium* which dehydroxylates cholate into deoxycholate, in people living in areas where cholera is endemic may disrupt *V. cholerae's* T6SS, leading to a less fit organism and a more positive disease outcome for the patient. Although our work does not demonstrate a necessity for the T6SS in colonization of the infant mouse, other work in the infant mouse, infant rabbit, zebra fish and fruit fly suggest the T6SS to have an important role for colonization (Chapter 4; Fu et al., 2018; Logan et al., 2018; Zhao et al., 2018).

As commensal organisms such as *Bifidobacterium* and *Bacteriodes* are lost through diarrheal purges during acute *V. cholerae* infection, the levels of bile acids repressing the T6SS might decrease (Monira et al., 2013). This would allow the pathogen to utilize its T6SS in a re-infection of patients recovering from a recent cholera episode, or during later stages of the purge, providing an opportunity for new therapies that introduce *Bifidobacterium* species at an early stage of *V. cholerae* infection to decrease pathogen T6SS activity.

In conclusion, *V. cholerae* infection is complex and involves host factors such as bile, mucins, and a microbiota that impact the pathogen and regulation of its T6SS. This work describes a novel mechanism for two-pronged regulation of a virulence pathway in *V. cholerae*, through mucins that activate the pathway and bile metabolites that repress it. This work adds to our understanding of how pandemic *V. cholerae* strains have evolved as such successful pathogens.

Chapter 6: Pandemic *V. cholerae's* T6SS interacts with the fly microbiome to impact disease

Figures 1 through 5 were published in

Fast, D.*, **Kostiuk, B.*,** Foley, E., and Pukatzki Commensal-Pathogen Competition Impacts Host Viability (PNAS), 2018

*Authors contributed equally

All experiments were conceived, carried out by and analyzed by Benjamin Kostiuk and David Fast.

5-1 Introduction

Studying the potential interactions between the T6SS of *V. cholerae* and commensal bacteria is extremely difficult due to the absence of a model where *V. cholerae* can interact with commensals without manipulation. In the infant mouse, the microbiome is underdeveloped in terms of microbial complexity and large variability exists between animals and amongst litters and commensals need to be added to see a T6SS phenotype (Zhao et al., 2018). Recent work has shown that commensal-pathogen interactions can be monitored in the infant mouse gut if commensal bacteria are added prior to infection (Zhao et al., 2018). However, this does not reconstitute the diversity of a robust microbiome. The adult mouse, while it houses a robust microbiome, is naturally refractory to *V. cholerae* colonization without the use of antibiotics (Olivier et al., 2007; Yoon et al., 2016). The mechanism of how this makes the mice susceptible to *V. cholerae* infection is unknown but the antibiotics do cause a reduction in commensals (Olivier et al., 2007).

The Mekalanos lab showed T6SS mediated killing of commensal *E. coli* in the infant mouse and while there were many interesting consequences of the killing there were a few notable disadvantages in this model (Zhao et al., 2018). The model requires manipulation of the microbiome to detect a phenotype, specifically the enrichment of T6SS-sensitve commensals (Zhao et al., 2018). The interactions with commensals appear to be specific commensals, as a combination of two *E. coli* strains isolated from the infant mouse appear to be necessary to see this phenotype (Zhao et al., 2018). Another accessible model used for *Vibrio cholerae* T6SS studies is the zebrafish model of infection (Runft et al., 2014). Recently, it was shown that while the T6SS contributes to pathogenesis in the zebrafish, this activity appears to not rely on the antibacterial activity of the system, and instead is dependent on the actin crosslinking domain of VgrG1 (Logan et al., 2018).

To help uncover the consequences of *V. cholerae*'s T6SS interacting with commensal bacteria we turned to using the *Drosophila melanogaster* model of cholera infection (Blow et al., 2005). This is an appropriate model to study pathogen-microbiome-host interactions: *V. cholerae* can cause disease symptoms and colonize the fly through its natural oral route of infection (Berkey et al., 2009; Hang et al., 2014; Purdy and Watnick, 2011; Wang et al., 2012). The microbiome of the fruit fly is well-defined with all the

bacteria sequenced and available in the Foley Laboratory (Petkau et al., 2016b). Additionally, the microbiome is relatively simple, with *Lactobacillus plantarum, Lactobacillus brevis* and *Acetobacter pasteurianus* responsible for the majority of the bacterial load (Petkau et al., 2016b). The microbiome is also easy to remove by antibiotic and antimycotic treatment, and reconstitute with defined members (Fast et al., 2016). Lastly, the host is remarkably similar to the mammal. The posterior midgut of the fruit fly resembles the small intestine of mammals and the innate immune systems share many conserved pathways (Lemaitre and Miguel-Aliaga, 2013).

In this study, we demonstrated that the T6SS contributes to the pathogenesis of *V. cholerae* and affects the fly in several different ways, including symptoms, colonization and death. The pathogenesis depends on the presence of the commensal bacteria, more specifically the Gram-negative *Acetobacter pasteurianus.* We implicate the immune system as a mediator of the pathogenesis and show through many disease markers the effects of the T6SS.

6-2 El Tor, but not classical strains, are able to kill the fruit fly

Furthering on our previous studies comparing 6th and 7th pandemic strains, we sought to compare the ability of strains from two separate pandemics. To kill the fruit fly, we infected flies with O395 from the sixth pandemic and C6706, from the seventh pandemic. We saw that C6706 was able to kill the flies in ~50 hours whereas O395 took almost double the time to kill the flies – nearly the same as flies fed plain LB broth, our uninfected controls (Figure 1A). This is an interesting observation as most of the virulence factors that are involved in killing the fruit fly (and causing disease in other model organisms) are encoded by both C6706 and O395. Specifically, for the fly, these include biofilm formation, quorum sensing, cholera toxin and acetyl-CoA Synthatse (Blow et al., 2005; Hang et al., 2014; Purdy & Watnick, 2011). However, many differences do exist between the pandemic strains. We focused on the difference in the T6SS. As shown in Chapter II, 6th pandemic strains have non-functional T6SSs due to disabling mutations in VCA0109 and VCA0120 (*vasK*). However, 7th pandemic strains have host-activated T6SSs (Bachmann et al., 2015). We next sought to determine the effect of the T6SS in the fruit fly model and if it contributes to the differences in pathogenesis between 6th and 7th pandemic strains.

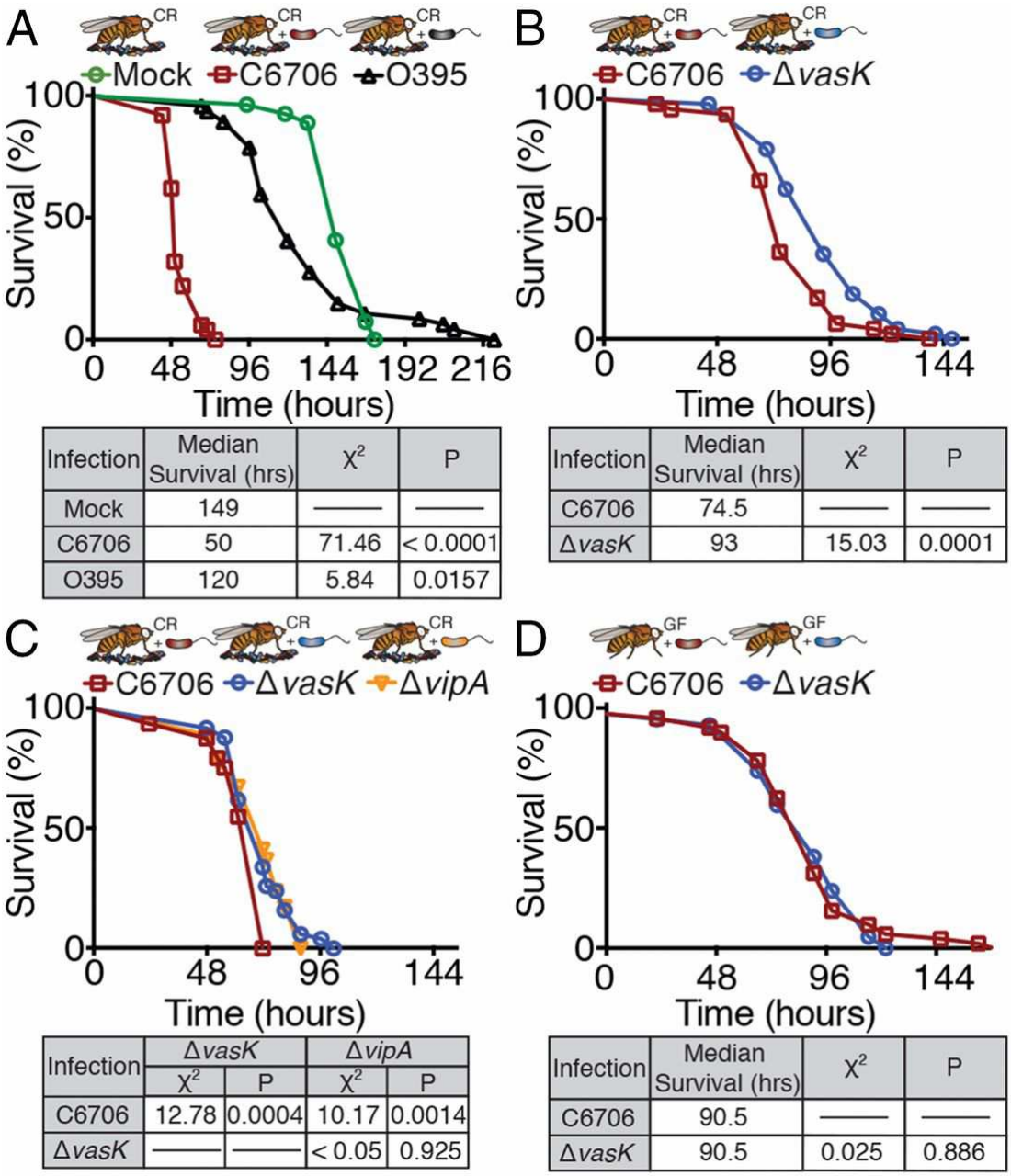

Infection	Median Survival (hrs)	X^2	P
Mock	149	———	———
C6706	50	71.46	< 0.0001
O395	120	5.84	0.0157

Infection	Median Survival (hrs)	X^2	P
C6706	74.5	———	———
Δ*vasK*	93	15.03	0.0001

Infection	Δ*vasK*		Δ*vipA*	
	X^2	P	X^2	P
C6706	12.78	0.0004	10.17	0.0014
Δ*vasK*	———	———	< 0.05	0.925

Infection	Median Survival (hrs)	X^2	P
C6706	90.5	———	———
Δ*vasK*	90.5	0.025	0.886

Figure 6-1. **T6SS contributes to the pathogenesis of *V. cholerae* in a commensal dependent manner.** (A) Survival curves of 5- to 6-d-old CR w1118 flies infected with the indicated *V. cholerae* strains. LB alone served as mock infection. (B and C) Survival curve of CR flies infected with T6SS functional (C6706) or T6SS nonfunctional (C6706Δ*vasK* and C6707Δ*vipA*) mutants. (D) Survival curve of GF flies infected with C6706 or C6706Δ*vasK*. D was performed at the same time and infected with the same bacterial cultures as B. The y axis shows percent survival, and x axis shows infection time. Tables show Longrank (Mantel−Cox) tests. In A, χ2 and P values are relative to mock infected flies; in B–D, χ2 and P values are relative to wild-type C6706 infected flies; n = 50 per group, for all experiments

6-3 The T6SS of El Tor *V. cholerae* interacts with commensal bacteria to influence host viability

To test the hypothesis that the T6SS is a virulence factor in the fruit fly we independently infected flies with two T6SS mutants in a C6706 background. The mutants lacked *vasK* and or *vipA*, both are routinely used in the study of the T6SS and are shown to not have pleotropic effects (Bachmann et al., 2015; Zhao et al., 2018). Both mutants demonstrated a reduction in their ability to kill fruit flies compared to WT, as the fruit flies lived ~15% longer when infected with each of the mutants vs WT C6706 (Figure 1BC). The mutations did not account for the entire difference between the virulence of these C6706 and O395, further studies are needed to understand additional virulence factors that contribute to the differences between these two strains.

Next we wanted to determine if this reduction in virulence is the result of bacteria-bacteria interactions or through the anti-eukaryotic effectors directly attacking the host. C6706 encodes two antibacterial effectors, VgrG-3 and TseL; one anti-eukaryotic effector, VgrG-1; and one cross-kingdom effector, VasX (Brooks et al., 2013; Miyata et al., 2011; Pukatzki et al., 2007; Unterweger et al., 2014a). To differentiate between these two hypotheses, we generated germ-free flies lacking a microbiome and measured whether or not a difference in virulence persisted. To accomplish this, we took flies immediately after enclosure and placed them on fly food containing a mixture of antibiotics and antimycotics (Fast et al., 2018). After four days growing on these conditions, flies were infected with C6706 and C6706Δ*vasK*. The pretreatment abolished the differences between the virulence of C6706 and C6706Δ*vasK* indicating that the commensals are necessary for the T6SS dependent virulence (Figure 1D). Interestingly, a model in which *V. cholerae* kills the commensal bacterial to simply replace their niche is not supported by the data. In a simple replacement model, we would expect a fly without a microbiome to fair worse against a *Vibrio cholerae* infection. This is not what we observed as the flies lacking a microbiome lived longer. This indicated both a host and a commensal component to T6SS mediated virulence (Figure 1BD).

To better understand the impact that the T6SS has on the pathogenesis, we sought to evaluate the symptomatic progression of cholera of the flies and evaluate the component that the T6SS is responsible for.

6-4 The T6SS contributes to disease symptoms.

The metrics we evaluated to describe the symptomatic condition of the fruit flies were the frequency of defecation, the volume of defecation, the fecal bacterial load and the histology of the posterior midgut of the fly.

To measure the frequency of defecation, we set up infection assays similar to those performed above; however, our LB culture was supplemented with a non-toxic, non-absorbable blue dye. This dye is often used to measure perforations within the intestine (Bhowmick et al., 2008). In this case, we used this dye to visualize and count diarrhea. After a 24-hour infection, we placed 5 groups of 5 flies each in a petri dish with a piece of filter paper covering the bottom. Each hour for four hours, we counted the number of blue dots on the filter paper – each dot representing a defecation event. We rationalized that a fly that defecates more frequently suffers from diarrhea. We performed this assay with flies receiving an oral infection of *V. cholerae* C6706, C6706Δ*vasK* or O395, as well as a mock-infected control and a solid food control. We observed no difference in defecation frequency between flies raised on solid or liquid diets, confirming that the bacterial growth medium does not cause diarrhea (Figure 2A). Likewise, O395 had no measurable effects on defecation frequency (Figure 2A). In contrast, we found that C6706 caused an increase in the number of fecal marks per fly (Figure 2A). Similarly, we found an increase in the number of fecal marks per fly from flies infected with C6706Δ*vasK* (Figure 2A). However, this increase was less pronounced than that of flies infected with C6706 ($p = 0.08$ vs $p = 0.009$) (Figure 2A). To assess the contributions of T6SS to defecation frequency, we performed a linear regression analysis on the groups indicated in Figure 2A. We noticed a significant increase in the number of fecal marks per fly over time from flies infected with C6706, but not from mock-infected flies. Furthermore, there was a significantly lower increase in the number of fecal marks per fly from C6706ΔvasK-infected flies, and a smaller portion of these fecal marks could be attributed to infection with C6706Δ*vasK* than wildtype infection(R^2 value of 0.2584 versus 0.4379), indicating that T6SS increases the

severity of diarrheal symptoms in infected flies (Figure 2A). However, T6SS inactivation does not abate diarrheal symptoms likely due to other virulence factors.

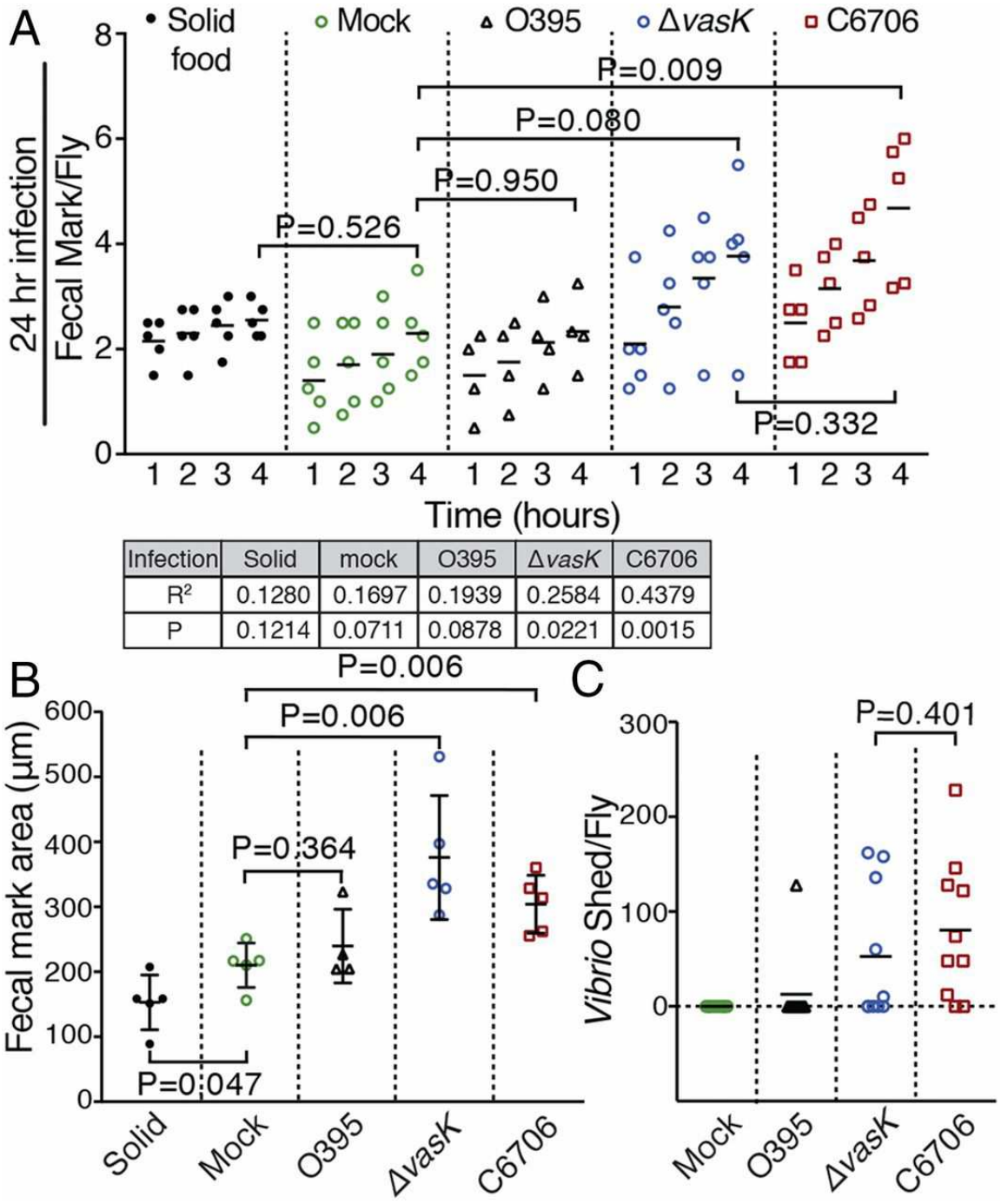

Infection	Solid	mock	O395	ΔvasK	C6706
R^2	0.1280	0.1697	0.1939	0.2584	0.4379
P	0.1214	0.0711	0.0878	0.0221	0.0015

Figure 6-2. **T6SS contributes to cholera-like disease.** (A) Fecal marks from w1118 flies fed solid fly food or LB broth (mock) supplemented with O395, C6706ΔvasK, or C6706 for 24 h. The table shows a linear regression analysis of each group, and P values are the result of a Student's t test at 4 h. (B) Fecal mark area, in micrometers, of spots counted. Each point is the average area of a given replicate. Statistics show Student's t tests for each group compared with solid food. (C) V. cholerae shed per fly fed LB or infected with V.

cholerae C6706, C6706ΔvasK, or O395 for 24 h. Each point is the number of Vibrio isolated from fecal matter of a single fly

In the same experiment, we were also able to measure the area of the blue dot, a characteristic we used as a proxy for the volume of diarrhea. This was performed by taking photographs of the filter papers after the four-hour time frame and imaging them using CellProfiler. This software was able to count all the images and give us the surface area of each fecal mark. The larger the fecal mark, the larger proportion of it we assumed was water – this was matched by a qualitative observation that the fecal mark was a paler blue. As watery diarrhea is a trademark symptom of cholera, we judged the larger fecal marks to be evident of more severe disease. We observed an increase in the area of fecal spots from mock-infected flies raised on a liquid diet compared with flies raised on a solid diet (Figure 2B). Infection with O395 did not impact defecation volume. In contrast, both C6706 and C6706Δ*vasK* significantly increased fecal volume relative to mock-infected controls, confirming enhanced diarrheal disease in flies infected with either strain (Figure 2B).

Next, we performed a similar experiment, without the blue dye, and this time placed each *V. cholerae*-infected fly individually into a 96-well plate with a piece of filter paper soaked in PBS+5% sucrose to attract the fly to the filter paper. After 4 hours, we removed the filter paper and vortexed it in 1mL PBS before performing serial dilutions. The next day we enumerated the number of bacteria that were expelled from the fly. These numbers were used as a measure of Bacterial load in the diarrheal purges. A high bacterial load is another characteristic of cholera diarrhea. Whereas we only detected *V. cholerae* in the feces of a single fly infected with the O395 strain, we found that 8 out of 10 flies infected with C6706 shed *V. cholerae* (Figure 2C). Consistent with contributions of T6SS to disease severity, we only found 5 out of 10 C6706Δ*vasK*-infected flies shed the bacteria (Figure 2C). In short, our results establish a role for T6SS in diarrheal symptoms during a *V. cholerae* infection: Loss of T6SS reduces defecation frequency, and lowers shedding of *V. cholerae* in the feces of infected animals.

All together, these data support the hypothesis that the T6SS contributes to the symptoms of cholera either directly, or indirectly by potentially improving colonization. These data are further supported by Ma *et al.* showing that an overactive T6SS promotes

increased inflammation in the gut. This caused us to look at the potential that this increased inflammation causes damage to the intestine.

6-5 *V. cholerae's* T6SS promotes damage to the intestinal epithelium.

In addition to the diarrheal symptoms associated with cholera, *V. cholerae* also causes changes to the intestinal ultrastructure and is associated with damage to the intestinal epithelium (Mathan et al., 1995). As the T6SS is involved in inflammation and diarrhea, we hypothesized that it also would be associated with the intestinal damage. To measure intestinal damage, we performed transmission electron microscopy (TEM) at a late stage in infection (48 hpi) and qualitatively examined the guts for signs of damage. The mock-infected posterior midguts looked healthy; they had a readily identifiable lumen, evenly spaced columnar epithelial cells, attached microvilli and normal looking cellular compartments such as the nuclei and mitochondria (Figure 3A-F). In contrast, major morphological differences were seen in the flies infected with C6706 to the point where we could not distinguish individual components on the intestine (Figure 3G-J). The lumen was filled with a mast of cells and microvilli that had presumably been shed from the intestine, and the borders between epithelial cells were unrecognizable. Tell tale signs of cell death are also observe, such as nuclear decondensation and fractured mitochondria (Figure 3 KL) (Buchon et al., 2010b). An intermediate phenotype was observed in flies infected with C6706Δ*vasK* (Figure 3 M-R). Flies infected with C6706Δ*vasK* retained aspects of a healthy gut. Individual epithelial cells and a relatively clean lumen could be identified (Figure 3 MN). Additionally, there were no visible signs of imminent cell death as the nuclear condensation was intact (Figure 3 QR). However, there were still signs of disease and intestinal damage (Vodovar et al., 2005). A disordered complement of microvilli and the shedding of epithelial cells into the lumen indicate that the intestine is being damaged Figure 3 M-P).

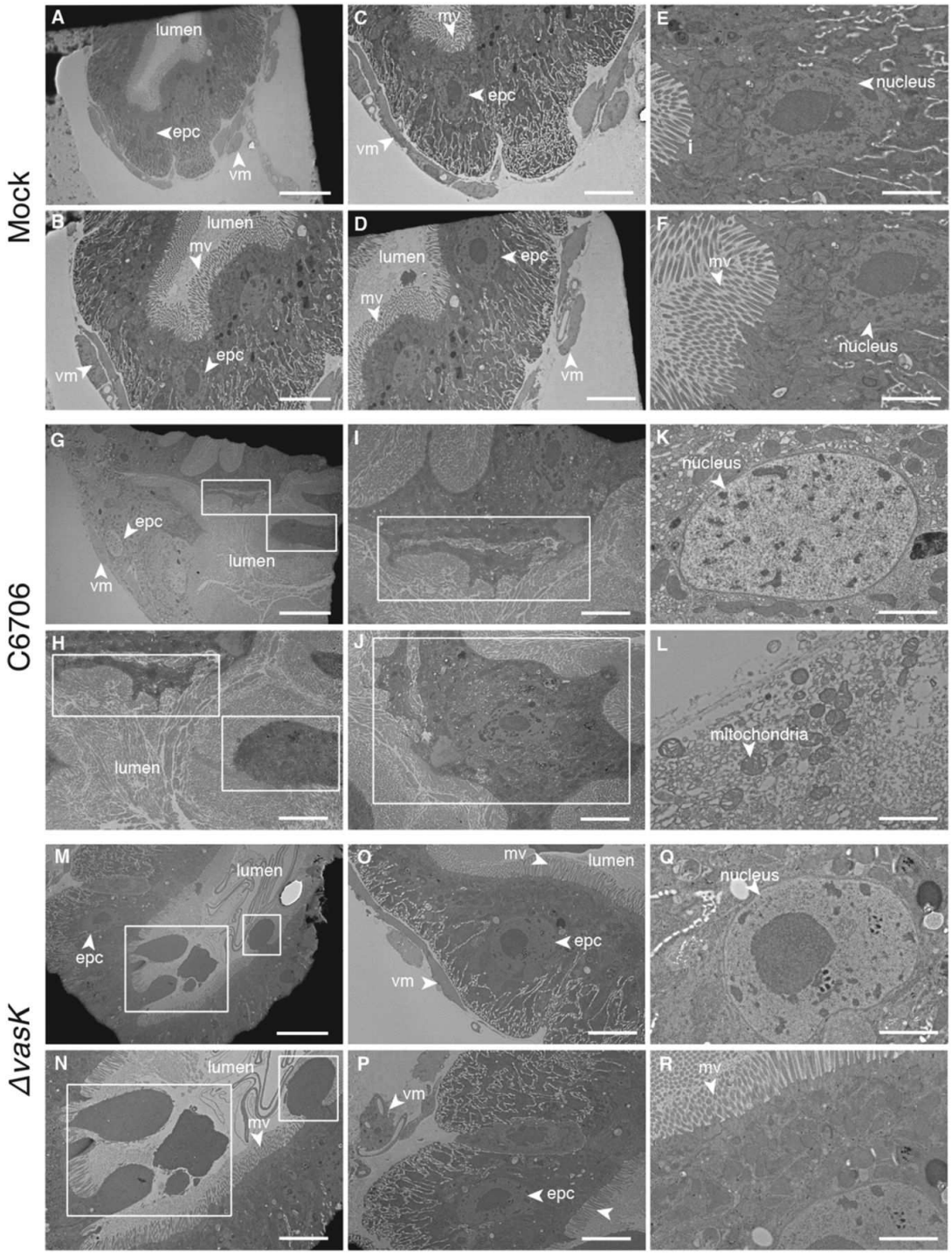

Figure 6-3. **T6SS contributes to V. cholerae intestinal pathogenesis**. TEM of the posterior midguts of flies, (A−F) mock-infected or (G−L) infected with C6706 or (M−R) C6706Δ*vasK* after 50 h of infection. Cells protruding into the lumen are indicated with boxes. (Large scale bars, 10 μm; small scale bars, 5 μm.) Epithelial cells, epc; microvilli, mv; visceral muscle, vm.

Now that we have a picture of how the T6SS contributes to pathogenesis of *V. cholerae* in the fruit fly model, we wanted to revisit how the microbiome contributes to this pathogenesis and virulence.

6-6 The T6SS of *V. cholerae* allows proliferation in flies with *A. pastuerianus*

As T6SS-assisted pathogenesis requires a microbiota, we asked if the T6SS influenced *V. cholerae* colonization numbers through interactions with the commensals. To test this hypothesis, we produced flies with a defined microbiota (Figure 4A). To accomplish this, we treated flies with the antibiotic/mycotic regiment that we used previously to generate germ-free flies. Following the generation of germ-free flies, they are starved for two hours to remove the antibiotics from their system and then are placed on a solution containing PBS, 5% sucrose and the bacteria that we wanted to colonize the fly with (OD of 16). After 16 hours, the flies are moved to autoclaved food vials free of microbes. The flies are left for 5 days so that their microbiome can standardize among vials. Using this technique, we generated germ-free flies and flies mono-associated with one of the two major commensal species in the fly, a Gram-positive –*Lactobcillus brevis* (*Lb*) and a Gram-negative *Acetobacter pasteurianus* (*Ap*) (Figure 4A). We then challenged these three fly populations with either C6706 or C6706Δ*vasK* and measured the change in bacterial load over time. We chose early time points in infection because as flies begun to die, we did not want to bias our results by choosing the flies that were living longer. The longest time point we chose was 24 hours as this is the last time point where >95% of the flies are alive. At each time point – 6, 12 and 24 hours – homogenized 5 groups of 5 flies and made serial dilutions to enumerate the *V. cholerae* numbers.

In the germ-free flies, both C6706 and C6706Δ*vasK* bloomed during infection increasing over 50x times between 6 and 25 hours (Figure 4B). The same trend was seen when *Lb* dominated the fly gut (Figure 4C). However, when the gut was instead colonized by a Gram-negative bacterium, *Ap,* the trend shifted. While the levels of *V. cholerae* C6706 increased statistically significantly between 6 and 24 hours the T6SS incompetent mutant failed to increase in levels over time (Figure 4D). While there are not statistically different numbers of *V. cholerae* between the WT and mutant at 24 hours, we argue it is likely biologically significant (Figure 4D).

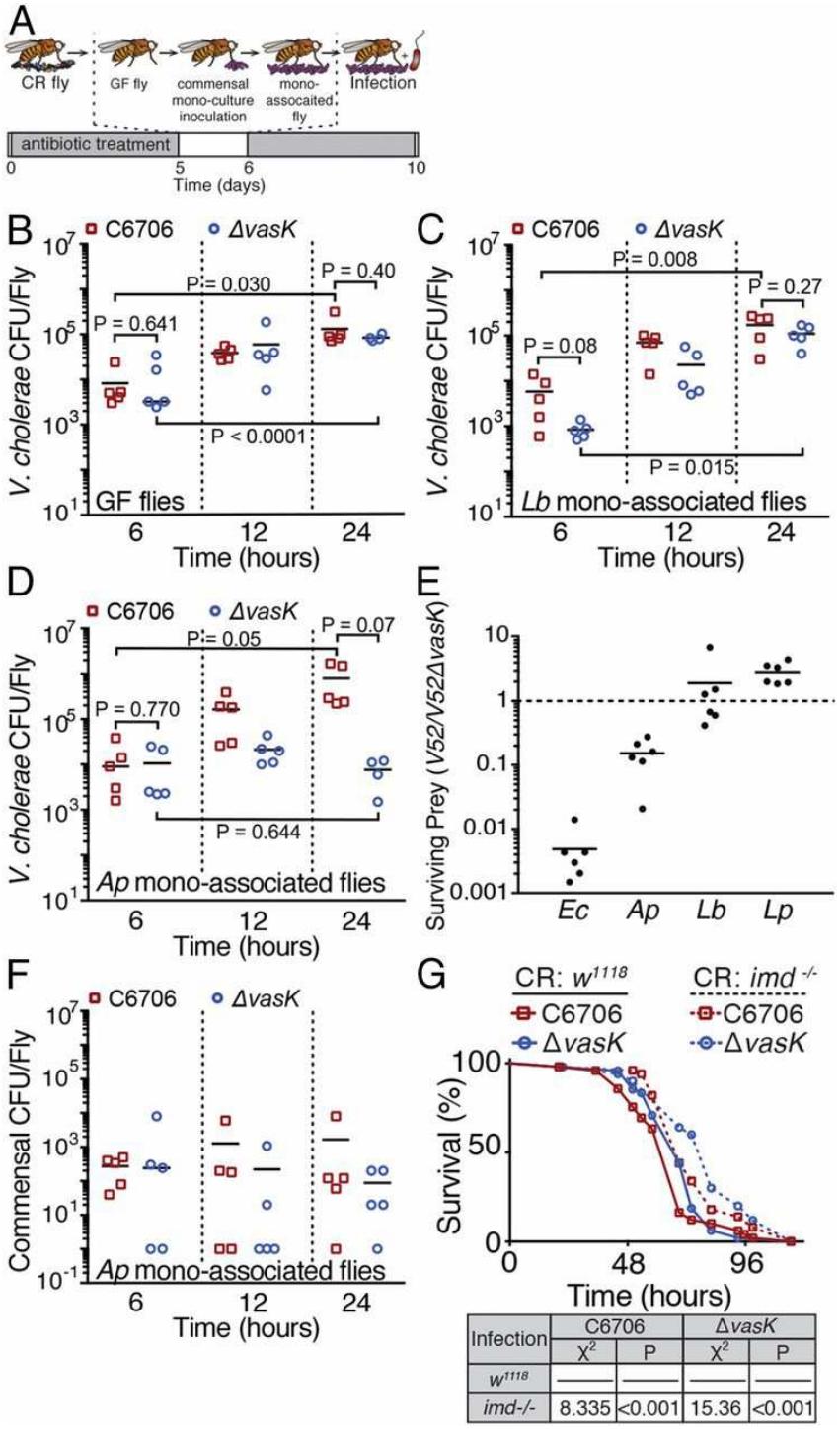

Infection	C6706		ΔvasK	
	X^2	P	X^2	P
w^{1118}	———	———	———	———
imd-/-	8.335	<0.001	15.36	<0.001

Figure 6-4. **Composition of the microbiome determines disease outcome.** T6SS-mediated gut infection. (A) Generation of monoassociated flies. (B−D) CFU/Fly of V. cholerae strains C6706 and C6706Δ*vasK* of surface-sterilized (B) GF, (C) *Lb* monoassociated flies, and (D) *Ap* monoassociated flies at indicated times. Each point represents a replicate of five randomly selected flies. P values are the result of Student's t tests. (E) An in vitro competitive assay between *V. cholerae* V52 and V52Δ*vasK* against *E. coli* as a positive control and *Ap*, *Lb*, and Lp. Bacteria were coincubated for 4 h at 37

°C. Surviving prey bacteria in the presence of T6SS were divided by the surviving prey in the absence of T6SS (Δ*vasK*). (F) CFU/Fly of *Ap* from flies infected with C6706 or C6706Δ*vasK*. Each point represents a biological replicate of five flies. (G) Survival of 5- to 6-d-old female CR w1118 or *imd* flies infected with C6706 or C6706Δ*vasK*. Tables show Long-rank (Mantel−Cox) test; $\chi 2$ and P values are relative to w1118 infected flies.

To determine if the bloom of *V. cholerae* was due to the T6SS activity against *Ap,* we wanted to set up these interactions *in-vitro* as a way to dissect the mechanism for this *V. cholerae* bloom. To accomplish this, we set up competition assays between V52, that has a constitutively active T6SS, and *Lb, Lp* and *Ap.* As a positive control for T6SS killing, we performed a competition assay between *V. cholerae* and *E. coli* and saw an >100x reduction in *E. coli* levels when exposed to V52 vs V52Δ*vasK* (Figure 4E). When *Ap* was exposed to V52 there was a 10x reduction in *Ap* levels indicating it is T6SS sensitive (Figure 4E). The two Gram-positive bacteria, aligning with previous studies, were resistant to the T6SS attacks (Figure 4E).

To see if the *Ap* levels dropped similarly *in vivo,* we infected *Ap* mono-associated flies with C6706 and C6706Δ*vasK* and plated 5 groups of 5 flies a 6, 12 and 24 hours for *Ap.* We found no significant difference in *Ap* levels. We did not detect obvious impacts of T6SS-positive C6706 on intestinal Ap numbers (Figure 4F). However, there is significant variability in the microbiome from fly to fly, so we cannot exclude the possibility the natural variation hides any T6SS-dependent killing. Alternatively, an infection with C6706 could lead to relocalization of *Ap* within the intestine, thereby exacerbating disease. Nonetheless, our data suggest that *V. cholerae* infection does not substantially alter total Ap numbers. As we did not detect a change in Ap numbers, we tested the alternate possibility that T6SS-mediated interactions with a subset of intestinal Ap induce secondary responses in the host that accelerate death. For example, mutations in the IMD antibacterial pathway attenuate *V. cholerae*-dependent killing of the host; IMD contributes to antibacterial responses in the fly gut, and is similar to the mammalian TNF pathway, a regulator of intestinal inflammation in mammals (Stokes et al., 2015). To determine whether T6SS-mediated interactions with the host involve pathological activation of immune responses, we infected wild-type and *imd* mutant flies with C6706 or C6706ΔvasK. Mutation of either *vasK* or *imd* prolonged host viability to near-equal extents (Figure 4G). Ablation of T6SS in combination with an *imd* mutation extended host viability

further. These data suggest that additive effects from the T6SS of *V. cholerae* and the IMD pathway of Drosophila synergistically control host viability.

6-7 The microbiome influences T6SS-dependent pathogenesis

T6SS contributes to *Drosophila* killing by *V. cholerae* (Figure 1BC), T6SS-assisted killing of Drosophila requires an intestinal microbiome (Figure 1D), and T6SS specifically targets the Gram-negative commensal *Ap* (Figure 4E) . These observations led us to ask whether interactions between T6SS and *Ap* are a prerequisite for T6SS-mediated killing of the host. To test this hypothesis, we examined host viability in adult flies that we associated exclusively with *Ap*, or *Lb*, and subsequently infected with C6706 or C6706Δ*vasK*. For each study, we ran a parallel infection study on CR flies with the same cultures of *V. cholerae*. Loss of T6SS in *V. cholerae* significantly impaired pathogenesis in each test with control, CR flies (Figure 5 D–F). However, loss of T6SS did not diminish *Vibrio* pathogenesis in adult flies that we associated exclusively with Lb (Figure 5A). As *Lb* also fails to block host colonization by a T6SS defective C6706 strain (Figure 4C), our data suggest that interactions between T6SS and *Lb* have minimal relevance for host viability. In contrast, we detected significant involvement of T6SS in the extermination of adults that we monoassociated with *Ap* (Figure 5B), indicating that *Ap* is sufficient for T6SS-mediated killing of the host. We then asked whether Gram-positive commensals can protect *Drosophila* from T6SS-dependent killing of *Ap*-associated flies. Here, we associated adult *Drosophila* with a 1:1:1 mixture of *Ap*, *Lb*, and *Lp*. We then challenged the flies with C6706 or C6706Δ*vasK*, and measured survival rates. In this experiment, we found that Gram-positive commensals do not impact T6SS-dependent killing of the host, suggesting that the presence of the common fly commensal *Ap* renders *Drosophila* sensitive to T6SS-dependent killing of the host irrespective of the presence of additional commensals Figure 6-5. These data, along with the extended lifespan of an IMD mutant suggest an interplay between the host, pathogen and commensal.

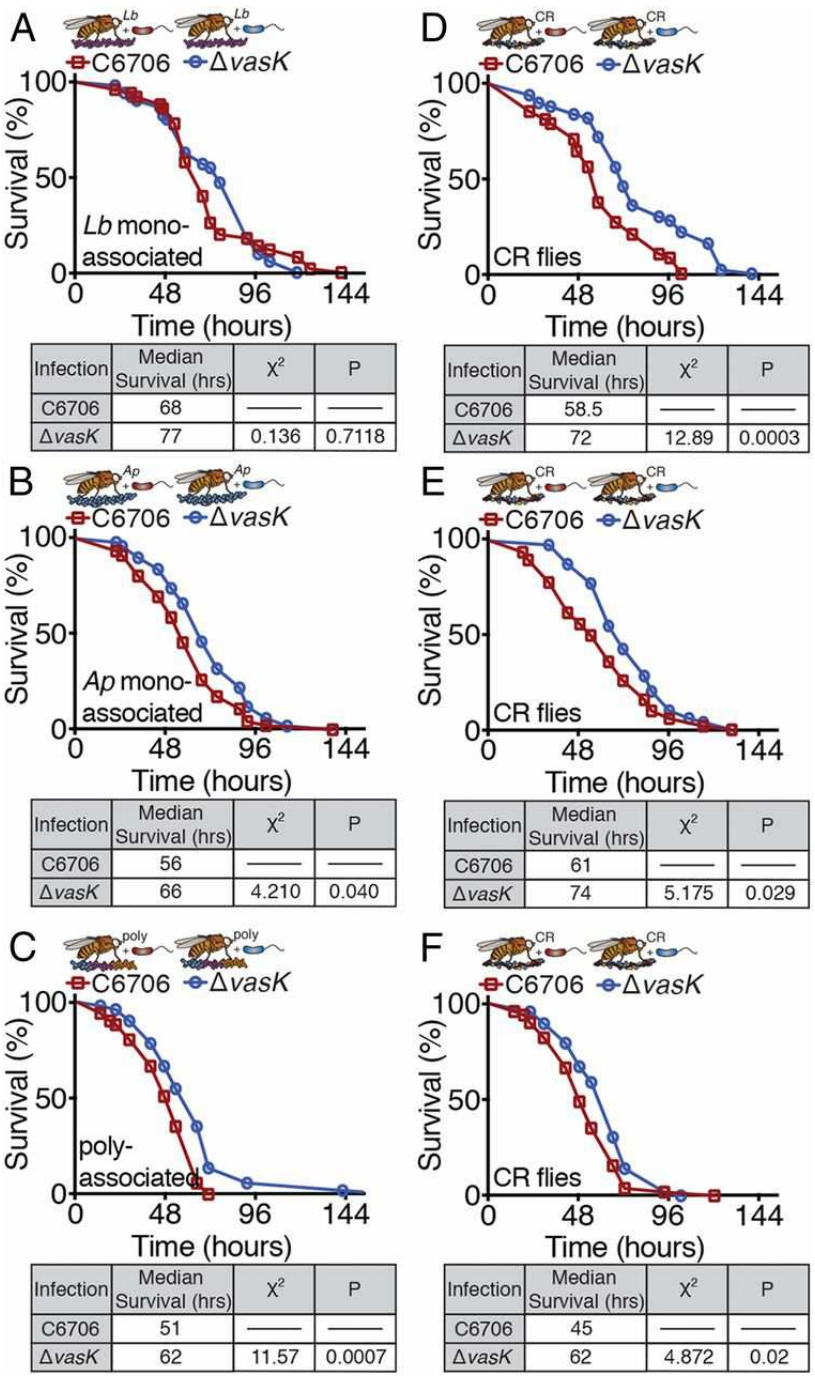

Infection	Median Survival (hrs)	X^2	P
C6706	68	——	——
Δ*vasK*	77	0.136	0.7118

Infection	Median Survival (hrs)	X^2	P
C6706	58.5	——	——
Δ*vasK*	72	12.89	0.0003

Infection	Median Survival (hrs)	X^2	P
C6706	56	——	——
Δ*vasK*	66	4.210	0.040

Infection	Median Survival (hrs)	X^2	P
C6706	61	——	——
Δ*vasK*	74	5.175	0.029

Infection	Median Survival (hrs)	X^2	P
C6706	51	——	——
Δ*vasK*	62	11.57	0.0007

Infection	Median Survival (hrs)	X^2	P
C6706	45	——	——
Δ*vasK*	62	4.872	0.02

Figure 6-5. **Composition of commensal microbes impacts T6SS virulence contributions *in vivo*.** (A) Survival curves for adult flies monoassociated with *Lb*. (B) Survival curves for adult flies monoassociated with *Ap*. (C) Survival curves for adult flies polyassociated with *Lb*, *Ap*, and *Lp*. In A–C, flies were infected as indicated. (D–F) Survival curves for parallel infection studies performed on CR flies. The y axis represents percent survival, and the x axis represents infection time in hours. Tables show Log-rank (Mantel−Cox) test.

6-8 *V. cholerae* and its T6SS impact the replication of intestinal stem cells

To this point, we have been focused on bacteria interactions in the gut of the fly; however, our data encouraged to us to dissect the host response to the T6SS in order to get a bigger picture of how the T6SS mechanistically acts as a virulence factor.

In order to get a wholistic view, we decided to take a transcriptomics approach and perform RNAseq on infected flies. We decided to look at C6706, C6706Δ*vasK* and mock infected flies, and just examine the intestinal progenitor cells. Using flow-cytometry we isolated the intestinal progenitor cells by driving GFP from the *esg* promoter that exists only in undifferentiated intestinal stem cells (Buchon et al., 2010b). The rationale for choosing this cell type was the observation that the number of *esg*+ cells was significantly higher in an infection with C6706Δ*vasK*, whereas they were significantly lower (equal to uninfected) in C6706 infected guts (Fast et al., 2018). This observation is at odds with the paradigm for intestinal infection in the fruit fly, where other pathogens like E*rwinia carotovora carotovora 15* will cause proliferation of this cell type (Buchon et al., 2010b). Intestinal progenitors proliferate in response to infection as a means of replacing the damaged epithelial cells with healthy ones, and concurrently sluffing the pathogen out of the host. In addition to responding to pathogens, intestinal progenitor cells also respond to cues from commensal bacteria, this is evidenced by germ-free flies having fewer. Lastly, genetically increasing or decreasing the proliferation of intestinal progenitor cells was shown to influence the success of survival for the fly (Buchon et al., 2009, 2010b). Altogether this positions intestinal progenitor cells as an important cell type in the study of *V. cholerae* pathogenesis as it responds to pathogens, the T6SS, and commensal bacteria.

To perform this experiment, 100 flies per experimental group were infected in triplicate with either C6706, C6706Δ*vasK* or LB alone. After 24 hours, their guts were dissected out and run through a flow cytometer to sort for the GFP positive progenitor cells. The total RNA was isolated, and reverse transcribed before sending to LITR for RNAseq. The data was then analyzed by the following pipeline. First, the reads were analyzed for quality by FastQC with all reads under a quality of 30 removed (Andrews, 2010). Next, the reads were trimmed using Trimmomatic and the reads were aligned to the *Drosophila melanogaster* genome (bdgp6_tran) using Hisat2 (Bolger et al., 2014; Kim et al., 2016). Samtools was used to convert, sort and index the resulting files (Li et al., 2009). Next, reads

were counted using RsubREAD (Chen et al.). EdgeR was used to generate a PCA plot and normalize the counts, and provide p-values for analysis (Chen et al.).

Gene Function	# of genes
SIGNALING	58
Wnt	7
Jax-stat	3
EGF	11
Notch	11
Other	26

Table 6-1. **Highlighted genes downregulated in intestinal stem cells by C6706 compared to mock infected *Drosophila melanogaster.***

This analysis provided insights into the effects of *V. cholerae* on the fruit fly as well as the role of the T6SS. When comparing the gene expression of intestinal progenitor cells in flies infected with *V. cholerae* with mock infected flies, the biggest differences were in the genes downregulated in the presence of wildtype *V. cholerae*. Overall, there was the downregulation of genes involved in DNA replication and cell division through inducing JAK-STAT, Wnt, EGF and Notch pathways (Buchon et al., 2009) (Table 1). These pathways are associated with promoting cell division in response to epithelial damage (Buchon et al., 2010b). This downregulation combined with the clear epithelial damage as evidenced by the TEM indicates that while *V. cholerae* is destroying epithelial cells, it is concurrently inhibiting the fly's ability to regenerate them (Figure 3). The upregulated genes associated with a *V. cholerae* infection indicate stress and apoptosis, through the upregulation of glutathione metabolism and p53 (Finkel and Holbrook, 2000) (Table 2). Additionally, there was a strong upregulation of genes associated with chitin binding proteins and chitin modeling proteins (Lehane, 1997) (Table 2). Chitin makes up the peritrophic matrix of a fly and is a natural defence against a pathogen, as *V. cholerae* encodes chitinases, we hypothesize that *V. cholerae* degrades the chitin layer, and the fly attempts

to fortify or replace it (Lehane, 1997).

Gene Function	# of genes	Gene Function	# of genes
CELL STRESS	112	INTESTINAL REPAIR	112
Metabolism	66	Chitin	14
Oxidative Stress	20	Actin	10
Apoptosis/autophagy	19	Cell adhesion	10
Ubiquitination	8	Mucin	1
Endoplasmic reticulum	6		

Table 6-2. **Highlighted genes upregulated in intestinal stem cells by C6706 compared to mock infected *Drosophila melanogaster*.**

Next, we compared mock-infected flies and C6706Δ*vasK* to isolate the component of the *V. cholerae* phenotype that the T6SS is responsible for. We saw a significantly lower number of genes that were expressed differentially between mock and C6706Δ*vasK* than mock and C6706. There are only 174 genes (< 2%) downregulated by C6706Δ*vasK,* about a third of what we noticed with C6706 (Figure 6). Interestingly, only 14 of these genes overlapped. Additionally, there is a complete absence of all genes involved in the JAK-STAT, Wnt, EGF and Notch pathways (Figure 6). To us that indicates that the cell division suppression might be T6SS mediated, or at least accelerated by the T6SS. An alternative hypothesis is that the increased bacterial load of C6706 over C6706Δ*vasK* might illicit a different celluar response. The upregulated genes followed a similar pattern to the genes upregulated by C6706, although to a lesser extent, while there were genes involved in stress, like proteases and heat shock proteins. Lastly, gene regulation by the T6SS appears to be mainly through supressing stem cell activity as the genes upregulated by C6706 and C6706Δ*vasK* are the same. The difference being that there are more genes in C6706 infected guts that are upregulated, albeit in the same class. This indicates that the disease from that perspective is similar, but that the disease progression is further along in C6706 than C6706Δ*vasK* (Table 1, 4).

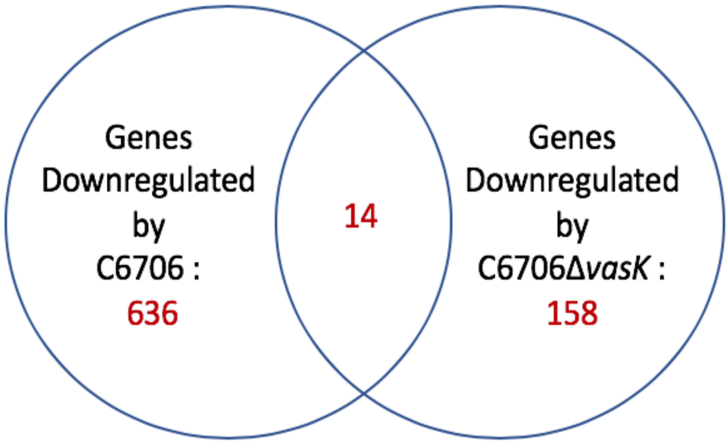

Figure 6-6. **Comparing the number of genes affected by C6706 and C6706Δ*vasK* in the stem cells of *Drosophila melanogaster*.** The number of downregulated genes compared between C6706 and C6706Δ*vasK*. A cutoff of a p-value of 0.05 was chosen, and the p-values were assigned by edgeR.

Concurrently, we attempted to isolate *V. cholerae* DNA and determine the pathogen's response to the environment that the T6SS contributes to. However, this approach failed due to the lack of reads generated.

Gene Function	# of genes	Gene Function	# of genes
CELL STRESS	20	INTESTINAL REPAIR	4
Metabolism	11	Chitin	2
Oxidative Stress	4	Actin	1
Apoptosis/autophagy	2	Cell adhesion	1
Ubiquitination	2	Mucin	0
Endoplasmic reticulum	1		

Table 6-3. **Highlighted genes downregulated in intestinal stem cells by C6706Δ*vasK* compared to mock infected *Drosophila melanogaster*.**

Altogether, the RNA Sequencing data suppors our experimental work that *V. cholerae*'s T6SS is actively involved in disease, epithelial destruction and the inhibition of epithelial renewal. In addition to supporting our hypotheses, this gives us lots of other exciting avenues to investigate. Especially the role that the cell division plays in the pathogenesis of the *V. cholerae*. This can be tested experimentally by artificially blocking

or overexpressing the JAK-STAT, Wnt, EGF and Notch pathways. Perhaps more interesting will be to determine if there is a link between pathogen-commensal interactions and host signaling.

6-9 Discussion

A dense community of commensal bacteria orchestrate growth, metabolism, and immune activity in the host intestine (Belkaid and Hand, 2014). Under homeostatic conditions, this bacterial community also forms a protective barrier that shields the host from microbial invaders. An example of this, is that *E. coli* Nissle 1917 are able to prevent *Salmonella* Typhimurium infection (Deriu et al., 2013). Another example is that *Clostridium difficile* only can affect a compromised microbiota (Weingarden et al., 2014). Thus, *V. cholerae* must navigate a complex pre-established microbiota to establish a productive infection. *V. cholerae* infections have been shown to interact with the microbiome in several ways. A correlation has been shown between the presence of the Gram-negative bacteria *Paracoccus aminovorans* and susceptibility to a *V. cholerae* infection (Midani et al., 2018). Additionally, an atypical *E. coli* strain unable to ferment lactose, also makes the adult mouse more susceptible to a *V. cholerae* infection due to its proliferation during infection (Yoon et al., 2016). Commensal bacteria also can help prevent a *V. cholerae* infection. The Gram-positive *Ruminococcus obeum* correlates with recovery from a *V. cholerae* infection in humans, and has been shown to block a *V. cholerae* infection in the infant mouse model (Hsiao et al., 2014). Lastly, *V. cholerae* also causes changes in the microbiome (Fast et al., 2018; Hsiao et al., 2014; Midani et al., 2018; Sheng et al., 2015; Yoon et al., 2016; Zhao et al., 2018).

Here, we used *Drosophila melanogaster* as a simple model to address how pathogen-commensal interactions contribute to host death. The fruit fly is a particularly good model as experimental endpoints of death are ethical. We were particularly interested in the T6SS of *V. cholerae* as a means of bacterial-bacterial competition. Using this model, we found that the T6SS contributes to *V. cholerae* pathogenesis, and that the T6SS accelerates host death through interactions with the commensal microbe *Acetobacter pasteurianus*. Removal of either the T6SS, or *Ap* from the *Vibrio-Drosophila* model extends the viability of infected adults, and inoculation of germ-free adult flies with *Ap*, a

symbiont, is sufficient to restore T6SS-dependent killing of the host. These results demonstrate an *in-vivo* contribution of the T6SS to *V. cholerae* pathogenesis.

We found that removal of all intestinal bacteria does not result in maximal host killing by T6SS-deficient *V. cholerae*, arguing against a simple replacement reaction where *V. cholerae* expands into a vacant niche left behind after T6SS-mediated killing of *Ap*. Therefore, it is not the *absence* of commensals but rather the *destruction* of commensals that is responsible for the phenotype. Indeed, an absence of commensal bacteria attenuates host killing by wild-type *V. cholerae*, suggesting that the presence of commensal bacteria is essential for T6SS-dependent killing of the host. Curiously, we did not see a substantial drop in *Ap* titers in flies challenged with *V. cholerae*, indicating that *Ap* persists during infection. This indicates that complete eradication of commensals is not a critical step in the T6SS mediated pathogenesis of *V. cholerae* – further arguing against the replacement model. Furthermore, as our data implicate interactions between *Ap,* a symbiont found in many healthy fly guts*,* and the T6SS of *V. cholerae* as pathogenic, this work reienforces that evaluation of host-symbiont relationships requires careful consideration of extraneous factors such as invasion by foreign microbes.

Finally, we found that inoculation of GF adults with *Ap*, either alone or in combination with *Lactobacilli*, was sufficient to restore T6SS-dependent killing of the host. These observations are in line with a model where T6SS-mediated killing of a proportion of intestinal *Ap* initiates secondary events that enhance host destruction by *V. cholerae*. As we cannot detect a decrease in *Ap,* I hypothesize that it is either just a small number of commensals that need to be killed, or else it is just the *Ap* in a specific location of the gut that need to be killed. The molecular basis for linking pathogen-commensal interaction and host death merits further investigation. We consider the host Immune Deficiency (IMD) pathway a possible mediator of such an effect. IMD is highly similar to the mammalian TNF pathway, a regulator of intestinal inflammation in mammals, and IMD regulates intestinal immune responses to Gram-negative bacteria (Lemaitre and Miguel-Aliaga, 2013). This model is supported by recent work in the infant mouse, demonstrating that the T6SS of *V. cholerae* activates the immune system to a greater extent when commensals are present (Zhao et al., 2018). Additionally, the T6SS of *V. choerae* modulates the intestines of the zebrafish during infection (Logan et al., 2018). We showed

that loss-of-function mutation in the IMD pathway extends the lifespan of flies infected with wild-type *V. cholerae* (C6706) to a similar extent as wild-type flies infected with a T6SS-negative strain (C6706*ΔvasK*) (Fast et al., 2018). *imd* mutant flies infected with the same T6SS-negative strain lived even longer, suggesting that activation of IMD and T6SS-dependent interactions with *Ap* programs the intestinal environment in a manner that supports *V. cholerae* pathogenesis (Fast et al., 2018). Our RNAseq data further implicate the relationship between the immune system and the T6SS. The T6SS greatly diminishes proliferation of intestinal progenitor cells indicating that the fly is unable to respond productively to the infection and repair the damaged epithelial layer. Whether this inhibition is direct through an anti-eukaryotic effector or works through the microbiome is unknown, however, if these phenotypes correlate with pathogenesis, we hypothesize that the commensals are also necessary for the signaling. If this is the case, this is a remarkable example of how interactions between commensals during infection cause host signaling changes. Deciphering the mechanism of immune activation can be completed by removing the anti-eukaryotic effectors from *V. cholerae* and performing qPCR to look at key immune gene activation. If this is shown to work though the microbiome, it would be interesting to know how this activation occurs. One way to uncover the mechanism would be to complete a metabolomic study on flies infected with their C6706 and C6706Δ*vasK,* and look for different metabolites that could potentially be released by dying *A. pasteurianus.* Additionally, we could feed T6SS-killed *A. pasteurianus* to the fruit fly and determine if that is sufficient for immune activation. Further to understanding the effect of *V. cholerae* on the host, there is also the question of how host changes influence *V. cholerae.* By pharmaceutically or genetically blocking the JAK-STAT, Wnt, EGF and Notch pathways we can measure downstream effects such as bacterial load or the expression of virulence factors. A recent study demonstrated that T6SS dependent immune activation results in the overexpression of other virulence factors, such as cholera toxin (Zhao et al., 2018). Altogether, this system presents a simple *in-vivo* model to define the host-microbe-pathogen interactions that determine T6SS-mediated death.

Chapter 7: Discussion

7-1 Diversity in regulating the T6SS of *V. cholerae*

The T6SS of *V. cholerae* is differentially regulated in different environments, in different subsets of strains as well as in different cholera pandemic strains. In this section, I will describe my work in the context of how T6SS is regulated in different environments, how regulation is different between strains, and finally how studying regulation gives insight into how the T6SS was used across multiple pandemics.

7-1.1 Regulation of the T6SS by cues in the environment.

V. cholerae sense its environment – whether inside or outside the host – to regulate its T6SS. In my thesis I focused mostly on uncovering the host signals that regulate the T6SS when *V. cholerae* is inside the host. I showed that mucin relieves repression of the T6SS *in-vivo,* a protein that is ubiquitous in the intestine. Mucin is a highly glycosylated protein that is the major component of mucus. While we were unable to dissect the component of mucin responsible for activation, I hypothesize that it is a sugar conjugated to the protein backbone of mucin – potentially a combination of N-acetylglucosamine, the sugar in chitin and other factors, or a related sugar. Chitin only induces the T6SS as a hexo-N-acetylglucosamine polymer, therefore, testing individual sugars like we did might be too simplistic of an approach (Borgeaud et al., 2015b; Meibom et al., 2005). Additionally, many factors in the crude mucin preparations might be necessary for activation of the T6SS as, as discussed in this section, many complex regulatory networks are involved in regulating the T6SS.

Mucin may positively regulate the T6SS through nutritional deprivation regulatory pathways. When *V. cholerae* is using less preferred carbon sources such as chitin or is in a low glucose or nucleotide environment the T6SS becomes active (Antonova et al., 2012; Borgeaud et al., 2015b; Ishikawa et al., 2009; Watve et al., 2015). The sugars on mucin, being similar to those of chitin, might qualify as nutritionally insufficient. This hypothesis is further supported by recent work that suggests that mucin might activate the chitin utilization pathway through recognition by ChiS (Chourashi et al., 2016b). ChiS is also necessary for other mucin related functions, such as motility, and it plays an important role for full virulence in the host. More research is needed to understand if mucin signals through ChiS to activate the T6SS in the host.

This response to nutritional deprivation, which may include mucin, suggests that a role of the T6SS could be to scavenge for nutrients by killing non-kin cells (Veening and Blokesch, 2017). This acquisition of nutrients would likely be mostly in the form of DNA, which is further supported by the linking of natural competence to import the DNA with the killing of kin cells. Although unconfirmed, this would be a new role for the T6SS of both *V. cholerae* and other species.

While mucin is responsible for turning on the T6SS of C6706, bile salts are able to modulate this system. Implicating bile in T6SS regulation introduces a spatially dependent aspect to *in-vivo* T6SS activity as the composition of bile changes throughout the intestine. We found that while conjugated bile salts, synthesized in the liver, are able to increase T6SS activity, the microbially dehydroxylated and deconjugated bile salts – such as deoxycholate – are able to inhibit the T6SS. While many colonic commensal bacteria are capable of metabolizing bile into deoxycholate, these bacteria do not inhabit the small intestine where *V. cholerae* primarily initiates disease (Bachmann et al., 2015; Begley et al., 2005; Gunn, 2000). This leads us to hypothesize that *V. cholerae* might only use its T6SS in specific stages of infection and it might be turned off as exiting the host. This hypothesis is supported by the observation that *V. cholerae* exits the host as a clonal culture and would have no need to be competitive (Dutta et al., 2013a).

Bile also regulates other *V. cholerae* virulence factors, giving us an opportunity to understand how *V. cholerae* coordinates the T6SS with other activities *in-vivo.* One example is that the bile acid deoxycholate has been shown to activate biofilm formation as well as inhibit T6SS activity (Hung et al., 2006). This indicates that The T6SS might not be important for competition in biofilms within the host. Other studies of bile, often do not dissect the individual components of bile responsible for gene regulation, however cholera toxin production and motility have been shown to be regulated by bile (Gupta and Chowdhury, 1997). A deeper understanding of how individual bile constituents regulate other virulence factors will aid in the understanding of when the T6SS is important during infection.

Altogether, *V. cholerae* responds to the host environment by activating it's T6SS in response to mucin and fine tuning this response based on the composition of bile. While the regulatory networks of these pathways need to be addressed, *Vibrios* response to both

cues have offered many starting points. Resolving these pathways will help elucidate how *V. cholerae* coordinates the T6SS relative to other virulence factors and bring us closer to a more complete understanding of the biological role of the T6SS.

7-1.2 Differences in regulation between *V. cholerae* strains

One facet of T6SS regulation that has become apparently during my research and throughout the literature is that different strains appear to not all respond to the regulatory cues of T6SSs in the same way. In my research, this spurred the identification of mucin and bile as regulators of C6706's T6SS as it did not respond to high osmotic pressures like other El Tor strains. The first example of this is the difference between strains that have a constitutively active and inactive system. The 7th pandemic strains N16961 and C6706 do not encode a constitutively active system, yet the non-pandemic strains do: V52, AM19226, DL4215 and 1587.

The reason behind this difference is unexplored from a regulatory perspective. However, recent work suggests – for at least V52 – this might be due to residual TfoY production (Metzger et al., 2016). It is also unknown if this is what causes constitutively active T6SSs in the other non-pandemic strains. One trend is clear, that non-pandemic *V. cholerae* strains are much more likely to have a constitutively active T6SS than pandemic strains (Bernardy et al., 2016). Despite this clear line, some mechanisms of regulation appear to be universal between the two groups of strains, including TfoY and quorum sensing.

The mechanisms of activation or repression that exist within pandemic strains are equally diverse. In my thesis, I describe mucin as the host signal to relieve repression of the T6SS. However, this is not necessary for all pandemics as, for example, while some labs have reported limited T6SS activity under laboratory conditions for A1552, yet others have seen no such effect (Borgeaud et al., 2015b; Ishikawa et al., 2012). For some strains, such as A1552, osmolarity has been seen to upregulate the T6SS, however no such effect was seen with C6706 (Ishikawa et al., 2012). This trend is the same for chitin-dependent activation, where chitin activates the T6SS of A1552 and some isolates of C6706, it has been shown that some C6706 isolates have a mutation in *luxO* which prevents T6SS activation in response to chitin (Stutzmann and Blokesch, 2016). This prevents maximal

T6SS activation from TfoX overproduction, however some T6SS activity is still observed (Stutzmann and Blokesch, 2016). This demonstrates the variability in how pandemic strains react to external stimuli to activate the T6SS. It is unknown the extent to which these differences exist in nature versus having accumulated in the laboratory under domesticated conditions.

7-1.3 The use of the T6SS across the pandemics

Another way that *V. cholerae* appears to control the activity of the T6SS is disabling mutations to remove T6SS activity altogether. This was explored extensively in Chapter II of my thesis (Figure 1). Our studies show that the T6SS was inactive in the 2nd and 6th pandemic classical strains, and potentially in the interim pandemics as well. There are two potential reasons to account for this. The first is that the system was redundant – that early pandemic strains had other mechanisms to compete with other bacteria. This could have come in the form of increased cholera toxin production which gives an increased growth rate by the release of nutrients alongside watery diarrhea (Pukatzki and Provenzano, 2013). This is potentially more important than killing neighbouring bacteria or the bacterial clearing properties of cholera toxin, which removes commensal bacteria along with mucin in diarrheal purges (Alexakis, 2017; Begum et al., 2018; Kaper et al., 1995; Monira et al., 2013; 1992). Alternatively, there could be another mechanism by which classical *V. cholerae* strains outcompete other bacteria. The second reason classical strains might have a dysfunctional T6SS is because that, while advantageous the T6SS also has significant drawbacks. The T6SS is immunogenic, and can cause unwanted inflammation that can severely reduce pathogenesis (Ma and Mekalanos, 2010a; Mougous et al., 2006). T6SS-dependent attacks can also activate the T6SS of neighboring bacteria, this turns neighbouring bacteria from being passive to a competitor (Basler et al., 2013). Lastly, the T6SS can cause competition between *V. cholerae* strains (Unterweger et al., 2014a). As discussed, *V. cholerae* competes with other *V. cholerae* strains and this competition could limit co-infections. Classical *V. cholerae* strains lack auxiliary hemolysins and other anti-eukaryotic effectors that are encoded by El Tor and non-pandemic strains (Beyhan et al., 2006). Therefore a co-infection could benefit classical strains if they are coninfecting with strains that encode such anti-eukaryotic activity (Olivier et al., 2007).

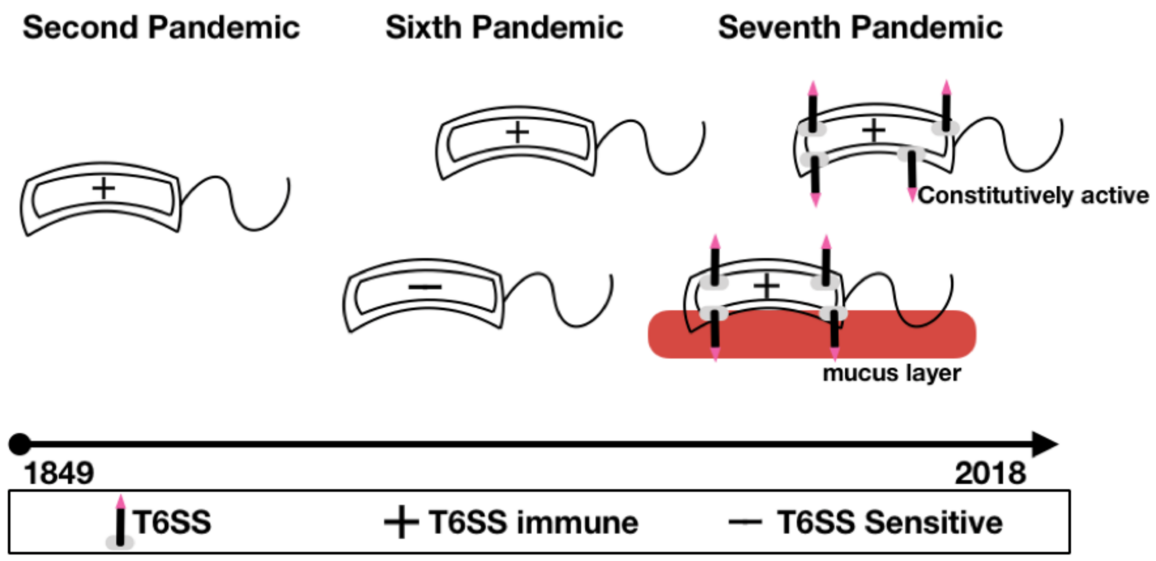

Figure 7-1. **The functionality of the T6SS across the pandemics.** The sole second pandemic strain, PA1849, has no T6SS activity, represented by the lack of a T6SS. However, the + sign represents it had resistance to a T6SS-mediated attack. Similarly, within the 6th pandemic, a subset of strains have T6SS immunity (+) and a subset does not (-). All sequenced representative of the 6th pandemic , however, lacked an active T6SS. Two groups of strains have been identified in the 7th pandemic. Whereas both have a fully functional T6SS system, some strains need activation through growth on mucin, chitin or high osmolarity, whereas recently isolated strains have a constitutively active system.

My data suggests that the 2nd pandemic strains lack T6SS activity due to a disabling in-frame 12-bp mutation in VCA0109. This mutation is also conserved in 6th pandemic strains. In addition to this mutation, 6th pandemic strains have also accumulated mutations in other T6SS genes including *vasK* and, in a subset of strains, *tsiV1.* The mutation is *vasK* is also sufficient to abolish T6SS activity, whereas the *tsiV1* mutation reduces the efficacy of the immunity protein resulting in TseL mediated toxicity. Coinciding with classical strains isolated with the defective *tsiV1,* was the isolation of El Tor pandemic strains that had a fully intact VCA0109, *vasK,* and *tsiV1.* These strains also had their T6SS activated in the host. Hypothetically, El Tor strains, such as C6706 would display a T6SS-mediated competitive advantage over the classical strains with the disabled *tsiV1*. Competition assays between these strains need to be performed *in-vivo* to test this hypothesis.

After El Tor *V. cholerae* was introduced to Haiti following the 2010 earthquake, it caused over 800,000 cases over 7 years, with over 10,000 dead, mostly caused by El Tor strains (Ali et al., 2011). Recently, strains isolated from this outbreak have been

demonstrated to have constitutively active T6SS (Zhao et al., 2018). This represents just another chapter in the evolution of the T6SS. It remains to be determined whether or not this trend will continue outside of Haiti and India, as strains become available from the current outbreak in Yemen, it will be interesting to sequence their T6SS gene clusters, and test their activity in competition assays within the *D. melanogaster* model of infection and under laboratory conditions. There are many advantages and disadvantages to utilizing the T6SS, and observation that its use has changed over the pandemics encourages a stronger molecular understanding of how the T6SS is used. If the trend continues, a constitutively active T6SS in modern El Tor strains would represent a massive change in T6SS activity over just sixty-years.

7-2 Diversification of T6SS modules

The T6SS encodes structural components, which are highly conserved and effector modules, which significantly vary. The effector modules are hypothesized and shown to be exchanged under pressure of T6SS attack. In chapter II of my thesis I studied the mechanisms of exchange as well as the consequence of exchange, both on competition between *V. cholerae* strains as well as horizontal gene exchange that occurs outside of the T6SS gene clusters following T6SS module exchange.

7-2.1 Mechanisms that govern diversification

T6SS module exchange has been predicted through bioinformatics and evidence of it occurring has been shown to be possible (Kirchberger et al., 2017a; Unterweger et al., 2015). There is, however, a conceptual problem with compatibility group switching. If a bacterium acquires a new effector module through horizontal recombination, it will be at the expense of the module they currently encode (Thomas et al., 2017). It was this type of exchange that has been observed with T6SS in the literature (Thomas et al., 2017). This would then place a single bacterium in competition with its sister cells, increasing and not reducing competition. Therefore a specialized recombination mechanism is required to incorporate the new effector module while retaining the old one. My thesis sought to experimentally demonstrate this mechanism. There are many examples of this occurring in *V. cholerae* strains, as arrays of open reading frames frequently follow effector modules in

the large cluster as well as auxiliary clusters 1 and 2 (Kirchberger et al., 2017a). Therefore, when integrating new effector modules, non-homologous recombination is likely to occur on the 3' side of the T6SS cluster between the effector and the immunity genes. This allows the old immunity gene to be retained. A recent study conceptually demonstrated these long arrays could be formed, and even demonstrated based on available sequences how some of the longer (5+) immunity arrays can be made (Kirchberger et al., 2017a).

On the 5' end, there is also benefit to specialized recombination. As discussed earlier, the structural components of the T6SS that appear on the 5' end of the gene clusters. The *vgrG* structural components (VC1416, VCA0020 & VCA0123) make a trimer. Some VgrG proteins have enzymatic roles in addition to their structural function (Pukatzki et al., 2007). Therefore, there may be an imperative to exchange effectors without disrupting the sequence of the *vgrG* genes. Our laboratory found a conserved 99-bp region within the adaptor genes (VC1417, VCA0019) of the two auxiliary clusters that could be used for such purposes (Unterweger et al., 2015) . As there is no *vgrG-3* adaptor gene, there is instead a conserved 99-bp region that is located between the structural and enzymatic domains. This allows recombination of new DNA without disrupting the structural components of the T6SS (Kirchberger et al., 2017a).

Altogether, the mechanism of preferred recombination must occur on the 5' end with a relatively short length of identity, 99-bp, and in the 3' end through non-homologous recombination. A mechanism that fits this description is homology facilitated illegitimate recombination (HFIR) (Figure 2) (Meier and Wackernagel, 2003; de Vries and Wackernagel, 2002). HFIR has been described in *Acinetobacter, Streptococcus* and *Pseudomonas* following natural transformation and in *E. coli* following conjugation (Amarir-Bouhram et al., 2011; Harms and Wackernagel, 2008; Meier and Wackernagel, 2003; de Vries and Wackernagel, 2002). HFIR is an extremely rare event that occurs at approximately 3-5 x 10^{-10} (Amarir-Bouhram et al., 2011; de Vries and Wackernagel, 2002). Like homologous recombination, this is RecA dependent, but unlike homologous recombination it is RecBCD and RecFOR independent (Harms and Wackernagel, 2008). It is currently unknown what proteins mediate the single crossover event.

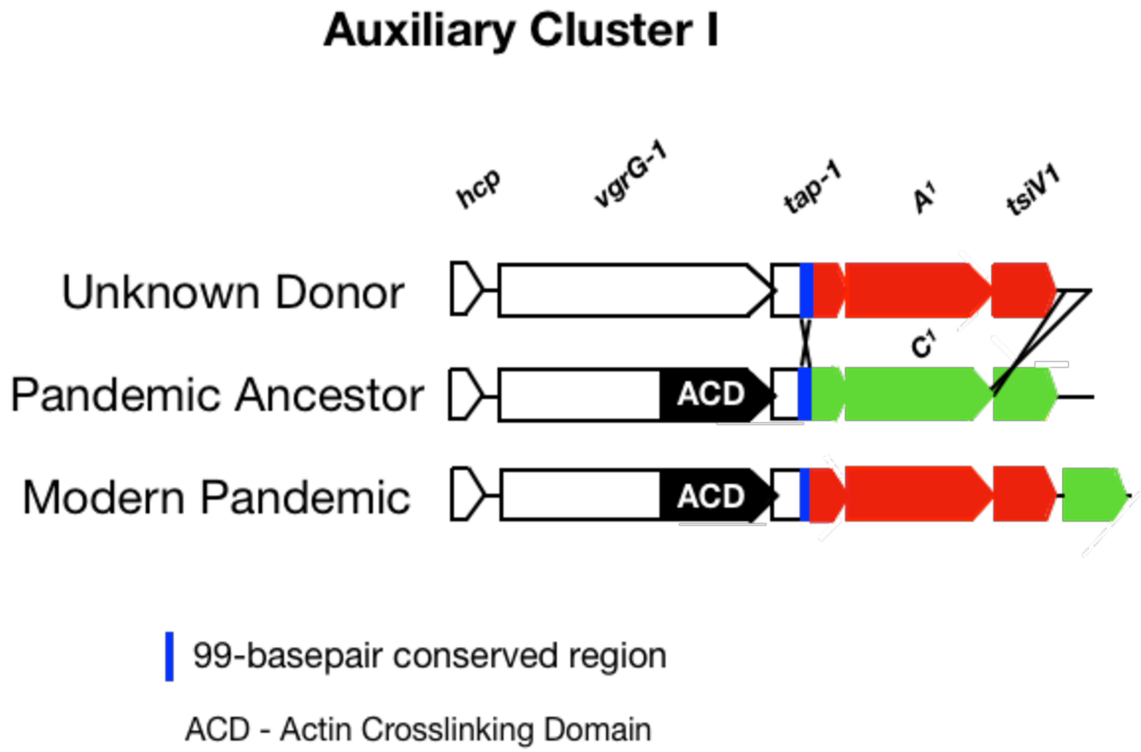

Figure 7-2. **Homology facilitated illegitimate recombination (HFIR) is a potential mechanism for T6SS effector module exchange.** This figure shows a potential mechanism whereby the precursor pandemic strains encoding the CAA module set acquired the A^1 gene to give the AAA module set encoded by modern pandemic strains. The genes in red represent the A^1 effector module, whereas the yellow genes represent the C^1 effector module. The blue region represents the region of identity shared between both strains.

We propose that HFIR is responsible for the exchange of *V. cholerae*'s T6SS effectors, demonstrating the first time HFIR has been observed in a *Vibrio* species. While a very rare event, we hypothesize that there is enough pressure to retain the original immunity gene while engaging in T6SS-mediated competition.

7-3 Consequences of T6SS diversification

We hypothesize that the compatibility group of a *V. cholerae* strain affects many areas of its physiology. This involves niche occupation in the host and the environment and evolution outside T6SS gene clusters.

7-3.1 Effector repertoire affects niche occupation

V. cholerae's T6SS effector repertoire affects how it competes with both eukaryotic and prokaryotic bacteria (Miyata et al., 2011; Thomas et al., 2017; Unterweger et al., 2012, 2014a). My doctoral work primarily expanded on the effect of effector repertoire on bacteria-bacteria competition. My thesis demonstrated that effector modules are readily exchanged between *V. cholerae* strains. This encourages us to revisit the differences between T6SS effectors, as we hypothesize that *V. cholerae* can collect the three effectors that best suit their environment.

We and others have shown that effectors differ in their ability to cause bacterial death (Thomas et al., 2017; Unterweger et al., 2012, 2014a; Wong et al., 2016). For example, in my thesis, I show that A^1 is more bacterially lytic than C^1 towards both *V. cholerae* and *E. coli*. The same trend was seen as A^M was stronger than C^M. This difference can also be observed amongst the three effectors that pandemic strains encode – the AAA effectors. This was shown by our laboratory, using deletion mutants. VasX was demonstrated to kill a *V. cholerae* strain lacking all their immunity genes to a greater extent (10-fold) compared to either VgrG-3 or TseL (Unterweger et al., 2014a). In addition to differences between effectors within a strain, effectors between strains also target eukaryotic cells to varying degrees (Miyata et al., 2011). In chapter two, I showed that exchanging effectors influences the ability of *V. cholerae* to compete with both *E. coli* and other *V. cholerae* compatibility groups.

The effector repertoire not only determines the magnitude of competitiveness but also the diversity of organisms you are able to compete with. For example, some effectors allow competition with eukaryotic cells, some prokaryotic cells, and some both (Miyata et al., 2011; Pukatzki et al., 2007; Unterweger et al., 2014a). A prominent example of this is the presence or absence of *vgrG*-1 (Kirchberger et al., 2017a). VgrG-1 with an actin crosslinking domain has been shown to be important for survival in phagocytic eukaryotic cells such as macrophage and amoeba (Pukatzki et al., 2007). This stresses the importance of exchanging effectors without changing the *vgrG-1* gene, as there are conceivable advantages to acquiring a new effector without losing the actin crosslinking domain of *vgrG-1*. In the infant mouse model of infection, the actin crosslinking activity of VgrG-1 induces expression of proinflammatory cytokines such as IL-1b, and the chemokine IP-10 (Ma and Mekalanos, 2010a). This results in diarrhea and a proliferative burst for *V.*

cholerae that potentially gives strains encoding this effector an advantage in host niches (Ma and Mekalanos, 2010a). Other effectors such as VasX, have the ability to target both eykaryotic and prokaryotic cells (Miyata et al., 2011, 2013). An *in-vivo* role has not been attributed specifically to VasX.

Another interesting aspect of effector repertoire is how it defines the compatibility group of *V. cholerae.* The compatibility group defines which strains can co-exist and which strains cannot as determined by T6SS-mediated competition (Unterweger et al., 2014a). While this compatibility rule has been tested predominately under laboratory conditions on LB-agar, there is emerging evidence it holds true in more biologically relevant conditions. Recently, *V. cholerae* complexes isolated from Falmouth, MA, USA showed that *V. cholerae* that are spatially close to one another belong to the same compatibility group (Kirchberger et al., 2016). In Chapter 4 of this thesis, we showed that the environmental isolates, DL4212 and DL2114 are excluded from the infant mouse intestine when coinnocuated with a T6SS positive C6706, but not when C6706Δ*vasK* was included. Additionally, recent work on chitin demonstrates that when two different compatibility groups are coinhabiting chitin, one will dominate and exclude the other strain from the niche (Thomas et al., 2017). An alternative to niche exclusion is compatibility group switching, where the effector repertoire of the two strains homogenize to favour cooperation over competition (Thomas et al., 2017).

Acquiring and losing effectors therefore has many consequences on *V. cholerae* biology – including which strains they can share a niche or coinfect with. Additionally, the effector repertoire also dictates what domain of life you are able to compete with. However the effect of effector exchange stretches beyond the T6SS and can result in the exchange of other DNA.

7-3.2 Genetic exchange following T6SS module exchange

I was encouraged to investigate genetic exchange between two strains beyond the T6SS based on a new technology, multiplex genome editing by natural transformation (MuGent). Through studies of natural competence and subsequent recombination in *V. cholerae,* researchers have found that on chitin that the two processes occur at a rate of approximately 1:1000 when there was selective pressure (the acquisition of an antibiotic

resistance cassette) (Meibom et al., 2005). Additionally, other researchers noticed that the recipient strain could acquire other genetic material during this process (Dalia et al., 2014). Specifically, the researchers fed linear DNA with an antibiotic resistance cassette concurrently with another linear piece of DNA that introduced a point mutation into *lacZ.* Therefore, if they plate the transformed *V. cholerae* onto plates with the appropriate antibiotics and X-gal, they can calculate both the transformation efficiency of acquiring the antibiotic resistance cassette as well as the ratio of the bacteria that acquired the antibiotic resistance cassette and the *lacZ* mutation that has no selective pressure (Dalia et al., 2014). They found that 50% of *V. cholerae* that acquired the antibiotic resistance cassette also acquired the *lacZ* mutation (Dalia et al., 2014, 2017). This phenotype could be expanded to multiple constructs without selection. This has since been used as a protocol to delete multiple genes at a time by allelic exchange (Dalia et al., 2017). While used primarily as a genetic tool, I expanded on this by studying the biological consequences of DNA exchange without a biological pressure.

We hypothesized that there was a biological consequence to acquiring DNA indiscriminately (Figure 3). To test this we modified the scenario described above and instead of feeding linear DNA constructs, we instead used genomic DNA (gDNA) with a transposon inserted into the T6SS gene cluster (Cameron et al., 2008). Through deep sequencing we found that along with the acquisition of the T6SS gene cluster, these hybrid strains also acquired several other genomic traits. In our experiments we saw mostly the acquisition of either gene clusters for motility or metabolism. This is likely due to a high degree of genetic identity. Therefore, it is likely this is a mechanism whereby similar alleles are exchanged. However, we cannot exclude the possibility that completely novel gene clusters can be transferred through these means.

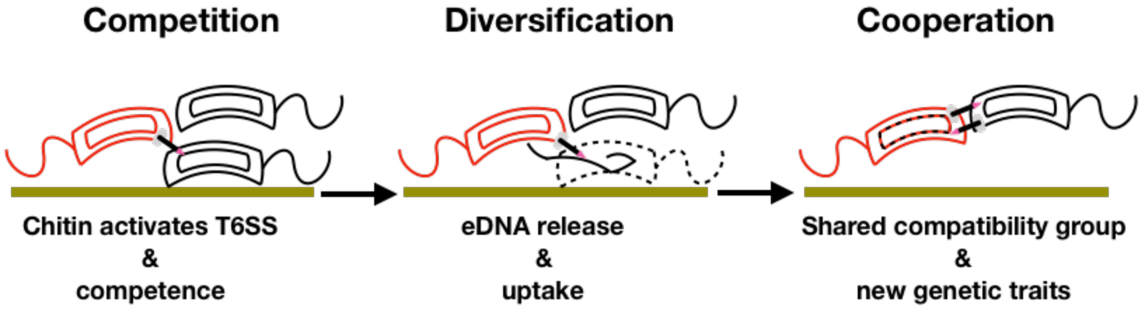

Figure 7-3. **Intraspecific competition results in cooperation and additional horizontal gene transfer.** The interaction between two incompatible strains results in T6SS

competition on chitin. Following this competition is the release of extracellular DNA (eDNA). This DNA is also internalized through natural competence as growth on chitin also activates the competency pathway. The pressure to acquire T6SS effector modules exists to prevent being outcompeted in a T6SS dependent manner. Along with the T6SS modules, T6SS-independent genes are also acquired resulting in diversification of the species.

Exchanging alleles can have a drastic effect on *V. cholerae* biology as a lot of *V. cholerae* diversity originates in very small changes within shared gene clusters. For example, the biosynthetic pathways responsible for the O-antigen could be exchanged this way as there is identity on the genetic level for strains that synthesize different O-antigens (Blokesch and Schoolnik, 2007). In our experiments we used gDNA from a pandemic strain and the natural competence of an environmental strain to model the flow of DNA from one strain to the other. One major reason for modeling it this way was to test the hypothesis that virulence factors could flow between pandemic and non-pandemic strains through natural competence. The other reason was that non-pandemic strains are significantly more likely to be naturally competent on chitin. One reason why this trend exists is that potentially evolution favours a more stable genome for pandemic strains due to their superior T6SS effectors and that they are well adapted to the human host. Alternatively, pandemic strains may benefit more from using extracellular gDNA as a carbon and nitrogen source rather than a source of genetic diversity.

Altogether this suggests many consequences of genetic diversification within the T6SS gene clusters. The exchange of effectors can cause *V. cholerae* to change its competitive tropism, whether other bacteria or eukaryotic cells. Additionally, changing effectors influences the compatibility group of the strain which influences niche occupation on chitin and in humans during coinfections. Lastly, the competitive pressure to acquire new T6SS modules will result in the acquisition of other genetic traits, representing an important means to diversify the genome through horizontal gene transfer.

7-4 Using the T6SS for interspecific competition

The T6SS as a secretion system for antibacterial proteins is not only a hallmark of *V. cholerae* but of many other studied T6SSs, including *Acinetobacter baumanii, Pseudomonas auruginosa, Salmonella* Typhimurium, and *Agrobacterium tumerfacies*

(Basler et al., 2013; Ma et al., 2014; Sana et al., 2016b; Weber et al., 2015). While the activities of the effectors are well studied, there is less known about the biological function of the T6SS and when it is essential for *V. cholerae* survival. In my thesis, I extensively study interspecific competition. First, it is used as a readout for T6SS activity, and as a determinant for evaluating the strength of effectors. Next, I study interspecific competition in the context of an *in-vivo* infection, demonstrating that T6SS killing of commensals in the host is productive for an infection. In this section I will briefly summarize the current models of the role the T6SS plays in both the environment and the host by competing with other species of bacteria before outlining the major questions facing the field and the difficulties to answer them

7-4.1 Interspecific competition in the environment

Chitin is the most abundant aminopolysaccharide polymer occurring in nature (Elieh-Ali-Komi and Hamblin, 2016). As such, it is home to a large diversity of microorganisms, both prokaryotic and eukaryotic (Kielak et al., 2013; Metcalfe et al., 2002). In fact, studies have shown that bacterial diversity increases in the presence of chitin compared to soil, with diversity increasing further with increased chitin degrading enzymes called chitinases (Kielak et al., 2013). *V. cholerae* encodes two extracellular chitinases and would therefore positively contribute to the environments potential to house increased biological diversity (Watve et al., 2015). To cope with this, *V. cholerae* must also have mechanisms to retain their niche. Such a mechanism could be *V. cholerae*'s T6SS. In my thesis, I explored how the repertoire of T6SS effectors affected competition with other bacterial species. I focused primarily on the AAA compatibility group as it is encoded by the strains of *V. cholerae* that represent the largest burden of disease towards humans. I showed that when competing with *E. coli,* both A^1 and A^M were superior to their non-toxigenic counterparts. However, more extensive studies need to be done as non-toxigenic strains are capable of encoding 117 different effectors. In this section I discuss the implications of superior competition.

As described earlier, using computational models and microscopy, three groups have independently demonstrated that the principal effect on population dynamics of T6SS-mediated competition is niche retention rather than niche invasion (Borenstein et al.,

2015; McNally et al., 2017; Wong et al., 2016). This is especially true if all bacteria have competition mechanisms (Borenstein et al., 2015). Another consequence of interspecific competition on chitin is the generation of eDNA for purposes of nutrition (Veening and Blokesch, 2017). DNA from distantly related bacteria is less likely to share identity with *V. cholerae* and therefore will potentially be used more for the carbon and nitrogen. Lastly, the eDNA could be used as a scaffold for biofilm formation on the chitin (Montanaro et al., 2011).

Competition on chitin also may allow bacterial numbers to increase through all three of the previously discussed mechanisms – more space, nutrients or a biofilm. As *V. cholerae* pathogenesis is dose dependent growing to high numbers on chitin would give *V. cholerae* an advantage during infection (Cohen et al., 1999).

There are many unanswered questions that would help clarify these models. One is the scope of T6SS killing. The large diversity of effectors allows us to speculate that certain effectors, or combinations of effectors can be superior under different environments. One example of this was recently published by Ringel *et al.* They showed that in *Acinetobacter baylyi* two different effectors kill bacteria in different ways, either through lysis, or without lysis (Ringel et al., 2017). This influenced the amount of DNA released by the prey bacteria. Through lysis, more eDNA is released more quickly and therefore could be more readily used for nutrition and horizontal gene transfer (Ringel et al., 2017). Wong *et al.* recently demonstrated a potential advantage to not lysing prey cells. This comes in the form of protecting established colonies (Wong et al., 2016). If a bacteria cell is killed through a non-lytic T6SS attack, the dead cell can act as a barrier that surrounds and protects the bacterial colony, simply because the dead cell cannot be replaced by a living cell (Wong et al., 2016). Beyond the mechanism of cell death, some effectors might be more adept at killing some species versus others. For example, VasX appears most proficient at killing other *V. cholerae* strains, whereas it appears to be the least important when competing with the Gram-negative bacteria *Aeromonas hydrophila* (Unterweger et al., 2014a; Wong et al., 2016). One could envision scenarios where the prey bacteria has a thicker peptidoglycan layer, and therefore be more resistant to peptidoglycan degrading enzymes. Alternatively, the structure of the peptidoglycan may make it more or less susceptible to one peptidoglycan degrading effector over another. Therefore the combination of effectors

encoded by *V. cholerae* might be acquired to best suit their specialized environment. For example, the ratio of anti-prokaryotic to anti-eukaryotic effectors might change based on the relative number of competitors.

7-4.2 Interspecific competition in the host

T6SS effectors on other bacterial species within the host environment have also been studied to a large degree. Recently three prominent studies have addressed the role of the T6SS in three different models of infection, the infant mouse, the infant zebrafish and – in my thesis – the fruit fly. In all three cases, the T6SS proved beneficial for the infection dependent on the presence of commensal organisms (Fast et al., 2018; Logan et al., 2018; Zhao et al., 2018). However, in all three models there were differences and similarities for both mechanism and outcome (Figure 4).

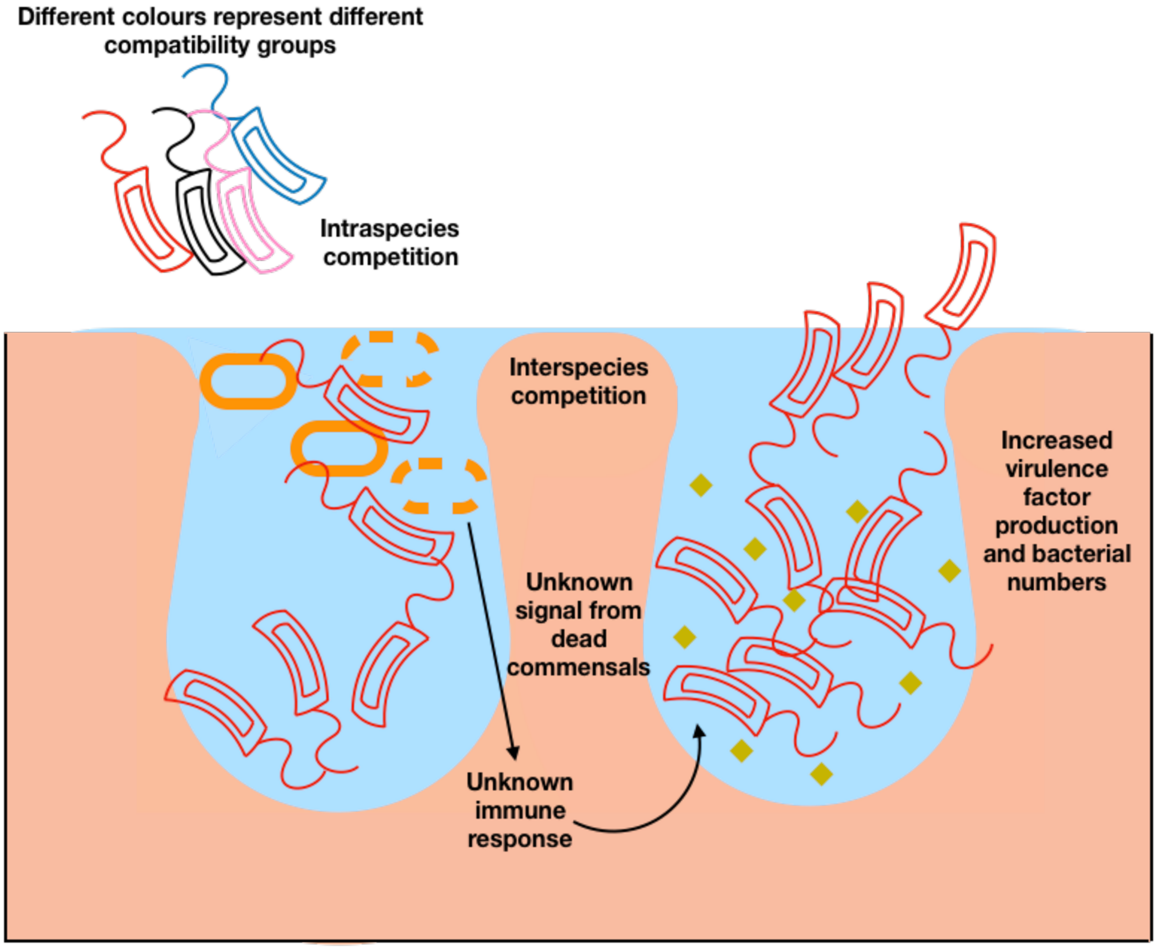

Figure 6-4. **Intraspecies and interspecies competition contribute to a productive *V. choelae* infection.** When a mix of *V. cholerae* strains are ingested into the host, there is activation of the T6SS when the bacteria come into contact with the mucous layer.

Following this, non-toxigenic strains are eliminated due to the lack of the membership to the AAA compatibility group. Next, *V. cholerae* must outcompete Gram-negative commensal bacteria. A direct result of a T6SS attack on the Gram-negative bacteria is the activation of the immune system. Unknown contributions of the immune response results in a milieu change that cause both the increase in virulence factor production by *V. cholerae* and also *V. cholerae* numbers in the host.

In my thesis, our work in the fruit fly suggested that the T6SS of *V. cholerae* killing the commensal *Acinetobacter pastuerianus* contributes positively to infection. We demonstrated this based on reduced lifespan and by increased diarrhea and transmission of *V. cholerae.* Next, we demonstrated that the T6SS benefitted the *V. cholerae* by allowing the bacteria to climb to higher titres. This increase was shown to be dependent on the presence of the T6SS-suceptible *A. pastuerianus.* Furthermore, I showed that the presence of the T6SS caused disruption of intestinal architecture through visualization with transmission electron microscopy. Finally, we showed that the T6SS activated the immune system of *V. cholerae.* It is unknown whether this activation is dependent on the presence of commensals. I hypothesize that it is, however, it could also be the actin-crosslinking domain or VasX that activates this system. Other models used to study the T6SS of *V. cholerae* suggest that both anti-bacterial and anti-eukaryotic effectors can activate the immune system (Logan et al., 2018; Ma and Mekalanos, 2010a; Zhao et al., 2018).

In the zebrafish model, the actin-crosslinking effector VgrG-1 was shown to be critical to activate the immune system and remove commensals from the organism (Logan et al., 2018). This effect is mediated through the immune system – causing contraction of the gut which results in the expulsion of the commensal *Aeromonas,* while *V. cholerae* is able to remain in the gut through an unknown mechanism (Logan et al., 2018). These data are similar to data shown in the infant mouse, where VgrG-1 is responsible for activation of the immune response and induction of diarrhea – although the state of the microbiome following this immune activation was not studied, I hypothesize that there would have been a great change in both commensal numbers and phylogenetic composition (Ma and Mekalanos, 2010a). This IMD activation in the fruit fly and the immune activation in the infant mouse appears to be dependent on the presence of commensals, however this was not tested in the zebrafish (Logan et al., 2018). The observation that VgrG-1 was necessary and sufficient for the immune activation in the zebrafish suggests that the microbiome is

not necessary for the activation as VgrG-1 targets eukaryotic cells only (Pukatzki et al., 2007).

In the fruit fly and infant mouse models, interaction between the T6SS of *V. cholerae* and Gram-negative commensals appear to be required to activate the immune system (Fast et al., 2018; Zhao et al., 2018). In the infant mouse this was tested by treatment with streptomycin and in the fruit fly, this was tested by generating germ-free animals. In both cases T6SS-mediated symptoms were abrogated (Fast et al., 2018; Zhao et al., 2018). This indicates that there is a signal from the dying commensals that is recognized by the host. Interestingly, the fate of the commensals differ in the two models. In the infant mouse, complete removal of two *E. coli* species occurred in a T6SS dependent manner, however, no statistically significant difference was found in commensal levels within the fruit fly (Fast et al., 2018; Zhao et al., 2018). This indicates that even a small or a localized loss of commensals can activate the immune system. Additionally, in the infant mouse there could be a combination of events that clears the commensal, for example, the T6SS could be used, like in the fruit fly, to remove a small percentage of the commensals, and then, as occurs in the zebra fish, the immune system could be responsible for clearing the rest of the commensals.

In the infant mouse, *V. cholerae* responds to the T6SS-commensal-immune system interaction by upregulating virulence factors such as cholera toxin, toxin-coregulated pilus and a proliferative growth response (Zhao et al., 2018). In the fruit fly, we did not look at the upregulation of virulence factors but we also observed an increased in *V. cholerae* CFUs (Fast et al., 2018).

Although it is difficult to integrate what we have learned from these models there are overlapping trends. The T6SS is activated when entering the host, presumably by mucins, and subsequently activates the immune system either though the anti-eukaryotic effector VgrG-1 or through interactions with the microbiome or both. This interaction between the immune system, the commensals, and the T6SS results in a more productive infection (Fast et al., 2018; Zhao et al., 2018).

A more complete model is needed to decipher the mechanism by which *V. cholerae*-commensal interactions causes an increased immune system as well as the environmental changes that result from the immune activation that appear to benefit *V.*

cholerae. This work might be best addressed in the fruit fly model as it is more readily assessible to manipulate the host genome to block or activate specific immune regulators.

Additionally, I would be interested in defining a role of the T6SS in persistence within the host. As discussed previously, El Tor *V. cholerae* strains persist longer in the host during infection than classical *V. cholerae* strains. This, combined with the observation that *V. cholerae* persists longer in a germ-free animal implicates the microbiome as a mechanism to clear *V. cholerae* infection (Ryan et al., 2000b). I hypothesize that the T6SS of *V. cholerae* can be used to increase the duration of a *V. cholerae* infection potentially through fending off the microbiome. This can be tested by infecting germ-free animals with *V. cholerae* or *V. cholerae* lacking a functional T6SS. Next, a variety of commensal bacteria can be administered to the animals. The CFUs of both the commensals and *V. cholerae* can then be measured over time to determine if the T6SS helps *V. cholerae* produce a prolonged infection.

Altogether, I hypothesize that the T6SS plays an important role in helping *V. cholerae* secure a niche in order to ensure that when they are ingested by a host they are at sufficient numbers to launch a production infection; after entering the intestine, *V. cholerae* uses its T6SS to outcompete the microbiome, secure its niche, enhance virulence factor production and potentially help prolong the infection.

7-5 Using the T6SS for intraspecific competition

Similar to interspecific competition, intraspecific competition has mostly been studied in the context of *in-vitro* killing assays. However, due to the diversity of both *V. cholerae* as a species and the T6SS effector modules, there is potential for competition on chitin and in the host. In this section I will briefly summarize the current models of the role the T6SS plays in both the environment and the host with respects to competing within *V. cholerae* as a species before outlining the major questions facing the field and the difficulties to answer them.

7-5.1 Intraspecific competition in the environment

In environmental samples, studies have found that toxigenic strains make up approximately 2.3% of the total proportion of *V. cholerae.* The non-toxigenic strains are

exceptionally diverse spanning many serogroups and compatibility groups (Faruque et al., 2004). This diversity and limited resources drives competition between *V. cholerae* strains. Knowing the outcome of this competition is important to understanding evolution and epidemiology of *V. cholerae*.

In contrast to the role of eDNA created by T6SS attacks outlined in interspecific competition, I hypothesize that the eDNA from intraspecific attacks will be more likely recombined into *V. cholerae* genomes. This can have two consequences. The first is that the DNA is used for genomic repair of highly conserved regions (Veening and Blokesch, 2017). The other consequence is acquiring new or new variations on genetic traits (Borgeaud et al., 2015b; Thomas et al., 2017).

One limitation in the study of intraspecific competition based on the T6SS is the difficulties associated with teasing apart various aspects of competition. For example, it is important to understand which effectors display increased bacterial killing compared to others. However, as discussed previously, the degree of killing by an effector might differ from target to target (Unterweger et al., 2014a; Wong et al., 2016). Furthermore, the degree that an effector can kill other bacteria might also depend on the environment. For example, in a hypertonic environment, a colicin – or pore forming – effector will have a higher degree of activity than in a hypotonic environment (Schwinghamer, 1980). *V. cholerae* inhabits many environments, including swimming planktonically, in biofilms, on the surface of various organisms (Almagro-Moreno and Taylor, 2013). Each of these environments will provide different osmolarity, and nutrition resulting in different growth conditions. Additionally, effectors may work in unison, the effect of multiple effectors might be additive, synergistic or even antagonize each other if they share a target.

Beyond the effectors encoded by *V. cholerae* the rate of firing, there also exists natural resistance through the production of a capsule (Borenstein et al., 2015; Toska et al., 2018). We must keep these differences in mind when fully evaluating the competition between two T6SS-positive *V. cholerae.*

As our library of *V. cholerae* strains is robust and growing, we are able to compare T6SS killing under laboratory conditions between two strains, and then repeat this competition assay using the same strain background but with the compatibility group switched (Unterweger et al., 2012, 2014a). For example, $V52_{AAA}$ and $DL4215_{CEC}$ can be

mixed in a competition assay and we observe that V52 "wins" by a magnitude of 100-fold (Unterweger et al., 2014a). However, what occurs when we mix $A1552_{AAA}$ with $A1552_{CEC}$ is currently unknown. A result with $A1552_{AAA}$ outcompeting $A1552_{CEC}$ would allow attribution to the effector modules, however, if $A1552_{CEC}$ outcompetes $A1552_{AAA}$, the rational for how V52 outcompeted DL4215 would need to be readdressed. For example the rate of T6SS firing can be measured through microscopy and the effect of any capsule can be determined through genetic mutants, additionally their growth rates can be measured. Repeating these killing assays on a variety of osmolarities, on chitin, or in the host my also give different results.

With the profound diversity of T6SS effectors and environments for *V. cholerae* to inhabit, it is tempting to hypothesize that there are effector combinations that best suit *V. cholerae* for the environment they are in. With that hypothesis in mind, I further speculate that as all toxigenic strains share the AAA-module set and that toxigenic strains appear to dominate in the host environment, that the AAA-module set is finely tuned for the intestine.

7-5.2 Intraspecific competition in the host

In addition to studying how *V. cholerae* interacts with other species in the gut, it is important to investigate how *V. cholerae* interacts in the context of a coinfection. This is important because in the environment, a very small proportion are toxigenic, yet cholera diarrhea is almost a pure culture of toxigenic *Vibrio cholerae* (Faruque et al., 2004; 1992). This is despite the fact that a proportion of these non-toxigenic strains are able to colonize the infant rabbit model of infection and are known to cause disease in humans (Faruque et al., 2004). Interestingly, while mixed infections are common in humans, as determined by multiple serogroups present in stool samples, this is not seen if there is a pandemic strain present (Dutta et al., 2013a). A similar observation was made in the infant rabbit, when mixed populations were fed to the infant rabbit (2.3% toxigenic) the percentage increased to over 60% after an 8-hour infection (Faruque et al., 2004). In my thesis, I explored the hypothesis that the mechanism behind this enrichment is the T6SS.

In my thesis, I demonstrated two instances of intraspecific competition. The first was between a T6SS-positive C6706 and a C6706 lacking three of its immunity genes. This demonstrated two important features, that the T6SS was active in the host, and that *V.*

cholerae density was sufficient to allow *Vibrio-Vibrio* competition. The strain lacking the immunity genes was outcompeted 10-fold. Next, we tested the ability of C6706 to outcompete non-toxigenic strains. The T6SS killing was localized to the proximal small intestine. This indicates that intraspecific competition might occur early in infection.

Recently in support of our work, in the infant rabbit, John Mekalanos's group demonstrated that C6706 gets in contact at distal areas of infection through the use of a conjugated plasmid (Fu et al., 2018). This conjugation event was not observed when the recipient strain was lacking its immunity genes indicating that it was killed instead of receiving the plasmid (Fu et al., 2018).

Toxigenic *V. cholerae* may use its T6SS to exclude strains that are not creating toxins for the common good, but are still receiving the benefits. I hypothesize at least two different classes of strains will be excluded for being so-called "cheaters". The first are non-toxigenic strains that do not produce cholera toxin. Cholera toxin benefits *V. cholerae* by creating an environment that allows for a proliferative burst in *V. cholerae* burden. Toxigenic *V. cholerae* strains would benefit from excluding non-toxigenic strains not producing the common good. Another common good is the T6SS, this allows clearance of commensals, and activation of the immune system which causes an increase in *V. cholerae.* Not only would toxigenic AAA *V. cholerae* strains exclude non-toxigenic strains of different compatibility groups, but our results in chapter 3 also suggest that classical pandemic strains would also be excluded due to a breached immunity gene.

To better understand this, it would be necessary to know when the T6SS is activated in the host, and when it participates in killing of other *vibrios*. I hypothesize that the T6SS of toxigenic strains will clear the non-toxigenic strains before cholera toxin is secreted. This could be studied through microscopy and translational fusions of both the T6SS and of cholera toxin with fluorescent proteins. One intriguing hypothesis is that the T6SS will occur between microcolony formation by TCP and cholera toxin secretion. Microcolony formation by TCP would bring *V. cholerae* into contact such that the T6SS can deliver toxin, following the purification of the culture, cholera toxin can then be released to cause watery diarrhea, amplification of *V. cholerae* and release into the environment.

Another question to be explored is whether the destruction of other *V. cholerae* is sufficient to induce the immune system of the infant mouse, and the subsequent increase

in cholera toxin production. If this is the case, this would be an additional benefit along with the removal of cheating strains.

Altogether *V. cholerae* uses its T6SS for competition and horizontal gene transfer between strains, but current experimental limitations make it difficult to understand which strains and T6SS effectors are best in which environments. I hypothesize that the AAA module set for toxigenic strains is superior in the host, and allows the removal of cheaters prior to cholera toxin mediated pathogenesis (Figure 4).

7-6 Taking advantage of the T6SS to prevent cholera

In this section I will discuss the current treatment strategies for cholera, as well as new technologies that are being used to treat the disease. Lastly, I will discuss two ways that our knowledge of the T6SS can be used to create new drugs and improve upon a cholera vaccine.

7-6.1 Current strategies to combat *V. cholerae*

V. cholerae contributes to an average of 100,000 mortalities worldwide, and over one million cases (Kaper et al., 1995). Recently, two major outbreaks have been responsible for a vast number of these. The first is the Haiti outbreak in early 2010 cause almost one million cases and left over 10,000 dead (Ali et al., 2011; Zarocostas, 2017). The second, starting in 2016 in Yemen and is ongoing and has already caused over 600,000 cases and over 2000 deaths (Camacho et al., 2018).

Front-line treatment of cholera is oral rehydration therapy – a buffered solution of glucose and sodium and potassium salts (Guerrant et al., 2003). This treatment simply replaces the upwards of 15L of water that is lost by diarrhea every day (Guerrant et al., 2003). Oral rehydration therapy reduces the mortality rate from 50% to 80% (Kaper et al., 1995). In high risk patients – both the very young, and very old – antibiotics can be used in conjugation with oral rehydration therapy (Kitaoka et al., 2011a; Mandal et al., 2012; Mhalu et al., 1979). Quinolones (which targets DNA gyrase) and tetracyclines (which targets translation) are the primary antibiotics used, however increasing antibiotic resistance have restricted their use (Kitaoka et al., 2011a).

Phage therapy is an emerging therapy for the treatment of cholera. This takes advantages of that natural ability of vibriophage to infect and lyse *Vibrio cholerae*. Unlike antibiotics, phage therapy is specific to *V. cholerae* and will not hurt the microbiome, risking secondary infections from such opportunistic pathogens a *C. difficile* (Yen et al., 2017). Phage therapy is also capable of auto dosing, i.e. the levels of the phage will increase to match the burden, and when the infection is cleared, the phage will have nothing left to infect and will also be cleared (Yen et al., 2017). Recent work has shown that the lytic phage ICP2 can reduce *V. cholerae* burden in disease (Seed et al., 2014). Furthermore, those bacteria that survive the therapy accumulated mutations to resist the phage – some of which come at the cost of attenuated virulence (Seed et al., 2014). Therefore, phage therapy may reduce disease burden both through lysis and forcing the evolution of *V. cholerae* towards mildness. More recently, Yen *et al.* demonstrated that combining ICP2 with two other phage, ICP1 and ICP3 can increase the efficacy of the treatment and could completely stop cholera if provided prophylactically (Yen et al., 2017).

The last treatment option is vaccines. Volunteers ingesting *V. cholerae* have been shown to have three years of protective immunity (Cash et al., 1974a, 1974b). The response of the adaptive immune response is primarily mediated by B-cells (Harris et al., 2009). However, due to the multiple serogroups and variation of the O-antigen, there is little cross-reactivity with other *V. cholerae* (Cash et al., 1974b). Lastly, patients of blood group O develop weak protection (Clemens et al., 1989).

Three cholera vaccines, Dukoral, Vaxchora and mORCVAX, are currently available and provide upwards of 50% protection for two years (World Health Organization Organisation mondiale de la Santé, 2017). These vaccines are whole bacteria killed, and Dukoral includes recombinant cholera toxin B-subunit (Jelinek and Kollaritsch, 2008).

The outlook for reducing the burden of cholera is bright, however, the best way to reduce disease burden still remains adequate clean drinking water and sanitation.

7-6.2 Breaching immunity

I believe that our knowledge of the T6SS can be utilized to derive treatment options for those suffering from cholera. Currently, when the T6SS is activated within the host, pandemic strains are able to kill non-toxigenic strains as well as the commensals but are

themselves protected due to their immunity proteins (Bachmann et al., 2015; Zhao et al., 2018). I hypothesize that by chemically inhibiting an immunity protein, *V. cholerae* will engage in sibling-mediated killing and will reduce the bacterial burden. We know that one compromised immunity gene is sufficient to reduce the fitness of *V. cholerae,* as witnessed by the compromised immunity system of the classical strain, O395. Because the T6SS is only used transiently, there is a small window of opportunity for the development of resistance. As T6SS immunity proteins require dimerization to bind and sequester the toxic effector, I propose screening small molecules to find a compound that prevents the dimerization of TsiV3 (the best studied effector from a biochemical standpoint) (Yang et al., 2014; Zhang et al., 2014) . This will prevent TsiV3 from being active, and *V. cholerae* will engage in sister-mediated killing.

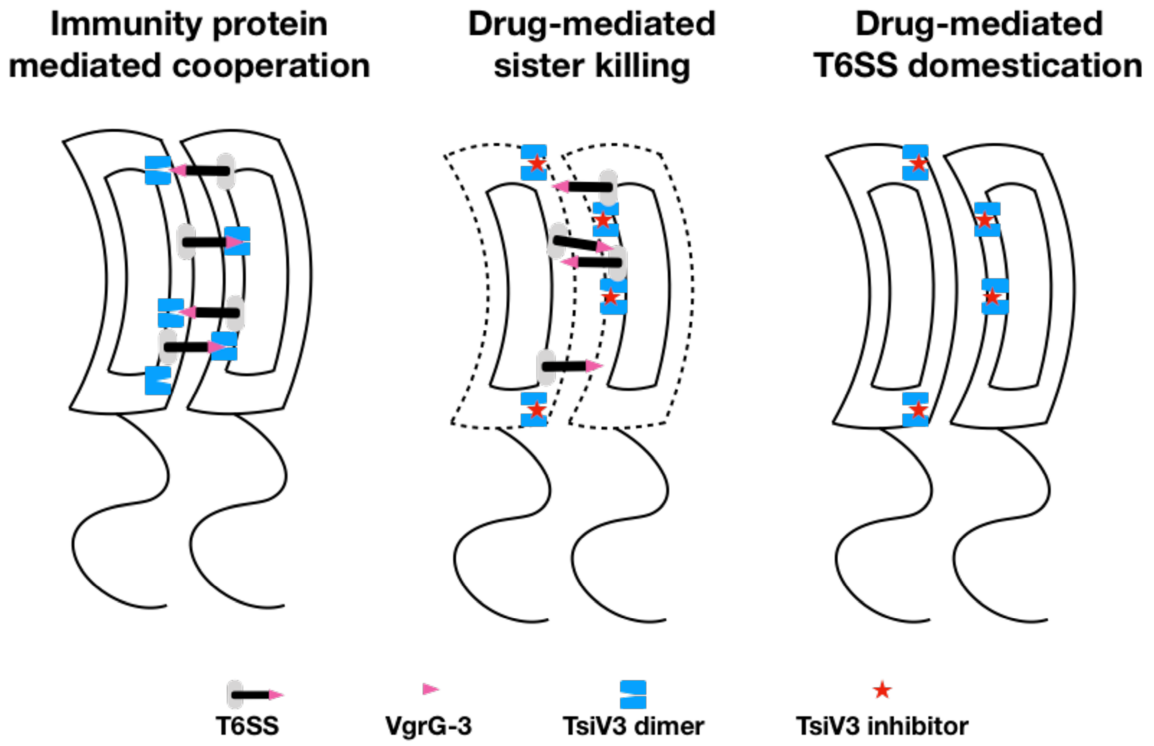

Figure 7-5. **Inhibiting dimerization of TsiV3 is a potential drug target to reduce *V. cholerae* virulence**. Under normal conditions, *V. cholerae* are protected from T6SS-dependent attacks from sister cells through the action of their immunity proteins. When a drug is administered that inhibits TsiV3 dimerization, we anticipate one of two situations. The first is that the dysfunctional immunity proteins will result in no protection and *V. cholerae* will participate in sister cell mediated killing. The second is that in order to prevent killing sister cells, mutations will occur in the T6SS to deactivate the system. In this case, *V. cholerae* will be result in a milder infection as it no longer has the ability to compete with other bacteria and eukaryotic cells.

One potential caveat, is that to prevent sister-mediated killing *V. cholerae* might genetically mutate its T6SS to not be active altogether. I hypothesize that in this case, *V. cholerae* will have also weakened itself and would have reduced virulence potential. Altogether, such a treatment would reduce *V. cholerae* burden through sister-mediated killing, then, after potential T6SS mutations occur, reduce the virulence of the remaining bacteria – preventing transmission of the pathogen (Figure 5). This treatment might work better as a prophylactic. Ideally, a commensal bacteria programmed with the biosynethic pathway of this small molecule would be employed.

6-6.2 Consideration of compatibility groups in rational vaccine design

A different vaccine strategy has recently been published, whereby a live attenuated bacteria is administered to an animal to protect from subsequent virulence (Hubbard et al., 2018). One problem with vaccines in the time it takes to provide immunity. As *V. cholerae* outbreaks are often difficult to predict, by the time a vaccine program is in place it might be too late to reduce disease burden in an area. The new vaccine, HaitiV, has a two pronged approach to protection. The first is to act as a probiotic, by occupying *V. cholerae's* niche (Hubbard et al., 2018). HaitiV lacks all toxins, antibiotic resistance cassettes and contains a CRISPR-Cas9 system that protects it from acquiring the cholera toxin phage (Hubbard et al., 2018). *V. cholerae* HaitiV provides protection within 24 hours in a probiotic manner without causing disease symptoms, and after the probiotic strain is cleared, lasting immunity is given through a humoral response.

As HaitiV requires colonization of the host to exclude *V. cholerae* strains from colonizing, I reason that it must be able to resist competition from the infecting strain. For that, it becomes imperative to know the compatibility group of the strain causing the outbreak. As T6SS killing can contribute to inflammation, it might be ideal for the compatibility group of the vaccine strain to match the strain causing the outbreak.

This would require that the compatibility group of outbreak strains to be investigated when looking at the molecular epidemiology.

6-7.1 Overall Summary of Conclusions

My thesis focused on examining unique characteristics of the T6SS encoded in pandemic *V. cholerae* strains. Previous observations from our laboratory showed that all pandemic strains encode the AAA-module set (Unterweger et al., 2014a). Further dissection of the T6SS gene clusters led to two hypotheses, that the T6SS effectors can be horizontally exchanged and that pandemic strains differ between one another in the structural components of the T6SS. These differences are deletions in structural components within 2nd and 6th pandemics and a SNP in an immunity gene in a subset of 6th pandemic strains compared to 7th pandemic strains.

First, I investigated both the mechanism and consequences of effector exchange. I tested a potential mechanism of effector exchange is homology facilitated illegitimate recombination (HFIR). HFIR allows effector module exchange between strains through a conserved region and the retention of the original immunity gene (de Vries and Wackernagel, 2002). This is necessary to preserve the *vgrG* genes as well as any enzymatic activity they may hold. Retaining the original immunity gene will potentially give an added benefit to *V. cholerae* and is a phenomenon seen many times through *V. cholerae* as a species. The effector modules acquired by pandemic strains are more bacteriolytic than other effectors encoded by *V. cholerae,* however, more exhaustive studies need to be performed. There are other factors to T6SS competition beyond the effectors encoded, such as the rate of T6SS firing. Therefore, even superior effectors can be outcompeted by a system delivering the toxins more frequently (Borenstein et al., 2015). I infer from this observation that the effectors are not the sole factor to determine the competitive outcome that the T6SS effector module set might be more useful in defining cooperative strains rather than which strain will outcompete another. From this I conclude that pandemic strains encode the same effectors so that they can co-exist and co-infect together.

Next, I studied the differences in the T6SS between the 7th, 6th and 2nd pandemics. We found that the 2nd and 6th pandemic strains contain mutations that when introduced into V52, a strain with a constitutively active T6SS, result in a completely non-functional T6SS. In addition, within the 6th pandemic, a subset of strains also accumulated a mutation within an immunity gene rendering them sensitive from T6SS attacks from the 7th pandemic strains. This could be a potential mechanism whereby the 7th pandemic replaced the 6th.

This indicates that the T6SS might be more important than it once was. This is supported by recent evidence that the T6SS of modern 7th pandemic strains isolated in Haiti have a constitutively active T6SS.

Next, I sought to understand the *in-vivo* regulation of the T6SS. We found that mucin is responsible for activating the system, and that the magnitude of the T6SS can be controlled by the composition of bile, with some components enhancing the system and others depressing it (Bachmann et al., 2015). As the composition of bile varies across the small and large intestine, this indicates that the T6SS might be fine-tuned to have maximum activity in a specific local (Begley et al., 2005). More work is needed to be done to investigate the spatial activation of the T6SS. We found that a mucin activated T6SS of pandemic strains was able to exclude non-pandemic strains in a coinfection, indicating that the T6SS serves an important role for intraspecific competition within the host (Bachmann et al., 2015).

Finally, we used the Drosophila model of cholera infection to investigate interspecies competition mediated by the T6SS (Fast et al., 2018). We found that *V. cholerae* was given a pathogenic advantage to encoding the T6SS, as the fly died more quickly, displayed a greater degree of diarrhea and had a more disorganized gut epithelial layer (Fast et al., 2018). This increased pathogenesis was due to the interaction between *V. cholerae* and the T6SS-sensitive bacteria *Acetobacter pasteurianus.* Reconstituting a microbiome without *Acetobacter pasteurianus* removed the T6SS dependent phenotype. Lastly, the T6SS was shown to activate the immune system, and the immune system appears to play a role in the increased pathogenesis (Fast et al., 2018).

These findings add to our knowledge of the T6SS in pandemic strains and how *V. cholerae* uses this sophisticated machine to interact with its environment. The acquired knowledge could have implications for the advancement of treatments of cholera.

References

Alam, A., LaRocque, R.C., Harris, J.B., Vanderspurt, C., Ryan, E.T., Qadri, F., and Calderwood, S.B. (2005). Hyperinfectivity of Human-Passaged Vibrio cholerae Can Be Modeled by Growth in the Infant Mouse. Infect. Immun. *73*, 6674–6679.

Alexakis, L.C. (2017). Cholera -"Rice water stools. Pan Afr. Med. J. *26*.

Ali, A., Chen, Y., Johnson, J.A., Redden, E., Mayette, Y., Rashid, M.H., Stine, O.C., and Morris, J.G. (2011). Recent Clonal Origin of Cholera in Haiti. Emerg. Infect. Dis. *17*, 699–701.

Ali, M., Lopez, A.L., You, Y.A., Kim, Y.E., Sah, B., Maskery, B., and Clemens, J. (2012). The global burden of cholera. Bull. World Health Organ. *90*, 209–218.

Almagro-Moreno, S., and Taylor, R.K. (2013). Cholera: Environmental Reservoirs and Impact on Disease Transmission. Microbiol. Spectr. *1*.

Altindis, E., Dong, T., Catalano, C., and Mekalanos, J. (2015). Secretome Analysis of Vibrio cholerae Type VI Secretion System Reveals a New Effector-Immunity Pair. MBio *6*, e00075-15.

Amarir-Bouhram, J., Goin, M., and Petit, M.-A. (2011). Low Efficiency of Homology-Facilitated Illegitimate Recombination during Conjugation in Escherichia coli. PLOS ONE *6*, e28876.

Anderson, A.M.L., Varkey, J.B., Petti, C.A., Liddle, R.A., Frothingham, R., and Woods, C.W. (2004). Non-O1 Vibrio cholerae septicemia: case report, discussion of literature, and relevance to bioterrorism. Diagn. Microbiol. Infect. Dis. *49*, 295–297.

Andrews, S. (2010). FastQC: a quality control tool for high throughput sequence data.

Ante, V.M., Bina, X.R., Howard, M.F., Sayeed, S., Taylor, D.L., and Bina, J.E. (2015). Vibrio cholerae leuO Transcription Is Positively Regulated by ToxR and Contributes to Bile Resistance. J. Bacteriol. *197*, 3499–3510.

Antonova, E.S., Bernardy, E.E., and Hammer, B.K. (2012). Natural competence in Vibrio cholerae is controlled by a nucleoside scavenging response that requires CytR-dependent anti-activation. Mol. Microbiol. *86*, 1215–1231.

Azman, A.S., Rudolph, K.E., Cummings, D.A.T., and Lessler, J. (2013). The incubation period of cholera: A systematic review. J. Infect. *66*, 432–438.

Bachmann, V., Kostiuk, B., Unterweger, D., Diaz-Satizabal, L., Ogg, S., and Pukatzki, S. (2015). Bile salts modulate the mucin-activated type VI secretion system of pandemic Vibrio cholerae. PLoS Negl. Trop. Dis. *9*, e0004031.

Baltrus, D.A. (2013). Exploring the costs of horizontal gene transfer. Trends Ecol. Evol. *28*, 489–495.

Bart, K.J., Huq, Z., Khan, M., Mosley, W.H., Nuruzzaman, M., and Golam Kibriya, A.K.M. (1970). Seroepidemiologic studies during a simultaneous epidemic of infection with El Tor Ogawa and classical Inaba Vibrio cholerae. J. Infect. Dis. *121*, S17–S24.

Barua, D. (1992). History of Cholera. In Cholera, (Springer, Boston, MA), pp. 1–36.

Basler, M. (2015). Type VI secretion system: secretion by a contractile nanomachine. Philos. Trans. R. Soc. B Biol. Sci. *370*.

Basler, M., and Mekalanos, J.J. (2012). Type 6 Secretion Dynamics Within and Between Bacterial Cells. Science *337*, 815–815.

Basler, M., Pilhofer, M., Henderson, P.G., Jensen, J.G., and Mekalanos, J. (2012). Type VI secretion requires a dynamic contractile phage tail-like structure. Nature *483*, 182–186.

Basler, M., Ho, B., and Mekalanos, J. (2013). Tit-for-tat: type VI secretion system counterattack during bacterial cell-cell interactions. Cell *152*, 884–894.

Beaber, J.W., Hochhut, B., and Waldor, M.K. (2004). SOS response promotes horizontal dissemination of antibiotic resistance genes. Nature *427*, 72–74.

Begley, M., Gahan, C.G.M., and Hill, C. (2005). The interaction between bacteria and bile. FEMS Microbiol. Rev. *29*, 625–651.

Begum, Y.A., Rydberg, H.A., Thorell, K., Kwak, Y.-K., Sun, L., Joffré, E., Qadri, F., and Sjöling, Å. (2018). In Situ Analyses Directly in Diarrheal Stool Reveal Large Variations in Bacterial Load and Active Toxin Expression of Enterotoxigenic Escherichia coli and Vibrio cholerae. MSphere *3*, e00517-17.

Belkaid, Y., and Hand, T.W. (2014). Role of the microbiota in immunity and inflammation. Cell *157*, 121–141.

Bendor, L., Weyrich, L.S., Linz, B., Rolin, O.Y., Taylor, D.L., Goodfield, L.L., Smallridge, W.E., Kennett, M.J., and Harvill, E.T. (2015). Type Six Secretion System of Bordetella bronchiseptica and Adaptive Immune Components Limit Intracellular Survival During Infection. PLOS ONE *10*, e0140743.

Benitez, J.A., and Silva, A.J. (2016). Vibrio cholerae hemagglutinin(HA)/protease: An extracellular metalloprotease with multiple pathogenic activities. Toxicon Off. J. Int. Soc. Toxinology *115*, 55–62.

Benz, J., and Meinhart, A. (2014). Antibacterial effector/immunity systems: it's just the tip of the iceberg. Curr. Opin. Microbiol. *17*, 1–10.

Berkey, C.D., Blow, N., and Watnick, P.I. (2009). Genetic analysis of Drosophila melanogaster susceptibility to intestinal Vibrio cholerae infection. Cell. Microbiol. *11*, 461–474.

Bernardy, E.E., Turnsek, M.A., Wilson, S.K., Tarr, C.L., and Hammer, B.K. (2016). Diversity of Clinical and Environmental Isolates of Vibrio cholerae in Natural Transformation and Contact-Dependent Bacterial Killing Indicative of Type VI Secretion System Activity. Appl. Environ. Microbiol. AEM.00351-16.

Beyhan, S., Tischler, A.D., Camilli, A., and Yildiz, F.H. (2006). Differences in Gene Expression between the Classical and El Tor Biotypes of Vibrio cholerae O1. Infect. Immun. *74*, 3633–3642.

Bhowmick, R., Ghosal, A., Das, B., Koley, H., Saha, D.R., Ganguly, S., Nandy, R.K., Bhadra, R.K., and Chatterjee, N.S. (2008). Intestinal adherence of Vibrio cholerae involves a coordinated interaction between colonization factor GbpA and mucin. Infect. Immun. *76*, 4968–4977.

Bina, J.E., and Mekalanos, J.J. (2001). Vibrio cholerae tolC Is Required for Bile Resistance and Colonization. Infect. Immun. *69*, 4681–4685.

Bina, X.R., Provenzano, D., Nguyen, N., and Bina, J.E. (2008). Vibrio cholerae RND Family Efflux Systems Are Required for Antimicrobial Resistance, Optimal Virulence Factor Production, and Colonization of the Infant Mouse Small Intestine. Infect. Immun. *76*, 3595–3605.

Bina, X.R., Taylor, D.L., Vikram, A., Ante, V.M., and Bina, J.E. (2013). Vibrio cholerae ToxR Downregulates Virulence Factor Production in Response to Cyclo(Phe-Pro). MBio *4*, e00366-13.

Bina, X.R., Howard, M.F., Ante, V.M., and Bina, J.E. (2016). Vibrio cholerae LeuO links the ToxR regulon to the expression of lipid A remodeling genes. Infect. Immun. IAI.00445-16.

Blokesch, M., and Schoolnik, G.K. (2007). Serogroup Conversion of Vibrio cholerae in Aquatic Reservoirs. PLOS Pathog. *3*, e81.

Blow, N.S., Salomon, R.N., Garrity, K., Reveillaud, I., Kopin, A., Jackson, F.R., and Watnick, P.I. (2005). Vibrio cholerae infection of Drosophila melanogaster mimics the human disease cholera. PLoS Pathog. *1*, e8.

Bolger, A.M., Lohse, M., and Usadel, B. (2014). Trimmomatic: a flexible trimmer for Illumina sequence data. Bioinformatics *30*, 2114–2120.

Borenstein, D.B., Ringel, P., Basler, M., and Wingreen, N.S. (2015). Established Microbial Colonies Can Survive Type VI Secretion Assault. PLOS Comput. Biol. *11*, e1004520.

Borgeaud, S., Metzger, L.C., Scrignari, T., and Blokesch, M. (2015a). The type VI secretion system of Vibrio cholerae fosters horizontal gene transfer. Science *347*, 63–67.

Borgeaud, S., Metzger, L.C., Scrignari, T., and Blokesch, M. (2015b). The type VI secretion system of Vibrio cholerae fosters horizontal gene transfer. Science *347*, 63–67.

Boucher, Y., Orata, F.D., and Alam, M. (2015). The out-of-the-delta hypothesis: dense human populations in low-lying river deltas served as agents for the evolution of a deadly pathogen. Front. Microbiol. *6*.

Boyer, F., Fichant, G., Berthod, J., Vandenbrouck, Y., and Attree, I. (2009). Dissecting the bacterial type VI secretion system by a genome wide in silico analysis: what can be learned from available microbial genomic resources? BMC Genomics *10*, 104.

Brooks, T.M., Unterweger, D., Bachmann, V., Kostiuk, B., and Pukatzki, S. (2013). Lytic activity of the Vibrio cholerae type VI secretion toxin VgrG-3 is inhibited by the antitoxin TsaB. J. Biol. Chem. *288*, 7618–7625.

Brunet, Y.R., Zoued, A., Boyer, F., Douzi, B., and Cascales, E. (2015). The Type VI Secretion TssEFGK-VgrG Phage-Like Baseplate Is Recruited to the TssJLM Membrane Complex via Multiple Contacts and Serves As Assembly Platform for Tail Tube/Sheath Polymerization. PLOS Genet. *11*, e1005545.

Buchon, N., Broderick, N.A., Poidevin, M., Pradervand, S., and Lemaitre, B. (2009). Drosophila Intestinal Response to Bacterial Infection: Activation of Host Defense and Stem Cell Proliferation. Cell Host Microbe *5*, 200–211.

Buchon, N., Broderick, N.A., Kuraishi, T., and Lemaitre, B. (2010a). Drosophila EGFR pathway coordinates stem cell proliferation and gut remodeling following infection. BMC Biol. *8*, 152.

Buchon, N., Broderick, N.A., Kuraishi, T., and Lemaitre, B. (2010b). Drosophila EGFR pathway coordinates stem cell proliferation and gut remodeling following infection. BMC Biol. *8*, 152.

Buffie, C.G., and Pamer, E.G. (2013). Microbiota-mediated colonization resistance against intestinal pathogens. Nat. Rev. Immunol. *13*, 790–801.

Camacho, A., Bouhenia, M., Alyusfi, R., Alkohlani, A., Naji, M.A.M., Radiguès, X. de, Abubakar, A.M., Almoalmi, A., Seguin, C., Sagrado, M.J., et al. (2018). Cholera epidemic in Yemen, 2016–18: an analysis of surveillance data. Lancet Glob. Health *6*, e680–e690.

Cameron, D.E., Urbach, J.M., and Mekalanos, J.J. (2008). A defined transposon mutant library and its use in identifying motility genes in Vibrio cholerae. Proc. Natl. Acad. Sci. U. S. A. *105*, 8736–8741.

Camilli, A., and Mekalanos, J.J. (1995). Use of recombinase gene fusions to identify Vibrio cholerae genes induced during infection. Mol. Microbiol. *18*, 671–683.

Cash, R.A., Music, S.I., Libonati, J.P., Snyder, M.J., Wenzel, R.P., and Hornick, R.B. (1974a). Response of Man to Infection with Vibrio cholerae. I. Clinical, Serologic, and Bacteriologic Responses to a Known Inoculum. J. Infect. Dis. *129*, 45–52.

Cash, R.A., Music, S.I., Libonati, J.P., Craig, J.P., Pierce, N.F., and Hornick, R.B. (1974b). Response of man to infection with Vibrio cholerae. II. Protection from illness afforded by previous disease and vaccine. J. Infect. Dis. *130*, 325–333.

Chaand, M., Miller, K.A., Sofia, M.K., Schlesener, C., Weaver, J.W.A., Sood, V., and Dziejman, M. (2015). Type Three Secretion System Island-Encoded Proteins Required for Colonization by Non-O1/Non-O139 Serogroup Vibrio cholerae. Infect. Immun. *83*, 2862–2869.

Chatterjee, A., and Chowdhury, R. (2008). Bile and Unsaturated Fatty Acids Inhibit the Binding of Cholera Toxin and Escherichia coli Heat-Labile Enterotoxin to GM1 Receptor. Antimicrob. Agents Chemother. *52*, 220–224.

Chen, H., Yang, D., Han, F., Tan, J., Zhang, L., Xiao, J., Zhang, Y., and Liu, Q. (2017). The Bacterial T6SS Effector EvpP Prevents NLRP3 Inflammasome Activation by Inhibiting the Ca2+-Dependent MAPK-Jnk Pathway. Cell Host Microbe *21*, 47–58.

Chen, Y., Lun, A.T., and Smyth, G.K. From reads to genes to pathways: differential expression analysis of RNA-Seq experiments using Rsubread and the edgeR quasi-likelihood pipeline [version 2; referees: 5 approved]. F1000Res. 2016; 5: 1438. PubMed Abstr. Publ. Full Text Free Full Text.

Chiang, S.L., and Mekalanos, J.J. (1998). Use of signature-tagged transposon mutagenesis to identify Vibrio cholerae genes critical for colonization. Mol. Microbiol. *27*, 797–805.

Chiavelli, D.A., Marsh, J.W., and Taylor, R.K. (2001). The Mannose-Sensitive Hemagglutinin ofVibrio cholerae Promotes Adherence to Zooplankton. Appl Env. Microbiol *67*, 3220–3225.

Childers, B.M., and Klose, K.E. (2007). Regulation of virulence in Vibrio cholerae: the ToxR regulon.

Choi, S.Y., Rashed, S.M., Hasan, N.A., Alam, M., Islam, T., Sadique, A., Johura, F.-T., Eppinger, M., Ravel, J., Huq, A., et al. (2016). Phylogenetic Diversity of Vibrio cholerae Associated with Endemic Cholera in Mexico from 1991 to 2008. MBio *7*.

Chourashi, R., Mondal, M., Sinha, R., Debnath, A., Das, S., Koley, H., and Chatterjee, N.S. (2016a). Role of a sensor histidine kinase ChiS of Vibrio cholerae in pathogenesis. Int. J. Med. Microbiol. IJMM *306*, 657–665.

Chourashi, R., Mondal, M., Sinha, R., Debnath, A., Das, S., Koley, H., and Chatterjee, N.S. (2016b). Role of a sensor histidine kinase ChiS of Vibrio cholerae in pathogenesis. Int. J. Med. Microbiol. IJMM *306*, 657–665.

Chun, J., Grim, C.J., Hasan, N.A., Lee, J.H., Choi, S.Y., Haley, B.J., Taviani, E., Jeon, Y.-S., Kim, D.W., Lee, J.-H., et al. (2009). Comparative genomics reveals mechanism for short-term and long-term clonal transitions in pandemic Vibrio cholerae. Proc. Natl. Acad. Sci. *106*, 15442–15447.

Clemens, J.D., Sack, D.A., Harris, J.R., Chakraborty, J., Khan, M.R., Huda, S., Ahmed, F., Gomes, J., Rao, M.R., and Svennerholm, A.-M. (1989). ABO blood groups and cholera: new observations on specificity of risk and modification of vaccine efficacy. J. Infect. Dis. *159*, 770–773.

Cohen, M.B., Giannella, R.A., Losonsky, G.A., Lang, D.R., Parker, S., Hawkins, J.A., Gunther, C., and Schiff, G.A. (1999). Validation and Characterization of a Human Volunteer Challenge Model for Cholera by Using Frozen Bacteria of the New Vibrio cholerae Epidemic Serotype, O139. Infect. Immun. *67*, 6346–6349.

Conner, J.G., Teschler, J.K., Jones, C.J., and Yildiz, F.H. (2016). Staying alive: Vibrio cholerae's cycle of environmental survival, transmission, and dissemination. Microbiol. Spectr. *4*.

Cordero, C.L., Sozhamannan, S., and Satchell, K.J.F. (2007). RTX Toxin Actin Cross-Linking Activity in Clinical and Environmental Isolates of Vibrio cholerae. J. Clin. Microbiol. *45*, 2289–2292.

de la Cruz, F., and Davies, J. (2000). Horizontal gene transfer and the origin of species: lessons from bacteria. Trends Microbiol. *8*, 128–133.

Dalia, A.B., McDonough, E., and Camilli, A. (2014). Multiplex genome editing by natural transformation. Proc. Natl. Acad. Sci. U. S. A. *111*, 8937–8942.

Dalia, T.N., Yoon, S.H., Galli, E., Barre, F.-X., Waters, C.M., and Dalia, A.B. (2017). Enhancing multiplex genome editing by natural transformation (MuGENT) via inactivation of ssDNA exonucleases. Nucleic Acids Res. *45*, 7527–7537.

Darling, A.E., Mau, B., and Perna, N.T. (2010). progressiveMauve: Multiple Genome Alignment with Gene Gain, Loss and Rearrangement. PLoS ONE *5*.

Das, M.M., Bhotra, T., Zala, D., and Singh, D.V. (2016). Phenotypic and genetic characteristics of Vibrio cholerae O1 carrying Haitian ctxB and attributes of classical and El Tor biotypes isolated from Silvassa, India. J. Med. Microbiol. *65*, 720–728.

David, L.A., Weil, A., Ryan, E.T., Calderwood, S.B., Harris, J.B., Chowdhury, F., Begum, Y., Qadri, F., LaRocque, R.C., and Turnbaugh, P.J. (2015). Gut Microbial Succession Follows Acute Secretory Diarrhea in Humans. MBio *6*, e00381-15.

Deriu, E., Liu, J.Z., Pezeshki, M., Edwards, R.A., Ochoa, R.J., Contreras, H., Libby, S.J., Fang, F.C., and Raffatellu, M. (2013). Probiotic Bacteria Reduce Salmonella Typhimurium Intestinal Colonization by Competing for Iron. Cell Host Microbe *14*, 26–37.

Devault, A.M., Golding, G.B., Waglechner, N., Enk, J.M., Kuch, M., Tien, J.H., Shi, M., Fisman, D.N., Dhody, A.N., Forrest, S., et al. (2014). Second-Pandemic Strain of Vibrio cholerae from the Philadelphia Cholera Outbreak of 1849. N. Engl. J. Med. *370*, 334–340.

Dionne, M.S., and Schneider, D.S. (2008). Models of infectious diseases in the fruit fly Drosophila melanogaster. Dis. Model. Mech. *1*, 43–49.

Dixit, S.M., Johura, F.-T., Manandhar, S., Sadique, A., Rajbhandari, R.M., Mannan, S.B., Rashid, M., Islam, S., Karmacharya, D., Watanabe, H., et al. (2014). Cholera outbreaks (2012) in three districts of Nepal reveal clonal transmission of multi-drug resistant Vibrio cholerae O1. BMC Infect. Dis. *14*, 392.

Domman, D., Chowdhury, F., Khan, A.I., Dorman, M.J., Mutreja, A., Uddin, M.I., Paul, A., Begum, Y.A., Charles, R.C., Calderwood, S.B., et al. (2018). Defining endemic cholera at three levels of spatiotemporal resolution within Bangladesh. Nat. Genet. *50*, 951–955.

Dong, T.G., and Mekalanos, J.J. (2012). Characterization of the RpoN regulon reveals differential regulation of T6SS and new flagellar operons in Vibrio cholerae O37 strain V52. Nucleic Acids Res. *40*, 7766–7775.

Dong, T.G., Ho, B.T., Yoder-Himes, D.R., and Mekalanos, J.J. (2013). Identification of T6SS-dependent effector and immunity proteins by Tn-seq in Vibrio cholerae. Proc. Natl. Acad. Sci. *110*, 2623–2628.

Dong, T.G., Dong, S., Catalano, C., Moore, R., Liang, X., and Mekalanos, J.J. (2015). Generation of reactive oxygen species by lethal attacks from competing microbes. Proc. Natl. Acad. Sci. U. S. A. *112*, 2181–2186.

Dutta, N.K., and Habbu, M.K. (1955). Experimental cholera in infant rabbits: a method for chemotherapeutic investigation. Br. J. Pharmacol. Chemother. *10*, 153–159.

Dutta, D., Chowdhury, G., Pazhani, G.P., Guin, S., Dutta, S., Ghosh, S., Rajendran, K., Nandy, R.K., Mukhopadhyay, A.K., Bhattacharya, M.K., et al. (2013a). Vibrio cholerae Non-O1, Non-O139 Serogroups and Cholera-like Diarrhea, Kolkata, India. Emerg. Infect. Dis. *19*, 464–467.

Dutta, D., Chowdhury, G., Pazhani, G.P., Guin, S., Dutta, S., Ghosh, S., Rajendran, K., Nandy, R.K., Mukhopadhyay, A.K., Bhattacharya, M.K., et al. (2013b). Vibrio cholerae non-O1, non-O139 serogroups and cholera-like diarrhea, Kolkata, India. Emerg. Infect. Dis. *19*, 464–467.

Elieh-Ali-Komi, D., and Hamblin, M.R. (2016). Chitin and Chitosan: Production and Application of Versatile Biomedical Nanomaterials. Int. J. Adv. Res. *4*, 411–427.

Faruque, S.M., Zhu, J., Asadulghani, null, Kamruzzaman, M., and Mekalanos, J.J. (2003a). Examination of diverse toxin-coregulated pilus-positive Vibrio cholerae strains fails to demonstrate evidence for Vibrio pathogenicity island phage. Infect. Immun. *71*, 2993–2999.

Faruque, S.M., Kamruzzaman, M., Meraj, I.M., Chowdhury, N., Nair, G.B., Sack, R.B., Colwell, R.R., and Sack, D.A. (2003b). Pathogenic Potential of Environmental Vibrio cholerae Strains Carrying Genetic Variants of the Toxin-Coregulated Pilus Pathogenicity Island. Infect. Immun. *71*, 1020–1025.

Faruque, S.M., Chowdhury, N., Kamruzzaman, M., Dziejman, M., Rahman, M.H., Sack, D.A., Nair, G.B., and Mekalanos, J.J. (2004). Genetic diversity and virulence potential of environmental Vibrio cholerae population in a cholera-endemic area. Proc. Natl. Acad. Sci. *101*, 2123–2128.

Faruque, S.M., Naser, I.B., Islam, M.J., Faruque, A.S.G., Ghosh, A.N., Nair, G.B., Sack, D.A., and Mekalanos, J.J. (2005). Seasonal epidemics of cholera inversely correlate with the prevalence of environmental cholera phages. Proc. Natl. Acad. Sci. U. S. A. *102*, 1702–1707.

Fast, D., Duggal, A., and Foley, E. (2016). Lactobacillus plantarum is a pathobiont for adult Drosophila. BioRxiv 049981.

Fast, D., Kostiuk, B., Foley, E., and Pukatzki, S. (2018). Commensal pathogen competition impacts host viability. Proc. Natl. Acad. Sci. *115*, 7099–7104.

Finkel, T., and Holbrook, N.J. (2000). Oxidants, oxidative stress and the biology of ageing.

Fu, Y., Waldor, M.K., and Mekalanos, J.J. (2013). Tn-Seq analysis of Vibrio cholerae intestinal colonization reveals a role for T6SS-mediated antibacterial activity in the host. Cell Host Microbe *14*, 652–663.

Fu, Y., Ho, B.T., and Mekalanos, J.J. (2018). Tracking Vibrio cholerae Cell-Cell Interactions during Infection Reveals Bacterial Population Dynamics within Intestinal Microenvironments. Cell Host Microbe *23*, 274-281.e2.

Fullner, K.J. (2003). Toxins of Vibrio cholerae: consensus and controversy. In Microbial Pathogenesis and the Intestinal Epithelial Cell, (American Society of Microbiology), pp. 481–502.

Gonzales, M.F., Brooks, T., Pukatzki, S.U., and Provenzano, D. (2013). Rapid Protocol for Preparation of Electrocompetent Escherichia coli and Vibrio cholerae. J. Vis. Exp. JoVE.

Guerrant, R.L., Carneiro-Filho, B.A., and Dillingham, R.A. (2003). Cholera, Diarrhea, and Oral Rehydration Therapy: Triumph and Indictment. Clin. Infect. Dis. *37*, 398–405.

Gunn, J.S. (2000). Mechanisms of bacterial resistance and response to bile. Microbes Infect. *2*, 907–913.

Gupta, S., and Chowdhury, R. (1997). Bile affects production of virulence factors and motility of Vibrio cholerae. Infect. Immun. *65*, 1131–1134.

Hammer, B.K., and Bassler, B.L. (2003). Quorum sensing controls biofilm formation in Vibrio cholerae. Mol. Microbiol. *50*, 101–104.

Hang, S., Purdy, A., Robins, W., Wang, Z., Mandal, M., Chang, S., Mekalanos, J., and Watnick, P. (2014). The acetate switch of an intestinal pathogen disrupts host insulin signaling and lipid metabolism. Cell Host Microbe *16*, 592–604.

Harms, K., and Wackernagel, W. (2008). The RecBCD and SbcCD DNases suppress homology-facilitated illegitimate recombination during natural transformation of Acinetobacter baylyi. Microbiol. Read. Engl. *154*, 2437–2445.

Harris, A.M., Bhuiyan, M.S., Chowdhury, F., Khan, A.I., Hossain, A., Kendall, E.A., Rahman, A., LaRocque, R.C., Wrammert, J., Ryan, E.T., et al. (2009). Antigen-Specific Memory B-Cell Responses to Vibrio cholerae O1 Infection in Bangladesh. Infect. Immun. *77*, 3850–3856.

Harris, J.B., LaRocque, R.C., Qadri, F., Ryan, E.T., and Calderwood, S.B. (2012). Cholera. Lancet Lond. Engl. *379*, 2466–2476.

Haugo, A.J., and Watnick, P.I. (2002). Vibrio cholerae CytR is a repressor of biofilm development. Mol. Microbiol. *45*, 471–483.

Hay, A.J., and Zhu, J. (2015). Host Intestinal Signal-Promoted Biofilm Dispersal Induces Vibrio cholerae Colonization. Infect. Immun. *83*, 317–323.

Heidelberg, J.F., Eisen, J.A., Nelson, W.C., Clayton, R.A., Gwinn, M.L., Dodson, R.J., Haft, D.H., Hickey, E.K., Peterson, J.D., Umayam, L., et al. (2000). DNA sequence of both chromosomes of the cholera pathogen Vibrio cholerae. Nature *406*, 477–483.

Herrington, D.A., Hall, R.H., Losonsky, G., Mekalanos, J.J., Taylor, R.K., and Levine, M.M. (1988). Toxin, toxin-coregulated pili, and the toxR regulon are essential for Vibrio cholerae pathogenesis in humans. | JEM.

Ho, B.T., Basler, M., and Mekalanos, J.J. (2013). Type 6 secretion system–mediated immunity to Type 4 secretion system–mediated gene transfer. Science *342*, 250–253.

Holmgren, J. (1981). Actions of cholera toxin and the prevention and treatment of cholera. Nature *292*, 413–417.

Hsiao, A., Shamsir Ahmed, A.M., Subramanian, S., Griffin, N.W., Drewry, L.L., Petri, W.A., Haque, R., Ahmed, T., and Gordon, J.I. (2014). Members of the human gut microbiota involved in recovery from Vibrio cholerae infection. Nature *515*, 423–426.

Hubbard, T.P., Billings, G., Dörr, T., Sit, B., Warr, A.R., Kuehl, C.J., Kim, M., Delgado, F., Mekalanos, J.J., Lewnard, J.A., et al. (2018). A live vaccine rapidly protects against cholera in an infant rabbit model. Sci. Transl. Med. *10*, eaap8423.

Hung, D.T., and Mekalanos, J.J. (2005). Bile acids induce cholera toxin expression in Vibrio cholerae in a ToxT-independent manner. Proc. Natl. Acad. Sci. U. S. A. *102*, 3028–3033.

Hung, D.T., Zhu, J., Sturtevant, D., and Mekalanos, J.J. (2006). Bile acids stimulate biofilm formation in Vibrio cholerae. Mol. Microbiol. *59*, 193–201.

Huq, A., Small, E.B., West, P.A., Huq, M.I., Rahman, R., and Colwell, R.R. (1983). Ecological relationships between Vibrio cholerae and planktonic crustacean copepods. Appl. Environ. Microbiol. *45*, 275–283.

Huq, A., West, P.A., Small, E.B., Huq, M.I., and Colwell, R.R. (1984). Influence of water temperature, salinity, and pH on survival and growth of toxigenic Vibrio cholerae serovar 01 associated with live copepods in laboratory microcosms. Appl. Environ. Microbiol. *48*, 420–424.

Ilangovan, A., Connery, S., and Waksman, G. (2015). Structural biology of the Gram-negative bacterial conjugation systems. Trends Microbiol. *23*, 301–310.

Ishikawa, T., Rompikuntal, P.K., Lindmark, B., Milton, D.L., and Wai, S.N. (2009). Quorum Sensing Regulation of the Two hcp Alleles in Vibrio cholerae O1 Strains. PLOS ONE *4*, e6734.

Ishikawa, T., Sabharwal, D., Bröms, J., Milton, D.L., Sjöstedt, A., Uhlin, B.E., and Wai, S.N. (2012). Pathoadaptive Conditional Regulation of the Type VI Secretion System in Vibrio cholerae O1 Strains. Infect. Immun. *80*, 575–584.

Jelinek, T., and Kollaritsch, H. (2008). Vaccination with Dukoral® against travelers' diarrhea (ETEC) and cholera. Expert Rev. Vaccines *7*, 561–567.

Jiang, F., Wang, X., Wang, B., Chen, L., Zhao, Z., Waterfield, N.R., Yang, G., and Jin, Q. (2016). The Pseudomonas aeruginosa Type VI Secretion PGAP1-like Effector Induces Host Autophagy by Activating Endoplasmic Reticulum Stress. Cell Rep. *16*, 1502–1509.

JONSON, G., SANCHEZ, J., and SVENNERHOLM, A.-M. (1989). Expression and Detection of Different Biotype-associated Cell-bound Haemagglutinins of Vibrio cholerae O1. Microbiology *135*, 111–120.

Jonson, G., Svennerholm, A.-M., and Holmgren, J. (1990). Expression of virulence factors by classical and El Tor Vibrio cholerae in vivo and in vitro. FEMS Microbiol. Lett. *74*, 221–228.

Joshi, A., Kostiuk, B., Rogers, A., Teschler, J., Pukatzki, S., and Yildiz, F.H. (2017). Rules of Engagement: The Type VI Secretion System in V. cholerae. Trends Microbiol. *25*, 267–279.

Jude, B.A., and Taylor, R.K. (2011). The physical basis of type 4 pilus-mediated microcolony formation by Vibrio cholerae O1. J. Struct. Biol. *175*, 1–9.

Kamareddine, L., Wong, A.C.N., Vanhove, A.S., Hang, S., Purdy, A.E., Kierek-Pearson, K., Asara, J.M., Ali, A., Morris Jr, J.G., and Watnick, P.I. (2018). Activation of Vibrio cholerae quorum sensing promotes survival of an arthropod host. Nat. Microbiol. *3*, 243–252.

Kaper, J.B., Morris, G., and Levine, M.M. (1995). CHOLERA (VOL 8, PG 51, 1995) (AMER SOC MICROBIOLOGY 1325 MASSACHUSETTS AVENUE, NW, WASHINGTON, DC 20005-4171).

Karaolis, D.K.R., Somara, S., Jr, D.R.M., Johnson, J.A., and Kaper, J.B. (1999). A bacteriophage encoding a pathogenicity island, a type-IV pilus and a phage receptor in cholera bacteria. Nature *399*, 375–379.

Kariisa, A.T., Grube, A., and Tamayo, R. (2015). Two nucleotide second messengers regulate the production of the Vibrio cholerae colonization factor GbpA. BMC Microbiol. *15*.

Karunasagar, I., Rivera, I., Joseph, B., Kennedy, B., Shetty, V.R., Huq, A., Karunasagar, I., and Colwell, R.R. (2003). ompU genes in non-toxigenic Vibrio cholerae associated with aquaculture. J. Appl. Microbiol. *95*, 338–343.

Kearse, M., Moir, R., Wilson, A., Stones-Havas, S., Cheung, M., Sturrock, S., Buxton, S., Cooper, A., Markowitz, S., Duran, C., et al. (2012). Geneious Basic: An integrated and extendable desktop software platform for the organization and analysis of sequence data. Bioinformatics *28*, 1647–1649.

Kelley, L.A., Mezulis, S., Yates, C.M., Wass, M.N., and Sternberg, M.J. (2015). The Phyre2 web portal for protein modelling, prediction and analysis. Nat. Protoc. *10*, 845–858.

Khan, M., and Shahidullah, M. (1980). Cholera due to the El Tor biotype equals the classical biotype in severity and attack rates. J. Trop. Med. Hyg. *83*, 35–39.

Kielak, A.M., Cretoiu, M.S., Semenov, A.V., Sørensen, S.J., and Elsas, J.D. van (2013). Bacterial Chitinolytic Communities Respond to Chitin and pH Alteration in Soil. Appl Env. Microbiol *79*, 263–272.

Kim, D., Langmead, B., and Salzberg, S.L. (2016). HISAT2 implementation.

Kirchberger, P.C., Orata, F.D., Barlow, E.J., Kauffman, K.M., Case, R.J., Polz, M.F., and Boucher, Y. (2016). A small number of phylogenetically distinct clonal complexes dominate a coastal Vibrio cholerae population. Appl. Environ. Microbiol. *82*, 5576–5586.

Kirchberger, P.C., Unterweger, D., Provenzano, D., Pukatzki, S., and Boucher, Y. (2017a). Sequential displacement of Type VI Secretion System effector genes leads to evolution of diverse immunity gene arrays in Vibrio cholerae. Sci. Rep. *7*, 45133.

Kirchberger, P.C., Unterweger, D., Provenzano, D., Pukatzki, S., and Boucher, Y. (2017b). Sequential displacement of Type VI Secretion System effector genes leads to evolution of diverse immunity gene arrays in Vibrio cholerae. Sci. Rep. *7*, 45133.

Kirn, T.J., Bose, N., and Taylor, R.K. (2003). Secretion of a soluble colonization factor by the TCP type 4 pilus biogenesis pathway in Vibrio cholerae. Mol. Microbiol. *49*, 81–92.

Kirn, T.J., Jude, B.A., and Taylor, R.K. (2005). A colonization factor links *Vibrio cholerae* environmental survival and human infection. Nature *438*, 863–866.

Kitaoka, M., Miyata, S.T., Unterweger, D., and Pukatzki, S. (2011a). Antibiotic resistance mechanisms of Vibrio cholerae. J. Med. Microbiol. *60*, 397–407.

Kitaoka, M., Miyata, S.T., Brooks, T.M., Unterweger, D., and Pukatzki, S. (2011b). VasH Is a Transcriptional Regulator of the Type VI Secretion System Functional in Endemic and Pandemic Vibrio cholerae. J. Bacteriol. *193*, 6471–6482.

Klose, K.E. (2000). The suckling mouse model of cholera YSTEM. *8*, 3.

Knop, J., and Rowley, D. (1975). Antibacterial mechanisms in the intestine. Elimination of V. cholerae from the intestines of infant mice and the role of antibody. Aust. J. Exp. Biol. Med. Sci. *53*, 147–154.

Koch, R. (1884). An Address on Cholera and its Bacillus. Br. Med. J. *2*, 453–459.

Kostiuk, B., Unterweger, D., Provenzano, D., and Pukatzki, S. (2018). T6SS intraspecific competition orchestrates Vibrio cholerae genotypic diversity. Int. Microbiol. *20*, 130–137.

Kovacikova, G., and Skorupski, K. (2000). Differential Activation of the tcpPH Promoter by AphB Determines Biotype Specificity of Virulence Gene Expression in Vibrio cholerae. J. Bacteriol. *182*, 3228–3238.

Krebs, S.J., and Taylor, R.K. (2011). Protection and Attachment of Vibrio cholerae Mediated by the Toxin-Coregulated Pilus in the Infant Mouse Model. J. Bacteriol. *193*, 5260–5270.

Labrie, S.J., Samson, J.E., and Moineau, S. (2010). Bacteriophage resistance mechanisms. Nat. Rev. Microbiol. *8*, 317–327.

Lancet, T. (2017). Cholera: ending a 50-year pandemic. The Lancet *390*, 1623.

Lehane, M.J. (1997). Peritrophic matrix structure and function. Annu. Rev. Entomol. *42*, 525–550.

Leiman, P.G., Basler, M., Ramagopal, U.A., Bonanno, J.B., Sauder, J.M., Pukatzki, S., Burley, S.K., Almo, S.C., and Mekalanos, J.J. (2009). Type VI secretion apparatus and phage tail-associated protein complexes share a common evolutionary origin. Proc. Natl. Acad. Sci. *106*, 4154–4159.

Lemaitre, B., and Miguel-Aliaga, I. (2013). The digestive tract of Drosophila melanogaster. Annu. Rev. Genet. *47*, 377–404.

Lertpiriyapong, K., Gamazon, E.R., Feng, Y., Park, D.S., Pang, J., Botka, G., Graffam, M.E., Ge, Z., and Fox, J.G. (2012). Campylobacter jejuni Type VI Secretion System: Roles in Adaptation to Deoxycholic Acid, Host Cell Adherence, Invasion, and In Vivo Colonization. PLOS ONE *7*, e42842.

Levine, M.M., Kaper, J.B., Herrington, D., Losonsky, G., Morris, J.G., Clements, M.L., Black, R.E., Tall, B., and Hall, R. (1988). Volunteer studies of deletion mutants of Vibrio cholerae O1 prepared by recombinant techniques. Infect. Immun. *56*, 161–167.

Li, H., and Durbin, R. (2009). Fast and accurate short read alignment with Burrows–Wheeler transform. Bioinformatics *25*, 1754–1760.

Li, H., Handsaker, B., Wysoker, A., Fennell, T., Ruan, J., Homer, N., Marth, G., Abecasis, G., and Durbin, R. (2009). The sequence alignment/map format and SAMtools. Bioinformatics *25*, 2078–2079.

Li-Hawkins, J., Lund, E.G., Turley, S.D., and Russell, D.W. (2000). Disruption of the Oxysterol 7α-Hydroxylase Gene in Mice. J. Biol. Chem. *275*, 16536–16542.

Liu, Z., Miyashiro, T., Tsou, A., Hsiao, A., Goulian, M., and Zhu, J. (2008). Mucosal penetration primes Vibrio cholerae for host colonization by repressing quorum sensing. Proc. Natl. Acad. Sci. *105*, 9769–9774.

Llosa, M., Gomis-Rüth, F.X., Coll, M., and Cruz, F. de la (2002). Bacterial conjugation: a two-step mechanism for DNA transport. Mol. Microbiol. *45*, 1–8.

Logan, S.L., Thomas, J., Yan, J., Baker, R.P., Shields, D.S., Xavier, J.B., Hammer, B.K., and Parthasarathy, R. (2018). The Vibrio cholerae type VI secretion system can modulate host intestinal mechanics to displace gut bacterial symbionts. Proc. Natl. Acad. Sci. 201720133.

Lombardo, M.-J., Michalski, J., Martinez-Wilson, H., Morin, C., Hilton, T., Osorio, C.G., Nataro, J.P., Tacket, C.O., Camilli, A., and Kaper, J.B. (2007). An in vivo expression technology screen for Vibrio cholerae genes expressed in human volunteers. Proc. Natl. Acad. Sci. *104*, 18229–18234.

Long, R.A., Rowley, D.C., Zamora, E., Liu, J., Bartlett, D.H., and Azam, F. (2005). Antagonistic Interactions among Marine Bacteria Impede the Proliferation of Vibrio cholerae. Appl. Environ. Microbiol. *71*, 8531–8536.

Lossi, N.S., Dajani, R., Freemont, P., and Filloux, A. (2011). Structure–function analysis of HsiF, a gp25-like component of the type VI secretion system, in Pseudomonas aeruginosa. Microbiology *157*, 3292–3305.

Ma, A.T., and Mekalanos, J.J. (2010a). In vivo actin cross-linking induced by Vibrio cholerae type VI secretion system is associated with intestinal inflammation. Proc. Natl. Acad. Sci. *107*, 4365–4370.

Ma, A.T., and Mekalanos, J.J. (2010b). In vivo actin cross-linking induced by Vibrio cholerae type VI secretion system is associated with intestinal inflammation. Proc. Natl. Acad. Sci. *107*, 4365–4370.

Ma, L.-S., Lin, J.-S., and Lai, E.-M. (2009). An IcmF family protein, ImpLM, is an integral inner membrane protein interacting with ImpKL, and its walker a motif is required for type VI secretion system-mediated Hcp secretion in Agrobacterium tumefaciens. J. Bacteriol. *191*, 4316–4329.

Ma, L.-S., Hachani, A., Lin, J.-S., Filloux, A., and Lai, E.-M. (2014). Agrobacterium tumefaciens Deploys a Superfamily of Type VI Secretion DNase Effectors as Weapons for Interbacterial Competition In Planta. Cell Host Microbe *16*, 94–104.

MacIntyre, D.L., Miyata, S.T., Kitaoka, M., and Pukatzki, S. (2010). The Vibrio cholerae type VI secretion system displays antimicrobial properties. Proc. Natl. Acad. Sci. *107*, 19520–19524.

Mandal, J., Dinoop, K.P., and Parija, S.C. (2012). Increasing Antimicrobial Resistance of Vibrio cholerae OI Biotype EI Tor Strains Isolated in a Tertiary-care Centre in India. J. Health Popul. Nutr. *30*, 12–16.

Mandlik, A., Livny, J., Robins, W.P., Ritchie, J.M., Mekalanos, J.J., and Waldor, M.K. (2011). RNA-Seq-Based Monitoring of Infection-Linked Changes in Vibrio cholerae Gene Expression. Cell Host Microbe *10*, 165–174.

Marraffini, L.A., and Sontheimer, E.J. (2008). CRISPR Interference Limits Horizontal Gene Transfer in Staphylococci by Targeting DNA. Science *322*, 1843–1845.

Marsh, J.W., and Taylor, R.K. (1998). Identification of the Vibrio cholerae type 4 prepilin peptidase required for cholera toxin secretion and pilus formation. Mol. Microbiol. *29*, 1481–1492.

Marteyn, B., Scorza, F.B., Sansonetti, P.J., and Tang, C. (2010). Breathing life into pathogens: the influence of oxygen on bacterial virulence and host responses in the gastrointestinal tract. Cell. Microbiol. *13*, 171–176.

Mathan, M.M., Chandy, G., and Mathan, V.I. (1995). Ultrastructural changes in the upper small intestinal mucosa in patients with cholera. Gastroenterology *109*, 422–430.

Matson, J.S. (2018). Infant Mouse Model of Vibrio cholerae Infection and Colonization. Methods Mol. Biol. Clifton NJ *1839*, 147–152.

Matthey, N., and Blokesch, M. (2016). The DNA-Uptake Process of Naturally Competent Vibrio cholerae. Trends Microbiol. *24*, 98–110.

Matz, C., McDougald, D., Moreno, A.M., Yung, P.Y., Yildiz, F.H., and Kjelleberg, S. (2005). Biofilm formation and phenotypic variation enhance predation-driven persistence of Vibrio cholerae. Proc. Natl. Acad. Sci. U. S. A. *102*, 16819–16824.

McNally, L., Bernardy, E., Thomas, J., Kalziqi, A., Pentz, J., Brown, S.P., Hammer, B.K., Yunker, P.J., and Ratcliff, W.C. (2017). Killing by Type VI secretion drives genetic phase separation and correlates with increased cooperation. Nat. Commun. *8*, ncomms14371.

Meibom, K.L., Li, X.B., Nielsen, A.T., Wu, C.-Y., Roseman, S., and Schoolnik, G.K. (2004). The Vibrio cholerae chitin utilization program. Proc. Natl. Acad. Sci. U. S. A. *101*, 2524–2529.

Meibom, K.L., Blokesch, M., Dolganov, N.A., Wu, C.-Y., and Schoolnik, G.K. (2005). Chitin induces natural competence in Vibrio cholerae. Science *310*, 1824–1827.

Meier, P., and Wackernagel, W. (2003). Mechanisms of homology-facilitated illegitimate recombination for foreign DNA acquisition in transformable Pseudomonas stutzeri. Mol. Microbiol. *48*, 1107–1118.

Merrell, D.S., and Camilli, A. (1999). The cadA gene of Vibrio cholerae is induced during infection and plays a role in acid tolerance. Mol. Microbiol. *34*, 836–849.

Merrell, D.S., and Camilli, A. (2002). Acid tolerance of gastrointestinal pathogens. Curr. Opin. Microbiol. *5*, 51–55.

Merrell, D.S., Bailey, C., Kaper, J.B., and Camilli, A. (2001). The ToxR-Mediated Organic Acid Tolerance Response of Vibrio cholerae Requires OmpU. J. Bacteriol. *183*, 2746–2754.

Merrell, D.S., Butler, S.M., Qadri, F., Dolganov, N.A., Alam, A., Cohen, M.B., Calderwood, S.B., Schoolnik, G.K., and Camilli, A. (2002a). Host-induced epidemic spread of the cholera bacterium. Nature *417*, 642–645.

Merrell, D.S., Hava, D.L., and Camilli, A. (2002b). Identification of novel factors involved in colonization and acid tolerance of Vibrio cholerae. Mol. Microbiol. *43*, 1471–1491.

Metcalf, W.W., Jiang, W., Daniels, L.L., Kim, S.-K., Haldimann, A., and Wanner, B.L. (1996). Conditionally Replicative and Conjugative Plasmids CarryinglacZα for Cloning, Mutagenesis, and Allele Replacement in Bacteria. Plasmid *35*, 1–13.

Metcalfe, A.C., Krsek, M., Gooday, G.W., Prosser, J.I., and Wellington, E.M.H. (2002). Molecular Analysis of a Bacterial Chitinolytic Community in an Upland Pasture. Appl. Environ. Microbiol. *68*, 5042–5050.

Metzger, L.C., Stutzmann, S., Scrignari, T., Van der Henst, C., Matthey, N., and Blokesch, M. (2016). Independent Regulation of Type VI Secretion in Vibrio cholerae by TfoX and TfoY. Cell Rep. *15*, 951–958.

Mhalu, F.S., Mmari, P.W., and Ijumba, J. (1979). Rapid emergence of El Tor Vibrio cholerae resistant to antimicrobial agents during first six months of fourth cholera epidemic in Tanzania. Lancet Lond. Engl. *1*, 345–347.

Midani, F.S., Weil, A.A., Chowdhury, F., Begum, Y.A., Khan, A.I., Debela, M.D., Durand, H.K., Reese, A.T., Nimmagadda, S.N., Silverman, J.D., et al. (2018). Human Gut Microbiota Predicts Susceptibility to Vibrio cholerae Infection. J. Infect. Dis. *218*, 645–653.

Mintz, E. (2018). Taking aim at cholera. The Lancet *391*, 1868–1870.

Miyata, S.T., Kitaoka, M., Wieteska, L., Frech, C., Chen, N., and Pukatzki, S. (2010a). The Vibrio Cholerae Type VI Secretion System: Evaluating its Role in the Human Disease Cholera. Front. Microbiol. *1*.

Miyata, S.T., Kitaoka, M., Wieteska, L., Frech, C., Chen, N., and Pukatzki, S. (2010b). The Vibrio Cholerae Type VI Secretion System: Evaluating its Role in the Human Disease Cholera. Front. Microbiol. *1*.

Miyata, S.T., Kitaoka, M., Brooks, T.M., McAuley, S.B., and Pukatzki, S. (2011). Vibrio cholerae requires the type VI secretion system virulence factor VasX to kill Dictyostelium discoideum. Infect. Immun. *79*, 2941–2949.

Miyata, S.T., Unterweger, D., Rudko, S.P., and Pukatzki, S. (2013). Dual expression profile of type VI secretion system immunity genes protects pandemic Vibrio cholerae. PLoS Pathog. *9*, e1003752.

Monira, S., Nakamura, S., Gotoh, K., Izutsu, K., Watanabe, H., Alam, N.H., Nakaya, T., Horii, T., Ali, S.I., Iida, T., et al. (2013). Metagenomic profile of gut microbiota in children during cholera and recovery. Gut Pathog. *5*, 1.

Montanaro, L., Poggi, A., Visai, L., Ravaioli, S., Campoccia, D., Speziale, P., and Arciola, C.R. (2011). Extracellular DNA in biofilms. Int. J. Artif. Organs *34*, 824–831.

Moore, S., Thomson, N., Mutreja, A., and Piarroux, R. (2014). Widespread epidemic cholera caused by a restricted subset of Vibrio cholerae clones. Clin. Microbiol. Infect. Off. Publ. Eur. Soc. Clin. Microbiol. Infect. Dis. *20*, 373–379.

Morris, J.J. (1990). Non-O group 1 Vibrio cholerae: a look at the epidemiology of an occasional pathogen. Epidemiol. Rev. *12*, 179–191.

Mougous, J.D., Cuff, M.E., Raunser, S., Shen, A., Zhou, M., Gifford, C.A., Goodman, A.L., Joachimiak, G., Ordoñez, C.L., and Lory, S. (2006). A virulence locus of Pseudomonas aeruginosa encodes a protein secretion apparatus. Science *312*, 1526–1530.

Murley, Y.M., Behari, J., Griffin, R., and Calderwood, S.B. (2000). Classical and El Tor Biotypes of Vibrio cholerae Differ in Timing of Transcription of tcpPHduring Growth in Inducing Conditions. Infect. Immun. *68*, 3010–3014.

Nair, G.B., Faruque, S.M., Bhuiyan, N.A., Kamruzzaman, M., Siddique, A.K., and Sack, D.A. (2002). New variants of Vibrio cholerae O1 biotype El Tor with attributes of the classical biotype from hospitalized patients with acute diarrhea in Bangladesh. J. Clin. Microbiol. *40*, 3296–3299.

Nalin, D.R., Daya, V., Reid, A., Levine, M.M., and Cisneros, L. (1979). Adsorption and growth of Vibrio cholerae on chitin. Infect. Immun. *25*, 768–770.

Narkevich, M.I., Onischenko, G.G., Lomov, J.M., Moskvitina, E.A., Podosinnikova, L.S., and Medinsky, G.M. (1993). The seventh pandemic of cholera in the USSR, 1961-89. Bull. World Health Organ. *71*, 189–196.

Nelson, E.J., Harris, J.B., Morris, J.G., Calderwood, S.B., and Camilli, A. (2009). Cholera transmission: the host, pathogen and bacteriophage dynamic. Nat. Rev. Microbiol. *7*.

Nishiura, H., Tsuzuki, S., and Asai, Y. (2018). Forecasting the size and peak of cholera epidemic in Yemen, 2017. Future Microbiol. *13*, 399–402.

Niyogi, S.G. (1979). Studies on cholera carriers and their role in transmission of the infection: a preliminary report. Indian J. Med. Res. *70*, 892–897.

Olivier, V., Salzman, N.H., and Satchell, K.J.F. (2007). Prolonged Colonization of Mice by Vibrio cholerae El Tor O1 Depends on Accessory Toxins. Infect. Immun. *75*, 5043–5051.

Oseasohn, R.S., Ahmad, S., Islam, M.A., and Rahman, A. (1966). Clinical and bacteriological findings among families of cholera patients. Lancet 340–42.

Pacini, F. (1854). Osservazioni microscopiche e deduzioni patologiche sul cholera asiatico (Federigo Bencini).

Perez-Vilar, J., and Hill, R.L. (1999). The Structure and Assembly of Secreted Mucins. J. Biol. Chem. *274*, 31751–31754.

Petkau, K., Fast, D., Duggal, A., and Foley, E. (2016a). Comparative evaluation of the genomes of three common Drosophila-associated bacteria. Biol. Open *5*, 1305–1316.

Petkau, K., Fast, D., Duggal, A., and Foley, E. (2016b). Comparative evaluation of the genomes of three common Drosophila-associated bacteria. Biol. Open bio.017673.

Provenzano, D., and Klose, K.E. (2000). Altered expression of the ToxR-regulated porins OmpU and OmpT diminishes Vibrio cholerae bile resistance, virulence factor expression, and intestinal colonization. Proc. Natl. Acad. Sci. *97*, 10220–10224.

Pukatzki, S., and Provenzano, D. (2013). Vibrio cholerae as a predator: lessons from evolutionary principles. Front. Microbiol. *4*.

Pukatzki, S., Ma, A.T., Sturtevant, D., Krastins, B., Sarracino, D., Nelson, W.C., Heidelberg, J.F., and Mekalanos, J.J. (2006a). Identification of a conserved bacterial protein secretion system in Vibrio cholerae using the Dictyostelium host model system. Proc. Natl. Acad. Sci. *103*, 1528–1533.

Pukatzki, S., Ma, A.T., Sturtevant, D., Krastins, B., Sarracino, D., Nelson, W.C., Heidelberg, J.F., and Mekalanos, J.J. (2006b). Identification of a conserved bacterial protein secretion system in Vibrio cholerae using the Dictyostelium host model system. Proc. Natl. Acad. Sci. *103*, 1528–1533.

Pukatzki, S., Ma, A.T., Revel, A.T., Sturtevant, D., and Mekalanos, J.J. (2007). Type VI secretion system translocates a phage tail spike-like protein into target cells where it cross-links actin. Proc. Natl. Acad. Sci. *104*, 15508–15513.

Purdy, A.E., and Watnick, P.I. (2011). Spatially selective colonization of the arthropod intestine through activation of Vibrio cholerae biofilm formation. Proc. Natl. Acad. Sci. *108*, 19737–19742.

Queen, J., and Satchell, K.J.F. (2012). Neutrophils are essential for containment of Vibrio cholerae to the intestine during the pro-inflammatory phase of infection. Infect. Immun. IAI.00356-12.

Quinlan, A.R., and Hall, I.M. (2010). BEDTools: a flexible suite of utilities for comparing genomic features. Bioinformatics *26*, 841–842.

Ray, A., Schwartz, N., de Souza Santos, M., Zhang, J., Orth, K., and Salomon, D. (2017). Type VI secretion system MIX-effectors carry both antibacterial and anti-eukaryotic activities. EMBO Rep. *18*, 1978–1990.

Redfield, R.J. (2001). Do bacteria have sex? Nat. Rev. Genet. *2*, 634–639.

Richardson, S.H. (1994). Animal Models in Cholera Research. Vibrio Cholerae Cholera 203–226.

Richardson, K., Michalski, J., and Kaper, J.B. (1986). Hemolysin production and cloning of two hemolysin determinants from classical Vibrio cholerae. Infect. Immun. *54*, 415–420.

Ringel, P.D., Hu, D., and Basler, M. (2017). The Role of Type VI Secretion System Effectors in Target Cell Lysis and Subsequent Horizontal Gene Transfer. Cell Rep. *21*, 3927–3940.

Ritchie, J.M., Rui, H., Bronson, R.T., and Waldor, M.K. (2010). Back to the Future: Studying Cholera Pathogenesis Using Infant Rabbits. MBio *1*, e00047-10.

Runft, D.L., Mitchell, K.C., Abuaita, B.H., Allen, J.P., Bajer, S., Ginsburg, K., Neely, M.N., and Withey, J.H. (2014). Zebrafish as a Natural Host Model for Vibrio cholerae Colonization and Transmission. Appl. Environ. Microbiol. *80*, 1710–1717.

Russell, A.B., LeRoux, M., Hathazi, K., Agnello, D.M., Ishikawa, T., Wiggins, P.A., Wai, S.N., and Mougous, J.D. (2013a). Diverse type VI secretion phospholipases are functionally plastic antibacterial effectors. Nature *496*, 508–512.

Russell, A.B., LeRoux, M., Hathazi, K., Agnello, D.M., Ishikawa, T., Wiggins, P.A., Wai, S.N., and Mougous, J.D. (2013b). Diverse type VI secretion phospholipases are functionally plastic antibacterial effectors. Nature *496*, 508–512.

Ryan, E.T., Crean, T.I., Kochi, S.K., John, M., Luciano, A.A., Killeen, K.P., Klose, K.E., and Calderwood, S.B. (2000a). Development of a ΔglnA Balanced Lethal Plasmid System for Expression of Heterologous Antigens by Attenuated Vaccine Vector Strains of Vibrio cholerae. Infect. Immun. *68*, 221–226.

Ryan, E.T., Crean, T.I., Kochi, S.K., John, M., Luciano, A.A., Killeen, K.P., Klose, K.E., and Calderwood, S.B. (2000b). Development of a DeltaglnA balanced lethal plasmid system for expression of heterologous antigens by attenuated vaccine vector strains of Vibrio cholerae. Infect. Immun. *68*, 221–226.

Saak, C.C., and Gibbs, K.A. (2016). The Self-Identity Protein IdsD Is Communicated between Cells in Swarming Proteus mirabilis Colonies. J. Bacteriol. *198*, 3278–3286.

Sack, R.B., Siddique, A.K., Longini, I.M., Nizam, A., Yunus, M., Islam, M.S., Morris, J.G., Ali, A., Huq, A., Nair, G.B., et al. (2003). A 4-year study of the epidemiology of Vibrio cholerae in four rural areas of Bangladesh. J. Infect. Dis. *187*, 96–101.

Salyers, A.A., Gupta, A., and Wang, Y. (2004). Human intestinal bacteria as reservoirs for antibiotic resistance genes. Trends Microbiol. *12*, 412–416.

Sana, T.G., Berni, B., and Bleves, S. (2016a). The T6SSs of Pseudomonas aeruginosa Strain PAO1 and Their Effectors: Beyond Bacterial-Cell Targeting. Front. Cell. Infect. Microbiol. *6*.

Sana, T.G., Flaugnatti, N., Lugo, K.A., Lam, L.H., Jacobson, A., Baylot, V., Durand, E., Journet, L., Cascales, E., and Monack, D.M. (2016b). Salmonella Typhimurium utilizes a T6SS-mediated antibacterial weapon to establish in the host gut. Proc. Natl. Acad. Sci. *113*, E5044–E5051.

Schwarz, S., Singh, P., Robertson, J.D., LeRoux, M., Skerrett, S.J., Goodlett, D.R., West, T.E., and Mougous, J.D. (2014). VgrG-5 is a Burkholderia type VI secretion system-exported protein required for multinucleated giant cell formation and virulence. Infect. Immun. *82*, 1445–1452.

Schwinghamer, E.A. (1980). A Method for Improved Lysis of Some Gram-Negative Bacteria. FEMS Microbiol. Lett. *7*, 157–162.

Scrudato, M.L., and Blokesch, M. (2012). The Regulatory Network of Natural Competence and Transformation of Vibrio cholerae. PLOS Genet. *8*, e1002778.

Seed, K.D., Yen, M., Shapiro, B.J., Hilaire, I.J., Charles, R.C., Teng, J.E., Ivers, L.C., Boncy, J., Harris, J.B., and Camilli, A. (2014). Evolutionary consequences of intra-patient phage predation on microbial populations. Elife *3*, e03497.

Seitz, P., Modarres, H.P., Borgeaud, S., Bulushev, R.D., Steinbock, L.J., Radenovic, A., Peraro, M.D., and Blokesch, M. (2014). ComEA Is Essential for the Transfer of External DNA into the Periplasm in Naturally Transformable Vibrio cholerae Cells. PLOS Genet. *10*, e1004066.

Shao, Y., and Bassler, B.L. (2014). Quorum regulatory small RNAs repress type VI secretion in Vibrio cholerae. Mol. Microbiol. *92*, 921–930.

Sharifi-Mood, B., and Metanat, M. (2014). Diagnosis, Clinical Management, Prevention, and Control of Cholera; A Review Study. Int. J. Infect. *1*.

Shaw, C.E., and Taylor, R.K. (1990). Vibrio cholerae O395 tcpA pilin gene sequence and comparison of predicted protein structural features to those of type 4 pilins. Infect. Immun. *58*, 3042–3049.

Sheng, Y., Fan, F., Jensen, O., Zhong, Z., Kan, B., Wang, H., and Zhu, J. (2015). Dual zinc transporter systems in Vibrio cholerae promote competitive advantages over gut microbiome. Infect. Immun. IAI.00447-15.

Shi, X., Chamankhah, M., Visal-Shah, S., Hemmingsen, S.M., Erlandson, M., Braun, L., Alting-Mees, M., Khachatourians, G.G., O'Grady, M., and Hegedus, D.D. (2004). Modeling the structure of the Type I peritrophic matrix: characterization of a Mamestra configurata intestinal mucin and a novel peritrophin containing 19 chitin binding domains. Insect Biochem. Mol. Biol. *34*, 1101–1115.

Shneider, M.M., Buth, S.A., Ho, B.T., Basler, M., Mekalanos, J.J., and Leiman, P.G. (2013). PAAR-repeat proteins sharpen and diversify the type VI secretion system spike. Nature *500*, 350–353.

Silva, A.J., and Benitez, J.A. (2016). Vibrio cholerae Biofilms and Cholera Pathogenesis. PLoS Negl. Trop. Dis. *10*, e0004330.

Silva, A.J., Pham, K., and Benitez, J.A. (2003). Haemagglutinin/protease expression and mucin gel penetration in El Tor biotype Vibrio cholerae. Microbiology *149*, 1883–1891.

Snow, J. (1857). Cholera, and the Water Supply in the South Districts of London. Br. Med. J. *1*, 864–865.

Son, M.S., Megli, C.J., Kovacikova, G., Qadri, F., and Taylor, R.K. (2011). Characterization of Vibrio cholerae O1 El Tor Biotype Variant Clinical Isolates from Bangladesh and Haiti, Including a Molecular Genetic Analysis of Virulence Genes ▿ . J. Clin. Microbiol. *49*, 3739–3749.

Stecher, B., Denzler, R., Maier, L., Bernet, F., Sanders, M.J., Pickard, D.J., Barthel, M., Westendorf, A.M., Krogfelt, K.A., Walker, A.W., et al. (2012). Gut inflammation can boost horizontal gene transfer between pathogenic and commensal Enterobacteriaceae. Proc. Natl. Acad. Sci. *109*, 1269–1274.

Stokes, B.A., Yadav, S., Shokal, U., Smith, L.C., and Eleftherianos, I. (2015). Bacterial and fungal pattern recognition receptors in homologous innate signaling pathways of insects and mammals. Front. Microbiol. *6*, 19.

Strating, H., and Clarke, A.J. (2001). Differentiation of bacterial autolysins by zymogram analysis. Anal. Biochem. *291*, 149–154.

Stutzmann, S., and Blokesch, M. (2016). Circulation of a Quorum-Sensing-Impaired Variant of Vibrio cholerae Strain C6706 Masks Important Phenotypes. MSphere *1*, e00098-16.

Suarez, G., Sierra, J.C., Erova, T.E., Sha, J., Horneman, A.J., and Chopra, A.K. (2010). A Type VI Secretion System Effector Protein, VgrG1, from Aeromonas hydrophila That Induces Host Cell Toxicity by ADP Ribosylation of Actin. J. Bacteriol. *192*, 155–168.

Sullivan, C., and Kim, C.H. (2008). Zebrafish as a model for infectious disease and immune function. Fish Shellfish Immunol. *25*, 341–350.

Takeya, K., Otohuji, T., and Tokiwa, H. (1981). FK phage for differentiating the classical and El T or groups of Vibrio cholerae. J. Clin. Microbiol. *14*, 222–224.

Tamamoto, T., Nakashima, K., Nakasone, N., Honma, Y., Higa, N., and Yamashiro, T. (1998). Adhesive property of toxin-coregulated pilus of Vibrio cholerae O1. Microbiol. Immunol. *42*, 41–45.

Tanaka, M., and Nakayama, J. (2017). Development of the gut microbiota in infancy and its impact on health in later life. Allergol. Int. *66*, 515–522.

Taylor, R.K., Miller, V.L., Furlong, D.B., and Mekalanos, J.J. (1987). Use of phoA gene fusions to identify a pilus colonization factor coordinately regulated with cholera toxin. Proc. Natl. Acad. Sci. *84*, 2833–2837.

Thomas, C.M., and Nielsen, K.M. (2005). Mechanisms of and Barriers to, Horizontal Gene Transfer between Bacteria. Nat. Rev. Microbiol. *3*, 711–721.

Thomas, J., Watve, S.S., Ratcliff, W.C., and Hammer, B.K. (2017). Horizontal Gene Transfer of Functional Type VI Killing Genes by Natural Transformation. MBio *8*, e00654-17.

Thurtle-Schmidt, D.M., and Lo, T.-W. (2018). Molecular biology at the cutting edge: A review on CRISPR/CAS9 gene editing for undergraduates. Biochem. Mol. Biol. Educ. Bimon. Publ. Int. Union Biochem. Mol. Biol. *46*, 195–205.

Toska, J., Ho, B.T., and Mekalanos, J.J. (2018). Exopolysaccharide protects Vibrio cholerae from exogenous attacks by the type 6 secretion system. Proc. Natl. Acad. Sci. 201808469.

Trunk, K., Peltier, J., Liu, Y.-C., Dill, B.D., Walker, L., Gow, N.A.R., Stark, M.J.R., Quinn, J., Strahl, H., Trost, M., et al. (2018). The type VI secretion system deploys antifungal effectors against microbial competitors. Nat. Microbiol. *3*, 920–931.

Turner, J.R. (2009). Intestinal mucosal barrier function in health and disease. Nat. Rev. Immunol. *9*, 799–809.

Úbeda, C., Maiques, E., Knecht, E., Lasa, Í., Novick, R.P., and Penadés, J.R. (2005). Antibiotic-induced SOS response promotes horizontal dissemination of pathogenicity island-encoded virulence factors in staphylococci. Mol. Microbiol. *56*, 836–844.

Unterweger, D., Kitaoka, M., Miyata, S.T., Bachmann, V., Brooks, T.M., Moloney, J., Sosa, O., Silva, D., Duran-Gonzalez, J., Provenzano, D., et al. (2012). Constitutive Type VI Secretion System Expression Gives Vibrio cholerae Intra- and Interspecific Competitive Advantages. PLOS ONE *7*, e48320.

Unterweger, D., Miyata, S.T., Bachmann, V., Brooks, T.M., Mullins, T., Kostiuk, B., Provenzano, D., and Pukatzki, S. (2014a). The Vibrio cholerae type VI secretion system employs diverse effector modules for intraspecific competition. Nat. Commun. *5*.

Unterweger, D., Miyata, S.T., Bachmann, V., Brooks, T.M., Mullins, T., Kostiuk, B., Provenzano, D., and Pukatzki, S. (2014b). The Vibrio cholerae type VI secretion system employs diverse effector modules for intraspecific competition. Nat. Commun. *5*.

Unterweger, D., Kostiuk, B., Ötjengerdes, R., Wilton, A., Diaz-Satizabal, L., and Pukatzki, S. (2015). Chimeric adaptor proteins translocate diverse type VI secretion system effectors in Vibrio cholerae. EMBO J. e201591163.

Unterweger, D., Kostiuk, B., and Pukatzki, S. (2017). Adaptor proteins of type VI secretion system effectors. Trends Microbiol. *25*, 8–10.

Unterweger, D., Kostiuk, B., and Pukatzki, S. (2018). A mutated type VI secretion system places classical biotype Vibrio cholerae at a competitive disadvantage.

Utada, A.S., Bennett, R.R., Fong, J.C.N., Gibiansky, M.L., Yildiz, F.H., Golestanian, R., and Wong, G.C.L. (2014). Vibrio cholerae use pili and flagella synergistically to effect motility switching and conditional surface attachment. Nat. Commun. *5*.

Vaitkevicius, K., Lindmark, B., Ou, G., Song, T., Toma, C., Iwanaga, M., Zhu, J., Andersson, A., Hammarström, M.-L., Tuck, S., et al. (2006). A Vibrio cholerae protease needed for killing of Caenorhabditis elegans has a role in protection from natural predator grazing. Proc. Natl. Acad. Sci. *103*, 9280–9285.

Valeru, S.P., Wai, S.N., Saeed, A., Sandström, G., and Abd, H. (2012). ToxR of Vibrio cholerae affects biofilm, rugosity and survival with Acanthamoeba castellanii. BMC Res. Notes *5*, 33.

Van der Henst, C., Scrignari, T., Maclachlan, C., and Blokesch, M. (2016). An intracellular replication niche for Vibrio cholerae in the amoeba Acanthamoeba castellanii. ISME J. *10*, 897–910.

Veening, J.-W., and Blokesch, M. (2017). Interbacterial predation as a strategy for DNA acquisition in naturally competent bacteria. Nat. Rev. Microbiol. *15*, 621–629.

Vettiger, A., Winter, J., Lin, L., and Basler, M. (2017a). The type VI secretion system sheath assembles at the end distal from the membrane anchor. Nat. Commun. *8*.

Vettiger, A., Winter, J., Lin, L., and Basler, M. (2017b). The type VI secretion system sheath assembles at the end distal from the membrane anchor. Nat. Commun. *8*, 16088.

Vodovar, N., Vinals, M., Liehl, P., Basset, A., Degrouard, J., Spellman, P., Boccard, F., and Lemaitre, B. (2005). Drosophila host defense after oral infection by an entomopathogenic Pseudomonas species. Proc. Natl. Acad. Sci. U. S. A. *102*, 11414–11419.

de Vries, J., and Wackernagel, W. (2002). Integration of foreign DNA during natural transformation of Acinetobacter sp. by homology-facilitated illegitimate recombination. Proc. Natl. Acad. Sci. *99*, 2094–2099.

Waldor, M.K., and Mekalanos, J.J. (1996). Lysogenic Conversion by a Filamentous Phage Encoding Cholera Toxin. Science *272*, 1910–1914.

Walker, B.J., Abeel, T., Shea, T., Priest, M., Abouelliel, A., Sakthikumar, S., Cuomo, C.A., Zeng, Q., Wortman, J., Young, S.K., et al. (2014). Pilon: An Integrated Tool for Comprehensive Microbial Variant Detection and Genome Assembly Improvement. PLoS ONE *9*.

Wan, B., Zhang, Q., Ni, J., Li, S., Wen, D., Li, J., Xiao, H., He, P., Ou, H., Tao, J., et al. (2017). Type VI secretion system contributes to Enterohemorrhagic Escherichia coli virulence by secreting catalase against host reactive oxygen species (ROS). PLOS Pathog. *13*, e1006246.

Wang, X., Wang, Q., Xiao, J., Liu, Q., Wu, H., Xu, L., and Zhang, Y. (2009). Edwardsiella tarda T6SS component evpP is regulated by esrB and iron, and plays essential roles in the invasion of fish. Fish Shellfish Immunol. *27*, 469–477.

Wang, Z., Berkey, C.D., and Watnick, P.I. (2012). The Drosophila protein mustard tailors the innate immune response activated by the immune deficiency pathway. J. Immunol. 1103301.

Watve, S.S., Thomas, J., and Hammer, B.K. (2015). CytR Is a Global Positive Regulator of Competence, Type VI Secretion, and Chitinases in Vibrio cholerae. PLOS ONE *10*, e0138834.

Weber, B.S., Ly, P.M., Irwin, J.N., Pukatzki, S., and Feldman, M.F. (2015). A multidrug resistance plasmid contains the molecular switch for type VI secretion in Acinetobacter baumannii. Proc. Natl. Acad. Sci. *112*, 9442–9447.

Weingarden, A.R., Chen, C., Bobr, A., Yao, D., Lu, Y., Nelson, V.M., Sadowsky, M.J., and Khoruts, A. (2014). Microbiota transplantation restores normal fecal bile acid composition in recurrent Clostridium difficile infection. Am. J. Physiol. Gastrointest. Liver Physiol. *306*, G310-319.

Willing, B.P., Vacharaksa, A., Croxen, M., Thanachayanont, T., and Finlay, B.B. (2011). Altering Host Resistance to Infections through Microbial Transplantation. PLOS ONE *6*, e26988.

Wong, M.J.Q., Liang, X., Smart, M., Tang, L., Moore, R., Ingalls, B., and Dong, T.G. (2016). Microbial Herd Protection Mediated by Antagonistic Interaction in Polymicrobial Communities. Appl. Environ. Microbiol. *82*, 6881–6888.

Woodward, W.E., and Mosley, W.H. (1972). The spectrum of cholera in rural Bangladesh II. Comparison of el tor ogawa and classical inaba infection. Am. J. Epidemiol. *96*, 342–351.

World Health Organization = Organisation mondiale de la Santé (2017). Cholera vaccines: WHO position paper – August 2017 – Vaccins anticholériques: Note de synthèse de l'OMS – août 2017. Wkly. Epidemiol. Rec. Relevé Épidémiologique Hebd. *92*, 477–498.

Yang, X., Xu, M., Wang, Y., Xia, P., Wang, S., Ye, B., Tong, L., Jiang, T., and Fan, Z. (2014). Molecular mechanism for self-protection against the type VI secretion system in Vibrio cholerae. Acta Crystallogr. D Biol. Crystallogr. *70*, 1094–1103.

Yen, M., Cairns, L.S., and Camilli, A. (2017). A cocktail of three virulent bacteriophages prevents *Vibrio cholerae* infection in animal models. Nat. Commun. *8*, 14187.

Yoon, S.S., and Mekalanos, J.J. (2006). 2,3-Butanediol Synthesis and the Emergence of the Vibrio cholerae El Tor Biotype. Infect. Immun. *74*, 6547–6556.

Yoon, M.Y., Min, K.B., Lee, K.-M., Yoon, Y., Kim, Y., Oh, Y.T., Lee, K., Chun, J., Kim, B.-Y., Yoon, S.-H., et al. (2016). A single gene of a commensal microbe affects host susceptibility to enteric infection. Nat. Commun. *7*, 11606.

Zarocostas, J. (2017). Cholera outbreak in Haiti—from 2010 to today. The Lancet *389*, 2274–2275.

Zhang, J., Zhang, H., Gao, Z., Hu, H., Dong, C., and Dong, Y.-H. (2014). Structural basis for recognition of the type VI spike protein VgrG3 by a cognate immunity protein. FEBS Lett. *588*, 1891–1898.

Zhao, W., Caro, F., Robins, W., and Mekalanos, J.J. (2018). Antagonism toward the intestinal microbiota and its effect on Vibrio cholerae virulence. Science *359*, 210–213.

Zheng, J., Shin, O.S., Cameron, D.E., and Mekalanos, J.J. (2010). Quorum sensing and a global regulator TsrA control expression of type VI secretion and virulence in Vibrio cholerae. Proc. Natl. Acad. Sci. U. S. A. *107*, 21128–21133.

Zheng, J., Ho, B., and Mekalanos, J.J. (2011). Genetic analysis of anti-amoebae and anti-bacterial activities of the type VI secretion system in Vibrio cholerae. PloS One *6*, e23876.

Zoued, A., Durand, E., Bebeacua, C., Brunet, Y.R., Douzi, B., Cambillau, C., Cascales, E., and Journet, L. (2013). TssK Is a Trimeric Cytoplasmic Protein Interacting with Components of Both Phage-like and Membrane Anchoring Complexes of the Type VI Secretion System. J. Biol. Chem. *288*, 27031–27041.

(1992). Cholera (New York: Plenum Medical Book Co).

Activation of Vibrio cholerae quorum sensing promotes survival of an arthropod host | Nature Microbiology.

Appendix A
RNASeq Data From *Drosophila* stem cells

FBgn	Fly Name	logFC	PValue	FDR
FBgn0051216	Naam	-2.114227	2.86E-09	2.91E-05
FBgn0031248	CG11912	5.86178275	6.25E-09	3.18E-05
FBgn0031080	CG12655	2.61322671	1.31E-08	3.37E-05
FBgn0004839	otk	-1.1463542	1.33E-08	3.37E-05
FBgn0019928	Ser8	4.47072842	3.42E-08	6.95E-05
FBgn0028534	CG7916	3.35700501	1.01E-07	0.00017032
FBgn0028533	CG7953	3.33951141	1.25E-07	0.00017868
FBgn0027601	pdgy	1.05716539	1.41E-07	0.00017868
FBgn0085481	CG34452	2.97022205	2.17E-07	0.00024562
FBgn0028920	CG8997	3.02146901	6.39E-07	0.00064966
FBgn0005664	Crys	3.17009866	7.04E-07	0.00065098
FBgn0038353	CG5399	1.48036035	9.75E-07	0.00082565
FBgn0030098	CG12057	3.66137824	1.30E-06	0.00101435
FBgn0011692	pav	-1.4356316	2.28E-06	0.00165436
FBgn0034317	CG14499	2.80052415	2.97E-06	0.00199389
FBgn0086356	tum	-1.5603933	3.14E-06	0.00199389
FBgn0264815	Pde1c	1.60813304	4.25E-06	0.00254374
FBgn0032105	borr	-1.8771589	5.57E-06	0.00314842
FBgn0038256	CG7530	-1.2767257	6.18E-06	0.00330563
FBgn0038866	CG5810	2.90241916	9.07E-06	0.00439948
FBgn0263324	CR43405	-1.597654	9.09E-06	0.00439948
FBgn0003124	polo	-1.0023429	9.96E-06	0.00460461
FBgn0031653	Jon25Biii	2.41993316	1.05E-05	0.00464556
FBgn0032297	CG17124	-1.1261932	1.10E-05	0.00464556
FBgn0040342	CG3706	2.52148434	1.24E-05	0.00502952
FBgn0263143	vret	-1.3739326	1.45E-05	0.00565105
FBgn0038842	hdly	1.13446751	1.52E-05	0.0057414
FBgn0000463	Dl	-1.5413387	1.59E-05	0.00577719
FBgn0002887	mus201	1.23033373	1.90E-05	0.00665715
FBgn0031515	CG9664	1.32509659	2.01E-05	0.00679829
FBgn0267237	CR45677	2.66361664	2.11E-05	0.00691043
FBgn0033459	CG12744	-1.3719056	2.46E-05	0.0078024
FBgn0030628	CG9114	-0.8965514	2.53E-05	0.00780549
FBgn0020906	Jon25Bi	4.29468969	2.79E-05	0.00814622
FBgn0267425	CR45778	-1.0039441	2.84E-05	0.00814622
FBgn0250837	dUTPase	-1.0030653	2.88E-05	0.00814622
FBgn0023395	Chd3	-1.2321912	3.27E-05	0.0089572
FBgn0031649	hoe2	2.2351254	3.35E-05	0.0089572
FBgn0043470	lambdaTry	1.9830286	3.66E-05	0.00954453

FBgn0260991	Incenp	-0.8567375	3.85E-05	0.00979194
FBgn0263855	BubR1	-1.0765284	4.65E-05	0.01125525
FBgn0052656	Muc11A	-3.5488414	4.65E-05	0.01125525
FBgn0265831	CR44620	3.41562711	5.43E-05	0.01284165
FBgn0029924	CG4586	1.66326214	5.99E-05	0.01383524
FBgn0263133	mEFG1	-1.1143767	6.30E-05	0.01424346
FBgn0030189	CG2909	1.38439125	6.67E-05	0.01473648
FBgn0031324	CG14342	1.94744292	7.31E-05	0.01582193
FBgn0024222	IKKbeta	-1.0399075	7.66E-05	0.01602308
FBgn0003068	per	-0.9632418	7.77E-05	0.01602308
FBgn0264904	CR44095	0.91386951	7.88E-05	0.01602308
FBgn0030576	CG15890	-3.0297431	8.07E-05	0.01608936
FBgn0038851	dmrt93B	-2.5052893	9.18E-05	0.01739139
FBgn0082928	snoRNA:Me28S-G3255a	-2.0843165	9.23E-05	0.01739139
FBgn0263492	CR43481	1.12184368	9.24E-05	0.01739139
FBgn0004569	aos	-1.2925601	0.00010044	0.01841593
FBgn0004629	Cys	0.89539295	0.00010302	0.01841593
FBgn0262148	CR42874	1.77944975	0.00010326	0.01841593
FBgn0028863	CG4587	2.07252359	0.00010543	0.01847902
FBgn0003984	vn	1.26332795	0.00011074	0.01908046
FBgn0263980	CG43729	1.42209627	0.00012123	0.02054106
FBgn0034312	CG10916	1.33396474	0.00012531	0.02062963
FBgn0266324	CR44989	-1.1163469	0.00012582	0.02062963
FBgn0023495	Lip3	2.23632838	0.00012988	0.02095749
FBgn0028331	l(1)G0289	0.82212659	0.00013267	0.02107414
FBgn0032682	grnd	1.61007122	0.00013615	0.02129309
FBgn0036024	CG18180	3.79760937	0.00015596	0.02347677
FBgn0267990	CR46257	0.85736457	0.00016088	0.02347677
FBgn0040609	CG3348	2.70315802	0.00016243	0.02347677
FBgn0025739	pon	-1.5167775	0.00016247	0.02347677
FBgn0003525	stg	-1.6114946	0.00016333	0.02347677
FBgn0016930	Dyrk2	-1.1105036	0.00016396	0.02347677
FBgn0000180	bib	-1.033807	0.00018244	0.02576009
FBgn0039137	CG13604	1.06884611	0.00019246	0.02650849
FBgn0035091	CG3829	1.74549176	0.00019296	0.02650849
FBgn0033490	CG12917	-2.0536701	0.00019773	0.02680166
FBgn0035157	CG13894	1.20809314	0.00020319	0.02711827
FBgn0039821	CG15556	-1.2644792	0.0002054	0.02711827
FBgn0045474	Gr77a	-1.5058933	0.00020947	0.02730114

FBgn0086672	snoRNA:Or-aca5	-1.2093524	0.00022304	0.02813258
FBgn0023094	cyc	-0.7136948	0.0002243	0.02813258
FBgn0266431	CG45061	1.29325813	0.00022469	0.02813258
FBgn0037882	CG17187	1.11924797	0.00022845	0.02813258
FBgn0265301	CR44274	1.6157468	0.00022969	0.02813258
FBgn0003041	pbl	1.23171407	0.00024047	0.02910213
FBgn0264507	CR43906	-1.3721218	0.00025125	0.02986938
FBgn0034671	CG13494	-1.4662443	0.00025268	0.02986938
FBgn0010435	emp	0.84399265	0.00025656	0.02997949
FBgn0033740	dgt5	-0.8578861	0.00025964	0.02999478
FBgn0035815	Snmp2	2.60027616	0.00026812	0.03062608
FBgn0035756	unc-13-4A	1.03965481	0.00028205	0.03173995
FBgn0031053	CG14223	-1.5995241	0.00028412	0.03173995
FBgn0010105	comm	-1.4719138	0.0002952	0.03243023
FBgn0029907	Atx-1	-1.6009641	0.00029668	0.03243023
FBgn0029818	GAA1	-0.7159061	0.00030141	0.03259684
FBgn0052368	CG32368	1.51690496	0.00031835	0.03406459
FBgn0010768	sqz	-0.9552955	0.00032168	0.03406459
FBgn0030261	CG15203	1.33818922	0.00033029	0.03410869
FBgn0039003	wfs1	1.09395221	0.00033213	0.03410869
FBgn0031745	rau	-1.138332	0.00033332	0.03410869
FBgn0038475	Keap1	1.16917083	0.00034031	0.03410869
FBgn0031939	CG13796	2.10533011	0.00034254	0.03410869
FBgn0264984	CR44135	1.24478616	0.00034367	0.03410869
FBgn0030246	CG1582	0.82985817	0.0003469	0.03410869
FBgn0034709	Swim	0.77583768	0.00034894	0.03410869
FBgn0032961	CG1416	-0.6844958	0.00035773	0.03447734
FBgn0266365	CR45013	2.03673194	0.00035949	0.03447734
FBgn0082943	snoRNA:Me28S-A982a	-2.0467242	0.0003667	0.03484028
FBgn0028978	trbl	1.04616225	0.00037739	0.03552354
FBgn0039350	jigr1	-0.8398619	0.00039129	0.03649443
FBgn0002873	mud	-1.7989105	0.00039775	0.03675925
FBgn0015721	ktub	-1.2223514	0.00040835	0.03739929
FBgn0030482	CG1673	1.89928474	0.00043863	0.03937905
FBgn0031528	CG15412	-2.412752	0.00044024	0.03937905
FBgn0015001	iotaTry	1.29088086	0.00044159	0.03937905
FBgn0037288	CG14661	1.73252978	0.000449	0.03969169
FBgn0010038	GstD2	2.63317606	0.00045443	0.03982532
FBgn0035763	CG8602	0.72340425	0.00047857	0.04144311
FBgn0262699	fzr	-0.7346408	0.0004833	0.04144311

FBgn0261385	scra	-0.8731591	0.00048512	0.04144311
FBgn0063496	GstE4	2.28077857	0.00050501	0.04278297
FBgn0037973	CG18547	1.12023221	0.00051347	0.04313997
FBgn0044324	Chro	-0.8174331	0.00052274	0.0435584
FBgn0039315	CG13658	1.91972994	0.00053772	0.04407293
FBgn0266894	CR45354	2.46030181	0.00054617	0.04407293
FBgn0001227	Hsp67Ba	1.23693037	0.00055447	0.04407293
FBgn0038742	Arc42	-0.8449957	0.0005583	0.04407293
FBgn0031114	cactin	1.10200697	0.00056068	0.04407293
FBgn0039250	Mink	-1.6552817	0.00056077	0.04407293
FBgn0040256	Ugt86Dd	1.64472356	0.00056181	0.04407293
FBgn0036896	wnd	1.30528869	0.00056359	0.04407293
FBgn0259236	comm3	2.35893666	0.00057241	0.04442046
FBgn0261850	Xpd	-0.7676635	0.00061131	0.04685473
FBgn0030710	CG8924	-1.2827347	0.00061299	0.04685473
FBgn0030749	AnxB11	0.76374776	0.00062304	0.04726742
FBgn0031249	CG11911	1.91926417	0.00063219	0.04760593
FBgn0003254	rib	2.78989804	0.00066973	0.05006265
FBgn0032061	CG9314	1.12231389	0.00068846	0.05105761
FBgn0002632	E(spl)m6-BFM	-1.5184769	0.00069352	0.05105761
FBgn0038118	timeout	-1.2724092	0.00069811	0.05105761
FBgn0263449	CR43472	-1.0955535	0.00071472	0.05189885
FBgn0263237	Cdk7	-0.8913473	0.00072996	0.05262992
FBgn0082962	snoRNA:Psi28S-3385a	-1.2678084	0.0007445	0.05329991
FBgn0264817	pre-lola-G	-0.8651296	0.0007501	0.05332557
FBgn0037310	Tim17b1	1.0820264	0.00075702	0.05344378
FBgn0085412	CG34383	1.15152319	0.00077021	0.05399954
FBgn0032835	CG16772	-1.6732028	0.0007972	0.05550884
FBgn0014135	bnl	0.92885606	0.00081001	0.05601753
FBgn0034452	Oseg6	1.82618981	0.00083663	0.0569398
FBgn0037431	CG17917	-1.3335376	0.00083928	0.0569398
FBgn0036419	CG13482	0.69292533	0.00084015	0.0569398
FBgn0003892	ptc	2.06235011	0.00088591	0.05964344
FBgn0260481	CG32454	-1.4831085	0.00089307	0.05971878
FBgn0024732	Drep1	-0.9439122	0.00089878	0.05971878
FBgn0024920	Ts	-1.5836073	0.00092417	0.0609099
FBgn0082979	snoRNA:Psi28S-3091a	-1.2809885	0.00093412	0.0609099
FBgn0015546	spel1	-0.796689	0.00093468	0.0609099
FBgn0028499	CG7985	-0.8081451	0.00095308	0.06171374
FBgn0263120	Acsl	0.69894052	0.00098447	0.06273301

FBgn0031575	Cep97	-1.011639	0.00098628	0.06273301
FBgn0037773	CG5359	-0.956075	0.00098734	0.06273301
FBgn0027889	ball	-0.7905334	0.00099674	0.06293686
FBgn0086675	fne	1.67504981	0.0010051	0.06307303
FBgn0050269	CG30269	1.24946716	0.0010986	0.06809967
FBgn0050273	CG30273	1.24946716	0.0010986	0.06809967
FBgn0037293	CG12007	0.74971929	0.00113476	0.06991469
FBgn0032382	Mal-B2	2.60887744	0.00115658	0.07082996
FBgn0020622	Pi3K21B	0.75099284	0.00116632	0.07099887
FBgn0005677	dac	1.38521661	0.00117917	0.0713356
FBgn0267691	CR46027	2.51273841	0.00118855	0.0713356
FBgn0032336	AstC	1.07599631	0.0011929	0.0713356
FBgn0038833	CG15696	-2.387936	0.0012299	0.07287741
FBgn0263763	CG43680	-2.1963575	0.00123302	0.07287741
FBgn0260755	CG42553	1.67822461	0.00126173	0.07360328
FBgn0032602	ppk17	1.46062324	0.00126259	0.07360328
FBgn0027279	l(1)G0196	-0.7411508	0.00126702	0.07360328
FBgn0038828	CG17270	-0.7999516	0.00128191	0.07386242
FBgn0259998	CG17571	2.49305824	0.00129043	0.07386242
FBgn0010314	Cks30A	-1.2515424	0.00129328	0.07386242
FBgn0038395	CG10407	-1.114116	0.0013308	0.07558053
FBgn0035495	CG14989	1.20743332	0.00136186	0.07638382
FBgn0004509	Fur1	0.85127323	0.00136334	0.07638382
FBgn0002578	Kaz-m1	2.17074969	0.00136816	0.07638382
FBgn0024352	Hop	-0.777879	0.00137626	0.07638382
FBgn0266810	CR45272	1.87973644	0.00138608	0.07638382
FBgn0003118	pnt	-1.0142114	0.00139003	0.07638382
FBgn0261285	Ppcs	0.69816786	0.00140071	0.07655701
FBgn0037149	CG14561	-1.0809672	0.0014251	0.07747381
FBgn0037265	spartin	0.82079316	0.00145365	0.07838674
FBgn0039128	CG13599	-1.4470375	0.00145732	0.07838674
FBgn0036754	CG5589	-0.7767073	0.00148448	0.07942735
FBgn0031643	CG3008	0.93013053	0.0015118	0.08010038
FBgn0003189		-0.8757794	0.00151281	0.08010038
FBgn0031533	CG2772	2.13365927	0.00158676	0.08336317
FBgn0030657	cerv	-0.9892094	0.00159344	0.08336317
FBgn0036565	CG5235	-1.1376773	0.00160618	0.08336317
FBgn0267766	CR46097	-1.6479696	0.00160724	0.08336317
FBgn0042086	Tsp42Eb	1.53060565	0.00163595	0.08415421
FBgn0032791	CG18094	0.82794	0.00163905	0.08415421

FBgn0038243	CG8066	0.69481932	0.00165204	0.08439498
FBgn0039637	CG11880	0.84817583	0.00172691	0.08743313
FBgn0259734	Nost	0.88200071	0.00172871	0.08743313
FBgn0050160	CG30160	1.55364392	0.00174021	0.08757904
FBgn0038071	Dtg	-0.8073227	0.00179023	0.08965256
FBgn0032934	CG8679	0.70411832	0.00182232	0.09081251
FBgn0035099	CG6845	-0.6777633	0.00184585	0.09153629
FBgn0038380	CG14877	0.87102843	0.00187409	0.09229813
FBgn0031914	CG5973	2.21523959	0.00187937	0.09229813
FBgn0039094	CG10184	-0.7262464	0.00190121	0.09292141
FBgn0036714	CG7692	0.93216403	0.00192717	0.09368494
FBgn0031602	CG15431	1.42942846	0.00193526	0.09368494
FBgn0082978	snoRNA:Psi28S-3091b	-1.3438701	0.00198469	0.09552886
FBgn0038381	CG3303	-0.8976951	0.00199214	0.09552886
FBgn0000024	Ace	0.80488411	0.00206692	0.09864929
FBgn0052649	CG32649	0.77110196	0.00207858	0.09874219
FBgn0034933	CG3735	-0.6434641	0.00210251	0.09941471
FBgn0051092	LpR2	0.74486631	0.00213928	0.10068476
FBgn0033312	CG8642	-0.7867174	0.00219497	0.10237484
FBgn0015376	cutlet	-0.8478249	0.00219567	0.10237484
FBgn0036203	Muc68D	4.67699061	0.0022054	0.10237484
FBgn0063649	CG6006	-0.8214514	0.00222845	0.10297461
FBgn0265535	CG44385	2.15985581	0.00224621	0.10301645
FBgn0270926	AsnS	0.96011328	0.00224962	0.10301645
FBgn0040765	luna	0.69280553	0.00226537	0.10327226
FBgn0262007	CG42825	2.57002667	0.00228432	0.10367125
FBgn0083013	snoRNA:Psi28S-1060	-1.8800188	0.0023349	0.10549592
FBgn0039215	CG6695	-0.5818449	0.00235568	0.10596408
FBgn0263131	CG43373	0.77716595	0.00239462	0.1071245
FBgn0034082	CG10734	2.43013344	0.00242666	0.1071245
FBgn0266405	CR45045	1.61793659	0.0024348	0.1071245
FBgn0010620	CG10939	1.42660461	0.00243539	0.1071245
FBgn0064116	CG33713	-0.5884768	0.00244471	0.1071245
FBgn0064117	SLIRP1	-0.5884768	0.00244471	0.1071245
FBgn0038344	obe	0.77250132	0.00246067	0.10736144
FBgn0262902	CR43257	0.70120732	0.00248761	0.1076245
FBgn0031848	Nse1	-1.1416372	0.00249802	0.1076245
FBgn0030748	Traf-like	0.73656171	0.00249846	0.1076245
FBgn0036910	Cyp305a1	-0.7310399	0.0025096	0.10764819
FBgn0004573	5-HT7	1.33054614	0.0025699	0.10939569

FBgn0015926	dah	-0.9045608	0.00257186	0.10939569
FBgn0019952	Orct	-1.0798946	0.0026195	0.11095761
FBgn0039002	CG17625	1.62864138	0.00264076	0.11139418
FBgn0035132	mthl10	-0.743457	0.00269262	0.11286215
FBgn0005648	Pabp2	-0.7219398	0.00269777	0.11286215
FBgn0031996	CG8460	-0.7566663	0.00272446	0.11351188
FBgn0034270	PIG-A	-0.9422725	0.00277279	0.11484676
FBgn0014388	sty	-0.7676716	0.0027791	0.11484676
FBgn0052549	CG32549	0.81515967	0.00282859	0.11641876
FBgn0037702	CG8176	-0.5974826	0.00293019	0.12011425
FBgn0035896	CG6983	-0.920557	0.00294754	0.12034
FBgn0083124	Uhg4	-0.6568214	0.00302842	0.12314787
FBgn0038102	CG14383	-0.8621843	0.00317324	0.12758596
FBgn0025456	CREG	1.36784968	0.00317556	0.12758596
FBgn0001149	GstD1	1.40343817	0.00319646	0.12758596
FBgn0037915	CG6790	1.23041749	0.00320353	0.12758596
FBgn0266111	ana3	-1.3681531	0.00320914	0.12758596
FBgn0039647	CG14509	1.34259224	0.00321287	0.12758596
FBgn0005619	Hdc	-1.2659905	0.00323471	0.12795368
FBgn0004914	Hnf4	0.93743083	0.0032757	0.12899142
FBgn0039101	CG16710	-1.0016263	0.00328632	0.12899142
FBgn0038827	Fancd2	-1.1991129	0.00337932	0.13213123
FBgn0259916	CG42445	0.67988904	0.00343944	0.13382913
FBgn0033544	CG7220	0.88447168	0.00344907	0.13382913
FBgn0038455	CG14907	0.84017807	0.00348889	0.13485947
FBgn0031530	pgant2	1.35325439	0.0035228	0.13513457
FBgn0037781	Fancl	2.11501703	0.0035333	0.13513457
FBgn0034670	CG13488	-0.7462403	0.00353588	0.13513457
FBgn0063667	CG32335	1.60628137	0.00355946	0.13527258
FBgn0034883	Eglp2	1.54579606	0.00357443	0.13527258
FBgn0038582	CG7988	0.71472785	0.00357941	0.13527258
FBgn0038020	GstD9	1.04568657	0.00363764	0.13650871
FBgn0034033	CG8204	0.88476866	0.00363898	0.13650871
FBgn0038547	CG17803	-1.1058065	0.0036574	0.13661273
FBgn0033372	CG13742	-0.8465309	0.00367759	0.13661273
FBgn0030993	Mec2	0.64273343	0.00368207	0.13661273
FBgn0053985	CG33985	1.22764827	0.00371136	0.13719879
FBgn0010041	GstD5	1.64248688	0.00378947	0.13885832
FBgn0261109	mrn	-0.701969	0.00381441	0.13885832
FBgn0259247	laccase2	0.93464865	0.00382326	0.13885832

FBgn0035235	CG7879	-0.6994717	0.00382901	0.13885832
FBgn0036547	CG17032	-1.2444438	0.00383107	0.13885832
FBgn0031498	CG17260	0.85106967	0.0038382	0.13885832
FBgn0260388	CG42514	0.77014269	0.00391666	0.14098224
FBgn0261817	CG42759	-1.1820891	0.00392465	0.14098224
FBgn0031654	Jon25Bii	3.39869079	0.00397804	0.14137309
FBgn0250753	kra	-0.6970881	0.00399572	0.14137309
FBgn0266350	CR44999	-0.883897	0.00399667	0.14137309
FBgn0259678	sqa	0.91647046	0.00400187	0.14137309
FBgn0050001	CG30001	-1.2936393	0.00400506	0.14137309
FBgn0015372	RabX1	0.62930195	0.00404605	0.14232588
FBgn0036624	RAF2	-0.8346904	0.00410273	0.14382182
FBgn0029795	CG15773	1.64512963	0.00414916	0.14494961
FBgn0053181	CG33181	1.07264319	0.0041713	0.14522415
FBgn0004598	Fur2	-0.6623013	0.0042181	0.14560389
FBgn0039776	PH4alphaEFB	-0.764035	0.00421822	0.14560389
FBgn0033696	Cyp6g2	2.1279885	0.00422518	0.14560389
FBgn0031419	CG15390	1.01485425	0.00427234	0.14673172
FBgn0259977	Tdc1	1.02990856	0.00433559	0.14840273
FBgn0040571	CG17193	-1.7741621	0.00435221	0.14847173
FBgn0265345	CR44299	1.11390226	0.00439871	0.14955626
FBgn0040290	RecQ4	-1.4532378	0.0044757	0.15137175
FBgn0010288	Uch	-0.5900771	0.00448189	0.15137175
FBgn0040238	Best1	-0.6591997	0.00451718	0.1520585
FBgn0025885	Inos	-0.6082634	0.00456084	0.15302129
FBgn0032793	CG10189	0.83893202	0.00458607	0.15336193
FBgn0036749	CG7460	-0.8401896	0.00460951	0.15364038
FBgn0004198	ct	-1.4052787	0.0047259	0.15665908
FBgn0051324	CG31324	-0.8810136	0.00474404	0.15665908
FBgn0035917	Zasp66	1.89810582	0.00474631	0.15665908
FBgn0004431	LysX	2.47131238	0.00476353	0.15670224
FBgn0265448	CR44348	1.1010415	0.00477845	0.15670224
FBgn0050169	Brca2	-0.8100674	0.00482121	0.15759605
FBgn0038035	lig3	0.91119943	0.00484901	0.15763495
FBgn0033989	CG7639	-0.5656097	0.00488312	0.15763495
FBgn0038608	WRNexo	-1.1819844	0.00491233	0.15763495
FBgn0020445	E23	-0.9586624	0.00491748	0.15763495
FBgn0029915	CG14434	-0.8200331	0.00493722	0.15763495
FBgn0001179	hay	0.85236819	0.00493769	0.15763495
FBgn0052461	CG32461	-1.4579389	0.00494206	0.15763495

FBgn0025835	CG17707	-1.1752579	0.00494644	0.15763495
FBgn0038100	Paip2	0.52535789	0.00500642	0.15869996
FBgn0050290	Ppcdc	0.8705988	0.0050267	0.15869996
FBgn0260222	CG42496	0.8705988	0.0050267	0.15869996
FBgn0034480	CG16898	1.62647494	0.00505201	0.15900538
FBgn0039735	Nph	-0.5719862	0.00506766	0.15900552
FBgn0032750	CG10495	-0.9165589	0.00510168	0.15915927
FBgn0037578	CG9601	-0.7437529	0.00510387	0.15915927
FBgn0034742	CG4294	0.657408	0.00512172	0.15922745
FBgn0023515	CG14814	-0.9078895	0.00514282	0.15939599
FBgn0026169	snoRNA:Psi18S-1820	-1.3136254	0.00517377	0.15963244
FBgn0003268	rod	-0.9764515	0.0052022	0.15963244
FBgn0029664	CG10802	1.9358801	0.00522246	0.15963244
FBgn0037834	Art1	-0.5700063	0.0052271	0.15963244
FBgn0261238	Alh	-0.7196784	0.00522896	0.15963244
FBgn0286007		-1.2774882	0.00526147	0.16014411
FBgn0265819	CR44608	-0.9955996	0.00530583	0.16101225
FBgn0037345	rev7	1.11075502	0.00533868	0.16132094
FBgn0036741	CG7510	-0.8377609	0.00535222	0.16132094
FBgn0263584	CR43609	-0.7639705	0.00536361	0.16132094
FBgn0038354	CG5404	1.33593297	0.00544134	0.16239763
FBgn0000412	D1	-0.5404934	0.00544703	0.16239763
FBgn0015924	crq	0.63119482	0.00544733	0.16239763
FBgn0031805	CG9505	0.88927482	0.00546907	0.16250296
FBgn0029608	CG3091	1.79343072	0.00548284	0.16250296
FBgn0260399	gwl	-1.0585421	0.00554011	0.16372299
FBgn0000639	Fbp1	-2.2734243	0.00561245	0.16482534
FBgn0030864	CG8173	-1.4148303	0.00562936	0.16482534
FBgn0262364	CG43062	-1.7025172	0.00563318	0.16482534
FBgn0030053	CG12081	-0.6405862	0.00564929	0.16482534
FBgn0002633	E(spl)m7-HLH	-0.9251941	0.00565847	0.16482534
FBgn0050025	CG30025	2.87897392	0.00572266	0.16571145
FBgn0031816	CG16947	-1.6513757	0.00573761	0.16571145
FBgn0042712	HBS1	0.65298205	0.0057378	0.16571145
FBgn0021768	nudC	-0.5613153	0.00586267	0.16883816
FBgn0264894	CG44085	0.78911431	0.0058895	0.16913185
FBgn0040346	CG3704	-0.5260492	0.00595113	0.17042023
FBgn0264442	ab	1.1232673	0.00601478	0.17097953
FBgn0035669	CG6592	2.41825428	0.00601502	0.17097953
FBgn0261530	nbs	0.58777835	0.00603171	0.17097953

FBgn0035755	CG14830	1.72524867	0.00604547	0.17097953
FBgn0036369	CG10089	1.49135123	0.00605475	0.17097953
FBgn0283741	prage	0.65733916	0.00611585	0.17222638
FBgn0029079	icln	-0.6865642	0.00614211	0.17248817
FBgn0035229	pns	-0.6294275	0.00617237	0.17286034
FBgn0031209	Ir21a	-0.7414049	0.00620393	0.17326677
FBgn0263240	Coop	-0.7496607	0.00624569	0.17349612
FBgn0037923	CG6813	-1.2065787	0.00624627	0.17349612
FBgn0032614	CG13284	0.78512466	0.00626742	0.17360915
FBgn0035392	CG1271	1.72732043	0.00629946	0.17371908
FBgn0266731	CR45204	0.63068498	0.00630556	0.17371908
FBgn0030358	CG10362	1.52419334	0.00636612	0.17491348
FBgn0032499	Uvrag	0.55090642	0.00640214	0.17517346
FBgn0259979	CG17337	-0.5523292	0.00643211	0.17517346
FBgn0003731	Egfr	-0.9386921	0.00644149	0.17517346
FBgn0031970	CG7227	1.72127407	0.00644451	0.17517346
FBgn0033635	Prip	0.77728684	0.00649831	0.17616474
FBgn0028738	ETH	0.68253613	0.00656732	0.17756204
FBgn0029657	CG12535	-0.6899879	0.00660141	0.17801036
FBgn0029761	SK	0.90930649	0.00664294	0.17832887
FBgn0035586	CG10671	0.71830814	0.00667259	0.17832887
FBgn0028530	mTTF	0.72736991	0.00668067	0.17832887
FBgn0035542	DOR	0.58509408	0.00668926	0.17832887
FBgn0015625	CycB3	-1.4935234	0.00670093	0.17832887
FBgn0042177	CG32164	-0.5729104	0.0067966	0.18040281
FBgn0026379	Pten	-0.6903838	0.00685113	0.1805367
FBgn0035041	CG13594	0.97540878	0.00685136	0.1805367
FBgn0005696	DNApol-alpha73	-1.9465982	0.00688462	0.1805367
FBgn0267728	otk2	-1.1607282	0.00691323	0.1805367
FBgn0034808	CG9896	1.29233162	0.00691356	0.1805367
FBgn0031461	daw	1.84745317	0.00691965	0.1805367
FBgn0259171	Pde9	1.7763077	0.00695101	0.1805367
FBgn0029937	CG8300	0.50642028	0.0069536	0.1805367
FBgn0052219	CG32219	-0.6997842	0.00696148	0.1805367
FBgn0053172	CG33172	-1.4064865	0.00699982	0.18106918
FBgn0004880	scrt	1.80677407	0.00707809	0.18176724
FBgn0039464	CG6330	0.99565163	0.00709514	0.18176724
FBgn0011260	Sema2a	-0.5603895	0.00709566	0.18176724
FBgn0027864	Ogg1	0.70780468	0.00710262	0.18176724
FBgn0085358	Diedel3	3.09760635	0.00711621	0.18176724

FBgn0036225	CG5883	3.09995236	0.0071599	0.1819704
FBgn0004587	B52	-0.5554653	0.00717428	0.1819704
FBgn0034646	Rae1	-0.67051	0.00717877	0.1819704
FBgn0039452	CG14245	-2.4142527	0.00719576	0.1819704
FBgn0051005	qless	0.59145566	0.00723534	0.18251733
FBgn0034908	CG5543	0.63209032	0.00726794	0.18288588
FBgn0043903	dome	-0.6131119	0.00746387	0.18735223
FBgn0025879	Timp	-0.6061125	0.00748563	0.18743573
FBgn0015336	CG15865	1.73833475	0.00752297	0.18790798
FBgn0004575	Syn	-0.5996449	0.00754147	0.18790828
FBgn0038242	CG14852	1.31141481	0.00757824	0.18836272
FBgn0020300	geko	1.63775952	0.00767678	0.1897897
FBgn0035996	CG3448	0.57120519	0.00769798	0.1897897
FBgn0085753	28SrRNA-Psi:CR40596	4.41939114	0.00769904	0.1897897
FBgn0000810	fs(1)K10	-0.522665	0.00771032	0.1897897
FBgn0263607	l(3)72Dp	0.915425	0.00775335	0.1897995
FBgn0264863	CR44054	-1.1050664	0.00776602	0.1897995
FBgn0025630	Rtca	-0.5737501	0.00776673	0.1897995
FBgn0032635	CG15141	-0.907776	0.00780502	0.18983592
FBgn0267191	CR45631	1.66102721	0.00780557	0.18983592
FBgn0033997	Ir51a	-1.2066666	0.00798516	0.19374019
FBgn0028543	NimB2	-1.0076576	0.00801516	0.19400501
FBgn0035761	RhoGEF4	-0.7666475	0.00809105	0.19491693
FBgn0051183	CG31183	0.80993167	0.00809118	0.19491693
FBgn0261429	CR42646	1.78958863	0.00816532	0.19592534
FBgn0033990	CG10265	-0.7653104	0.0081857	0.19592534
FBgn0039205	CG13623	1.36898251	0.00819086	0.19592534
FBgn0032935	Atg18b	0.70291876	0.00826286	0.19708097
FBgn0033375	CG8078	-0.554761	0.00827794	0.19708097
FBgn0267792	rgr	-0.5517735	0.00829965	0.19713601
FBgn0030272	CG15201	-1.4629237	0.00837485	0.19845723
FBgn0261349	Mst36Fb	1.3857081	0.00839432	0.19845723
FBgn0267558	CR45898	-1.0562932	0.0084293	0.198822
FBgn0035989	CG3967	-0.78754	0.00845514	0.19896986
FBgn0026418	Hsc70Cb	-0.5896657	0.00848963	0.19931993
FBgn0035028	Start1	0.53066804	0.00855618	0.20041967
FBgn0033226	CG1882	0.88813549	0.00860534	0.20073841
FBgn0040251	Ugt86Di	1.12453822	0.00860928	0.20073841
FBgn0022027	Vps25	0.65141041	0.00864936	0.20083794
FBgn0053532	lectin-37Da	2.01158752	0.00865306	0.20083794

FBgn0050463	CG30463	-0.5950958	0.00869699	0.20139775
FBgn0033564	Pex6	0.84767796	0.00874219	0.20198422
FBgn0033423	CG1809	1.3420041	0.00878066	0.20241306
FBgn0038720	CG6231	1.00214957	0.00881496	0.20272861
FBgn0033204	CG2065	1.24309724	0.00885397	0.20272861
FBgn0014427	CG11899	1.39115863	0.0088646	0.20272861
FBgn0082936	snoRNA:Me28S-C2645c	-1.0824376	0.00887411	0.20272861
FBgn0010358	deltaTry	1.58853244	0.00893396	0.20363821
FBgn0004643	Zw10	-0.6129285	0.00896501	0.20372662
FBgn0037900	CG5276	0.63230747	0.00897792	0.20372662
FBgn0033458	CG18446	1.01847433	0.00904112	0.20465437
FBgn0034491	Hsl	-0.5609801	0.00907483	0.20465437
FBgn0082942	snoRNA:Me28S-A982b	-1.0890625	0.0090792	0.20465437
FBgn0035726	CG9953	-0.515992	0.00920802	0.20709898
FBgn0035438	PHGPx	0.81435172	0.00924946	0.20740791
FBgn0266966	CR45417	1.35942483	0.00926256	0.20740791
FBgn0035206	CG9186	0.53056216	0.00931046	0.20800067
FBgn0035951	CG5068	-0.5958761	0.00933266	0.20800067
FBgn0029831	CG5966	2.19194259	0.00935041	0.20800067
FBgn0033584	CG7737	-1.0264147	0.00937735	0.2081443
FBgn0037727	CG8358	3.54449876	0.00939884	0.20816692
FBgn0033206	DCTN4-p62	0.7389683	0.00945048	0.20825249
FBgn0035358	CG14949	1.14497823	0.00945391	0.20825249
FBgn0011274	Dif	-1.0403863	0.00946416	0.20825249
FBgn0053506	CG33506	-0.6799611	0.00953891	0.20944393
FBgn0263606	Hsc20	1.09304111	0.00956513	0.20956697
FBgn0038404	CG8925	1.24840941	0.00961683	0.21024664
FBgn0036844	Mkp3	-0.8956552	0.00969667	0.21153733
FBgn0035833	CG7565	0.53170748	0.00975316	0.21231406
FBgn0036126	Irbp18	0.75722376	0.00983823	0.21370812
FBgn0000636	Fas3	0.78630417	0.00986984	0.21371302
FBgn0083015	snoRNA:Psi18S-920	-1.3011211	0.00992617	0.21371302
FBgn0259707	CG42361	0.71748368	0.00994662	0.21371302
FBgn0264078	Flo2	0.62984055	0.00996084	0.21371302
FBgn0051163	SKIP	-0.560633	0.01001087	0.21371302
FBgn0051313	CG31313	1.24019459	0.01001875	0.21371302
FBgn0043806	CG32032	2.18313242	0.01003762	0.21371302
FBgn0013726	pnut	0.5524609	0.0100389	0.21371302
FBgn0040064	yip2	0.80810553	0.010067	0.21371302

FBgn0025709	CG8083	2.12465997	0.01007198	0.21371302
FBgn0038881	CG16791	0.56431587	0.01009065	0.21371302
FBgn0264979	CG4267	0.62817079	0.01009072	0.21371302
FBgn0051102	CG31102	0.7707999	0.01013754	0.21425391
FBgn0033543	CG12338	1.11994514	0.01017699	0.21425391
FBgn0031878	sip2	-0.8288778	0.01017948	0.21425391
FBgn0050151	CG30151	2.07055269	0.01022414	0.2147478
FBgn0039773	CG2224	0.64477033	0.0102452	0.2147478
FBgn0000109	Aprt	0.81084353	0.01030295	0.21477374
FBgn0031474	CG2991	0.50685819	0.0103267	0.21477374
FBgn0035120	wac	-0.7230887	0.01032834	0.21477374
FBgn0265298	SC35	-0.4968942	0.01033094	0.21477374
FBgn0036320	CG10943	1.42986753	0.01035665	0.21486889
FBgn0264001	bru3	0.69909698	0.01052823	0.21772422
FBgn0000451	ect	-0.6045935	0.01055658	0.21772422
FBgn0039642	CG11882	-1.2280679	0.01056502	0.21772422
FBgn0051288	CG31288	1.06394286	0.01057995	0.21772422
FBgn0001281	janB	-0.7737585	0.01063768	0.21782315
FBgn0004395	unk	0.51318454	0.01064424	0.21782315
FBgn0033188	Drat	1.15395846	0.01064904	0.21782315
FBgn0053306	CG33306	1.80304938	0.01067251	0.21786495
FBgn0265531	CR44381	-1.2385131	0.01069412	0.21786863
FBgn0031010	CG8028	-1.1909018	0.01076161	0.21839421
FBgn0033205	CG2064	1.15726789	0.01076289	0.21839421
FBgn0010217	ATPsynbeta	-0.5499637	0.01091463	0.22103223
FBgn0038854	CG7044	0.97955631	0.01098043	0.22154486
FBgn0050359	Mal-A5	1.70293884	0.01098353	0.22154486
FBgn0031142	r-cup	-0.8004508	0.01105567	0.22255836
FBgn0037667	CG16734	-0.9715272	0.01113207	0.22365332
FBgn0038766	CG4854	0.82017215	0.0111812	0.22419747
FBgn0030056	CG11284	-0.5209705	0.01129041	0.22509214
FBgn0285926		0.53470866	0.01130354	0.22509214
FBgn0026080	Tip60	0.51804154	0.01131638	0.22509214
FBgn0262524	ver	0.76782255	0.01132863	0.22509214
FBgn0053099	CG33099	-0.6460991	0.01136895	0.22509214
FBgn0085290	CG34261	-0.8598904	0.0113953	0.22509214
FBgn0052283	Drsl3	1.9763144	0.01139839	0.22509214
FBgn0027608	CG2082	-0.5290686	0.01140947	0.22509214
FBgn0004597	CycC	0.57984228	0.0114251	0.22509214
FBgn0036502	CG7841	1.25573463	0.01148109	0.22575784

FBgn0037518	CG2641	-0.7476697	0.01151878	0.22578988
FBgn0030992	CG33253	0.7320414	0.01152714	0.22578988
FBgn0039877	CG2118	-0.5752325	0.01159477	0.22637406
FBgn0266317	CR44982	0.90630416	0.01160876	0.22637406
FBgn0032877	CG2617	-0.7246647	0.01162377	0.22637406
FBgn0003257	r-l	-0.5118789	0.0116582	0.22661037
FBgn0036996	mag	2.57598146	0.01173955	0.22735227
FBgn0036348	CG17687	1.92982215	0.01174109	0.22735227
FBgn0030196	Psf3	-0.6726217	0.01183138	0.22866512
FBgn0034938	CG3803	-0.8971272	0.01199138	0.23120279
FBgn0037974	CG12224	0.68581877	0.01202827	0.23120279
FBgn0014879	Set	-0.5605132	0.01204616	0.23120279
FBgn0035691	CG7386	1.2390593	0.01205543	0.23120279
FBgn0259748	CG42397	2.56827184	0.0120805	0.23120279
FBgn0040813	Nplp2	0.66071587	0.01210868	0.23120279
FBgn0051041	CG31041	2.66408227	0.01215217	0.23120279
FBgn0023197	Jon74E	2.85368233	0.01220182	0.23120279
FBgn0032428	CG6405	-0.9891781	0.01222068	0.23120279
FBgn0029147	NtR	-0.9983484	0.01224252	0.23120279
FBgn0263256	CG43394	1.9353926	0.01224914	0.23120279
FBgn0259985	Mppe	-0.8045037	0.01225458	0.23120279
FBgn0265715	CR44522	1.95553457	0.01225834	0.23120279
FBgn0051036	CG31036	-1.2195158	0.0123421	0.23130947
FBgn0030407	CG2543	0.95155909	0.01235312	0.23130947
FBgn0262656	Myc	-0.6364796	0.01239339	0.23130947
FBgn0027621	Pfrx	0.56491455	0.01239382	0.23130947
FBgn0023530	CG3740	0.94614106	0.01240435	0.23130947
FBgn0003380	Sh	0.84967127	0.01240969	0.23130947
FBgn0261283	SREBP	-0.5067369	0.01243619	0.23130947
FBgn0023000	mth	-0.5844445	0.01244602	0.23130947
FBgn0030057	Ppt1	-0.605283	0.01247208	0.23137081
FBgn0260940	lsn	0.67283629	0.01252491	0.23192764
FBgn0036772	CG5290	-0.567196	0.01255694	0.23209797
FBgn0035410	CG14964	-1.5092924	0.01263158	0.23305376
FBgn0043578	PGRP-SB1	-1.4958928	0.01269147	0.23373456
FBgn0000330	cm	0.53104267	0.01283462	0.23594351
FBgn0036767	CG16775	2.31893584	0.01287313	0.23622424
FBgn0036335	mRpL20	-0.7476161	0.01290665	0.23641254
FBgn0085813	18SrRNA-Psi:CR41602	1.74512251	0.01293548	0.23651451
FBgn0037248	srl	-0.5719261	0.01303691	0.23741633

FBgn0034507	CG11192	1.09763933	0.01310175	0.23741633
FBgn0032873	CG2614	-0.5571033	0.01312388	0.23741633
FBgn0039316	CG11893	1.53756134	0.01312774	0.23741633
FBgn0263081	CG43349	1.42147224	0.0131312	0.23741633
FBgn0035158	CG13895	0.6260992	0.01315058	0.23741633
FBgn0036759	CG5577	0.85664932	0.01315763	0.23741633
FBgn0266918	CG32486	-0.5869853	0.01318359	0.23741633
FBgn0037720	CG8312	1.66087137	0.01319499	0.23741633
FBgn0262736	Vha16-1	0.58100361	0.01322853	0.23759932
FBgn0000723	FER	-0.6479891	0.0132903	0.23811111
FBgn0036833	CG3819	3.81733932	0.01330387	0.23811111
FBgn0010315	CycD	-0.4859799	0.01332856	0.23813389
FBgn0033686	Hen1	-0.6110689	0.01338526	0.23872727
FBgn0020391	Nrk	-1.0051873	0.01345161	0.23949052
FBgn0035987	CG3689	-0.6374814	0.01350156	0.23995945
FBgn0003502	Btk29A	-0.6632119	0.01354857	0.24003878
FBgn0031437	Arpc5	0.50316144	0.01355324	0.24003878
FBgn0036121	CG6310	-1.0080902	0.01358012	0.24009648
FBgn0266819	CR45281	1.15781422	0.01364977	0.24072371
FBgn0004449	Ten-m	0.54504749	0.01368647	0.24072371
FBgn0033733	CG8834	2.04786896	0.01368663	0.24072371
FBgn0034588	CG9394	1.70366522	0.01374881	0.24139962
FBgn0031579	CG15422	1.17103356	0.01379786	0.24184326
FBgn0031279	CG3544	-0.5841929	0.01388957	0.24269174
FBgn0027079	ValRS	0.96097613	0.01394814	0.24269174
FBgn0037975	CG3397	1.2710501	0.01400154	0.24269174
FBgn0031435	Elba2	-0.8683622	0.01400802	0.24269174
FBgn0035213	CG2199	-0.4741731	0.01404196	0.24269174
FBgn0083068	CG33947	0.65627324	0.01404761	0.24269174
FBgn0040091	Ugt58Fa	-1.4695124	0.01407511	0.24269174
FBgn0033371	CNT1	-0.810986	0.01411432	0.24269174
FBgn0037753	CG12947	-1.3158579	0.01412105	0.24269174
FBgn0030881	CG12985	1.03734027	0.01412158	0.24269174
FBgn0034860	CG9812	1.95303807	0.01414275	0.24269174
FBgn0037668	CG16736	-1.9968749	0.01414504	0.24269174
FBgn0014455	Ahcy	-0.5078284	0.01415662	0.24269174
FBgn0010043	GstD7	1.51139896	0.01423461	0.24320946
FBgn0040965	CR13130	-0.8674008	0.01423467	0.24320946
FBgn0267814	CR46139	1.27088441	0.01437364	0.24517185
FBgn0263316	Mrp4	0.94668822	0.01441149	0.24540569

FBgn0037888	scpr-B	-1.3238777	0.01454946	0.24734084
FBgn0052707	APC4	-0.9100908	0.01462141	0.24814897
FBgn0046874	Pif1B	0.72062929	0.01470502	0.24915207
FBgn0036290	CG10638	0.80962409	0.01478303	0.25005697
FBgn0001280	janA	-0.5548448	0.01490322	0.25030389
FBgn0053317	CR33317	0.86772695	0.0149092	0.25030389
FBgn0033354	FANCI	-1.1311057	0.01492944	0.25030389
FBgn0035983	CG4080	-0.5193097	0.01493458	0.25030389
FBgn0033243	CG14763	-0.9152163	0.01494822	0.25030389
FBgn0034717	CG5819	1.08681372	0.01495624	0.25030389
FBgn0031049	Sec61gamma	-0.4850254	0.01496997	0.25030389
FBgn0265901	CR44690	0.99719472	0.01499676	0.25034004
FBgn0052068	Adi1	0.55116545	0.01504333	0.2507057
FBgn0029882	CG3226	-0.6126802	0.01514187	0.25193499
FBgn0034029	eIF2Bgamma	0.6777877	0.01523546	0.25307793
FBgn0011606	Klp3A	-0.7923288	0.01537804	0.25424249
FBgn0038756	CG4783	1.8284861	0.01538758	0.25424249
FBgn0267348	LanB2	-0.5409933	0.0154079	0.25424249
FBgn0027562	CG10345	5.13745325	0.01541512	0.25424249
FBgn0266044	CR44809	1.08390068	0.01543673	0.25424249
FBgn0028381	Decay	0.66841837	0.01545562	0.25424249
FBgn0041604	dlp	-0.6500004	0.01555012	0.25538378
FBgn0038839	Ktl	-0.8575568	0.01561227	0.2554466
FBgn0001991	Ca-alpha1D	1.02657958	0.01561976	0.2554466
FBgn0036341	Syx13	0.59985099	0.01563567	0.2554466
FBgn0032702	CG10376	0.53434215	0.01565613	0.2554466
FBgn0004584	Rrp1	-0.6677936	0.01567959	0.2554466
FBgn0036381	CG8745	1.67225199	0.01593588	0.25888031
FBgn0261015	Pif1A	0.7182458	0.01594128	0.25888031
FBgn0031887	CG11289	1.02305333	0.01602361	0.2598023
FBgn0052076	Alg10	-0.6120812	0.01608422	0.26011796
FBgn0262570	CG43110	1.18219454	0.01609426	0.26011796
FBgn0031191	Cp110	-0.5302011	0.0161358	0.26037544
FBgn0038083	CG5999	2.08987862	0.01617034	0.26051937
FBgn0015805	HDAC1	-0.5637729	0.01624426	0.26129616
FBgn0051345	CG31345	-0.878503	0.01628434	0.2614112
FBgn0034225	veil	1.22138581	0.01630284	0.2614112
FBgn0036715	Cad74A	2.0644258	0.0163323	0.26147113
FBgn0069354	Porin2	-1.2057333	0.01643962	0.26185782
FBgn0262580	CG43120	0.94870625	0.01644482	0.26185782

FBgn0042178	CG32165	-0.587553	0.01646147	0.26185782
FBgn0046247	CG5938	0.50367039	0.01647395	0.26185782
FBgn0030955	CG6891	0.53966568	0.01650956	0.26185782
FBgn0034422	CG7137	-0.7827962	0.016511	0.26185782
FBgn0032633	Lrch	-0.6334407	0.01663056	0.26294622
FBgn0033177	CG11141	0.48322223	0.01666683	0.26294622
FBgn0032524	CG9267	-0.5313813	0.01670882	0.26294622
FBgn0053062	CG33062	-1.0046871	0.01673346	0.26294622
FBgn0004362	HmgD	-0.6770003	0.01674833	0.26294622
FBgn0052062	Rbfox1	-0.7890079	0.01675912	0.26294622
FBgn0285963		-0.5262238	0.01676069	0.26294622
FBgn0050031	CG30031	2.07142052	0.01683654	0.26372927
FBgn0265311	CR44284	-1.0374362	0.0169613	0.26527471
FBgn0267408	AOX1	0.83000522	0.01700781	0.265399
FBgn0032191	CG5734	0.50874693	0.01702146	0.265399
FBgn0029596	CG14054	-1.2001052	0.01708289	0.26563744
FBgn0030747	CG4301	0.57184719	0.01708901	0.26563744
FBgn0050010	CG30010	0.82470148	0.01711953	0.26564577
FBgn0041184	Socs36E	-0.6502505	0.01714181	0.26564577
FBgn0028484	Ack	-0.5141702	0.01717412	0.26574134
FBgn0086708	stv	0.63635259	0.01727079	0.26683113
FBgn0030294	Pa1	-0.5966424	0.01730158	0.26690122
FBgn0086358	Tab2	-0.660397	0.01736682	0.26734417
FBgn0030468	CG1622	-0.4605682	0.0174375	0.26734417
FBgn0030321	CG1703	0.86475188	0.01744401	0.26734417
FBgn0267181	CR45621	0.92009337	0.01745219	0.26734417
FBgn0027783	SMC2	-0.7538755	0.01749145	0.26734417
FBgn0264997	CR44148	0.71725448	0.01753381	0.26734417
FBgn0264816	koko	-0.632196	0.01753921	0.26734417
FBgn0264574	Glut1	-0.9239853	0.01754068	0.26734417
FBgn0037443	Dmtn	0.61438776	0.01760129	0.26775592
FBgn0037772	Spn85F	-0.8745995	0.01764652	0.26775592
FBgn0005670	Cyp4d1	1.30766284	0.01764671	0.26775592
FBgn0086608	CG34112	0.62623511	0.01772097	0.26848195
FBgn0044020	Roc2	-0.814963	0.01775933	0.26866277
FBgn0024555	flfl	-0.5186169	0.01781375	0.26908559
FBgn0030911	CR15061	0.81743512	0.01790517	0.27006528
FBgn0039719	CG15515	-1.3386735	0.01795695	0.27009473
FBgn0034195	Spn53F	2.03603227	0.01796026	0.27009473
FBgn0260768	CG42566	0.72732233	0.01807788	0.27146197

FBgn0262189	mir-2500	-0.9544665	0.01810802	0.27149726
FBgn0035523	CG1311	-0.4606893	0.01813365	0.27149726
FBgn0029174	FKBP59	-0.4474506	0.01825385	0.271613
FBgn0027363	Stam	0.5009952	0.01825981	0.271613
FBgn0261873	sdt	0.77438073	0.01830268	0.271613
FBgn0024957	Irp-1B	0.83233301	0.01830321	0.271613
FBgn0263447	CR43470	1.54836294	0.01831621	0.271613
FBgn0265872	CR44661	1.63033659	0.01832559	0.271613
FBgn0063493	GstE7	1.33229488	0.0183284	0.271613
FBgn0029506	Tsp42Ee	0.94706694	0.0183903	0.27175365
FBgn0034439	CG10062	-3.7994041	0.01841843	0.27175365
FBgn0037057	CG10512	-0.6822183	0.01845903	0.27175365
FBgn0031646	CG2837	-1.4317303	0.01846825	0.27175365
FBgn0004797	mdy	0.70680684	0.01847155	0.27175365
FBgn0266393	CR45033	-0.5090247	0.01850393	0.27183664
FBgn0027550	CG6495	-0.5704834	0.01869046	0.27311116
FBgn0038868	CG5862	0.50054477	0.01872527	0.27311116
FBgn0036493	CG7255	1.08718237	0.01874147	0.27311116
FBgn0033494	KCNQ	1.00518729	0.01874784	0.27311116
FBgn0036571	Strumpellin	0.47935013	0.01877397	0.27311116
FBgn0030638	CG11655	0.84384409	0.01877422	0.27311116
FBgn0034179	CG6805	0.81640925	0.01881115	0.27311116
FBgn0039165	CG6204	-1.0184183	0.01881638	0.27311116
FBgn0266400	CR45040	1.26202898	0.01885037	0.27311116
FBgn0013773	Cyp6a22	2.08844742	0.01885934	0.27311116
FBgn0265419	CR44331	0.65156812	0.01911411	0.2764069
FBgn0002542	lds	-0.9188481	0.01921321	0.27744535
FBgn0038860	Ice2	-1.1419131	0.0193077	0.27841433
FBgn0032908	CG9270	0.81022193	0.01936077	0.27878418
FBgn0039543	CG12428	0.76547918	0.0195309	0.28047339
FBgn0036397	Nprl3	-0.6148182	0.01953326	0.28047339
FBgn0001098	Gdh	-0.5050459	0.01972526	0.28275978
FBgn0264446	CR43864	-1.0335061	0.01974813	0.28275978
FBgn0031412	CG16995	1.98102952	0.01977723	0.2827782
FBgn0037117	CG11248	0.63142058	0.01985	0.28327157
FBgn0034741	CG4269	1.66932905	0.01988169	0.28327157
FBgn0266626	CR45133	1.18230198	0.01990738	0.28327157
FBgn0035934	TrpA1	-0.5663447	0.01998006	0.28327157
FBgn0032124	CG17855	0.57901683	0.02002882	0.28327157
FBgn0034156	CG5348	0.6864816	0.02003274	0.28327157

FBgn0267024	CR45468	-0.8297854	0.02005387	0.28327157
FBgn0035112	CG13877	-1.5591433	0.02007576	0.28327157
FBgn0014396	tim	-0.6941711	0.02008017	0.28327157
FBgn0030506	Lig4	0.65360718	0.02011632	0.28327157
FBgn0034723	CG13506	-0.5758376	0.02013793	0.28327157
FBgn0265853	CR44642	1.57871859	0.02015076	0.28327157
FBgn0062440	CG17680	0.54394632	0.02017397	0.28327157
FBgn0267507	pre-rRNA:CR45847	-1.3920258	0.02023356	0.28371635
FBgn0029121	Sras	0.5419911	0.02029202	0.28384467
FBgn0052107	CG32107	1.88441076	0.02029855	0.28384467
FBgn0031739	CG14005	-0.6436739	0.02038378	0.28445641
FBgn0267790	rump	-0.4777813	0.02039826	0.28445641
FBgn0267497	28SrRNA:CR45837	2.31972324	0.02042868	0.28449042
FBgn0035241	CG12105	-2.2500225	0.02050869	0.28521388
FBgn0050424	CG30424	0.55243333	0.02055822	0.28551205
FBgn0031514	CG3332	1.42127565	0.02060609	0.28575189
FBgn0035400	CG11537	0.43339457	0.0206317	0.28575189
FBgn0261933	SmD1	-0.6726955	0.02074949	0.28613856
FBgn0265915	CR44704	-0.6132853	0.02076161	0.28613856
FBgn0001258	ImpL3	0.65499081	0.02076665	0.28613856
FBgn0038349	AOX3	0.65872906	0.02077221	0.28613856
FBgn0263605	l(3)72Dn	-0.5321686	0.02087878	0.28669143
FBgn0040687	CG14645	1.04396413	0.02090141	0.28669143
FBgn0016983	smid	-0.5080148	0.02093904	0.28669143
FBgn0000644	Fcp3C	-0.8051565	0.02096295	0.28669143
FBgn0003863	alphaTry	2.03837458	0.02098334	0.28669143
FBgn0058354	CR40354	0.83735074	0.0209911	0.28669143
FBgn0039488	CG6066	0.63378247	0.02101887	0.28669143
FBgn0003475	spir	-0.5901694	0.02103795	0.28669143
FBgn0028552	gammaSnap1	0.60245928	0.02119264	0.28748271
FBgn0052695	CG32695	1.7807264	0.02119589	0.28748271
FBgn0002631	E(spl)m5-HLH	-1.1789125	0.02120624	0.28748271
FBgn0038519	Prx3	-0.5670338	0.02120913	0.28748271
FBgn0050287	CG30287	-0.9334522	0.02133808	0.28863006
FBgn0050077	Blos1	0.60616301	0.02135056	0.28863006
FBgn0030500	Ndc80	-0.7372582	0.02138336	0.28868958
FBgn0038145	Droj2	-0.540791	0.02146388	0.28917559
FBgn0265193	Atf-2	-0.5736906	0.02147645	0.28917559
FBgn0266430	CG45060	0.61577968	0.0215047	0.28917559
FBgn0050022	CG30022	0.69643724	0.0215467	0.28935766

FBgn0051792	CG31792	1.61258353	0.02160712	0.28978621
FBgn0046114	Gclm	0.72091042	0.02168959	0.28992762
FBgn0005612	Sox14	0.53223802	0.02169632	0.28992762
FBgn0035977	PGRP-LF	-0.7340452	0.02170322	0.28992762
FBgn0000442	Pkg21D	-0.5497909	0.02180863	0.29093756
FBgn0010359	gammaTry	2.39175792	0.02183667	0.29093756
FBgn0031758	Ucp4B	-1.4490034	0.02197594	0.29093756
FBgn0263442	CR43465	-1.4490034	0.02197594	0.29093756
FBgn0051633	CG31633	0.93972001	0.02198352	0.29093756
FBgn0037371	Sym	-0.6929965	0.02198848	0.29093756
FBgn0038487	TwdlW	-0.9506559	0.02204698	0.29093756
FBgn0051231	CG31231	-1.6264853	0.02206081	0.29093756
FBgn0038306	Art3	-0.5745577	0.02207418	0.29093756
FBgn0030701	CG16952	-0.4866862	0.02208685	0.29093756
FBgn0262532	CR43086	1.0235643	0.02211937	0.29093756
FBgn0052037	CG32037	-1.3371727	0.02212569	0.29093756
FBgn0266394	CR45034	-1.204141	0.02215086	0.29093756
FBgn0265542	CR44392	0.7491684	0.02217975	0.29094105
FBgn0032694	MESR3	-0.6733868	0.02229889	0.29205245
FBgn0261274	Ero1L	0.54773014	0.02232193	0.29205245
FBgn0085354	CG34325	-0.8720389	0.02239869	0.29268009
FBgn0085257	CG34228	0.82491964	0.02246939	0.29322703
FBgn0259936	Uhg3	-0.5437574	0.02260665	0.29464006
FBgn0284220	Top2	-0.8626349	0.02263662	0.2946528
FBgn0037750	Whamy	0.86148661	0.02268248	0.2948723
FBgn0086676	spin	-0.8316647	0.02273182	0.29513622
FBgn0024191	sip1	0.75442006	0.02277005	0.29518108
FBgn0053303	CG33303	-0.4503646	0.02279335	0.29518108
FBgn0039109	CG10365	-0.5013041	0.02290123	0.2958497
FBgn0037439	CG10286	-0.4859039	0.02297765	0.2958497
FBgn0267808	CR46133	0.86162681	0.02302313	0.2958497
FBgn0004107	Cdk2	-1.0975348	0.02303078	0.2958497
FBgn0033863	CG13337	1.60804811	0.02305398	0.2958497
FBgn0036363	CG10140	1.81530752	0.02307562	0.2958497
FBgn0038425	CG14881	-0.613804	0.02309867	0.2958497
FBgn0026428	HDAC6	0.56007672	0.02310256	0.2958497
FBgn0051793	CG31793	0.58576177	0.02311305	0.2958497
FBgn0264460	CR43868	0.7782324	0.02313599	0.2958497
FBgn0035270	CG13933	0.55915369	0.02321591	0.2962658
FBgn0017577	Mcm5	-1.2017501	0.02322682	0.2962658

FBgn0033605	CG9067	0.8436357	0.02328062	0.29657989
FBgn0266670	Sec5	0.43845582	0.02339952	0.2974321
FBgn0039325	CG10560	1.04768957	0.02340603	0.2974321
FBgn0266570	CG2982	-0.5164541	0.02345738	0.29771249
FBgn0051690	CG31690	0.86362543	0.0234944	0.29781051
FBgn0016797	fz2	-0.7549456	0.02360211	0.29880325
FBgn0259224	CG42324	1.41657487	0.02363842	0.29889083
FBgn0021872	Xbp1	0.61784757	0.02369785	0.29926997
FBgn0034569	dgt3	-1.6314663	0.0237313	0.29932062
FBgn0035727	CG10063	-0.6077472	0.02394922	0.30148458
FBgn0031881	MME1	0.9847384	0.02396218	0.30148458
FBgn0035263	CG12035	1.48498178	0.0240542	0.30157648
FBgn0050021	metro	-1.0598421	0.02407352	0.30157648
FBgn0004636	Rap1	0.44583874	0.02410627	0.30157648
FBgn0265575	yin	1.48809045	0.02410802	0.30157648
FBgn0030612	CG5599	-0.4753506	0.0241433	0.30157648
FBgn0031277	CG13947	-1.8393018	0.02414748	0.30157648
FBgn0066101	LpR1	3.05433212	0.02430022	0.30270025
FBgn0037354	CG12171	0.69699644	0.0243475	0.30270025
FBgn0085399	CG34370	-1.1484598	0.02439597	0.30270025
FBgn0036557	mRpS31	-0.452212	0.02440633	0.30270025
FBgn0039809	CG15547	0.50001524	0.02443509	0.30270025
FBgn0036386	CG8833	0.52699497	0.02443515	0.30270025
FBgn0026577	CG8677	0.44704365	0.02447027	0.30270025
FBgn0259101	CG42249	1.67394564	0.02447566	0.30270025
FBgn0050385	CG30385	1.47934052	0.02450639	0.30271196
FBgn0067864	Patj	0.44244398	0.02473727	0.30519301
FBgn0259738	CG42392	0.66560854	0.02476964	0.30521042
FBgn0053971	Ir62a	0.9710928	0.02485022	0.30521042
FBgn0038583	CG7183	0.54577919	0.02485038	0.30521042
FBgn0264978	Slh	0.70840109	0.02490828	0.30521042
FBgn0266633	CR45140	0.49928127	0.0249271	0.30521042
FBgn0052801	CG32801	-1.0630059	0.02493295	0.30521042
FBgn0013269	FK506-bp1	-0.4863339	0.02494884	0.30521042
FBgn0030499	CG11178	0.48414049	0.02507214	0.30635027
FBgn0267991	CR46258	-1.1398439	0.02512769	0.30643865
FBgn0266933	CR45384	-1.2722588	0.02513966	0.30643865
FBgn0065080	snoRNA:Me18S-A1374	-0.45497	0.02527536	0.30768373
FBgn0039254	Nmnat	0.69086172	0.02530234	0.30768373
FBgn0063497	GstE3	0.99470314	0.02534516	0.30783619

FBgn0063498	GstE2	1.06957792	0.02543264	0.30791879
FBgn0028360	Cdc7	-0.5752799	0.02545509	0.30791879
FBgn0032805	CG10337	0.49570135	0.02546261	0.30791879
FBgn0003358	Jon99Ci	1.98295539	0.02547312	0.30791879
FBgn0029689	CG6428	0.57175912	0.02553969	0.30800149
FBgn0260653	serp	1.69279524	0.02554055	0.30800149
FBgn0264962	Pcf11	-0.5527634	0.02560009	0.30803922
FBgn0032084	CG13101	-0.9075993	0.02562975	0.30803922
FBgn0030467	CG1764	-0.6397614	0.0256378	0.30803922
FBgn0261625	GLS	0.47189122	0.02566719	0.30803922
FBgn0004378	Klp61F	-0.75925	0.02571741	0.30803922
FBgn0032197	CG5694	-0.5105311	0.02572813	0.30803922
FBgn0053640	CG33640	1.14664843	0.02575579	0.30803922
FBgn0035065	CG3589	0.46422003	0.02587625	0.30809574
FBgn0020513	ade5	-0.5060042	0.02590562	0.30809574
FBgn0034282	Mapmodulin	-0.4872802	0.02590911	0.30809574
FBgn0063298	CR31429	-0.4826634	0.02594162	0.30809574
FBgn0266736	CR45209	-0.4854754	0.02597657	0.30809574
FBgn0032252	loh	0.89417797	0.02600264	0.30809574
FBgn0046685	Wsck	0.59875545	0.02602195	0.30809574
FBgn0037468	CG1943	0.44942949	0.02603428	0.30809574
FBgn0086906	sls	1.14115689	0.02603854	0.30809574
FBgn0261934	dikar	0.47127298	0.02611831	0.30809574
FBgn0015036	Cyp4ae1	1.33233716	0.02613063	0.30809574
FBgn0035300	CG1139	1.88025172	0.0261521	0.30809574
FBgn0283451	br	0.65899254	0.0261545	0.30809574
FBgn0265664	CR44471	1.59057923	0.02619661	0.30823471
FBgn0040078	pont	-0.4540249	0.0262388	0.30830821
FBgn0085732	CR40190	-0.444803	0.02628831	0.30830821
FBgn0053258	CG33258	3.50014299	0.02629384	0.30830821
FBgn0038365	CG9593	0.90468111	0.02636404	0.30877519
FBgn0033137	Tsp42Ep	-0.9449532	0.02639473	0.30877889
FBgn0266853	CR45314	1.96771051	0.02646985	0.30930174
FBgn0020224	Cbl	-0.4614971	0.02653879	0.30975127
FBgn0267679	CR46015	1.52203086	0.02660407	0.30983632
FBgn0029890	CG4095	-0.5201727	0.02666056	0.30983632
FBgn0037391	CG2017	0.84652972	0.02666091	0.30983632
FBgn0035941	CG13313	1.62081826	0.02666905	0.30983632
FBgn0028997	nmdyn-D7	-0.7277962	0.02669847	0.30983632
FBgn0038095	Cyp304a1	1.65130802	0.02678888	0.31050781

FBgn0031011	CG8034	0.48684976	0.02681742	0.31050781
FBgn0063494	GstE6	0.96839919	0.02694982	0.31134345
FBgn0031948	CG7149	-0.9815178	0.02695084	0.31134345
FBgn0264326	DNApol-epsilon255	-1.3778499	0.02698488	0.31138283
FBgn0032706	Irk3	-0.8451485	0.0271367	0.31277972
FBgn0266019	rudhira	0.5292078	0.02721811	0.3133628
FBgn0001233	Hsp83	-0.6407358	0.02732537	0.31375449
FBgn0003334	Scm	-0.424699	0.02736679	0.31375449
FBgn0033777	CG17574	0.48580474	0.02737073	0.31375449
FBgn0004390	RasGAP1	-0.7214683	0.02737559	0.31375449
FBgn0051956	pgant4	1.96596237	0.02745425	0.31430172
FBgn0010357	betaTry	2.18007671	0.02755991	0.31466004
FBgn0033075	Pld	0.44440503	0.0275888	0.31466004
FBgn0035889	mkg-p	0.54120547	0.02768172	0.31466004
FBgn0053057	CG33057	0.54120547	0.02768172	0.31466004
FBgn0285892	tea	-0.6877278	0.02768863	0.31466004
FBgn0022893	Df31	-0.7305179	0.02769651	0.31466004
FBgn0020493	Dad	-0.6895446	0.02772461	0.31466004
FBgn0050345	CG30345	0.69323742	0.02776293	0.31466004
FBgn0039118	CG10208	-0.6882233	0.02776412	0.31466004
FBgn0037153	olf413	1.04718539	0.02783797	0.31510819
FBgn0036740	Vps60	0.46917239	0.02788034	0.31510819
FBgn0040299	Myo28B1	0.50310371	0.02791608	0.31510819
FBgn0032377	CG14937	-2.0159479	0.02792765	0.31510819
FBgn0034113	CG8060	0.5972339	0.02811303	0.31673586
FBgn0052010	CR32010	1.04897362	0.0281517	0.31673586
FBgn0041627	Ku80	0.97605127	0.02817823	0.31673586
FBgn0262582	cic	-0.5575266	0.02822914	0.31673586
FBgn0030744	CG9992	-0.6139996	0.028245	0.31673586
FBgn0040493	grsm	-0.4477978	0.02826075	0.31673586
FBgn0002914	Myb	-0.4619802	0.02830258	0.31673586
FBgn0035209	msd1	-1.3414577	0.02832116	0.31673586
FBgn0052856	CG32856	-0.7625611	0.02842116	0.31750492
FBgn0264562	Hr4	0.67056916	0.02854103	0.3184941
FBgn0052040	CG32040	-0.5617709	0.0286488	0.31934615
FBgn0265071	CR44182	0.63500432	0.02876363	0.32027494
FBgn0036646	CR18217	-0.576633	0.02883569	0.32040052
FBgn0025454	Cyp6g1	2.05866746	0.02883794	0.32040052
FBgn0086408	stl	0.82610981	0.02887438	0.32045516
FBgn0034564	CG9344	-0.6060945	0.02897196	0.32087372

FBgn0260477	CG30283	-0.5311255	0.02902309	0.32087372
FBgn0052027	CR32027	-1.0792689	0.02902655	0.32087372
FBgn0264836	CG44044	1.07603926	0.0290674	0.32087372
FBgn0053523	CG33523	-0.5407871	0.02906991	0.32087372
FBgn0035670	CG10472	2.27709354	0.02910374	0.32089869
FBgn0032774	CG17549	1.86412303	0.02916485	0.32122412
FBgn0069056	CG33226	-0.9501131	0.02922084	0.32138418
FBgn0013772	Cyp6a8	1.44702349	0.0292739	0.32138418
FBgn0036240	CG6928	0.60729447	0.02927422	0.32138418
FBgn0264490	Eip93F	0.47527027	0.02936049	0.32198358
FBgn0259152	Clbn	0.60270862	0.02946767	0.32252987
FBgn0032358	Ppt2	0.49218572	0.02947376	0.32252987
FBgn0030691	Efhc1.1	-2.5976651	0.02955078	0.32302497
FBgn0040823	dpr6	0.97268243	0.02972339	0.32372553
FBgn0039525	CG5646	0.77227327	0.02973174	0.32372553
FBgn0250848	26-29-p	-0.4839317	0.02976839	0.32372553
FBgn0036354	Poc1	-0.6657145	0.0297727	0.32372553
FBgn0036298	nst	0.56466871	0.02978573	0.32372553
FBgn0086668	snoRNA:Psi28S-3436a	-1.4846785	0.0298376	0.32372553
FBgn0015568	alpha-Est1	1.10114808	0.02985397	0.32372553
FBgn0265830	CR44619	-0.8437709	0.02986962	0.32372553
FBgn0028539	CG31731	0.48152583	0.02998312	0.3246096
FBgn0034030	CG8192	0.89347882	0.03007886	0.32529971
FBgn0262870	axo	2.1215504	0.03017955	0.32571965
FBgn0003008	or	0.67275685	0.03018674	0.32571965
FBgn0032733	CG15170	1.19654109	0.03021573	0.32571965
FBgn0029896	CG3168	-1.4725747	0.03024585	0.32571965
FBgn0026415	Idgf4	2.20766205	0.03028862	0.32583508
FBgn0283467	Pol32	-0.6287994	0.03044138	0.32713224
FBgn0265186	CG44251	0.59839796	0.03061058	0.32860314
FBgn0033081	geminin	-0.5109884	0.03064868	0.32866504
FBgn0032726	CG10621	1.57916442	0.03076021	0.32951349
FBgn0010786	l(3)02640	1.09782164	0.03082084	0.32981548
FBgn0260798	Gprk1	-0.5144465	0.03086368	0.32992656
FBgn0002609	E(spl)m3-HLH	-0.8915063	0.03117039	0.33285526
FBgn0038398	sxe2	1.35060727	0.03125121	0.33336812
FBgn0262141	CG42867	0.85267886	0.03132239	0.3334507
FBgn0034142	CG8306	-0.4840432	0.03132455	0.3334507
FBgn0264855	AP-2alpha	-0.4878492	0.03136147	0.33349441
FBgn0038129	TBC1D5	-0.5163941	0.03139976	0.33355273

FBgn0024432	Dlc90F	0.4290672	0.03144317	0.33366524
FBgn0030725	CG8958	-0.9765728	0.03154633	0.33441079
FBgn0031078	Nup205	-1.1237382	0.03171248	0.33527717
FBgn0027518	Wdr24	-0.7950421	0.03171814	0.33527717
FBgn0036684	CG3764	-0.439527	0.031727	0.33527717
FBgn0032453	CG6180	-0.485318	0.03177825	0.33534168
FBgn0053468	CG33468	1.22094158	0.03179907	0.33534168
FBgn0039087	CG10168	0.94519491	0.03193463	0.33618182
FBgn0039829	CG15561	-0.5701171	0.03194668	0.33618182
FBgn0027548	nito	-0.4651729	0.03197795	0.33618182
FBgn0259227	CG42327	1.41330088	0.03210209	0.33713832
FBgn0037555	Ada2b	0.45103953	0.03215826	0.33737967
FBgn0034915	eIF6	0.71028082	0.03223165	0.33765881
FBgn0010173	RpA-70	0.81272695	0.03228311	0.33765881
FBgn0043853	scaRNA:MeU5-C46	-1.5014982	0.03228451	0.33765881
FBgn0260243	E(var)3-9	-0.5400929	0.03233273	0.3378155
FBgn0027537	Nup93-1	-0.4347192	0.03249381	0.33914999
FBgn0051463	CG31463	1.19559958	0.03263358	0.34025942
FBgn0032401	Plzf	0.76914596	0.03267153	0.34030615
FBgn0086704	stops	1.21166032	0.03274706	0.34074376
FBgn0015766	Msr-110	2.29023821	0.03278566	0.34078512
FBgn0266331	CR44996	1.58519569	0.03281808	0.34078512
FBgn0025697	santa-maria	1.91567146	0.03287578	0.34103592
FBgn0036405	CG6833	-0.4664256	0.03300431	0.34202018
FBgn0266421	RPA3	0.86073784	0.03309383	0.34227103
FBgn0039380	CG5890	2.24803822	0.03310262	0.34227103
FBgn0065032	Arpc3B	0.56507521	0.03312952	0.34227103
FBgn0261822	Bsg	0.42661352	0.03318014	0.34232777
FBgn0029587	CG14797	-0.9081267	0.03320236	0.34232777
FBgn0034046	tun	-0.4816928	0.03329006	0.34248198
FBgn0267516	pre-rRNA-Psi:CR45856	1.17365808	0.0332965	0.34248198
FBgn0037025	Spc105R	-1.3317742	0.03331838	0.34248198
FBgn0037150	CG7133	-0.4334027	0.03343231	0.34330595
FBgn0039145	CG6000	0.78181107	0.03349272	0.34342078
FBgn0034432	CG7461	0.46731691	0.03351106	0.34342078
FBgn0260741	CG3281	0.57304096	0.03355065	0.34348023
FBgn0037251	CG9804	-0.5453389	0.0336537	0.34360986
FBgn0262962	CG43273	1.02079264	0.03366079	0.34360986
FBgn0085452	CG34423	0.77286865	0.03366471	0.34360986
FBgn0031062	CG14230	-0.4822375	0.03388052	0.34534244

FBgn0264908	pHCl-1	1.21441152	0.0339024	0.34534244
FBgn0031824	CG9547	-0.4366043	0.03406748	0.34601096
FBgn0053140	CG33140	2.19240518	0.03409396	0.34601096
FBgn0260006	drd	1.42872567	0.03410676	0.34601096
FBgn0033124	Tsp42Ec	1.02982474	0.03420013	0.34601096
FBgn0028336	l(1)G0255	-0.4533833	0.03420066	0.34601096
FBgn0264906	CR44097	0.77970938	0.03423963	0.34601096
FBgn0003483	spn-E	-1.8319977	0.03427012	0.34601096
FBgn0085446	CG34417	1.20978897	0.03429064	0.34601096
FBgn0265961	CR44748	-0.611626	0.03429839	0.34601096
FBgn0264351	CR43807	1.52528763	0.03430839	0.34601096
FBgn0286006		-0.9868916	0.03435361	0.3461237
FBgn0038013	CG10038	-0.5614925	0.03446388	0.34643746
FBgn0265042	Irk1	0.57892749	0.03447034	0.34643746
FBgn0050015	CG30015	-0.577118	0.03450227	0.34643746
FBgn0011659	Mlh1	-0.5903795	0.03452106	0.34643746
FBgn0030410	Aven	0.65054373	0.03460298	0.34691707
FBgn0035689	CG7376	0.69904813	0.0346644	0.34719047
FBgn0284226	CG46310	0.58008267	0.03485185	0.34820311
FBgn0038640	CG7706	0.55955204	0.03488605	0.34820311
FBgn0050486	CG30486	-0.7397423	0.03491058	0.34820311
FBgn0035211	CG2211	0.73180115	0.03493504	0.34820311
FBgn0061476	Zwilch	-0.9173269	0.03494479	0.34820311
FBgn0265978	CR44757	-0.9808235	0.03497102	0.34820311
FBgn0003300	run	1.26148299	0.03510831	0.34915007
FBgn0039588	mIF2	0.59729592	0.03515035	0.34915007
FBgn0027949	msb1l	-0.7537464	0.03516916	0.34915007
FBgn0087035	AGO2	0.4824276	0.03521986	0.34931225
FBgn0035159	CG13896	0.72710965	0.03529009	0.34966774
FBgn0036997	CG5955	-1.6569516	0.03540701	0.35048454
FBgn0028342	ATPsyndelta	-0.4256869	0.0354416	0.35048573
FBgn0052251	Claspin	-1.1336368	0.03548624	0.35058614
FBgn0264087	Slob	0.63310156	0.03554631	0.35083866
FBgn0035517	CG1265	0.62268026	0.03564359	0.35119597
FBgn0031042	CG14221	-0.9728495	0.03565468	0.35119597
FBgn0266993	CR45444	-1.2164202	0.03574152	0.35119597
FBgn0035083	Tina-1	-0.4712441	0.03575147	0.35119597
FBgn0039459	IntS12	0.52935633	0.03579356	0.35119597
FBgn0030912	CG6023	-1.0228648	0.0358007	0.35119597
FBgn0011768	Fdh	-0.4787434	0.03582434	0.35119597

FBgn0014861	Mcm2	-0.722059	0.03598598	0.35244075
FBgn0004552	Akh	-1.0400289	0.0360511	0.35273866
FBgn0034797	nahoda	0.64342065	0.03609832	0.35286109
FBgn0020633	Mcm7	-1.401084	0.03624548	0.3539592
FBgn0261560	Thor	0.56025265	0.03637217	0.35485553
FBgn0028467	CG11070	0.43841173	0.03640984	0.35488253
FBgn0004646	ogre	-0.8681464	0.03653665	0.35512875
FBgn0082988	snoRNA:Psi28S-2442b	-0.7326581	0.0365477	0.35512875
FBgn0033692	wash	0.45245124	0.03654839	0.35512875
FBgn0035957	CG5144	1.49164735	0.03657484	0.35512875
FBgn0035039	Adck	0.69392104	0.0367399	0.35639109
FBgn0031516	CG9663	0.66801564	0.03682832	0.35670362
FBgn0031393	CG15382	-0.7672796	0.03691187	0.35670362
FBgn0038221	CG3259	-0.9921166	0.03693556	0.35670362
FBgn0037630	Ir85a	0.89138926	0.03693895	0.35670362
FBgn0054021	CG34021	-1.1135335	0.03695592	0.35670362
FBgn0016041	Tom40	-0.396817	0.03698265	0.35670362
FBgn0042133	CG18810	-1.3420022	0.03708561	0.35720181
FBgn0040388	boi	-0.8505738	0.03710458	0.35720181
FBgn0037517	CG10086	0.60874544	0.03715242	0.357205
FBgn0025626	CG4281	-0.4430073	0.03717518	0.357205
FBgn0053002	mRpL27	-0.5441401	0.0372521	0.35760608
FBgn0037185	CG11367	-0.5678668	0.03743587	0.35903115
FBgn0010039	GstD3	1.0315825	0.03747979	0.35911365
FBgn0030841	CG8568	-1.1465994	0.0376233	0.36006904
FBgn0000256	capu	1.05878309	0.03765034	0.36006904
FBgn0035286	CG13924	-1.8509874	0.03773788	0.36033225
FBgn0027539	lili	-0.5485968	0.03775532	0.36033225
FBgn0030085	CG6999	-1.6576658	0.0377842	0.36033225
FBgn0035855	CG7366	-1.8022939	0.03788217	0.36092801
FBgn0003356	Jon99Cii	1.90673261	0.03792004	0.36095051
FBgn0029861	CG3815	-0.4354368	0.03796004	0.36099323
FBgn0051935	CG31935	0.57773151	0.03800218	0.36105626
FBgn0050357	CG30357	-0.5355084	0.03808727	0.36134123
FBgn0265982	CR44761	-0.7714186	0.03810327	0.36134123
FBgn0038974	CG5377	0.7273668	0.03818072	0.36173832
FBgn0037845	CG14694	1.77309274	0.03822258	0.36179768
FBgn0003357	Jon99Ciii	1.88889951	0.03832503	0.36212695
FBgn0000617	e(y)1	-0.4765295	0.03835395	0.36212695
FBgn0051643	CG31643	0.63228374	0.03836423	0.36212695

FBgn0266362	CR45010	0.95371214	0.03842776	0.36216202
FBgn0023171	rnh1	-0.4556168	0.03843919	0.36216202
FBgn0050392	CG30392	0.54939007	0.03847854	0.36219711
FBgn0031693	Cyp4ac1	1.63668786	0.03855748	0.3626044
FBgn0266526	CG45093	0.41521292	0.03862901	0.36260624
FBgn0050497	CG30497	0.41521292	0.03862901	0.36260624
FBgn0086051	snoRNA:Me28S-U2134a	-0.9624707	0.03872478	0.36316985
FBgn0031769	CG9135	-0.5390325	0.0389548	0.36484031
FBgn0031401	papi	-0.436555	0.03905963	0.36484031
FBgn0034948	PPP1R15	0.46234853	0.03907971	0.36484031
FBgn0261286	Mat89Ba	-0.4772788	0.03908398	0.36484031
FBgn0040285	Scamp	0.44761111	0.03911418	0.36484031
FBgn0038530	AttD	1.40394239	0.03911823	0.36484031
FBgn0034249	RhoGAP54D	1.02639855	0.03922282	0.36548042
FBgn0002466	sti	-0.829911	0.03932577	0.36610421
FBgn0051072	Lerp	0.71154288	0.03945939	0.36701205
FBgn0001085	fz	0.62311665	0.0395934	0.36737364
FBgn0082927	snoRNA:Me28S-G3255b	-1.4288481	0.03960395	0.36737364
FBgn0003701	thr	-0.8501213	0.03960778	0.36737364
FBgn0031450	Hrs	0.39158418	0.03964847	0.36737364
FBgn0261553	CG42671	0.6200099	0.03967895	0.36737364
FBgn0013305	Nmda1	0.47541977	0.03978512	0.36796424
FBgn0038294	Mf	1.76240129	0.03981514	0.36796424
FBgn0035176	CG13905	-1.7299637	0.03997515	0.3691075
FBgn0263769	CR43686	0.93556846	0.04003727	0.36931014
FBgn0035697	CG10163	1.57650068	0.04006975	0.36931014
FBgn0034293	CG14495	1.71667867	0.0402379	0.37052404
FBgn0030915	CG6179	-0.4516677	0.04031856	0.37093076
FBgn0050340	CG30340	0.96000523	0.04040549	0.37139437
FBgn0033465	Etf-QO	0.58691257	0.04056994	0.37256908
FBgn0035231	Pcyt2	-0.638866	0.04069833	0.3734109
FBgn0031683	CG4230	0.4281733	0.04084836	0.37444939
FBgn0267531	CR45871	-1.4433369	0.04109907	0.3762768
FBgn0052026	CG32026	-1.1692885	0.04114323	0.3762768
FBgn0260450	CalpC	-0.4218555	0.04118551	0.3762768
FBgn0034137	CG4945	-0.7984607	0.04119576	0.3762768
FBgn0036353	CG10171	-0.5291765	0.04144578	0.37794254
FBgn0034583	CG10527	-0.542265	0.04145248	0.37794254
FBgn0263597	Acp98AB	-0.6841986	0.04158204	0.37873009

FBgn0033737	Nup54	-0.6212601	0.04161337	0.37873009
FBgn0040257	Ugt86Dc	0.52382507	0.04175581	0.37962273
FBgn0036915	Prp3	-0.4623107	0.04178613	0.37962273
FBgn0036775	CG5147	-0.4077794	0.04191798	0.38048056
FBgn0037703	JHDM2	-0.4063781	0.04205895	0.38141949
FBgn0037521	CG2993	-0.7681726	0.04222988	0.38255844
FBgn0039319	CG13659	1.07213285	0.0422598	0.38255844
FBgn0034527	CG9945	0.40167193	0.04241918	0.38326558
FBgn0031904	CG5149	-0.4978703	0.04243325	0.38326558
FBgn0035960	CG4942	0.70526012	0.04245102	0.38326558
FBgn0039183	Dis3	-0.5067635	0.04257246	0.38402093
FBgn0030803	CG4880	-0.6970254	0.04262935	0.38419327
FBgn0034935	Orcokinin	0.86781775	0.04280136	0.38540177
FBgn0052687	CG32687	1.3373718	0.04300883	0.38692727
FBgn0030679	CG8206	0.66837106	0.04318939	0.3882081
FBgn0082989	snoRNA:Psi28S-2442a	-0.7009217	0.04330928	0.3889418
FBgn0040477	cid	-1.3515283	0.04336438	0.38909296
FBgn0285925		1.38922984	0.04344497	0.38947231
FBgn0026083	tyf	0.43334772	0.04358223	0.3900951
FBgn0036337	AdenoK	-0.4294216	0.04359119	0.3900951
FBgn0259148	CG42263	-0.8898519	0.04369479	0.39061651
FBgn0053318	CR33318	1.00580295	0.0437263	0.39061651
FBgn0032154	mtDNA-helicase	-0.4964583	0.04378308	0.39078033
FBgn0026374	Rhp	0.92634985	0.04385626	0.39088509
FBgn0027844	CAH1	0.76428599	0.04389113	0.39088509
FBgn0054045	CG34045	0.62586489	0.04396446	0.39088509
FBgn0003302	rux	-0.6229785	0.04399791	0.39088509
FBgn0051140	CG31140	0.6050666	0.04403937	0.39088509
FBgn0031497	SerRS	0.72372229	0.04405101	0.39088509
FBgn0034058	Pex11	0.48624078	0.04406397	0.39088509
FBgn0031630	CG15629	-0.8151678	0.04417915	0.39156516
FBgn0037566	mRpL1	-0.4411069	0.0442177	0.39156546
FBgn0002069	AspRS	0.64128142	0.04429332	0.39189369
FBgn0261085	Syt12	-1.5721369	0.04435477	0.39209619
FBgn0035805	CG7506	0.82799052	0.04444631	0.39256401
FBgn0050069	CG30069	0.81543747	0.04455492	0.39265311
FBgn0037151	CG7130	1.10378	0.04470692	0.39265311
FBgn0050491	CG30491	0.59397466	0.0447116	0.39265311
FBgn0044872	FucTC	0.86337677	0.04471468	0.39265311
FBgn0038845	CG10827	1.79937179	0.04475251	0.39265311

FBgn0011205	fbl	0.61142006	0.04478701	0.39265311
FBgn0035073	CG16896	-0.6829332	0.04478995	0.39265311
FBgn0035622	TM9SF3	-0.4115228	0.044811	0.39265311
FBgn0037483	CG14609	-1.4867498	0.04482681	0.39265311
FBgn0039084	CG10175	-0.555311	0.04484264	0.39265311
FBgn0035401	CG1291	0.50239846	0.04508203	0.39419065
FBgn0040723	CG5011	1.30722292	0.04509578	0.39419065
FBgn0038402	Fer2	-0.6933311	0.04520275	0.39478622
FBgn0263979	Caf1-55	-0.4453564	0.04541607	0.39616593
FBgn0022382	Pka-R2	0.83311656	0.04546083	0.39616593
FBgn0051158	Efa6	-0.5314341	0.04547764	0.39616593
FBgn0034360	CG10927	-0.4351924	0.04557131	0.39664208
FBgn0033853	CG6145	0.49241215	0.04572241	0.39761676
FBgn0032298	CG6724	-0.4184085	0.04581117	0.39804821
FBgn0037549	CG7878	-0.424574	0.04587862	0.39817088
FBgn0030683	CG8239	-0.423799	0.04597251	0.39817088
FBgn0031392	AIF	-0.5138302	0.04599454	0.39817088
FBgn0039219	CG13630	-0.4560474	0.04600925	0.39817088
FBgn0038257	smp-30	1.56930495	0.04602113	0.39817088
FBgn0031611	FIG4	0.56116865	0.04610528	0.39826071
FBgn0065097	snmRNA:357	2.11779488	0.04622689	0.39826071
FBgn0260632	dl	-0.4745544	0.04629209	0.39826071
FBgn0010240	Lcch3	-0.6018482	0.04629807	0.39826071
FBgn0031707	CG14020	0.65299298	0.04637042	0.39826071
FBgn0035715	CG10103	0.48372606	0.04637258	0.39826071
FBgn0051373	CG31373	-0.7707291	0.0463752	0.39826071
FBgn0035167	Gr61a	-1.0008513	0.04639335	0.39826071
FBgn0038032	CG10096	2.18312281	0.04646513	0.39826071
FBgn0038033	CG10097	2.18312281	0.04646513	0.39826071
FBgn0038598	CG7131	-0.8045314	0.04650699	0.39826071
FBgn0032393	CG12264	0.58912403	0.04656674	0.39826071
FBgn0032042	CG13398	0.40451976	0.04657418	0.39826071
FBgn0036702	CG6512	0.5708305	0.04661479	0.39826071
FBgn0031050	Arp10	-0.4069929	0.04661915	0.39826071
FBgn0263080	CG43348	1.56210092	0.04684113	0.39917476
FBgn0267813	CR46138	-0.4167266	0.046883	0.39917476
FBgn0011774	Irbp	0.52301641	0.04688325	0.39917476
FBgn0004861	ph-p	-0.6528789	0.04695065	0.39917476
FBgn0037560	CR18228	0.60668612	0.0471092	0.39917476
FBgn0002932	neur	-0.4116688	0.04712574	0.39917476

FBgn0024947	NTPase	0.74859976	0.04716677	0.39917476
FBgn0040392	CG14050	-1.1078401	0.04717318	0.39917476
FBgn0039751	CG1983	0.58232543	0.04719004	0.39917476
FBgn0011638	La	0.53365331	0.04720295	0.39917476
FBgn0266681	CR45171	-0.7910194	0.04725248	0.39917476
FBgn0015277	Pi3K59F	0.39956716	0.04728477	0.39917476
FBgn0265340	CR44294	0.78038293	0.04730214	0.39917476
FBgn0035160	hng3	0.72893957	0.04735717	0.39917476
FBgn0264775	CG44013	2.50290629	0.04738123	0.39917476
FBgn0267758	CR46089	0.73870767	0.04738715	0.39917476
FBgn0001142	Gs1	-0.7662138	0.04739366	0.39917476
FBgn0024734	PRL-1	0.42482985	0.04765759	0.40039215
FBgn0051446	CG31446	1.41737771	0.04767157	0.40039215
FBgn0031746	CG9029	-1.2450275	0.04769187	0.40039215
FBgn0015351	CG14906	0.48282821	0.04769574	0.40039215
FBgn0040361	CG14627	0.69415409	0.04787385	0.40155578
FBgn0016754	sba	-0.4629657	0.04792688	0.40166912
FBgn0034091	mrj	-0.4645686	0.04799466	0.40177375
FBgn0083940	RhoU	-0.7536707	0.0480184	0.40177375
FBgn0030177	CG2972	-0.4384882	0.0481078	0.40205955
FBgn0265590	CR44417	0.59398681	0.04813784	0.40205955
FBgn0031690	CG7742	0.85604771	0.04817121	0.40205955
FBgn0029512	Aos1	-0.4664034	0.0482395	0.40229922
FBgn0051694	CG31694	0.46618071	0.04837681	0.40311366
FBgn0034045	CG8249	1.22908762	0.0485056	0.40339386
FBgn0020388	Gcn5	0.6195723	0.04850781	0.40339386
FBgn0265699	CR44506	1.31951682	0.04856438	0.40339386
FBgn0003386	Shaw	0.89374239	0.04856916	0.40339386
FBgn0000351	cort	-0.740662	0.04861291	0.40342764
FBgn0052350	Vps11	0.41331659	0.04872881	0.40405959
FBgn0039044	p53	0.59565225	0.04891201	0.40500184
FBgn0015513	mbc	-0.7216382	0.04892271	0.40500184
FBgn0266634	CR45141	0.63722817	0.04898565	0.40500184
FBgn0015391	glu	-0.7040017	0.0490018	0.40500184
FBgn0001321	knk	-1.7295295	0.04907986	0.40531753
FBgn0031298	Atg4a	0.52623643	0.0491723	0.40575134
FBgn0014033	Sr-CI	-0.8030065	0.0494429	0.40729723
FBgn0261808	cu	0.46353682	0.04947582	0.40729723
FBgn0265053	CR44168	0.81827046	0.04951716	0.40729723
FBgn0265512	mlt	0.38966485	0.04952596	0.40729723

FBgn0085484	Pdxk	0.82490329	0.04955997	0.40729723
FBgn0030091	CG7065	-0.4539755	0.04972588	0.40737855
FBgn0261439	SdhA	-0.3684355	0.04972985	0.40737855
FBgn0051864	Qtzl	0.94154775	0.04974195	0.40737855
FBgn0259221	CG42321	-0.4943809	0.04974447	0.40737855
FBgn0016081	fry	0.40088584	0.04977023	0.40737855
FBgn0263930	dally	-0.5259328	0.04982365	0.40748769
FBgn0267484	CR45834	0.61071866	0.04987868	0.40760985
FBgn0085425	CG34396	1.37946032	0.04995016	0.40786613

Table A-1. Fly genes with different expression levels between mock infected flies and those infected with WT C6706 as determined with a P-value of >0.05. FBgn – Fly Base gene name. LogFC – log fold change. FDR – false discovery rate.

FBgn	**Gene Name**	**logFC**	**PValue**	**FDR**
FBgn0030261	CG15203	2.21995812	2.98E-08	0.00030248
FBgn0005670	Cyp4d1	2.80595269	2.04E-06	0.0103569
FBgn0031248	CG11912	4.94828613	3.19E-06	0.01079831
FBgn0037850	CG14695	1.9500492	1.66E-05	0.04223436
FBgn0031981	CG7466	-1.6184565	4.10E-05	0.08345288
FBgn0032266	CG18302	2.07533013	8.09E-05	0.12740811
FBgn0040950	Muc26B	-1.7849781	9.96E-05	0.12740811
FBgn0031649	hoe2	2.26416719	0.00010026	0.12740811
FBgn0032602	ppk17	1.87088155	0.00013343	0.14876856
FBgn0040813	Nplp2	1.09357871	0.00014634	0.14876856
FBgn0039821	CG15556	-1.4498261	0.00027247	0.25181555
FBgn0085813	18SrRNA-Psi:CR41602	-3.2872446	0.00031778	0.26920894
FBgn0023495	Lip3	2.15956458	0.00048364	0.3561333
FBgn0036953	CG17145	-3.8516162	0.00053691	0.3561333
FBgn0082937	snoRNA:Me28S-C2645b	1.66932151	0.00054712	0.3561333
FBgn0046874	Pif1B	1.11307749	0.0005629	0.3561333
FBgn0261015	Pif1A	1.11599339	0.00059554	0.3561333
FBgn0035495	CG14989	1.36543057	0.00082263	0.46460349
FBgn0038173	Adgf-C	-2.317257	0.00110284	0.56840572
FBgn0022774	Oat	-2.3463561	0.00111825	0.56840572
FBgn0032336	AstC	1.14844986	0.00144388	0.64153327
FBgn0035041	CG13594	1.24532554	0.00146956	0.64153327
FBgn0030358	CG10362	1.90434561	0.00157439	0.64153327
FBgn0264877	CR44068	-3.1067419	0.00159518	0.64153327
FBgn0032590	CG4631	-2.6957858	0.00162976	0.64153327

FBgn0035917	Zasp66	2.24290682	0.00164075	0.64153327
FBgn0265535	CG44385	2.40204791	0.00174431	0.65676434
FBgn0037630	Ir85a	1.44707532	0.00185337	0.67290481
FBgn0000644	Fcp3C	-1.2805251	0.00221346	0.77593128
FBgn0015001	iotaTry	1.20302693	0.0024693	0.81051009
FBgn0002773	Mlc2	1.42624316	0.00247155	0.81051009
FBgn0085481	CG34452	1.97583677	0.00260859	0.82699365
FBgn0039341	CG5112	-0.7851857	0.00269153	0.82699365
FBgn0265068	CR44179	-0.7908092	0.00276587	0.82699365
FBgn0038365	CG9593	1.30281229	0.00288948	0.83927077
FBgn0031910	CG15818	-5.0324739	0.00329976	0.87716508
FBgn0031533	CG2772	2.09965751	0.00332677	0.87716508
FBgn0267551	CR45891	1.27813778	0.00335378	0.87716508
FBgn0054045	CG34045	0.99487152	0.00336508	0.87716508
FBgn0033945	CG12868	1.06482686	0.0037315	0.92665153
FBgn0010549	l(2)03659	-1.1283667	0.00373723	0.92665153
FBgn0034935	Orcokinin	1.33858312	0.00408125	0.98465806
FBgn0005677	dac	1.32839344	0.00422207	0.98465806
FBgn0053140	CG33140	3.14503244	0.00426175	0.98465806
FBgn0028534	CG7916	1.79376738	0.00455525	1
FBgn0032066	LManIII	2.63544914	0.0046588	1
FBgn0010329	Tbh	1.31102777	0.0046904	1
FBgn0038973	Pebp1	-2.287141	0.00472617	1
FBgn0028863	CG4587	1.58771473	0.00507311	1
FBgn0087021	Spc25	-1.8757993	0.00541487	1
FBgn0263980	CG43729	1.1059644	0.00557118	1
FBgn0030587	CG9522	-3.6687445	0.00580276	1
FBgn0036833	CG3819	4.44469561	0.00596319	1
FBgn0043470	lambdaTry	1.40112848	0.00597131	1
FBgn0004169	up	1.1628147	0.00600563	1
FBgn0033540	Elp2	-1.07016	0.00644043	1
FBgn0259998	CG17571	2.20139403	0.00650109	1
FBgn0003499	sr	-1.6336201	0.00653961	1
FBgn0033458	CG18446	1.1494703	0.00660767	1
FBgn0263763	CG43680	-2.1767517	0.00685888	1
FBgn0051463	CG31463	1.62933066	0.00692014	1
FBgn0004878	cas	1.53436529	0.00713208	1
FBgn0266933	CR45384	-1.8924647	0.0071516	1
FBgn0013275	Hsp70Aa	-1.0873229	0.0071882	1
FBgn0001226	Hsp27	-1.7254583	0.00725138	1

FBgn0264815	Pde1c	1.01244566	0.00742974	1
FBgn0053306	CG33306	2.01305608	0.00750822	1
FBgn0031091	Phf7	1.20897477	0.00766776	1
FBgn0037534	CG2781	-1.4128965	0.00775579	1
FBgn0013276	Hsp70Ab	-1.0013531	0.00778733	1
FBgn0042205	CG18764	-0.8897166	0.00785549	1
FBgn0040658	CG13516	-0.9168825	0.0082851	1
FBgn0036150	Ir68a	-2.1230951	0.00849237	1
FBgn0031837	DIP-iota	-0.9951396	0.00859693	1
FBgn0030777	CG9672	-2.8571133	0.00874555	1
FBgn0036574	elg1	-1.0113814	0.00883962	1
FBgn0039486	caix	-1.7882343	0.00932951	1
FBgn0014007	Ptp69D	-0.6999458	0.00933501	1
FBgn0032856	CG16798	-1.4855374	0.00942812	1
FBgn0002772	Mlc1	2.35677686	0.00959433	1
FBgn0033072	CG17994	-2.3388302	0.00969622	1
FBgn0005664	Crys	1.67268272	0.00972182	1
FBgn0036715	Cad74A	2.33596061	0.00973572	1
FBgn0283471	wupA	2.13790929	0.00995206	1
FBgn0082949	snoRNA:Me18S-U1356a	1.49501988	0.01004199	1
FBgn0031653	Jon25Biii	1.46938985	0.01005621	1
FBgn0033778	CG3790	-1.679717	0.01032112	1
FBgn0265831	CR44620	2.31886792	0.01052726	1
FBgn0085460	CG34431	-1.7508312	0.01060417	1
FBgn0000473	Cyp6a2	-2.9651541	0.01081435	1
FBgn0263446	CR43469	-1.6366011	0.01143975	1
FBgn0001224	Hsp23	-1.4285189	0.01148628	1
FBgn0035838	ldbr	-1.2280305	0.01159029	1
FBgn0035669	CG6592	2.32999461	0.0116267	1
FBgn0037409	Osi24	0.95201077	0.01185044	1
FBgn0037176	CG14456	-2.2380096	0.01256582	1
FBgn0051956	pgant4	2.3696314	0.01275961	1
FBgn0262719	CG43163	-1.8646231	0.0131358	1
FBgn0033661	CG13185	-0.7758821	0.01323669	1
FBgn0032033	CG13392	-1.1668477	0.01358002	1
FBgn0004880	scrt	1.77556765	0.01378717	1
FBgn0032252	loh	1.0703617	0.01445752	1
FBgn0085415	CG34386	1.45073237	0.01463753	1
FBgn0030855	CG5800	0.76795985	0.01478423	1

FBgn0035103	Vdup1	-2.5040332	0.01488963	1
FBgn0032922	CG9249	-0.8433615	0.01516199	1
FBgn0031249	CG11911	1.44269153	0.01532151	1
FBgn0038658	CG14292	-1.5979865	0.0153465	1
FBgn0003380	Sh	-0.9644127	0.01551563	1
FBgn0038903	RpI12	0.7131691	0.01574322	1
FBgn0261085	Syt12	-2.3206236	0.01593601	1
FBgn0035756	unc-13-4A	0.7498304	0.016102	1
FBgn0038878	CG3301	-1.2723677	0.01631275	1
FBgn0029995	CG2256	-1.6642538	0.01691955	1
FBgn0031515	CG9664	0.8027943	0.01726331	1
FBgn0050049	CG30049	-0.8029554	0.01784867	1
FBgn0082981	snoRNA:Psi28S-2949	1.3065446	0.01793614	1
FBgn0029909	mAChR-C	0.79843142	0.01799798	1
FBgn0002917	na	-1.9897457	0.0183837	1
FBgn0263206	CG43376	0.94451659	0.01839287	1
FBgn0034529	FAM21	-0.7248998	0.01855156	1
FBgn0039052	CG6733	-1.6911053	0.01899639	1
FBgn0035154	CG3344	-3.6955604	0.01924352	1
FBgn0266862	CR45323	1.57874178	0.01982006	1
FBgn0027780	U26	-0.5314744	0.01999759	1
FBgn0013277	Hsp70Ba	-1.0952236	0.02000707	1
FBgn0039844	CG1607	-1.8492153	0.02011276	1
FBgn0032253	LManI	2.83465963	0.02024043	1
FBgn0039049	CG6726	-0.6843682	0.02031494	1
FBgn0261625	GLS	0.53961824	0.02046314	1
FBgn0039050	CG17110	-0.6727355	0.02057673	1
FBgn0001145	Gs2	-1.626194	0.02059305	1
FBgn0085400	CG34371	1.36569858	0.02105215	1
FBgn0083124	Uhg4	0.55970064	0.02117172	1
FBgn0041111	lilli	-0.5775791	0.02122381	1
FBgn0263771	CR43688	-2.4841751	0.02155609	1
FBgn0267990	CR46257	0.57044657	0.0220394	1
FBgn0039761	CG18404	-4.2642074	0.02212287	1
FBgn0033876	Syngr	-1.0597659	0.02226822	1
FBgn0020294	ko	-1.3639323	0.02234892	1
FBgn0037669	Ibf2	-1.1135482	0.0227873	1
FBgn0259162	RunxB	-2.3549179	0.02330078	1
FBgn0040297	Nhe2	-0.672062	0.02346308	1
FBgn0030724	Nipsnap	-0.6633604	0.02355535	1

FBgn0036742	CG7497	-0.8108883	0.02355741	1
FBgn0030725	CG8958	-1.2039472	0.02371242	1
FBgn0011555	thetaTry	-3.5437431	0.0237361	1
FBgn0031961	CG7102	-1.3038878	0.02385278	1
FBgn0027608	CG2082	-0.5379124	0.02387256	1
FBgn0001225	Hsp26	-1.3434031	0.02416036	1
FBgn0065107	snmRNA:128	-0.9263553	0.0244981	1
FBgn0266405	CR45045	1.30922788	0.02499732	1
FBgn0267991	CR46258	-1.3596431	0.02507337	1
FBgn0001230	Hsp68	-1.1943163	0.02542831	1
FBgn0034885	Eglp4	-1.9905445	0.02568289	1
FBgn0259740	CG42394	0.61790593	0.02621562	1
FBgn0051547	CG31547	1.14010463	0.02626272	1
FBgn0041336	Cyp6t2Psi	1.88869311	0.02639269	1
FBgn0051953	CR31953	-1.1000738	0.02646893	1
FBgn0039696	CG7837	-1.1254802	0.02647284	1
FBgn0038582	CG7988	0.59721013	0.02648472	1
FBgn0039355	CG4730	0.67291262	0.02688693	1
FBgn0001228	CG4456	-1.2135797	0.02691319	1
FBgn0001223	Hsp22	-1.2135766	0.02694019	1
FBgn0025387	CG12184	-1.4581217	0.02695642	1
FBgn0040342	CG3706	1.3472906	0.02704154	1
FBgn0263659	CR43650	-0.7692592	0.02716943	1
FBgn0041780	Ssl2	-1.0336509	0.02755569	1
FBgn0040359	CG11380	1.04475776	0.02830789	1
FBgn0029986	CG15332	-1.9299315	0.02831358	1
FBgn0036836	CG11619	-0.7235004	0.02841482	1
FBgn0262405	mir-998	-1.0557292	0.02842055	1
FBgn0037719	bocks	0.67664087	0.02851071	1
FBgn0037760	FBXO11	0.45221822	0.02892658	1
FBgn0039920	CG11360	-0.5984606	0.0290746	1
FBgn0030028	Corp	1.08420875	0.02919455	1
FBgn0000056	Adhr	-3.3577505	0.02931379	1
FBgn0025835	CG17707	-1.0517445	0.0295024	1
FBgn0000055	Adh	-3.3528918	0.02955588	1
FBgn0003507	srp	-0.7200207	0.02986245	1
FBgn0039768	CG15533	1.89039528	0.03000559	1
FBgn0260775	DnaJ-60	0.45112768	0.0302524	1
FBgn0260770	CG42568	0.45112768	0.0302524	1
FBgn0030687	CG17209	-0.6424461	0.0306396	1

FBgn0051116	ClC-a	-2.3560596	0.03064282	1
FBgn0015663	Dot	-0.8311906	0.03162897	1
FBgn0035670	CG10472	2.34859205	0.0316882	1
FBgn0036348	CG17687	1.77639189	0.0317116	1
FBgn0034317	CG14499	1.31596495	0.03181969	1
FBgn0052984	CG32984	-2.5983316	0.03193994	1
FBgn0065083	snmRNA:765	-1.1230908	0.0322381	1
FBgn0052479	Usp10	-0.4796715	0.03228442	1
FBgn0266218	CR44913	-1.1189674	0.03233642	1
FBgn0013279	Hsp70Bc	-1.2012395	0.03244468	1
FBgn0265140	Meltrin	-0.5458434	0.03277213	1
FBgn0037936	CG6908	-2.71275	0.032933	1
FBgn0032169	CG4709	-0.6505623	0.03303064	1
FBgn0085285	CG34256	-0.7555666	0.03351555	1
FBgn0265296	Dscam2	-1.1989275	0.03389526	1
FBgn0040959	Peritrophin-15a	-1.8002222	0.03396211	1
FBgn0062517	CG16984	-0.7256264	0.03402119	1
FBgn0004842	RYa-R	1.981969	0.03414756	1
FBgn0052182	CG32182	-1.3406674	0.03446829	1
FBgn0028853	CG15263	-4.1606372	0.03472687	1
FBgn0051495	CG31495	-0.9779022	0.03491991	1
FBgn0266742	CR45215	-1.6550772	0.03557413	1
FBgn0034618	CG9485	-0.6516992	0.03577498	1
FBgn0034617	Panx	-0.7019894	0.03605921	1
FBgn0034797	nahoda	0.70579973	0.03643861	1
FBgn0037975	CG3397	1.15839111	0.03722988	1
FBgn0050089	CG30089	-0.9671399	0.03761157	1
FBgn0267455	CR45805	-0.8816723	0.03808227	1
FBgn0266786	CR45251	0.94193452	0.03827638	1
FBgn0030509	CG11162	2.2310197	0.03846171	1
FBgn0031630	CG15629	-0.9714985	0.0385731	1
FBgn0010425	epsilonTry	-3.2841863	0.03868753	1
FBgn0023534	CG17778	0.6156941	0.03872296	1
FBgn0039293	CG11851	-0.7074383	0.03882332	1
FBgn0036652	CG13032	-1.5774818	0.03882427	1
FBgn0040600	CG13631	-2.2301979	0.03893937	1
FBgn0039003	wfs1	0.68456763	0.03896596	1
FBgn0028945	CG7631	1.6852266	0.03905997	1
FBgn0028533	CG7953	1.30019466	0.03912126	1
FBgn0052181	CG32181	-1.3881525	0.03946277	1

FBgn0023536	CG3156	-0.8506003	0.03960273	1
FBgn0262149	CR42875	-1.0595575	0.03967311	1
FBgn0024943	PIP82	-1.3300131	0.03977586	1
FBgn0050147	Hil	0.73517442	0.03992708	1
FBgn0000395	cv-2	0.71955858	0.0399328	1
FBgn0030456	CG4332	-0.5510336	0.04012096	1
FBgn0035424	CG11505	-0.5247143	0.04044046	1
FBgn0051648	CG31648	-0.6684714	0.04059161	1
FBgn0031676	senju	-0.5625536	0.04089251	1
FBgn0037098	Wnk	-0.6762102	0.0409148	1
FBgn0030066	CG1885	-0.9443165	0.0409897	1
FBgn0051354	Hsp70Bbb	-1.2147026	0.0411161	1
FBgn0052791	DIP-alpha	-2.1857712	0.04116551	1
FBgn0085358	Diedel3	-2.9015689	0.04118032	1
FBgn0011236	ken	0.5020824	0.04157663	1
FBgn0032877	CG2617	-0.6695672	0.04191283	1
FBgn0036398	upSET	-0.5295133	0.04242262	1
FBgn0040290	RecQ4	-1.1992294	0.0426225	1
FBgn0039002	CG17625	1.22733541	0.04270601	1
FBgn0035941	CG13313	1.57349693	0.04285132	1
FBgn0036935	CG14186	-0.9679527	0.04286918	1
FBgn0031561	IM33	2.13305521	0.04291947	1
FBgn0266549	CR45102	-0.5988269	0.04341554	1
FBgn0028532	CG7968	1.53557308	0.04358252	1
FBgn0264822	CR44030	0.58126577	0.04361766	1
FBgn0266197	CR44892	0.76574631	0.04372727	1
FBgn0034439	CG10062	-4.095198	0.04375929	1
FBgn0284223	CG46307	-0.6380705	0.04394156	1
FBgn0036152	CG6175	-0.6979752	0.04396012	1
FBgn0265942	CR44729	-1.3701822	0.04397092	1
FBgn0039380	CG5890	2.1955897	0.04397377	1
FBgn0051694	CG31694	0.52241481	0.04411508	1
FBgn0267091	CR45535	-1.7274598	0.044369	1
FBgn0029504	CHES-1-like	-0.5814139	0.0444525	1
FBgn0033821	CG10799	-2.1286811	0.04448612	1
FBgn0250815	Jon65Aiv	-2.3862229	0.04483957	1
FBgn0053503	Cyp12d1-d	-2.2335093	0.04488601	1
FBgn0035356	CG16986	-2.4772616	0.04488965	1
FBgn0038702	CG3739	-2.504512	0.04508211	1
FBgn0266180	CR44886	1.29778436	0.04529312	1

FBgn0262354	CG43052	0.98355335	0.04534744	1
FBgn0032068	LManV	2.26527871	0.04537665	1
FBgn0033195	CG1360	-1.0807893	0.04546223	1
FBgn0034978	CG3257	-1.9105476	0.04561662	1
FBgn0027843	CAH2	-1.8458441	0.04573155	1
FBgn0004367	mei-41	-1.156764	0.04598931	1
FBgn0031747	CG9021	0.59120384	0.04605359	1
FBgn0031258	CG4297	-0.7230694	0.04612348	1
FBgn0086254	CG6084	-0.6023556	0.04645941	1
FBgn0264991	CG44142	-1.5652769	0.04661491	1
FBgn0034318	CG14500	-1.9570414	0.04694123	1
FBgn0039760	CG9682	-3.005939	0.04701417	1
FBgn0029896	CG3168	-1.6030542	0.04733753	1
FBgn0026176	SkpB	0.62737514	0.04740083	1
FBgn0036142	CG7616	-1.0109232	0.047626	1
FBgn0033792	CG13325	-3.2396749	0.04773064	1
FBgn0034856	yellow-d2	-0.9262119	0.04780451	1
FBgn0037780	ohgt	-0.6376842	0.04803724	1
FBgn0039588	mIF2	-0.6499592	0.04826846	1
FBgn0026430	Grip84	-0.5354155	0.04846275	1
FBgn0261836	Msp300	-0.5533386	0.04882635	1
FBgn0039354	Lgr3	0.96560191	0.04882997	1
FBgn0038733	CG11407	-3.817749	0.04894041	1
FBgn0023523	Or2a	-1.5602482	0.04927382	1
FBgn0259224	CG42324	1.32416257	0.04953263	1
FBgn0263031	CG43326	-1.4251712	0.04979669	1
FBgn0032048	Dh31	0.71207135	0.04982554	1
FBgn0029924	CG4586	0.88591859	0.04984945	1
FBgn0040670	e(y)2b	0.95285953	0.04985757	1

Table A-2. Fly genes with different expression levels between mock infected flies and those infected with C6706Δ*vasK* as determined with a P-value of >0.05. FBgn – Fly Base gene name. LogFC – log fold change. FDR – false discovery rate.

FBgn	Gene Name	logFC	PValue	FDR
FBgn0004839	otk	-1.336282	1.13E-09	1.15E-05
FBgn0038851	dmrt93B	-3.4408278	8.03E-08	0.00040837
FBgn0085813	18SrRNA-Psi:CR41602	5.03323866	3.85E-07	0.00112466
FBgn0083124	Uhg4	-1.2165236	5.35E-07	0.00112466
FBgn0260991	Incenp	-1.1370498	5.74E-07	0.00112466
FBgn0033459	CG12744	-1.7456668	6.64E-07	0.00112466
FBgn0082943	snoRNA:Me28S-A982a	-2.8804394	9.18E-07	0.00133309
FBgn0086356	tum	-1.734476	1.55E-06	0.00186244
FBgn0003068	per	-1.273743	1.65E-06	0.00186244
FBgn0027601	pdgy	1.09631457	1.99E-06	0.0020224
FBgn0051216	Naam	-1.7890062	2.22E-06	0.0020562
FBgn0044324	Chro	-1.1930603	3.60E-06	0.00305228
FBgn0035157	CG13894	1.80230479	4.17E-06	0.00325965
FBgn0003380	Sh	1.81414336	8.72E-06	0.00633453
FBgn0020906	Jon25Bi	5.97850648	9.84E-06	0.00667067
FBgn0032297	CG17124	-1.1981042	1.69E-05	0.0106675
FBgn0003984	vn	1.64293166	1.83E-05	0.0106675
FBgn0263492	CR43481	1.4340545	1.89E-05	0.0106675
FBgn0038842	hdly	1.28739612	2.23E-05	0.01190772
FBgn0082937	snoRNA:Me28S-C2645b	-2.0530446	2.64E-05	0.01332345
FBgn0033375	CG8078	-0.9658652	2.75E-05	0.01332345
FBgn0086672	snoRNA:Or-aca5	-1.4857583	2.94E-05	0.01357519
FBgn0083015	snoRNA:Psi18S-920	-2.1199565	4.66E-05	0.01981446
FBgn0037409	Osi24	-1.5603321	4.68E-05	0.01981446
FBgn0015546	spel1	-1.0634014	5.30E-05	0.02021992
FBgn0025739	pon	-1.7533218	5.35E-05	0.02021992
FBgn0264877	CR44068	3.92501027	5.41E-05	0.02021992
FBgn0031324	CG14342	2.4256649	5.57E-05	0.02021992
FBgn0259936	Uhg3	-1.0443471	6.38E-05	0.02237652
FBgn0022774	Oat	2.93748875	7.19E-05	0.02436174
FBgn0037265	spartin	1.18978483	7.49E-05	0.0245654
FBgn0263855	BubR1	-1.1349358	8.06E-05	0.02559335
FBgn0259977	Tdc1	1.69031216	9.03E-05	0.02690661
FBgn0038256	CG7530	-1.1959844	9.23E-05	0.02690661
FBgn0034933	CG3735	-0.8962324	9.26E-05	0.02690661
FBgn0267792	rgr	-0.8937546	9.76E-05	0.02757242
FBgn0011692	pav	-1.2732802	0.00010793	0.02965362
FBgn0033312	CG8642	-1.0814962	0.00011469	0.03068306

FBgn0003124	polo	-0.9504619	0.00012542	0.03180589
FBgn0053099	CG33099	-1.0677343	0.00012796	0.03180589
FBgn0013275	Hsp70Aa	1.57867873	0.00012827	0.03180589
FBgn0038866	CG5810	2.98410374	0.000139	0.03312449
FBgn0013276	Hsp70Ab	1.45662165	0.00014129	0.03312449
FBgn0082928	snoRNA:Me28S-G3255a	-2.1938186	0.00014458	0.03312449
FBgn0052649	CG32649	1.10040158	0.00014663	0.03312449
FBgn0031528	CG15412	-2.7306851	0.00015699	0.03469456
FBgn0039588	mIF2	1.24728826	0.00017834	0.03845533
FBgn0002633	E(spl)m7-HLH	-1.358611	0.00018348	0.03845533
FBgn0051036	CG31036	-1.9316779	0.00019243	0.03845533
FBgn0031981	CG7466	1.45954962	0.00019343	0.03845533
FBgn0038903	RpI12	-1.1002275	0.00019902	0.03845533
FBgn0001230	Hsp68	2.05917114	0.00020005	0.03845533
FBgn0051092	LpR2	1.04152108	0.00020049	0.03845533
FBgn0004449	Ten-m	0.94629647	0.00020576	0.03873582
FBgn0031745	rau	-1.2738993	0.00021564	0.0392113
FBgn0085358	Diedel3	6.00056546	0.000216	0.0392113
FBgn0004573	5-HT7	1.96432644	0.00023083	0.04116868
FBgn0266810	CR45272	2.63670573	0.00025153	0.04408724
FBgn0031419	CG15390	1.54446802	0.0002766	0.04765892
FBgn0010768	sqz	-1.0444867	0.00030926	0.05239951
FBgn0082981	snoRNA:Psi28S-2949	-2.0607625	0.00032125	0.05262704
FBgn0036759	CG5577	1.46297306	0.00032394	0.05262704
FBgn0032682	grnd	1.79396187	0.00032614	0.05262704
FBgn0036754	CG5589	-0.9587855	0.00033425	0.0530935
FBgn0045474	Gr77a	-1.5688692	0.00034075	0.05329375
FBgn0260481	CG32454	-1.7228732	0.00035134	0.05411747
FBgn0033564	Pex6	1.34972186	0.00036877	0.05595345
FBgn0038306	Art3	-0.9742551	0.00038091	0.0569458
FBgn0051313	CG31313	2.0607097	0.00039297	0.0572584
FBgn0031053	CG14223	-1.7090078	0.00039426	0.0572584
FBgn0024732	Drep1	-1.0958829	0.00040335	0.05775331
FBgn0001224	Hsp23	2.0466113	0.00041987	0.05903492
FBgn0024222	IKKbeta	-1.0078162	0.00042935	0.05903492
FBgn0010620	CG10939	1.98275918	0.00043115	0.05903492
FBgn0039776	PH4alphaEFB	-1.0262742	0.00043553	0.05903492
FBgn0039325	CG10560	1.99147269	0.00044371	0.05935227
FBgn0036024	CG18180	4.39207372	0.00045389	0.05992504

FBgn0039145	CG6000	1.5173165	0.00048439	0.06313221
FBgn0266393	CR45033	-0.8251519	0.00049465	0.06321291
FBgn0264906	CR44097	1.51562837	0.0005029	0.06321291
FBgn0082936	snoRNA:Me28S-C2645c	-1.5534627	0.00050466	0.06321291
FBgn0053181	CG33181	1.53032402	0.00051498	0.06321291
FBgn0030993	Mec2	0.88245905	0.0005161	0.06321291
FBgn0001227	Hsp67Ba	1.44144702	0.00056416	0.06827687
FBgn0040609	CG3348	2.98028358	0.00057111	0.06830478
FBgn0263120	Acsl	0.83229494	0.00061144	0.07227807
FBgn0036150	Ir68a	2.71622646	0.0006323	0.07388492
FBgn0004569	aos	-1.2241779	0.00065663	0.07515149
FBgn0032033	CG13392	1.61801077	0.00065793	0.07515149
FBgn0038349	AOX3	1.12454915	0.00067239	0.07594995
FBgn0000473	Cyp6a2	4.18918061	0.00068019	0.07598664
FBgn0019928	Ser8	3.00906327	0.00070209	0.07675236
FBgn0036142	CG7616	1.75611947	0.00071808	0.07675236
FBgn0037534	CG2781	1.78814647	0.00072593	0.07675236
FBgn0083013	snoRNA:Psi28S-1060	-2.2056665	0.00072686	0.07675236
FBgn0010314	Cks30A	-1.4190725	0.00073095	0.07675236
FBgn0035120	wac	-1.0382522	0.00073782	0.07675236
FBgn0264894	CG44085	1.11976704	0.00073989	0.07675236
FBgn0050151	CG30151	3.52934421	0.00077584	0.07887461
FBgn0030576	CG15890	-2.709345	0.00077646	0.07887461
FBgn0030628	CG9114	-0.7825094	0.00078568	0.07887461
FBgn0036749	CG7460	-1.0818504	0.00079868	0.07887461
FBgn0264817	pre-lola-G	-0.9404848	0.00079914	0.07887461
FBgn0038118	timeout	-1.3614198	0.00083323	0.0803748
FBgn0032105	borr	-1.4927777	0.00083591	0.0803748
FBgn0267181	CR45621	1.53083271	0.00084544	0.0803748
FBgn0263584	CR43609	-0.9999173	0.00084597	0.0803748
FBgn0263324	CR43405	-1.295522	0.0008602	0.08097058
FBgn0035103	Vdup1	3.4114138	0.00087962	0.0816963
FBgn0040256	Ugt86Dd	1.86912058	0.00088399	0.0816963
FBgn0266317	CR44982	1.40904584	0.00090111	0.08252893
FBgn0052010	CR32010	1.99404916	0.00091256	0.08275019
FBgn0031209	Ir21a	-0.9807532	0.00091981	0.08275019
FBgn0261283	SREBP	-0.7376923	0.00092898	0.08284203
FBgn0032061	CG9314	1.27653759	0.00094087	0.08317302
FBgn0013277	Hsp70Ba	1.57968968	0.00097019	0.08502587

FBgn0030864	CG8173	-1.8115358	0.00099228	0.08621821
FBgn0027844	CAH1	1.47115747	0.00100154	0.08628513
FBgn0034885	Eglp4	3.06412173	0.00103018	0.08770312
FBgn0002632	E(spl)m6-BFM	-1.5796043	0.00103525	0.08770312
FBgn0264078	Flo2	0.921246	0.00105486	0.08862537
FBgn0040959	Peritrophin-15a	2.91354225	0.00108847	0.09070029
FBgn0041629	Hexo2	-0.7759794	0.00109786	0.09073871
FBgn0050287	CG30287	-1.4254998	0.00112544	0.09226759
FBgn0082942	snoRNA:Me28S-A982b	-1.4511143	0.00116269	0.09455933
FBgn0034046	tun	-0.805406	0.00118351	0.09548838
FBgn0259916	CG42445	0.86374708	0.00122183	0.09780444
FBgn0040297	Nhe2	0.96378689	0.00125589	0.09884988
FBgn0010358	deltaTry	2.3982727	0.00126897	0.09884988
FBgn0001228	CG4456	1.80812062	0.00127798	0.09884988
FBgn0001223	Hsp22	1.80811707	0.00128049	0.09884988
FBgn0262699	fzr	-0.74253	0.00128687	0.09884988
FBgn0265301	CR44274	1.63771392	0.00129564	0.09884988
FBgn0023171	rnh1	-0.7756959	0.00130862	0.09884988
FBgn0035989	CG3967	-1.0483541	0.00132041	0.09884988
FBgn0029831	CG5966	3.43772503	0.00132413	0.09884988
FBgn0259162	RunxB	3.35523256	0.00133767	0.09884988
FBgn0015376	cutlet	-0.9698395	0.00134185	0.09884988
FBgn0001134	Grd	1.12880492	0.00135247	0.09891523
FBgn0031142	r-cup	-1.097904	0.00136397	0.09904382
FBgn0038404	CG8925	1.83714146	0.00140873	0.10156832
FBgn0038973	Pebp1	2.61808493	0.00143309	0.10259723
FBgn0035213	CG2199	-0.6757109	0.00145534	0.10346159
FBgn0013772	Cyp6a8	2.65598553	0.00146741	0.10359486
FBgn0261385	scra	-0.866231	0.0015472	0.1080037
FBgn0264904	CR44095	0.83651903	0.00155111	0.1080037
FBgn0038146	CG9799	-0.7922098	0.00159346	0.11019837
FBgn0004431	LysX	3.48056117	0.00162439	0.11102694
FBgn0259236	comm3	2.60756637	0.00162729	0.11102694
FBgn0030407	CG2543	1.40580142	0.00168669	0.11431276
FBgn0036203	Muc68D	6.44010668	0.00169965	0.1144284
FBgn0263607	l(3)72Dp	1.25907831	0.00171099	0.1144335
FBgn0031791	AANATL2	4.33232919	0.00173172	0.11486295
FBgn0035761	RhoGEF4	-0.9894432	0.00174602	0.11486295
FBgn0051643	CG31643	1.11284944	0.0017513	0.11486295
FBgn0036652	CG13032	2.24808084	0.00177637	0.11500632

FBgn0031514	CG3332	2.347318	0.00177668	0.11500632
FBgn0024920	Ts	-1.611197	0.00178743	0.11500632
FBgn0250753	kra	-0.8271182	0.00181303	0.11591979
FBgn0003358	Jon99Ci	3.55390194	0.00183477	0.11657694
FBgn0002775	msl-3	-0.7896907	0.00185555	0.11716503
FBgn0050269	CG30269	1.38323711	0.00189945	0.11803567
FBgn0050273	CG30273	1.38323711	0.00189945	0.11803567
FBgn0260464	CG9288	0.92279442	0.00191579	0.11803567
FBgn0259721	CG42375	0.92279442	0.00191579	0.11803567
FBgn0036152	CG6175	1.07736652	0.00194348	0.11902067
FBgn0031080	CG12655	1.51696239	0.00198566	0.11978657
FBgn0028331	l(1)G0289	0.75767872	0.00200974	0.11978657
FBgn0030915	CG6179	-0.7455258	0.00202473	0.11978657
FBgn0031910	CG15818	5.1962249	0.00203242	0.11978657
FBgn0003448	sna	-1.2650485	0.00203442	0.11978657
FBgn0267425	CR45778	-0.8079938	0.0020439	0.11978657
FBgn0250837	dUTPase	-0.8079939	0.00204507	0.11978657
FBgn0004629	Cys	0.81116847	0.00205046	0.11978657
FBgn0050496	CG30496	0.84321811	0.00206368	0.11978657
FBgn0032382	Mal-B2	3.00751151	0.00207481	0.11978657
FBgn0028658	Adat1	1.34512094	0.00209422	0.11978657
FBgn0263239	dar1	-1.0400791	0.00209738	0.11978657
FBgn0030710	CG8924	-1.2486126	0.00211716	0.12024047
FBgn0037780	ohgt	0.99055536	0.00213626	0.12065143
FBgn0010105	comm	-1.3417439	0.00216224	0.12144378
FBgn0038395	CG10407	-1.1550491	0.00217695	0.12159836
FBgn0086668	snoRNA:Psi28S-3436a	-2.1985886	0.0022457	0.12300192
FBgn0031654	Jon25Bii	4.67502249	0.00224895	0.12300192
FBgn0027583	CG7601	0.90392696	0.00225103	0.12300192
FBgn0032922	CG9249	1.06738482	0.00225381	0.12300192
FBgn0010425	epsilonTry	5.3369532	0.00226258	0.12300192
FBgn0002578	Kaz-m1	2.4813339	0.0023079	0.12327366
FBgn0036240	CG6928	0.98112393	0.00230815	0.12327366
FBgn0259734	Nost	0.98775251	0.00231376	0.12327366
FBgn0038881	CG16791	0.76469954	0.00232532	0.12327366
FBgn0260450	CalpC	-0.6910396	0.00232821	0.12327366
FBgn0263133	mEFG1	-0.9224875	0.00234636	0.1234416
FBgn0036565	CG5235	-1.1891675	0.00236543	0.1234416
FBgn0030583	CG14410	-1.4866235	0.00237031	0.1234416
FBgn0028530	mTTF	0.93952109	0.00239218	0.1234416

FBgn0035679	CG10467	0.96256901	0.00239734	0.1234416
FBgn0028484	Ack	-0.7193161	0.00240423	0.1234416
FBgn0016032	lbm	-0.7683293	0.0024577	0.12550452
FBgn0001226	Hsp27	1.96544886	0.0024691	0.12550452
FBgn0034717	CG5819	1.5923899	0.0025322	0.12754708
FBgn0026379	Pten	-0.8438223	0.00253438	0.12754708
FBgn0030053	CG12081	-0.7647567	0.0025853	0.12946861
FBgn0034045	CG8249	2.30433601	0.00266561	0.13283644
FBgn0027843	CAH2	2.90417038	0.00268108	0.13295551
FBgn0029121	Sras	0.80360701	0.00273523	0.13488727
FBgn0036386	CG8833	0.8069115	0.00274657	0.13488727
FBgn0035697	CG10163	2.90662232	0.0027775	0.13575014
FBgn0003870	ttk	-0.7073236	0.00280872	0.13661945
FBgn0003525	stg	-1.3694668	0.00283938	0.13739475
FBgn0001098	Gdh	-0.7099183	0.00285169	0.13739475
FBgn0259738	CG42392	1.02200941	0.00291794	0.13936637
FBgn0028920	CG8997	2.04615243	0.00293775	0.13936637
FBgn0032079	CG31886	0.95007754	0.00294163	0.13936637
FBgn0030177	CG2972	-0.7246206	0.00294745	0.13936637
FBgn0284223	CG46307	0.94608204	0.00299739	0.14107175
FBgn0039052	CG6733	2.12741708	0.00306639	0.14365392
FBgn0030500	Ndc80	-1.0345664	0.00308587	0.14390336
FBgn0037831	Cap-H2	-0.7694938	0.00312285	0.14496295
FBgn0030189	CG2909	1.17668083	0.00315972	0.14600793
FBgn0031091	Phf7	-1.3207766	0.00319624	0.14702724
FBgn0262580	CG43120	1.37129664	0.0032183	0.14737476
FBgn0267516	pre-rRNA-Psi:CR45856	1.95102691	0.00325614	0.14794885
FBgn0031042	CG14221	-1.4698506	0.0032669	0.14794885
FBgn0050069	CG30069	1.40553926	0.00328241	0.14794885
FBgn0039696	CG7837	1.5053334	0.00328905	0.14794885
FBgn0038353	CG5399	1.00924662	0.00332396	0.14829533
FBgn0026169	snoRNA:Psi18S-1820	-1.4701569	0.00332614	0.14829533
FBgn0029907	Atx-1	-1.4184334	0.00334051	0.14829533
FBgn0039250	Mink	-1.5059148	0.00338501	0.14877363
FBgn0000463	Dl	-1.1266602	0.0033874	0.14877363
FBgn0086768	Pcmt	-0.686498	0.00339519	0.14877363
FBgn0034491	Hsl	-0.6909948	0.00342744	0.14902879
FBgn0030701	CG16952	-0.6835615	0.00343033	0.14902879
FBgn0030683	CG8239	-0.6816073	0.00346999	0.14905559
FBgn0015926	dah	-0.9618415	0.00347342	0.14905559

FBgn0038828	CG17270	-0.7940528	0.00347493	0.14905559
FBgn0065080	snoRNA:Me18S-A1374	-0.6530896	0.00349205	0.14916042
FBgn0011236	ken	-0.7177655	0.00355345	0.15114783
FBgn0051354	Hsp70Bbb	1.76537806	0.00363594	0.15401254
FBgn0002914	Myb	-0.6725339	0.00368542	0.15546067
FBgn0027343	fz3	-2.2832953	0.00371112	0.15553673
FBgn0039350	jigr1	-0.7518873	0.00371783	0.15553673
FBgn0082979	snoRNA:Psi28S-3091a	-1.2219143	0.00376517	0.15687198
FBgn0035542	DOR	0.71365201	0.00379213	0.15712189
FBgn0020445	E23	-1.0725641	0.00381424	0.15712189
FBgn0037443	Dmtn	0.8602906	0.00383143	0.15712189
FBgn0019830	colt	0.84720994	0.00384723	0.15712189
FBgn0004797	mdy	1.00230373	0.00384845	0.15712189
FBgn0037923	CG6813	-1.3535659	0.00386486	0.15716067
FBgn0028533	CG7953	2.03930235	0.00389691	0.1572531
FBgn0267814	CR46139	1.79373503	0.00389807	0.1572531
FBgn0010549	l(2)03659	1.11461946	0.00394603	0.15855879
FBgn0263143	vret	-0.9921344	0.00400208	0.16017777
FBgn0040238	Best1	-0.7319423	0.00402664	0.16026362
FBgn0000180	bib	-0.8644841	0.00403576	0.16026362
FBgn0001145	Gs2	2.05390342	0.00405783	0.16051314
FBgn0035763	CG8602	0.67751799	0.00407788	0.16068105
FBgn0263605	l(3)72Dn	-0.7243212	0.00417561	0.16388863
FBgn0259171	Pde9	2.27029572	0.00419418	0.16388863
FBgn0030777	CG9672	3.16598119	0.00420765	0.16388863
FBgn0063496	GstE4	2.22141427	0.00423102	0.16416989
FBgn0038416	CG17930	1.85220345	0.00425711	0.16427552
FBgn0082927	snoRNA:Me28S-G3255b	-2.0826225	0.00426606	0.16427552
FBgn0002036	CG10561	1.05826085	0.00433387	0.16577096
FBgn0039128	CG13599	-1.4003482	0.00435312	0.16577096
FBgn0262148	CR42874	1.50147762	0.00435381	0.16577096
FBgn0003041	pbl	1.09770712	0.00439662	0.16677612
FBgn0038827	Fancd2	-1.2653287	0.00441618	0.16689538
FBgn0004509	Fur1	0.86679557	0.00444774	0.16714516
FBgn0003499	sr	1.71384818	0.00445567	0.16714516
FBgn0027949	msb11	-1.109755	0.00452285	0.16903387
FBgn0034518	CG13430	0.85303411	0.00458884	0.16903387
FBgn0034519	CG18065	0.85303411	0.00458884	0.16903387
FBgn0031579	CG15422	1.58986065	0.00458997	0.16903387

FBgn0037850	CG14695	-1.2456346	0.00463687	0.16903387
FBgn0260741	CG3281	0.87897385	0.0046427	0.16903387
FBgn0030600	hiw	1.37078445	0.00466129	0.16903387
FBgn0036354	Poc1	-0.9469312	0.00466276	0.16903387
FBgn0050031	CG30031	3.0702458	0.00466847	0.16903387
FBgn0001225	Hsp26	1.70919627	0.00468302	0.16903387
FBgn0038858	CG5793	1.6828397	0.00468892	0.16903387
FBgn0031676	senju	0.77650545	0.00473599	0.16926984
FBgn0266431	CG45061	1.13805787	0.00473881	0.16926984
FBgn0001248	Idh	1.44598111	0.00475367	0.16926984
FBgn0035159	CG13896	1.13971245	0.00476207	0.16926984
FBgn0085734	CR40450	2.37078727	0.00481512	0.17018716
FBgn0039453	CG6403	5.98380443	0.00482136	0.17018716
FBgn0265298	SC35	-0.6001661	0.0048715	0.17094673
FBgn0033124	Tsp42Ec	1.62240267	0.00487651	0.17094673
FBgn0051231	CG31231	-2.1103262	0.00493116	0.1722688
FBgn0043578	PGRP-SB1	-1.7928677	0.00498107	0.17308733
FBgn0038243	CG8066	0.70715496	0.00500668	0.17308733
FBgn0029117	Surf1	1.41799949	0.0050137	0.17308733
FBgn0033494	KCNQ	1.40692696	0.0050227	0.17308733
FBgn0033543	CG12338	1.43295031	0.00504446	0.17312734
FBgn0265872	CR44661	2.42422523	0.00505792	0.17312734
FBgn0036714	CG7692	0.97075684	0.0051071	0.17422396
FBgn0038363	Acyp2	-0.8662286	0.00514145	0.17480922
FBgn0030098	CG12057	2.31530533	0.00518034	0.17507047
FBgn0053971	Ir62a	1.42839936	0.00518357	0.17507047
FBgn0050025	CG30025	3.64948706	0.00523862	0.17634374
FBgn0030769	CG13012	2.14164689	0.00534399	0.17929715
FBgn0051116	ClC-a	3.13970103	0.00540066	0.18060227
FBgn0086358	Tab2	-0.8444938	0.00543308	0.18109085
FBgn0037248	srl	-0.7020858	0.0054856	0.1822439
FBgn0040687	CG14645	1.47594139	0.0056105	0.18563691
FBgn0037439	CG10286	-0.6503759	0.00562425	0.18563691
FBgn0261836	Msp300	0.78172606	0.00566291	0.18630796
FBgn0039755	CG15531	-0.8616885	0.00569921	0.18689726
FBgn0015623	Cpr	1.53244675	0.0058022	0.18955545
FBgn0003892	ptc	2.01048313	0.00581756	0.18955545
FBgn0040359	CG11380	-1.3069354	0.00591702	0.19123181
FBgn0039773	CG2224	0.7920303	0.00593904	0.19123181
FBgn0011274	Dif	-1.1957013	0.00595593	0.19123181

FBgn0082949	snoRNA:Me18S-U1356a	-1.5834423	0.0059601	0.19123181
FBgn0038100	Paip2	0.58549739	0.00598	0.19123181
FBgn0031688	Cyp28d2	1.33417997	0.00598187	0.19123181
FBgn0038071	Dtg	-0.7758373	0.00602877	0.19212703
FBgn0004425	LysB	3.3447921	0.00606308	0.19234449
FBgn0086608	CG34112	0.83635476	0.00607344	0.19234449
FBgn0033541	CG12934	-0.6699623	0.00612245	0.19329454
FBgn0003118	pnt	-0.9439854	0.00619998	0.19513625
FBgn0053207	pxb	-1.0782475	0.00626222	0.19642804
FBgn0031939	CG13796	1.87232413	0.00627967	0.19642804
FBgn0013279	Hsp70Bc	1.55191514	0.00636004	0.19833192
FBgn0263111	cac	0.70858709	0.0064479	0.19942316
FBgn0013278	Hsp70Bb	1.28019509	0.00645968	0.19942316
FBgn0037882	CG17187	0.94637544	0.00647066	0.19942316
FBgn0036571	Strumpellin	0.63376253	0.00649832	0.19942316
FBgn0266731	CR45204	0.71774596	0.00651089	0.19942316
FBgn0032197	CG5694	-0.6839062	0.00651274	0.19942316
FBgn0037307	Tim17a2	1.60509913	0.00653326	0.19945086
FBgn0034628	Acox57D-p	1.7074366	0.00659187	0.20063768
FBgn0034742	CG4294	0.72888131	0.00661919	0.20086767
FBgn0034142	CG8306	-0.6682492	0.00682546	0.20650614
FBgn0085290	CG34261	-0.9962452	0.00684562	0.20650614
FBgn0032635	CG15141	-1.0031766	0.00690317	0.2066008
FBgn0038235	CG8461	1.41446979	0.00691808	0.2066008
FBgn0261530	nbs	0.65935545	0.00692658	0.2066008
FBgn0041780	Ssl2	1.27078974	0.00695687	0.2066008
FBgn0034360	CG10927	-0.6452669	0.00695717	0.2066008
FBgn0265042	Irk1	0.84978299	0.00697069	0.2066008
FBgn0030066	CG1885	1.25515206	0.00701151	0.20664801
FBgn0031707	CG14020	1.0275659	0.00702906	0.20664801
FBgn0043903	dome	-0.6776909	0.00703327	0.20664801
FBgn0263597	Acp98AB	-0.9856289	0.00706863	0.20708833
FBgn0033188	Drat	1.42424253	0.00710424	0.20753352
FBgn0034195	Spn53F	2.88081558	0.00714184	0.20803433
FBgn0024957	Irp-1B	1.09885602	0.00723665	0.20981705
FBgn0050345	CG30345	0.97740424	0.00725511	0.20981705
FBgn0031831	COX5BL	-1.2311546	0.00726496	0.20981705
FBgn0038746	Surf6	-0.7690768	0.0073449	0.21020634
FBgn0031703	CG12512	2.28205393	0.00735119	0.21020634

FBgn0035392	CG1271	2.02102218	0.00735699	0.21020634
FBgn0053503	Cyp12d1-d	3.09642452	0.00736115	0.21020634
FBgn0035206	CG9186	0.62305329	0.00740704	0.21092431
FBgn0036381	CG8745	2.24764703	0.00746727	0.21114981
FBgn0038145	Droj2	-0.6905059	0.00746874	0.21114981
FBgn0052191	CG32191	3.3237592	0.0074936	0.21114981
FBgn0262357	CG43055	3.73175248	0.00749804	0.21114981
FBgn0039109	CG10365	-0.6465138	0.00758597	0.21267069
FBgn0031392	AIF	-0.7538706	0.00759389	0.21267069
FBgn0016930	Dyrk2	-0.8541512	0.00762153	0.21285855
FBgn0020513	ade5	-0.6652684	0.00766803	0.21357032
FBgn0034312	CG10916	1.06087162	0.00774074	0.21467514
FBgn0038173	Adgf-C	1.95128128	0.00774993	0.21467514
FBgn0259173	corn	-0.6801478	0.00780682	0.21549032
FBgn0266354	CG45002	1.70644025	0.00785687	0.21549032
FBgn0050001	CG30001	-1.2966057	0.00787154	0.21549032
FBgn0031848	Nse1	-1.0861033	0.00788207	0.21549032
FBgn0005670	Cyp4d1	-1.4989636	0.00788749	0.21549032
FBgn0050010	CG30010	1.06639094	0.00790654	0.21549032
FBgn0023395	Chd3	-0.8674496	0.00797309	0.21619721
FBgn0040268	Top3alpha	-0.6251255	0.00797501	0.21619721
FBgn0267481	CR45831	0.96412393	0.00799778	0.21623777
FBgn0263606	Hsc20	1.30549996	0.00805889	0.21705248
FBgn0038401	CG5916	-0.7583311	0.00807061	0.21705248
FBgn0040346	CG3704	-0.5573012	0.00811586	0.2172124
FBgn0010357	betaTry	3.31392625	0.00812204	0.2172124
FBgn0035383	CPT2	0.70944374	0.00814066	0.2172124
FBgn0032266	CG18302	-1.3494742	0.00835876	0.22068185
FBgn0086708	stv	0.80881448	0.0083656	0.22068185
FBgn0034709	Swim	0.65063097	0.00838493	0.22068185
FBgn0259152	Clbn	0.83885119	0.00840242	0.22068185
FBgn0028375	heix	0.75068754	0.00841576	0.22068185
FBgn0020493	Dad	-0.9013288	0.00843852	0.22068185
FBgn0051102	CG31102	0.90896719	0.00844033	0.22068185
FBgn0085322	CG34293	1.20548868	0.00845121	0.22068185
FBgn0034671	CG13494	-1.1397814	0.00846606	0.22068185
FBgn0040600	CG13631	2.92965401	0.00849829	0.22071005
FBgn0004427	LysD	3.28556339	0.00851056	0.22071005
FBgn0031498	CG17260	0.8880494	0.00858361	0.22146113
FBgn0004395	unk	0.60152522	0.00858391	0.22146113

FBgn0284226	CG46310	0.82992452	0.00864063	0.22146113
FBgn0039828	CG1542	-0.7481841	0.00865229	0.22146113
FBgn0025390	Mur2B	0.78336293	0.00865734	0.22146113
FBgn0039488	CG6066	0.82836	0.00867023	0.22146113
FBgn0039315	CG13658	1.69009053	0.00874131	0.22147322
FBgn0266680	CR45170	1.51458954	0.00874495	0.22147322
FBgn0031062	CG14230	-0.6546707	0.00874698	0.22147322
FBgn0032961	CG1416	-0.5524608	0.00875856	0.22147322
FBgn0033584	CG7737	-1.1222987	0.0087816	0.22147322
FBgn0263256	CG43394	2.45706425	0.00880509	0.22147322
FBgn0038242	CG14852	1.52805172	0.0088574	0.22147322
FBgn0029830	Grip	-0.585965	0.00888763	0.22147322
FBgn0037756	CG8507	-0.5696086	0.00888768	0.22147322
FBgn0038407	CG6126	-1.1265888	0.00889712	0.22147322
FBgn0260477	CG30283	-0.6982507	0.00891034	0.22147322
FBgn0267779	CR46110	1.05990113	0.00896058	0.22154808
FBgn0033465	Etf-QO	0.8620579	0.00899643	0.22154808
FBgn0266400	CR45040	1.66441682	0.00901759	0.22154808
FBgn0031422	PIG-Wa	-1.4740984	0.00905772	0.22154808
FBgn0013717	not	0.79721474	0.0090605	0.22154808
FBgn0266626	CR45133	1.56295715	0.00907188	0.22154808
FBgn0039321	CG10550	1.33991723	0.00910549	0.22154808
FBgn0030756	CG9903	1.82681249	0.00910726	0.22154808
FBgn0267408	AOX1	1.04923528	0.00913021	0.22154808
FBgn0038037	Cyp9f2	0.77306647	0.00913232	0.22154808
FBgn0264982	CR44133	3.4110309	0.00915308	0.22154808
FBgn0038924	CG6028	1.39816884	0.00927526	0.22397221
FBgn0031049	Sec61gamma	-0.570142	0.00935044	0.22399755
FBgn0262736	Vha16-1	0.69629351	0.00937926	0.22399755
FBgn0082988	snoRNA:Psi28S-2442b	-0.9889249	0.00939492	0.22399755
FBgn0030484	GstT4	1.90388183	0.00939576	0.22399755
FBgn0039766	CG15536	1.00116708	0.00939754	0.22399755
FBgn0027864	Ogg1	0.78283131	0.00942573	0.22399755
FBgn0027279	l(1)G0196	-0.6544622	0.00943055	0.22399755
FBgn0024984	CG3457	-1.5240112	0.00949157	0.22492143
FBgn0034512	CG18067	0.69006627	0.00953925	0.22521405
FBgn0039254	Nmnat	0.92294593	0.00954823	0.22521405
FBgn0024352	Hop	-0.6888545	0.00962603	0.22556404
FBgn0042712	HBS1	0.69884166	0.00962722	0.22556404
FBgn0038475	Keap1	0.96754648	0.00962963	0.22556404

FBgn0052350	Vps11	0.619199	0.00971963	0.22653303
FBgn0029915	CG14434	-0.8220683	0.00972769	0.22653303
FBgn0032358	Ppt2	0.66815467	0.00973785	0.22653303
FBgn0027616	YT521-B	0.62130059	0.00976854	0.22672827
FBgn0285926		0.62121759	0.00983022	0.2276402
FBgn0039215	CG6695	-0.5432749	0.00986054	0.22782324
FBgn0010315	CycD	-0.5572914	0.00993769	0.22908521
FBgn0087007	bbg	0.8426766	0.01003167	0.23032382
FBgn0033544	CG7220	0.89385571	0.01003674	0.23032382
FBgn0031417	CG3597	0.61860413	0.01013587	0.23159003
FBgn0037174	CG14457	1.48110317	0.01013747	0.23159003
FBgn0035154	CG3344	4.14019452	0.01019309	0.23162938
FBgn0031050	Arp10	-0.5782127	0.01020569	0.23162938
FBgn0015721	ktub	-0.9615257	0.01020755	0.23162938
FBgn0027376	rha	3.75501647	0.01029112	0.23231391
FBgn0035410	CG14964	-1.6702355	0.01030196	0.23231391
FBgn0063491	GstE9	2.30768294	0.01031054	0.23231391
FBgn0030587	CG9522	3.30022526	0.01032913	0.23231391
FBgn0259227	CG42327	2.03803716	0.01036355	0.23257358
FBgn0002466	sti	-1.1202256	0.01045112	0.23309199
FBgn0041111	lilli	0.64263156	0.01045117	0.23309199
FBgn0265901	CR44690	1.22186848	0.01045543	0.23309199
FBgn0036298	nst	0.76279773	0.01047906	0.23310746
FBgn0036575	CG5157	1.28601696	0.01058981	0.23505682
FBgn0004914	Hnf4	0.9357531	0.01064539	0.23528637
FBgn0042086	Tsp42Eb	1.44233595	0.01067385	0.23528637
FBgn0037153	olf413	1.43688511	0.010681	0.23528637
FBgn0039544	CG12877	0.756621	0.01071037	0.23528637
FBgn0037888	scpr-B	-1.4714024	0.01072548	0.23528637
FBgn0050160	CG30160	1.47271344	0.01073902	0.23528637
FBgn0004428	LysE	3.26310865	0.0107841	0.23569356
FBgn0019968	Khc-73	0.64647345	0.01080397	0.23569356
FBgn0265068	CR44179	0.67054111	0.01089957	0.23634218
FBgn0053985	CG33985	1.25192935	0.01090661	0.23634218
FBgn0030410	Aven	0.90688675	0.01094761	0.23634218
FBgn0035483	Mul1	1.01232046	0.01094975	0.23634218
FBgn0031689	Cyp28d1	1.409212	0.01094995	0.23634218
FBgn0033989	CG7639	-0.5619197	0.01101879	0.23732412
FBgn0040091	Ugt58Fa	-1.6201077	0.0111369	0.23807057
FBgn0039326	CG10562	1.95985221	0.01113766	0.23807057

FBgn0250815	Jon65Aiv	3.12031895	0.01114091	0.23807057
FBgn0040765	luna	0.65621409	0.01114712	0.23807057
FBgn0267521	18SrRNA-Psi:CR45861	2.25088581	0.0111917	0.23821498
FBgn0052055	CG32055	-0.866756	0.01121399	0.23821498
FBgn0265830	CR44619	-1.0459036	0.01124146	0.23821498
FBgn0039137	CG13604	0.82863338	0.01125712	0.23821498
FBgn0051793	CG31793	0.74922222	0.01127738	0.23821498
FBgn0085452	CG34423	1.07385975	0.01129447	0.23821498
FBgn0004597	CycC	0.66340397	0.01135705	0.23903883
FBgn0000256	capu	1.52172008	0.01142018	0.23941808
FBgn0014135	bnl	0.7992703	0.01142217	0.23941808
FBgn0050361	mtt	2.4148382	0.01145032	0.23944967
FBgn0264707	RhoGEF3	0.61661612	0.01151117	0.23944967
FBgn0027528	goe	1.66095361	0.01154453	0.23944967
FBgn0051324	CG31324	-0.8591264	0.01155862	0.23944967
FBgn0031895	CG4497	1.25916541	0.01155881	0.23944967
FBgn0035806	PGRP-SD	0.89485086	0.011565	0.23944967
FBgn0035476	CG12766	2.43680793	0.01163412	0.24039123
FBgn0032910	CG9265	0.70491065	0.01174351	0.24215333
FBgn0265193	Atf-2	-0.6880791	0.01177964	0.24215333
FBgn0266324	CR44989	-0.8036909	0.01180494	0.24215333
FBgn0033061	SmydA-5	-2.1023725	0.01181468	0.24215333
FBgn0036910	Cyp305a1	-0.6668121	0.01184781	0.24234378
FBgn0041604	dlp	-0.7402252	0.01187404	0.24239256
FBgn0039341	CG5112	0.65561335	0.01192557	0.24295656
FBgn0039354	Lgr3	-1.2338725	0.01195704	0.24311049
FBgn0264490	Eip93F	0.62538907	0.01199931	0.2433802
FBgn0014388	sty	-0.7050165	0.01201818	0.2433802
FBgn0031638	CG11927	0.80214304	0.01208595	0.24426584
FBgn0038344	obe	0.7296449	0.01223782	0.24643733
FBgn0033696	Cyp6g2	2.22053272	0.01224187	0.24643733
FBgn0026374	Rhp	1.350286	0.01231227	0.24736464
FBgn0267237	CR45677	1.74638235	0.01235523	0.24773818
FBgn0030657	cerv	-0.8569887	0.01242377	0.24859931
FBgn0085446	CG34417	1.69799411	0.01244708	0.24859931
FBgn0265186	CG44251	0.79379331	0.01248167	0.24872688
FBgn0261575	tobi	3.99008404	0.01253178	0.24872688
FBgn0033638	CG9005	0.61373966	0.01253831	0.24872688
FBgn0051495	CG31495	1.14562919	0.01255134	0.24872688
FBgn0036502	CG7841	1.45298332	0.01261224	0.24900956

FBgn0050414	CG30414	-0.7656716	0.01261459	0.24900956
FBgn0038402	Fer2	-0.9392025	0.01265241	0.24927205
FBgn0041630	Hexo1	0.80086691	0.01270055	0.24973653
FBgn0040950	Muc26B	1.14950386	0.01287443	0.25186585
FBgn0039044	p53	0.86736553	0.01288571	0.25186585
FBgn0010044	GstD8	4.00501422	0.01289821	0.25186585
FBgn0033354	FANCI	-1.2549749	0.01290794	0.25186585
FBgn0085409	smal	-0.671295	0.01301262	0.25311483
FBgn0033540	Elp2	0.972288	0.01302174	0.25311483
FBgn0267766	CR46097	-1.3810906	0.0130641	0.25345354
FBgn0032049	Bace	3.56850343	0.01316505	0.2549256
FBgn0037781	Fancl	2.1349928	0.01320121	0.25513971
FBgn0050489	Cyp12d1-p	2.72100823	0.01324652	0.2555296
FBgn0015372	RabX1	0.61737733	0.01328587	0.25580341
FBgn0010226	GstS1	-0.5489151	0.01333774	0.25588648
FBgn0036419	CG13482	0.58329686	0.0133816	0.25588648
FBgn0082989	snoRNA:Psi28S-2442a	-0.9279725	0.01340338	0.25588648
FBgn0266361	CR45009	1.33484741	0.0134077	0.25588648
FBgn0263493	CR43482	2.40677228	0.01344279	0.25588648
FBgn0067783	att-ORFA	0.69827528	0.01345478	0.25588648
FBgn0266428	CR43463	-0.7123815	0.01346638	0.25588648
FBgn0033079	Fmo-2	0.96072419	0.01350713	0.25618195
FBgn0038095	Cyp304a1	2.23089689	0.01356585	0.25681654
FBgn0026418	Hsc70Cb	-0.606931	0.01360814	0.25695915
FBgn0046114	Gclm	0.89217178	0.01362444	0.25695915
FBgn0031878	sip2	-0.8690691	0.01364922	0.25695915
FBgn0038035	lig3	0.91621403	0.01371931	0.25773215
FBgn0032401	Plzf	1.02970954	0.01374297	0.25773215
FBgn0034058	Pex11	0.68222963	0.01378837	0.25773215
FBgn0050359	Mal-A5	1.96908502	0.01379169	0.25773215
FBgn0033635	Prip	0.80727254	0.01389896	0.25926032
FBgn0039844	CG1607	1.91499729	0.0139434	0.25951436
FBgn0029006	Smurf	-0.5241198	0.01396364	0.25951436
FBgn0035689	CG7376	0.93841625	0.01435022	0.26592825
FBgn0027657	glob1	-0.6280487	0.01436756	0.26592825
FBgn0000253	Cam	0.63380093	0.01441211	0.26592825
FBgn0036896	wnd	1.06203896	0.01441338	0.26592825
FBgn0036199	Bmcp	-0.5801364	0.01446876	0.26643254
FBgn0036837	CG18135	1.15894781	0.01449313	0.26643254
FBgn0003863	alphaTry	2.64704873	0.0145277	0.26658584

FBgn0058354	CR40354	1.02678654	0.01456707	0.26682664
FBgn0032726	CG10621	2.16588708	0.01467947	0.26840191
FBgn0063368	Gpb5	-0.8346025	0.01470773	0.26843583
FBgn0032124	CG17855	0.69453183	0.01474286	0.26859475
FBgn0039870	CG1896	-0.5940259	0.01476973	0.26860308
FBgn0000546	EcR	-0.6311922	0.0149216	0.26935256
FBgn0003502	Btk29A	-0.7160397	0.0149276	0.26935256
FBgn0062412	Ctr1B	1.79412879	0.01497295	0.26935256
FBgn0002887	mus201	0.79317676	0.01498649	0.26935256
FBgn0034617	Panx	0.81502003	0.01499125	0.26935256
FBgn0050344	CG30344	0.6418361	0.014992	0.26935256
FBgn0031398	CG10880	0.62255953	0.01499641	0.26935256
FBgn0052815	CG32815	-0.6223114	0.01506419	0.26964055
FBgn0039637	CG11880	0.75150726	0.0150655	0.26964055
FBgn0031500	CG17221	1.03188087	0.01510611	0.26989223
FBgn0001970	Pgant35A	-0.7020504	0.01540768	0.27479739
FBgn0010053	Jheh1	1.14716022	0.0154395	0.27488267
FBgn0052282	Drsl4	2.66286377	0.01554265	0.27546234
FBgn0036493	CG7255	1.30984468	0.015545	0.27546234
FBgn0037252	CG14650	-0.5229624	0.01559213	0.27546234
FBgn0266742	CR45215	1.93016978	0.0156309	0.27546234
FBgn0035300	CG1139	2.49888848	0.01564337	0.27546234
FBgn0030748	Traf-like	0.67128574	0.01564998	0.27546234
FBgn0033447	dila	-1.1242779	0.01566174	0.27546234
FBgn0034156	CG5348	0.81691161	0.01570273	0.27570639
FBgn0037025	Spc105R	-1.624103	0.01583402	0.27753223
FBgn0001149	GstD1	1.33146736	0.01599806	0.27992481
FBgn0015571	alpha-Est3	1.53977948	0.01609247	0.28109283
FBgn0264571	CR43943	-1.1602991	0.01617827	0.28210684
FBgn0037936	CG6908	3.10543177	0.01622052	0.2821646
FBgn0004426	LysC	3.41513607	0.01625351	0.2821646
FBgn0038681	Cyp12a4	1.40494576	0.01627607	0.2821646
FBgn0035484	CG11594	1.34157918	0.0162926	0.2821646
FBgn0023094	cyc	-0.5103606	0.01635047	0.28268513
FBgn0016797	fz2	-0.8726836	0.01643897	0.28373274
FBgn0035833	CG7565	0.56144838	0.01651207	0.28451136
FBgn0035039	Adck	0.92079658	0.01658694	0.28497724
FBgn0039856	CG1774	1.35245785	0.01659517	0.28497724
FBgn0000636	Fas3	0.83755902	0.016649	0.28541951
FBgn0265819	CR44608	-0.9355786	0.01679617	0.28745774

FBgn0263458	snoRNA:CG43051-a	-0.5526389	0.01687274	0.28828284
FBgn0036534	DCP2	0.52486576	0.01694611	0.28859105
FBgn0260632	dl	-0.6242401	0.01701591	0.28859105
FBgn0030839	CG5613	1.23975811	0.01701912	0.28859105
FBgn0038608	WRNexo	-1.0868324	0.01702096	0.28859105
FBgn0034318	CG14500	2.38662304	0.0170736	0.28859105
FBgn0037746	CG8478	-1.6786098	0.01708667	0.28859105
FBgn0028978	trbl	0.80033783	0.0170895	0.28859105
FBgn0016081	fry	0.5546407	0.01720652	0.29008541
FBgn0023000	mth	-0.6116356	0.01735504	0.29210481
FBgn0023535	arg	1.36736864	0.01741008	0.2925469
FBgn0039274	CG11920	-0.6317403	0.01746698	0.29263066
FBgn0035983	CG4080	-0.5575052	0.01747264	0.29263066
FBgn0002567	Rab32	-0.603737	0.01750582	0.29270414
FBgn0005696	DNApol-alpha73	-1.8328457	0.01755762	0.29306803
FBgn0035586	CG10671	0.7186375	0.01761114	0.29306803
FBgn0052104	CG32104	-0.86705	0.01761406	0.29306803
FBgn0259707	CG42361	0.75931596	0.01766448	0.29342656
FBgn0016054	phr6-4	-0.8342167	0.01793592	0.29615757
FBgn0004598	Fur2	-0.6010857	0.01794007	0.29615757
FBgn0025815	Mcm6	-1.0660394	0.0179402	0.29615757
FBgn0037659	Kdm2	-0.6987853	0.01794541	0.29615757
FBgn0034670	CG13488	-0.6619303	0.01809844	0.29819895
FBgn0034029	eIF2Bgamma	0.75555279	0.01821153	0.29957675
FBgn0044872	FucTC	1.1835262	0.01829436	0.30003431
FBgn0283471	wupA	-1.9030174	0.01831661	0.30003431
FBgn0261266	zuc	-0.8214372	0.01832789	0.30003431
FBgn0030766	mthl1	-0.664631	0.01846723	0.30121128
FBgn0002631	E(spl)m5-HLH	-1.3196904	0.01849029	0.30121128
FBgn0031779	CG9175	0.92032205	0.01849832	0.30121128
FBgn0033072	CG17994	2.10393857	0.0185183	0.30121128
FBgn0032835	CG16772	-1.3309371	0.01872891	0.30352564
FBgn0023416	Ac3	1.01294646	0.01874244	0.30352564
FBgn0039528	dsd	0.77446148	0.01876397	0.30352564
FBgn0028467	CG11070	0.56131386	0.0188029	0.30352564
FBgn0034494	CG10444	-0.6406874	0.01880987	0.30352564
FBgn0038868	CG5862	0.56938443	0.01896687	0.30557399
FBgn0038083	CG5999	2.47406538	0.01901381	0.30584557
FBgn0266115	CR44841	-0.5959482	0.01930312	0.30935576
FBgn0267730	CR46061	0.80658359	0.01931741	0.30935576

FBgn0262619	DNA-ligI	-1.0146819	0.01939737	0.30935576
FBgn0015575	alpha-Est7	2.47360214	0.01940769	0.30935576
FBgn0270926	AsnS	0.84083819	0.01945577	0.30935576
FBgn0267803	CR46128	1.51063504	0.01948895	0.30935576
FBgn0038275	CG3817	-0.5331486	0.01949162	0.30935576
FBgn0063492	GstE8	1.27475151	0.01950051	0.30935576
FBgn0039774	CDase	-0.5005912	0.01950591	0.30935576
FBgn0010482	l(2)01289	0.98850015	0.01963074	0.31036944
FBgn0260935	Vps15	0.66751681	0.0196597	0.31036944
FBgn0037900	CG5276	0.6440972	0.01966141	0.31036944
FBgn0040364	CG11378	0.64791981	0.01974366	0.31118465
FBgn0036953	CG17145	2.47952685	0.01977447	0.31118774
FBgn0085423	CG34394	0.61934255	0.01990061	0.31268866
FBgn0265934	CR44723	-1.1908186	0.01996453	0.31303892
FBgn0031381	Npc2a	0.67597688	0.020032	0.31303892
FBgn0035356	CG16986	2.93016434	0.02003989	0.31303892
FBgn0250830	CG12547	0.52060874	0.0200959	0.31303892
FBgn0267691	CR46027	2.12228997	0.02011264	0.31303892
FBgn0039342	CG5107	3.22115505	0.02015079	0.31303892
FBgn0003159	CG2841	0.65995272	0.02015275	0.31303892
FBgn0052009	CR32009	0.98215352	0.02016924	0.31303892
FBgn0031575	Cep97	-0.7763858	0.02022911	0.31327672
FBgn0283741	prage	0.63467278	0.02024619	0.31327672
FBgn0001330	kz	-0.6752601	0.02040002	0.31517722
FBgn0029155	Men-b	1.1187985	0.02044392	0.31537621
FBgn0035951	CG5068	-0.5837917	0.02055231	0.31636777
FBgn0033789	CG13324	2.70246121	0.02062458	0.31636777
FBgn0035760	CG8607	-0.9081303	0.02063719	0.31636777
FBgn0003257	r-l	-0.5168444	0.02069811	0.31636777
FBgn0067782	att-ORFB	0.70234076	0.0207198	0.31636777
FBgn0011206	bol	0.54993091	0.02072563	0.31636777
FBgn0038487	TwdlW	-1.042597	0.02075576	0.31636777
FBgn0263770	CR43687	1.22109076	0.02075716	0.31636777
FBgn0015036	Cyp4ae1	1.64096168	0.02082949	0.31698461
FBgn0035047	Pof	0.6068539	0.02085999	0.31698461
FBgn0039417	CG6073	-0.6280998	0.02098217	0.31791628
FBgn0035249	CG17249	0.64806729	0.02100539	0.31791628
FBgn0001992	Cyp303a1	0.74599411	0.02104266	0.31791628
FBgn0035632	Ppat-Dpck	0.70724799	0.02106791	0.31791628
FBgn0261286	Mat89Ba	-0.5863879	0.02107767	0.31791628

FBgn0035401	CG1291	0.66181413	0.0211621	0.31837863
FBgn0035665	Jon65Aiii	3.10978484	0.02117096	0.31837863
FBgn0267742	CR46073	0.90819516	0.02120662	0.31844392
FBgn0064116	CG33713	-0.4922968	0.02131322	0.3190926
FBgn0064117	SLIRP1	-0.4922968	0.02131322	0.3190926
FBgn0030747	CG4301	0.62997714	0.02134399	0.3190926
FBgn0266579	tau	0.77962848	0.02138115	0.31917877
FBgn0063667	CG32335	1.48613551	0.02144773	0.31970319
FBgn0263337	CR43418	3.31021207	0.02150433	0.31986483
FBgn0033774	CG12374	3.86602748	0.0215215	0.31986483
FBgn0051076	CG31076	1.22716257	0.02158283	0.32020679
FBgn0285962		0.8163264	0.02161938	0.32020679
FBgn0015391	glu	-0.8974665	0.021639	0.32020679
FBgn0030261	CG15203	-0.8820491	0.02175897	0.32151412
FBgn0051065	ppk31	1.02263845	0.02185724	0.32249745
FBgn0035298	SCOT	0.56584626	0.02190253	0.32269724
FBgn0085802	18SrRNA:CR41548	1.11217819	0.02202446	0.32402417
FBgn0005624	Psc	-0.660952	0.02207248	0.32426129
FBgn0024992	CG2658	0.74408427	0.02218098	0.32476552
FBgn0039709	Cad99C	1.91901175	0.02220608	0.32476552
FBgn0085412	CG34383	0.89340793	0.02221825	0.32476552
FBgn0004228	mex1	1.10682251	0.02224118	0.32476552
FBgn0032873	CG2614	-0.5650029	0.02226653	0.32476552
FBgn0038381	CG3303	-0.7266889	0.02233574	0.32522902
FBgn0036481	CG16959	1.05547493	0.02237801	0.32522902
FBgn0028572	qtc	1.07939809	0.0224125	0.32522902
FBgn0039494	grass	1.59233143	0.02245229	0.32522902
FBgn0054040	CG34040	3.16875976	0.02247784	0.32522902
FBgn0033538	CG11883	-0.8735804	0.02250749	0.32522902
FBgn0037772	Spn85F	-0.9211613	0.02252225	0.32522902
FBgn0036299	Tsf2	0.66572304	0.02269848	0.32730891
FBgn0001085	fz	0.79034427	0.02285494	0.32909818
FBgn0029664	CG10802	1.85837736	0.02295753	0.33010787
FBgn0021818	cnk	-0.4998602	0.02305304	0.33080882
FBgn0259678	sqa	0.82933804	0.02307338	0.33080882
FBgn0035065	CG3589	0.53868656	0.02311237	0.33080882
FBgn0037702	CG8176	-0.5017582	0.02316851	0.33080882
FBgn0038783	CG4367	-1.8365589	0.02316898	0.33080882
FBgn0036738	CG7542	4.10163326	0.02327356	0.33124039
FBgn0051300	CG31300	2.63555449	0.02335664	0.33124039

FBgn0023169	AMPKalpha	-0.4743909	0.0233854	0.33124039
FBgn0284221	Sema5c	0.71495378	0.02338606	0.33124039
FBgn0010395	Itgbn	0.65549535	0.02343923	0.33124039
FBgn0032935	Atg18b	0.68894055	0.02347268	0.33124039
FBgn0050360	Mal-A6	3.40498664	0.02350745	0.33124039
FBgn0039084	CG10175	-0.6895591	0.02352632	0.33124039
FBgn0051288	CG31288	1.09098459	0.02354163	0.33124039
FBgn0030662	CG9220	-0.5036008	0.02357429	0.33124039
FBgn0002719	Men	0.72510716	0.02358291	0.33124039
FBgn0028534	CG7916	1.56322821	0.02359147	0.33124039
FBgn0031805	CG9505	0.8307093	0.02362279	0.33124039
FBgn0037973	CG18547	0.83229198	0.02378148	0.33232659
FBgn0031279	CG3544	-0.5891843	0.02379506	0.33232659
FBgn0259979	CG17337	-0.5041339	0.02379832	0.33232659
FBgn0036547	CG17032	-1.0609112	0.02384078	0.33246272
FBgn0035231	Pcyt2	-0.7686647	0.02388046	0.33255995
FBgn0029608	CG3091	1.71301835	0.02395855	0.33319097
FBgn0086603	snoRNA:Or-CD2	-0.9222172	0.02406813	0.33425761
FBgn0036935	CG14186	1.08128227	0.0241326	0.33469582
FBgn0037751	topi	0.96871421	0.0242059	0.335255
FBgn0028853	CG15263	4.50652673	0.02430629	0.33618742
FBgn0038893	Archease	0.77836813	0.02434721	0.33629589
FBgn0035424	CG11505	0.57613281	0.02451285	0.33812435
FBgn0000451	ect	-0.5829246	0.02477632	0.33944156
FBgn0031948	CG7149	-1.0796081	0.02479336	0.33944156
FBgn0003268	rod	-0.8526557	0.02479868	0.33944156
FBgn0051648	CG31648	0.73373389	0.02484336	0.33944156
FBgn0037924	CG14712	-1.0613238	0.02488191	0.33944156
FBgn0003356	Jon99Cii	2.5295328	0.02489772	0.33944156
FBgn0037842	CG6567	0.58940087	0.02489836	0.33944156
FBgn0010359	gammaTry	2.88785044	0.02490702	0.33944156
FBgn0039543	CG12428	0.84538515	0.02493517	0.33944156
FBgn0035977	PGRP-LF	-0.7826298	0.02494224	0.33944156
FBgn0051414	Gba1b	1.2324742	0.02503709	0.33994314
FBgn0039501	CG5987	-1.2661549	0.02507591	0.33994314
FBgn0260775	DnaJ-60	-0.4658934	0.02514015	0.33994314
FBgn0260770	CG42568	-0.4658934	0.02514015	0.33994314
FBgn0034179	CG6805	0.89569593	0.0251463	0.33994314
FBgn0023129	aay	1.24030069	0.0254347	0.34266722
FBgn0036563	CG13075	4.35760526	0.02545338	0.34266722

FBgn0025620	CG13360	3.17525908	0.02549136	0.34266722
FBgn0034219	mthl4	-0.8263676	0.02549747	0.34266722
FBgn0040089	meso18E	-1.0593658	0.02551634	0.34266722
FBgn0030482	CG1673	1.38491779	0.02576119	0.3454192
FBgn0029158	Las	0.90229045	0.02578922	0.3454192
FBgn0037993	dpr15	1.46824604	0.02586471	0.34597458
FBgn0034137	CG4945	-0.9485415	0.02593296	0.34643157
FBgn0020909	Rtc1	-0.5227089	0.02596956	0.34646532
FBgn0026702	l(1)G0045	-0.6654848	0.0261537	0.34846458
FBgn0035431	CG14968	0.69683015	0.02625522	0.34878108
FBgn0040827	CG13315	2.21136001	0.02626014	0.34878108
FBgn0037773	CG5359	-0.7086099	0.02628038	0.34878108
FBgn0028539	CG31731	0.56180845	0.0263173	0.34881569
FBgn0285963		-0.5368911	0.02639468	0.34904475
FBgn0011828	Pxn	2.84382313	0.02642569	0.34904475
FBgn0011659	Mlh1	-0.6781409	0.02649061	0.34904475
FBgn0265299	CR44272	-1.3508667	0.0265131	0.34904475
FBgn0265873	CR44662	2.19673021	0.02658982	0.34904475
FBgn0051158	Efa6	-0.6460737	0.02659299	0.34904475
FBgn0004556	Dbp73D	-0.666677	0.02659584	0.34904475
FBgn0263030	CG43325	1.86681114	0.0266382	0.34904475
FBgn0036697	rogdi	0.66758606	0.02668322	0.34904475
FBgn0034317	CG14499	1.48453538	0.02669714	0.34904475
FBgn0038530	AttD	1.80120992	0.02671226	0.34904475
FBgn0000566	Eip55E	0.72997215	0.02681429	0.34992815
FBgn0001321	knk	-2.0451839	0.02698163	0.35096465
FBgn0264501	CR43900	0.69209028	0.02698986	0.35096465
FBgn0261822	Bsg	0.50376557	0.02699728	0.35096465
FBgn0039751	CG1983	0.74457852	0.02703285	0.35097827
FBgn0085484	Pdxk	1.078958	0.02715092	0.35199202
FBgn0033821	CG10799	2.36564731	0.02718018	0.35199202
FBgn0023536	CG3156	0.90718484	0.02729851	0.35262758
FBgn0011672	Mvl	-0.5661484	0.02730197	0.35262758
FBgn0037146	CG7470	3.01346155	0.02733744	0.35262758
FBgn0051759	CG31759	0.81247091	0.02736801	0.35262758
FBgn0038720	CG6231	0.97321919	0.02745661	0.35309297
FBgn0029082	hbs	-0.5170695	0.02748039	0.35309297
FBgn0031877	CG10399	0.9124934	0.02764053	0.35309297
FBgn0010241	Mdr50	1.61033649	0.02765653	0.35309297
FBgn0263342	CR43423	1.26915157	0.02766572	0.35309297

FBgn0030723	dpr18	-0.5849813	0.02769018	0.35309297
FBgn0000810	fs(1)K10	-0.4762308	0.02770144	0.35309297
FBgn0004391	shtd	-0.9857115	0.02770454	0.35309297
FBgn0015034	Cyp4e1	2.34560683	0.02773706	0.35309297
FBgn0038179	CG9312	1.5459581	0.02775145	0.35309297
FBgn0262353	CR43051	-0.5195592	0.02786197	0.35362581
FBgn0026393	Or43b	-0.5405787	0.0278629	0.35362581
FBgn0260003	Dys	-0.4912173	0.02799543	0.3548648
FBgn0036844	Mkp3	-0.8265856	0.02819069	0.35655665
FBgn0033792	CG13325	3.65711913	0.02822594	0.35655665
FBgn0267506	pre-rRNA:CR45846	-1.8786492	0.02826416	0.35655665
FBgn0035189	CG9119	1.62969555	0.0282692	0.35655665
FBgn0034281	CG14490	-1.5297647	0.02831422	0.35662776
FBgn0000442	Pkg21D	-0.5769801	0.028345	0.35662776
FBgn0052438	SMC5	-0.5318514	0.02854908	0.35756517
FBgn0051953	CR31953	1.08686956	0.028564	0.35756517
FBgn0031611	FIG4	0.70781564	0.0286127	0.35756517
FBgn0040723	CG5011	1.6999834	0.02862028	0.35756517
FBgn0035355	CG16985	1.67316162	0.02862928	0.35756517
FBgn0037667	CG16734	-0.9160977	0.02875527	0.35756517
FBgn0032187	CG4839	1.94126997	0.02880463	0.35756517
FBgn0033081	geminin	-0.5683712	0.0288107	0.35756517
FBgn0267348	LanB2	-0.5363252	0.02888282	0.35756517
FBgn0053136	CG33136	-0.8053253	0.02891757	0.35756517
FBgn0033736	CG13154	1.19168836	0.02891907	0.35756517
FBgn0034394	CG15096	3.00172519	0.02895294	0.35756517
FBgn0262009	CG42827	-0.9543356	0.02897258	0.35756517
FBgn0039537	CG5590	0.74747733	0.02897513	0.35756517
FBgn0053054	CG33054	-0.7411716	0.02898112	0.35756517
FBgn0015336	CG15865	1.66850247	0.02898226	0.35756517
FBgn0004378	Klp61F	-0.8120264	0.02909536	0.35852535
FBgn0036369	CG10089	1.39971012	0.02913776	0.35861317
FBgn0051104	CG31104	3.31754962	0.02931942	0.35963141
FBgn0034602	Lapsyn	1.52824561	0.02935357	0.35963141
FBgn0014380	RhoL	-0.706691	0.02940419	0.35963141
FBgn0082978	snoRNA:Psi28S-3091b	-1.0466153	0.02945199	0.35963141
FBgn0262738	norpA	0.72457518	0.02945567	0.35963141
FBgn0027082	ProRS-m	1.22074231	0.029467	0.35963141
FBgn0265419	CR44331	0.69433888	0.02946813	0.35963141
FBgn0003357	Jon99Ciii	2.42637022	0.02951721	0.35979847

FBgn0038756	CG4783	1.95347679	0.02964886	0.36059289
FBgn0038680	Cyp12a5	2.65174521	0.02974983	0.36059289
FBgn0030048	CG12112	0.62016424	0.02977474	0.36059289
FBgn0033686	Hen1	-0.5894982	0.02977587	0.36059289
FBgn0010194	Wnt5	-0.642312	0.02979512	0.36059289
FBgn0034002	CG8079	0.77623983	0.0297952	0.36059289
FBgn0032779	CG16771	0.64919571	0.02986321	0.36079643
FBgn0004362	HmgD	-0.6722362	0.02992022	0.36079643
FBgn0032242	CG5355	0.60892778	0.03000736	0.36079643
FBgn0264939	CR44108	-0.5301157	0.03006892	0.36079643
FBgn0001090	bnb	1.14069781	0.03008114	0.36079643
FBgn0030638	CG11655	0.89847942	0.0300841	0.36079643
FBgn0026616	alpha-Man-IIb	-1.1292902	0.03008878	0.36079643
FBgn0032350	CG6287	1.4742277	0.03011639	0.36079643
FBgn0036035	CG18178	-0.4865366	0.03013144	0.36079643
FBgn0050021	metro	-1.0965024	0.03025184	0.36181197
FBgn0030478	CG1640	0.88015595	0.03041381	0.36284573
FBgn0263234	Phae1	2.46470831	0.03044036	0.36284573
FBgn0028970	betaggt-II	0.70319209	0.03046713	0.36284573
FBgn0036336	ste14	0.66137356	0.03049532	0.36284573
FBgn0260940	lsn	0.66601891	0.03051673	0.36284573
FBgn0284442	Mcm3	-0.8041937	0.03065887	0.36398516
FBgn0004636	Rap1	0.48548515	0.03068417	0.36398516
FBgn0033982	Cyp317a1	-0.5875077	0.0311535	0.36912174
FBgn0031708	CG7382	0.61089519	0.03120853	0.36932113
FBgn0013347	TfIIA-S	-0.5017338	0.03124298	0.36932113
FBgn0263451	CR43474	-1.0098282	0.03144804	0.37131333
FBgn0031970	CG7227	1.60431233	0.03151003	0.37161367
FBgn0050460	CG30460	-0.6029841	0.03168669	0.37326407
FBgn0046685	Wsck	0.66056219	0.03174237	0.37348722
FBgn0031732	CG11149	2.41855019	0.0317881	0.37359284
FBgn0037057	CG10512	-0.6796815	0.03186026	0.37400855
FBgn0037750	Whamy	0.93546708	0.03203225	0.37559383
FBgn0263510	nclb	-0.5744831	0.03214644	0.37565946
FBgn0051472	sgll	0.77872998	0.03216971	0.37565946
FBgn0035619	CG10592	3.11070835	0.03219695	0.37565946
FBgn0028962	AlaRS-m	0.62522846	0.03228518	0.37565946
FBgn0038878	CG3301	1.12701604	0.03230125	0.37565946
FBgn0002552	lin	-0.4839821	0.03230925	0.37565946
FBgn0022787	Hel89B	-0.4766975	0.03232114	0.37565946

FBgn0083120	Uhg8	-0.6425012	0.03234917	0.37565946
FBgn0028421	Kap3	-0.5714152	0.03237042	0.37565946
FBgn0034396	CG15097	-0.679348	0.0325255	0.37676664
FBgn0038902	CG6800	-0.9917807	0.03258275	0.37676664
FBgn0029932	CG4607	2.61427107	0.0326053	0.37676664
FBgn0030881	CG12985	1.04523823	0.03261407	0.37676664
FBgn0063497	GstE3	1.10227457	0.03284998	0.3788477
FBgn0038466	CG8907	1.20970612	0.03286875	0.3788477
FBgn0038429	CG14882	-0.6377472	0.0330123	0.38007141
FBgn0036366	CG10133	0.80469767	0.03314939	0.38116289
FBgn0032476	CG5439	0.49355254	0.03322898	0.38116289
FBgn0005664	Crys	1.49735288	0.03325509	0.38116289
FBgn0028436	ECSIT	0.66970949	0.03325708	0.38116289
FBgn0002735	E(spl)mgamma-HLH	-0.7446838	0.0333342	0.38161649
FBgn0263240	Coop	-0.6394684	0.03344881	0.38168862
FBgn0039407	CG14544	-0.7684374	0.03346646	0.38168862
FBgn0034247	CG6484	2.66375114	0.03351802	0.38168862
FBgn0004643	Zw10	-0.5475637	0.03360811	0.38168862
FBgn0038354	CG5404	1.16084247	0.033656	0.38168862
FBgn0037777	CG11722	0.78769589	0.03368082	0.38168862
FBgn0038394	CG10264	-1.0023129	0.03370611	0.38168862
FBgn0035235	CG7879	-0.5639067	0.033761	0.38168862
FBgn0013323	Ptth	-0.6559788	0.03377327	0.38168862
FBgn0050354	UQCR-11L	1.69053853	0.03378701	0.38168862
FBgn0085753	28SrRNA-Psi:CR40596	4.37064992	0.0338573	0.38168862
FBgn0264962	Pcf11	-0.5766542	0.03385953	0.38168862
FBgn0047334	BG642312	2.21392036	0.03388725	0.38168862
FBgn0024329	Mekk1	-0.4896878	0.03391134	0.38168862
FBgn0025454	Cyp6g1	2.43209326	0.03394371	0.38168862
FBgn0037834	Art1	-0.4768244	0.03397401	0.38168862
FBgn0037722	CG8319	-0.6691926	0.03397877	0.38168862
FBgn0031881	MME1	1.07180969	0.03410287	0.38265975
FBgn0032839	CG10659	2.69392206	0.03423828	0.38353223
FBgn0037845	CG14694	2.19333547	0.03425608	0.38353223
FBgn0265800	CR44589	0.91210613	0.03431995	0.38361406
FBgn0011555	thetaTry	3.27548027	0.03433885	0.38361406
FBgn0038854	CG7044	0.93790793	0.03454717	0.38551761
FBgn0085437	CG34408	0.62417532	0.03458767	0.38554636
FBgn0038742	Arc42	-0.5685424	0.03470423	0.38642196
FBgn0265185	CG44250	0.76455215	0.03476226	0.38664453

FBgn0034422	CG7137	-0.753444	0.03480868	0.38673773
FBgn0260027	CG42495	0.84589739	0.03494399	0.38781726
FBgn0010877	l(3)05822	-0.5835667	0.03501197	0.38814801
FBgn0030412	Tomosyn	0.50097429	0.03517763	0.38955965
FBgn0263771	CR43688	2.23091883	0.03532258	0.3907392
FBgn0042092	CG13773	-0.5811954	0.0353798	0.39079305
FBgn0033205	CG2064	1.10532313	0.03540433	0.39079305
FBgn0034488	CG11208	0.60159765	0.0356532	0.39277839
FBgn0034605	CG15661	2.27462235	0.03566147	0.39277839
FBgn0035132	mthl10	-0.5697691	0.03578239	0.39351719
FBgn0014949	btn	-1.3570922	0.03581655	0.39351719
FBgn0026602	Ady43A	0.71293563	0.03586215	0.39351719
FBgn0023530	CG3740	0.91450713	0.03588338	0.39351719
FBgn0010038	GstD2	1.80970358	0.03595066	0.3938302
FBgn0003575	su(sable)	-0.6230736	0.03600365	0.39398607
FBgn0039639	CG14512	0.80570295	0.03605364	0.39410896
FBgn0038739	CG4686	0.58631366	0.03609667	0.3941555
FBgn0003254	rib	1.93745223	0.0363105	0.39606491
FBgn0030687	CG17209	0.61919906	0.03641316	0.39675903
FBgn0038380	CG14877	0.66727344	0.03651194	0.39740935
FBgn0025626	CG4281	-0.4893442	0.03659891	0.39792992
FBgn0052137	CG32137	1.18345354	0.03669856	0.39858717
FBgn0034082	CG10734	1.94937067	0.03673926	0.39860331
FBgn0036806	Cyp12c1	1.3656409	0.03685028	0.39879131
FBgn0031814	retm	0.58149637	0.03687186	0.39879131
FBgn0031766	CG9117	1.05285987	0.03689269	0.39879131
FBgn0040823	dpr6	1.08520315	0.0369135	0.39879131
FBgn0086442	mib2	-0.4582403	0.03699821	0.39908933
FBgn0265715	CR44522	1.93954577	0.0370196	0.39908933
FBgn0041184	Socs36E	-0.6225016	0.03712405	0.39927169
FBgn0004885	tok	2.58498753	0.03713645	0.39927169
FBgn0034406	Jheh3	0.65962442	0.03715434	0.39927169
FBgn0014427	CG11899	1.28717817	0.03735451	0.40099894
FBgn0266700	CR45190	0.72658595	0.03742969	0.40138215
FBgn0051344	CG31344	1.10641896	0.03747903	0.40143676
FBgn0035702	CG10147	0.69049266	0.03754539	0.40143676
FBgn0052687	CG32687	1.63175287	0.03756317	0.40143676
FBgn0037838	CG4089	-0.8607821	0.03761621	0.40143676
FBgn0031897	CG13784	0.50190191	0.03766236	0.40143676
FBgn0000723	FER	-0.5957924	0.03770407	0.40143676

FBgn0051087	CG31087	1.12722619	0.0377112	0.40143676
FBgn0051072	Lerp	0.82637375	0.03777868	0.40173435
FBgn0033788	CG13323	1.95923005	0.03781825	0.40173491
FBgn0039355	CG4730	-0.6258996	0.03787297	0.4018963
FBgn0030724	Nipsnap	0.60774552	0.03798418	0.40265613
FBgn0042175	CG18858	0.79481168	0.03807438	0.40319177
FBgn0004919	gol	-0.6770767	0.03815763	0.4035422
FBgn0052656	Muc11A	-1.8219882	0.03818686	0.4035422
FBgn0263467	snoRNA:nop5-x16-a	-0.9774627	0.03829368	0.40402014
FBgn0034476	Toll-7	-0.9996469	0.03834418	0.40402014
FBgn0032066	LManIII	-1.8903152	0.03841211	0.40402014
FBgn0004369	Ptp99A	-0.5582789	0.03843035	0.40402014
FBgn0051852	Tap42	0.77242081	0.03843953	0.40402014
FBgn0029999	CG1575	-0.5227899	0.03847054	0.40402014
FBgn0026149	BCL7-like	0.57249461	0.03860663	0.40452237
FBgn0025885	Inos	-0.4873015	0.0386157	0.40452237
FBgn0033712	mIF3	0.55479175	0.03863774	0.40452237
FBgn0030749	AnxB11	0.52339561	0.03868699	0.40462129
FBgn0039205	CG13623	1.24314386	0.03877317	0.4051059
FBgn0039472	CG17192	3.06129109	0.03883392	0.40532408
FBgn0033381	GstE13	-0.5353333	0.03888828	0.40547509
FBgn0037504	CG1142	-0.5013562	0.03893424	0.40553843
FBgn0028341	Ptpmeg2	-0.5762565	0.03902247	0.4057271
FBgn0039272	CG11836	-1.0198521	0.03903218	0.4057271
FBgn0032225	CG5022	-0.7788594	0.03917593	0.4068054
FBgn0039840	pHCl-2	2.93336703	0.03921911	0.40683819
FBgn0032040	CG13386	2.39156548	0.03928761	0.40713339
FBgn0033117	CG3358	0.55434995	0.03938448	0.40752015
FBgn0033787	CG13321	2.01828166	0.03959709	0.40752015
FBgn0031645	CG3036	-0.8179813	0.03965928	0.40752015
FBgn0021979	l(2)k09913	0.49428583	0.0397148	0.40752015
FBgn0039829	CG15561	-0.5999283	0.03974521	0.40752015
FBgn0033945	CG12868	-0.7539985	0.03980232	0.40752015
FBgn0032196	CG5708	-0.5050655	0.03980727	0.40752015
FBgn0035438	PHGPx	0.73614636	0.03985693	0.40752015
FBgn0083068	CG33947	0.62683443	0.03987114	0.40752015
FBgn0264296	CG43774	1.70340199	0.03989196	0.40752015
FBgn0042106	CG18754	-1.3787908	0.0399382	0.40752015
FBgn0265053	CR44168	0.99771405	0.03998196	0.40752015
FBgn0030320	CG2247	-0.4689066	0.04001425	0.40752015

FBgn0266365	CR45013	1.31701083	0.04002082	0.40752015
FBgn0032083	CG9541	-0.8064013	0.04002895	0.40752015
FBgn0004050		-0.4543007	0.04003358	0.40752015
FBgn0038020	GstD9	0.84617062	0.04003921	0.40752015
FBgn0082994	snoRNA:Psi28S-1837c	-0.8583996	0.04004649	0.40752015
FBgn0033502	CG12910	-0.5463221	0.04012329	0.40789337
FBgn0039920	CG11360	0.56201808	0.04020978	0.40803535
FBgn0026563	CG1979	2.58668101	0.04026298	0.40803535
FBgn0265345	CR44299	0.92262127	0.04027147	0.40803535
FBgn0266362	CR45010	1.10230423	0.04029781	0.40803535
FBgn0037703	JHDM2	-0.4515852	0.04043243	0.40899111
FBgn0035539	slow	0.9794577	0.04054656	0.40952425
FBgn0004463	RpIII128	-0.5715422	0.0406228	0.40952425
FBgn0052017	CG32017	0.51640063	0.04062313	0.40952425
FBgn0034282	Mapmodulin	-0.4924777	0.04064627	0.40952425
FBgn0043806	CG32032	2.06126132	0.04070125	0.40960604
FBgn0032639	CG18563	-1.1199619	0.04073497	0.40960604
FBgn0015393	hoip	-0.7291881	0.04082804	0.4096821
FBgn0264510	CR43909	1.5299973	0.04085572	0.4096821
FBgn0004910	Eip63F-1	1.06416501	0.04087535	0.4096821
FBgn0032889	CG9331	0.5423683	0.04090373	0.4096821
FBgn0036225	CG5883	2.82582228	0.04095607	0.4098026
FBgn0265853	CR44642	1.64002085	0.04115984	0.4108513
FBgn0033296	Mal-A7	2.70492342	0.04116357	0.4108513
FBgn0000639	Fbp1	-1.7667796	0.04118561	0.4108513
FBgn0063449	Uhg2	-0.9543429	0.04123322	0.4108513
FBgn0038974	CG5377	0.82353404	0.04126295	0.4108513
FBgn0000326	clt	0.70047911	0.04136821	0.41108105
FBgn0037856	Leash	0.672999	0.04139377	0.41108105
FBgn0032750	CG10495	-0.7283957	0.04140734	0.41108105
FBgn0039309	CG11891	2.08214489	0.04154504	0.41148605
FBgn0039308	CG11889	2.08214489	0.04154504	0.41148605
FBgn0265101	Sgt1	0.53072693	0.04156956	0.41148605
FBgn0001179	hay	0.70556688	0.04162427	0.41158211
FBgn0033010	Atf6	0.48471234	0.04177767	0.41158211
FBgn0025781	Cdc16	0.74814363	0.04179677	0.41158211
FBgn0037345	rev7	0.93386354	0.0418142	0.41158211
FBgn0036205	CG14131	1.39173709	0.0418161	0.41158211
FBgn0032633	Lrch	-0.5894755	0.04190283	0.41158211
FBgn0032590	CG4631	1.76714696	0.04192094	0.41158211

FBgn0039051	CG17109	1.74580066	0.04194766	0.41158211
FBgn0030348	CG10352	1.05165066	0.04198839	0.41158211
FBgn0033740	dgt5	-0.5257292	0.04203009	0.41158211
FBgn0001075	ft	-1.5731368	0.04205962	0.41158211
FBgn0051659	CG31659	2.04344433	0.04207715	0.41158211
FBgn0267794	CR43174	-0.746831	0.04211364	0.41158211
FBgn0086451	l(2)k09022	-0.57955	0.04216252	0.41158211
FBgn0266657	CR45164	0.51990264	0.04218656	0.41158211
FBgn0264001	bru3	0.63334426	0.04226738	0.41197529
FBgn0035360	CG1246	1.92424565	0.04233878	0.41227585
FBgn0004364	18w	-0.7012848	0.04240551	0.41248856
FBgn0031224	CG11454	0.53723394	0.04244177	0.41248856
FBgn0033733	CG8834	2.00382107	0.04253781	0.41302711
FBgn0266372	CR45016	-0.7014585	0.04280935	0.4150291
FBgn0263081	CG43349	1.35489038	0.04285935	0.4150291
FBgn0030963	CG7101	-0.7912738	0.04288503	0.4150291
FBgn0038972	CG7054	1.01491257	0.0429073	0.4150291
FBgn0035523	CG1311	-0.4347197	0.04305144	0.4160275
FBgn0265071	CR44182	0.67494868	0.04316915	0.41660164
FBgn0036300	Pmm2	0.81235489	0.04320452	0.41660164
FBgn0052054	CG32054	1.63403007	0.04323379	0.41660164
FBgn0031690	CG7742	1.02488679	0.04355743	0.41862874
FBgn0266316	CR44981	-0.5182714	0.04363405	0.41862874
FBgn0034687	CG11475	-0.932309	0.04363858	0.41862874
FBgn0036752	Adgf-A	-0.4509731	0.04364024	0.41862874
FBgn0267497	28SrRNA:CR45837	2.44616673	0.04368257	0.41862874
FBgn0027780	U26	0.45999835	0.04369124	0.41862874
FBgn0028543	NimB2	-0.8529928	0.0439967	0.42034015
FBgn0037778	mtTFB2	0.83018578	0.04406741	0.42034015
FBgn0038251	Hexim	-0.5049524	0.04409481	0.42034015
FBgn0030056	CG11284	-0.4557234	0.04416323	0.42034015
FBgn0036886	CG9300	-0.5356196	0.04416513	0.42034015
FBgn0002773	Mlc2	-0.9273594	0.04417614	0.42034015
FBgn0030929	CG15043	1.83471329	0.04419272	0.42034015
FBgn0038733	CG11407	3.91753435	0.04420063	0.42034015
FBgn0039886	CG2003	1.83080636	0.04428784	0.42077591
FBgn0031914	CG5973	1.65971224	0.04435167	0.42093921
FBgn0261535	l(2)34Fd	-0.605059	0.04439388	0.42093921
FBgn0051286	CG31286	2.28266732	0.04442925	0.42093921
FBgn0024555	flfl	-0.483463	0.04455564	0.42174361

FBgn0036786	skl	-1.7744651	0.04470278	0.42248423
FBgn0053265	Muc68E	3.02631617	0.044717	0.42248423
FBgn0036827	CG6843	0.5267819	0.04486581	0.42349662
FBgn0015618	Cdk8	0.71173602	0.04502839	0.42463693
FBgn0266268	FeCH	0.65185542	0.04511123	0.42487184
FBgn0265140	Meltrin	0.51152436	0.04513689	0.42487184
FBgn0031990	PAPLA1	0.68676685	0.04520661	0.42501337
FBgn0027505	Rab3-GAP	0.56293202	0.04530079	0.42501337
FBgn0027784	Prp18	0.56488267	0.04533739	0.42501337
FBgn0051865	Ada1-1	0.90095673	0.04534837	0.42501337
FBgn0019949	Cdk9	0.69200399	0.0454125	0.42501337
FBgn0267081	CR45525	-0.5644175	0.04541699	0.42501337
FBgn0263077	CG43340	1.20717891	0.04544457	0.42501337
FBgn0037185	CG11367	-0.5985781	0.04552563	0.42528047
FBgn0065107	snmRNA:128	0.82479371	0.0455568	0.42528047
FBgn0039854	CG1635	0.70999889	0.04571644	0.42637924
FBgn0032727	CG10623	0.63420508	0.0457866	0.4266421
FBgn0015929	dpa	-0.8192554	0.04589219	0.4269501
FBgn0038585	Non3	-0.5072883	0.04590365	0.4269501
FBgn0033177	CG11141	0.45708072	0.04613829	0.42851649
FBgn0035867	CG13671	0.74769183	0.04615636	0.42851649
FBgn0026376	Rgl	-0.8443336	0.04636538	0.42979665
FBgn0082962	snoRNA:Psi28S-3385a	-0.8299123	0.0463788	0.42979665
FBgn0063495	GstE5	1.76517337	0.04663582	0.43178481
FBgn0283462	IMPPP	-1.0735266	0.04674412	0.4321105
FBgn0033582	CG9084	1.10743447	0.04675601	0.4321105
FBgn0260755	CG42553	1.1885456	0.04689594	0.43301012
FBgn0086695	hd	-1.409576	0.04702469	0.43366085
FBgn0010397	LamC	-0.537549	0.04709196	0.43366085
FBgn0260243	E(var)3-9	-0.550096	0.04709846	0.43366085
FBgn0013269	FK506-bp1	-0.4737218	0.04714205	0.43366085
FBgn0264507	CR43906	-0.8253158	0.04721458	0.43366085
FBgn0037150	CG7133	-0.4455657	0.04722236	0.43366085
FBgn0052115	CG32115	0.77621309	0.04727457	0.43374847
FBgn0038488	m-cup	-0.4841794	0.04736951	0.4342276
FBgn0039210	CG13625	0.53200609	0.04756348	0.43561293
FBgn0038257	smp-30	1.8645155	0.04794252	0.43618475
FBgn0050377	CG30377	0.8620641	0.0479453	0.43618475
FBgn0050290	Ppcdc	0.70117744	0.04797265	0.43618475
FBgn0260222	CG42496	0.70117744	0.04797265	0.43618475

FBgn0267575	CR45915	1.09890019	0.04811357	0.43618475
FBgn0027783	SMC2	-0.6847791	0.04812828	0.43618475
FBgn0033297	Mal-A8	2.58522035	0.04815095	0.43618475
FBgn0020278	loco	-0.592267	0.04818407	0.43618475
FBgn0026755	Ugt37b1	3.00579585	0.04818691	0.43618475
FBgn0003353	sei	0.58924939	0.04820565	0.43618475
FBgn0032524	CG9267	-0.4828949	0.04821616	0.43618475
FBgn0034588	CG9394	1.60615327	0.04822864	0.43618475
FBgn0029818	GAA1	-0.430498	0.04824418	0.43618475
FBgn0035620	CG5150	3.65406268	0.04824885	0.43618475
FBgn0032665	CG15152	1.26386311	0.04826951	0.43618475
FBgn0083953	CG34117	0.71879414	0.04838983	0.4368837
FBgn0264822	CR44030	-0.5675534	0.04846072	0.43713549
FBgn0029823	CG3011	-0.4340196	0.04851872	0.43727066
FBgn0033980	Cyp6a20	0.85888658	0.04858281	0.43743875
FBgn0036287	CG10663	-0.7342285	0.04864228	0.43743875
FBgn0000251	cad	-0.5739257	0.04867801	0.43743875
FBgn0085460	CG34431	1.3501507	0.04873007	0.43743875
FBgn0027596	Kank	-0.6342511	0.04875252	0.43743875
FBgn0033778	CG3790	1.27791443	0.04881191	0.43758545
FBgn0028381	Decay	0.62073773	0.04888955	0.43789531
FBgn0044020	Roc2	-0.7370685	0.04895263	0.43804174
FBgn0053533	lectin-37Db	1.62462304	0.04899208	0.43804174
FBgn0051974	CG31974	1.1239324	0.04906903	0.43834427
FBgn0031412	CG16995	1.99574305	0.04913656	0.43849472
FBgn0037870	CG18577	1.49087267	0.04917214	0.43849472
FBgn0031535	CG12795	0.64865859	0.04941811	0.44030195
FBgn0052283	Drsl3	1.81983186	0.04950112	0.44050605
FBgn0037549	CG7878	-0.4598117	0.04952768	0.44050605
FBgn0053301	CG33301	2.63900614	0.04966482	0.44130011
FBgn0037960	mthl5	-0.75826	0.04970378	0.44130011
FBgn0267439	CR45789	-0.6436074	0.04981617	0.44191201
FBgn0032393	CG12264	0.66490551	0.04987626	0.4420593
FBgn0037065	CG12974	1.24396447	0.04994028	0.44224123

Table A-2. Fly genes with different expression levels between flies infected with WT C6706 and those infected with C6706Δ*vasK* as determined with a P-value of >0.05. FBgn – Fly Base gene name. LogFC – log fold change. FDR – false discovery rate.